



HAL
open science

Contributions to the Optimization of Wireless Broadcast/Broadband Systems: Differentiated and Convergent Approaches

Matthieu Crussière

► **To cite this version:**

Matthieu Crussière. Contributions to the Optimization of Wireless Broadcast/Broadband Systems: Differentiated and Convergent Approaches. Engineering Sciences [physics]. Université de rennes 1, 2017. tel-04361987

HAL Id: tel-04361987

<https://hal.science/tel-04361987>

Submitted on 22 Dec 2023

HAL is a multi-disciplinary open access archive for the deposit and dissemination of scientific research documents, whether they are published or not. The documents may come from teaching and research institutions in France or abroad, or from public or private research centers.

L'archive ouverte pluridisciplinaire **HAL**, est destinée au dépôt et à la diffusion de documents scientifiques de niveau recherche, publiés ou non, émanant des établissements d'enseignement et de recherche français ou étrangers, des laboratoires publics ou privés.



Mémoire

Habilitation à Diriger des Recherches

Contributions to the Optimization of Wireless Broadcast/Broadband Systems : Differentiated and Convergent Approaches

Matthieu CRUSSIÈRE

Maître de Conférences à l'INSA de Rennes
Laboratoire IETR / Équipe de recherche SYSCOM

Soutenue le 24/11/2017 devant le jury composé de

Rapporteurs

Geneviève Baudoin
Andrea Tonello
Jean-Marie Gorce

Professeure à l'ESIEE, Paris
Professeur à l'Université de Klagenfurt, Autriche
Professeur à l'INSA Lyon

Examineurs

Marie-Laure Boucheret
Catherine Douillard
Jean-François Hérald
Michel Terré
Bernard Uguen
Luc Vanderdorpe

Professeure à l'ENSEEIH, Toulouse
Professeure à l'IMT-A, Brest
Professeur à l'INSA Rennes
Professeur au CNAM, Paris
Professeur à l'Université de Rennes 1
Professeur à l'Université de catholique de Louvain, Belgique

*A mes très chers enfants,
Suzanna, Gaston, Marceau et Angéline,
sans qui tout cela n'aurait pas de sens.*

Note : la mise en page de ce document a été réalisée à partir du style de mise en forme personnalisé disponible sous <http://coursonline.insa-rennes.fr/course/view.php?id=90>, en tant qu'évolution de la proposition opensource disponible sur <http://ctan.org/pkg/pas-cv>.

Introduction

Ce mémoire d'HdR se décompose en deux grandes parties. La première présente de façon détaillée tous les éléments factuels d'appréciation de mon parcours professionnel tant sur le plan de l'enseignement que de la recherche. Cette première partie est rédigée en français. La seconde partie propose une synthèse de mes activités de recherche, en faisant ressortir une structuration en trois axes et en mettant l'accent sur les principales contributions de ma recherche. Cette partie est rédigée en anglais. Enfin, de façon complémentaire à cette partie de synthèse une sélection de trois articles de revues est fournie en annexe du document concernant des points de ma recherche non développés dans le corps du document.

This HdR manuscript consists of two main parts. The first part contains all the details of my carrier path, exhaustively providing the elements to assess my teaching and research activities. This part is written in french. The second part of the document focuses on the main results of my research and provides a synthesis of the work according to three main axes. This part is written is english. Complementary to such an overview, a selection of three journal papers is given in appendix to highlight other contributions not detailed in the document.

Sommaire

	Introduction	iii
Part.	I Parcours Professionnel	1
	Préambule	3
Chap.	1 Curriculum Vitae succinct	5
	1 État Civil	5
	2 Situation professionnelle actuelle	5
	3 Titres et qualifications	5
	4 Parcours	6
Chap.	2 Activités liées à l'enseignement	7
	1 Structuration des enseignements	7
	2 Thématiques des enseignements	9
	3 Investissements pédagogiques	10
	4 Responsabilités administratives	12
Chap.	3 Activités liées à la recherche	14
	1 Axes de recherche	14
	2 Encadrement de la recherche	15
	3 Contrats et projets collaboratifs	19
	4 Production et valorisation scientifique	21
	5 Responsabilités scientifiques, Rayonnement	24
Chap.	4 Publications	26
Part.	II Synthesis of the Research Works	35
	Preliminaries	37
Chap.	5 Overview of the Research Activities	39
	1 Classification	39
	2 Overview of the studies	40
	2.1 Wireless broadcast transmissions	40
	2.2 Wireless broadband access	41
	2.3 Broadcast/broadband convergent networks	42
Chap.	6 Optimization of Wireless Broadcast Transmissions	43
	1 MIMO Schemes for Broadcast Systems	43
	1.1 Motivations	43
	1.2 Capacity of OFDM-MIMO Systems in SFN	44
	1.3 Robust Distributed STBC for SFN	46
	1.4 Fast Decodable Distributed STBC	49
	1.5 conclusion	52
	2 Practical design of PAPR reduction algorithms	52
	2.1 Motivations	52

Sommaire

	2.2	PAPR Reduction and Tone Reservation Algorithms	53
	2.3	Existing practical solutions	55
	2.4	Proposed Algorithm based on New Kernel Definition	55
	2.5	Performance results and analysis	59
	2.6	Conclusion	63
	3	Theoretical Analysis of Joint PAPR Reduction and Predistortion	64
	3.1	Motivation	64
	3.2	Transmitter Architecture Model	64
	3.3	Analytical Derivations of the EVM	67
	3.4	Application to Optimal Setting of the Transmitter	72
	3.5	Conclusion	73
Chap.	7	Optimization of the Wireless Broadband Access	75
	1	Analysis of Time-Reversal Based Communications	75
	1.1	Motivations	75
	1.2	Time Reversal Filter Concept	76
	1.3	TR-OFDM System Design	80
	1.4	Achievable Rate in Single User Scenarios	83
	1.5	Bit Error Rate Performance Analysis	86
	1.6	Conclusion	88
	2	Spatial Filtering for MU-MIMO in Moderate-Scale Antenna regime	89
	2.1	Motivations	89
	2.2	MU-MIMO Achievable Rate in the Moderate-scale antenna Regime	90
	2.3	BER Performance with Partial Bandwidth Overlap	93
	2.4	Extension to SS-OFDM waveform	99
	2.5	Conclusion	102
	3	Practical Beamforming Strategy for mmWave Communications	103
	3.1	Motivations	103
	3.2	System Model with Geometric-Based Channel Description	103
	3.3	Digital Beamsteering Strategies	106
	3.4	Leakage based power allocation	108
	3.5	Leakage based power allocation	110
	3.6	Conclusion	111
Chap.	8	Broadcast / Broadband Convergence Studies	113
	1	Semi-analytic analysis of dual mode Broadcast/Unicast Networks	113
	1.1	Motivation	113
	1.2	System Level Hybrid Broadband/Broadcast Wireless Network Model	114
	1.3	Semi-Analytic Hybrid Network Performance Evaluation	118
	1.4	Hybrid access performance analysis	119
	1.5	Conclusion	121
	2	Wireless hybrid broadcast/broadband network optimization	122
	2.1	Motivation	122
	2.2	Hybrid Network with adaptive broadcast coverage	123
	2.3	Service Capacity Maximization	125
	2.4	Energy Consumption Minimization	130
	2.5	Conclusion	133
Chap.	9	Research Perspectives	135
	1	General context	135
	2	Proposed Research tracks	135
	2.1	Unified Model of High Power Transmitters Efficiency	135
	2.2	Spatial Filtering for mmWave Systems	135

	2.3 Optimized multi-mode communication networks	135
	Bibliography	137
Part.	III Annexes	147
Ann.	1 Article de revue R.7.	149
Ann.	2 Article de revue R.8.	173
Ann.	3 Article de revue R.14.	189
Ann.	4 Article de revue R.17.	191
Ann.	5 Article de conférence C.67.	203

Partie



Parcours Professionnel

Cette première partie de manuscrit a pour objectif d'apporter une vue générale de mon parcours tant sur le plan de la recherche que de l'enseignement. Elle aborde donc de façon synthétique mais néanmoins exhaustive l'ensemble des éléments représentatifs de mon activité, depuis ma thèse certes, mais surtout depuis ma nomination en tant que Maître de Conférences en février 2017. C'est dans cette partie que sont notamment consignés les différents éléments quantitatifs de mon dossier recherche : publications, encadrement doctoral, collaborations, activités contractuelles, etc. Mais, c'est également au sein de cette partie que je décris mon implication dans le processus de formation de mon établissement d'affectation, tant sur le plan strict de l'enseignement que des responsabilités administratives.

Plan de la partie

Chapitre 1 : <i>Curriculum Vitae succinct</i>	p.5
Chapitre 2 : <i>Activités liées à l'enseignement</i>	p.7
Chapitre 3 : <i>Activités liées à la recherche</i>	p.14
Chapitre 4 : <i>Publications</i>	p.26

1 ÉTAT CIVIL

Nom Crussière
Prénom Matthieu
Date et lieu de naissance 22 octobre 1979
Marennes (Charente-Maritime)
Situation familiale Marié
4 enfants
Adresse Professionnelle INSA de Rennes
Département SRC, bât. 6
20, Avenue des Buttes de Coësmes
CS 70839
35708 Rennes Cedex 7
Tél. +33 (0)2 2323 8581
Mél. matthieu.crussiere@insa-rennes.fr
Web www.ietr.fr/perso/mcrussie

2 SITUATION PROFESSIONNELLE ACTUELLE

► Maître de Conférence de classe normale, 63^e section CNU

Etablissement d'affectation INSA Rennes
Département "Systèmes et Réseaux de Communication" (SRC)
Laboratoire de Recherche Institut d'Électronique et de Télécommunications de Rennes (IETR)
UMR CNRS 6164
Département "Communications"
Équipe "Systèmes de Communications" (SYSCOM)

3 TITRES ET QUALIFICATIONS

Depuis 2008 **Détenteur** de la PEDR/PES sans interruption, 63^e section CNU
Première attribution : PEDR au 01/10/2008
Deuxième attribution : PES au 01/10/2012
Troisième attribution : PEDR au 01/10/2016
Dernier classement global au rang A
Classement par critère (Publ./Encadr./Rayon./Resp.) : A/A/A/B

- 2006 Qualification** aux fonctions de Maître de Conférences
Section 63 : "Électronique, Optronique et Systèmes"
Section 61 : "Génie Informatique, Automatique et Traitement du Signal"
- 2002–2005 Doctorat** de l'INSA de Rennes, mention Electronique
Mention Très honorable
Date de soutenance : 25 novembre 2005
Titre de la Thèse : "Étude et optimisation de communications à haut-débit sur lignes d'énergie : exploitation de la combinaison OFDM/CDMA"
Jury : Claude Berrou (P), Marie-Laure Boucheret (R), Pierre Duhamel (R), Jean-Marc Brossier (E), Jean-Yves Baudais (E), Jean-François Hérald (E)
- 2002 Diplôme d'Etudes Approfondies (DEA)** de l'INSA de Rennes
Spécialité : Électronique, Réseaux et Communications
- 1997–2002 Titre d'Ingénieur** de l'INSA de Rennes
Option : Électronique et Systèmes de Communications
- 1996–1997 Baccalauréat**, Académie de Poitiers
Série : Scientifique
Mention : Bien

4 PARCOURS

- Depuis septembre 2013** **Chercheur associé** à l'Institut de Recherche en Technologies B-COM à Rennes
Laboratoire Infrastructures Réseaux (I&R)
Mise à disposition à 20%
- Depuis février 2007** **Maître de Conférences** à l'INSA de Rennes
Département Systèmes et Réseaux de Communications (SRC)
Classe Normale
- 2005–2007 Attaché Temporaire d'Enseignement et de Recherche (ATER)** à l'Institut National des Sciences Appliquées de Rennes
Département Électronique et Systèmes de Communications (ESC)
Durée : 18 mois
- 2002–2005 Doctorant** à l'Institut d'Électronique et de Télécommunications de Rennes, groupe Communications-Propagation-Radar (CPR)
Direction de thèse : Prof. J.-F. Hérald
Co-encadrement : CR CNRS J.-Y. Baudais
Contributions au projet RNRT IDILE portant sur l'optimisation de systèmes multipor-teuses à étalement de spectre dans le contexte de communications à haut-débit sur courant porteur en ligne.

Comme indiqué dans mon CV au chapitre 1, mon établissement d'appartenance est l'INSA de Rennes, et je suis affecté au département d'enseignement SRC (Systèmes et Réseaux de Communication). Comme cela va être détaillé dans cette partie, j'effectue la quasi intégralité de mes enseignements au sein de ce département qui accueille des étudiants de niveau L3 à M2. Depuis la rentrée 2016, j'interviens également auprès des étudiants de la formation par apprentissage CDTI (Conception et Développement de Technologies Innovantes) de l'INSA de Rennes. Cette partie du document sera également l'occasion de détailler les différentes missions et responsabilités administratives que j'ai pu exercer en lien avec l'enseignement.

1 STRUCTURATION DES ENSEIGNEMENTS

Une vue d'ensemble de mes activités d'enseignement depuis mon poste d'ATER jusqu'à aujourd'hui est présentée sur les histogrammes de la figure 2.1. Ces histogrammes permettent de mettre rapidement en évidence deux aspects de mon déroulé de carrière en tant qu'enseignant :

- L'aspect **volumétrique**
- L'aspect **typologique**

Ces deux points sont commentés plus en détails ci-après. Par ailleurs, sur les histogrammes sont marquées par des noeuds numérotés (\mathbf{Ni}) les principales étapes de refontes/modifications de programmes d'enseignement que j'ai effectuées ou auxquelles j'ai participé. Ces aspects seront détaillés dans le paragraphe 3.

► Volumétrie

Mon service d'enseignement annuel est bien entendu calibré sur la charge statutaire de 192 Heq TD, volume nominal auquel s'ajoutent tous les ans quelques dizaines d'heures supplémentaires. Comme le montrent les histogrammes, deux facteurs sont venus conditionner le volume total d'heures dispensées :

- Mon nombre d'heures complémentaires est borné à 50 Heq TD depuis l'obtention de la PEDR en octobre 2008, un an après ma nomination. J'ai ainsi effectué un service stable de 2008 à 2013 de 242 Heq TD par an.
- Depuis ma mise à disposition en septembre 2013 en tant que chercheur associé à l'institut de recherche et de technologie (IRT) B-com à Rennes, à hauteur de 20% de mon temps de travail, je bénéficie d'une décharge de service en équivalence horaire de 38 Heq TD à l'année. Depuis 4 ans, ma charge annuelle d'enseignement est donc réduite à 204 Heq TD (service réduit + heures complémentaires).

► Typologie

Mon investissement en cours, TD, TP et projets affiche une stabilité relative au cours des années. Il en est de même si l'on s'intéresse aux niveaux d'études auxquels correspondent mes enseignements : License (L2, L3), Maîtrise (M1, M2) ou Apprentissage (AP). Les fluctuations au cours du temps sont essentiellement dues aux évolutions des programmes d'enseignement et aux ventilations d'heures entre collègues en fonction des besoins/opportunités. Pour résumer les types d'enseignements dans lesquels je suis investi, deux points peuvent être notés :

- J'ai eu la chance de prendre la charge de deux cours magistraux dès ma prise de fonction, représentant un total d'environ 50 Heq TD. Aux modifications structurelles des maquettes d'enseignement prêt, ces cours constituent le socle stable de mon service depuis 10 ans. Pour le reste de ma charge, j'interviens selon les années, au sein de divers enseignements, en travaux pratiques et projets essentiellement, et en séances

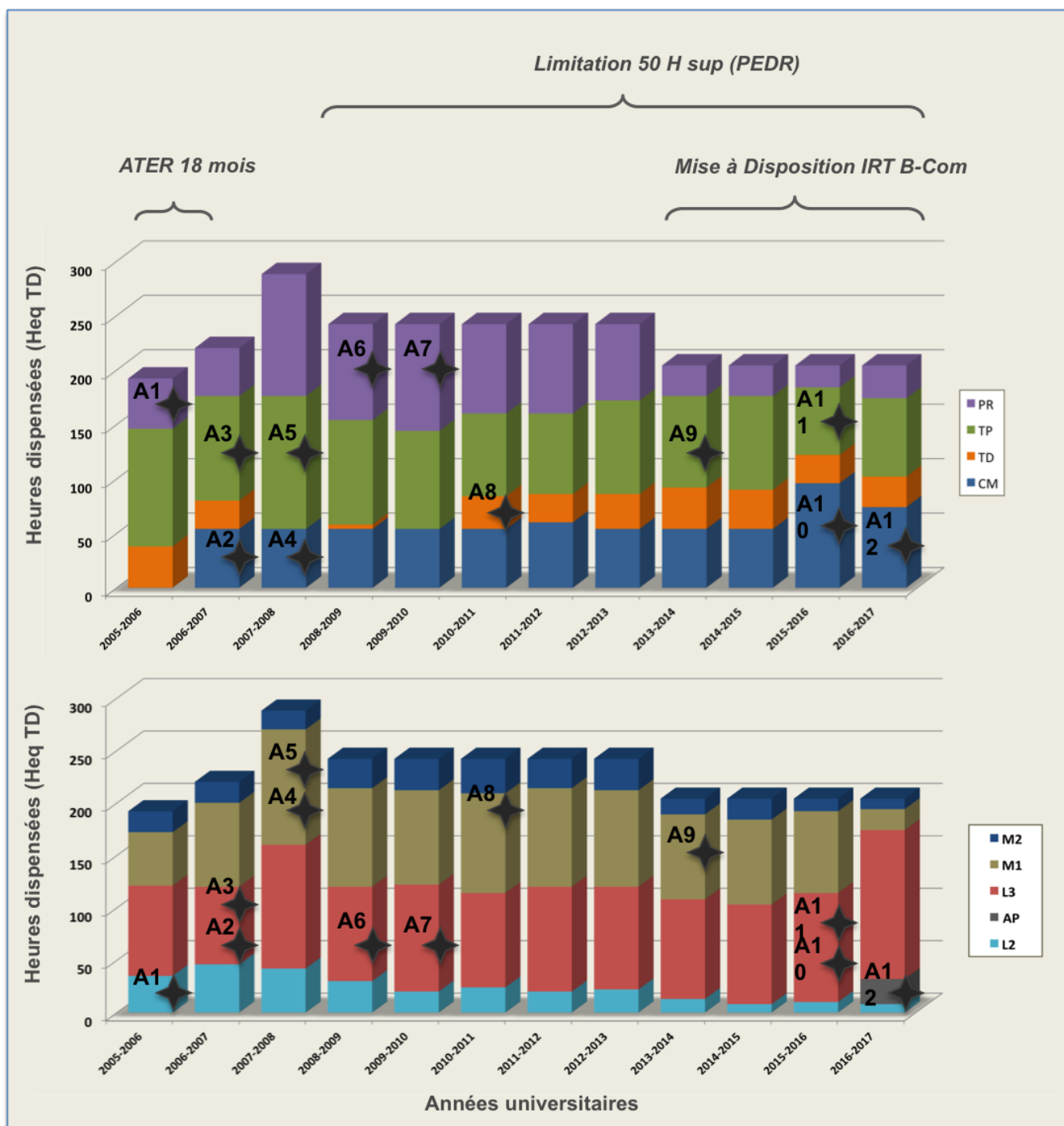


FIGURE 2.1– Volume et type d'enseignements dispensés par année, de 2005 à 2017. En haut, volumes répartis par type : CM=cours magistral, TD=travaux dirigés, TP=travaux pratiques, PR=projets. En bas, volumes répartis par niveau : L2/L3=2e et 3e année de licence, M1/M2=1e et 2e année de master, AP=apprentissage.

2. Thématiques des enseignements

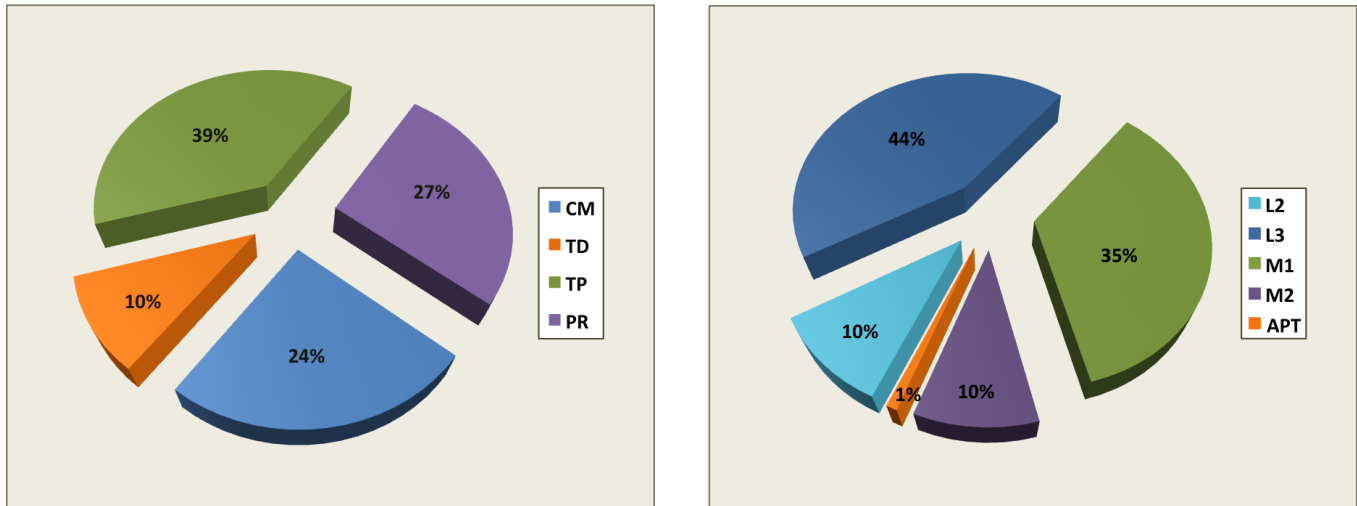


FIGURE 2.2– Répartition moyenne des enseignements sur toute la carrière en % du volume total. A gauche : répartition en CM/TD/TP/PR. A droite : répartition par niveau L2/L3, M1/M2 et AP

de travaux dirigés plus rarement. Cette tendance moyenne est reflétée par le diagramme de gauche de la figure 2.2.

- Jusqu'en 2015, mes enseignements étaient focalisés à environ 80% sur les niveaux L3 et M1. Depuis 2016, deux changements importants dans les enseignements à l'INSA ont fait évoluer cet équilibre. D'une part, des modifications importantes de maquettes pédagogiques ont conduit à redéployer un certain nombre des cours auxquels je participe du M1 vers la L3. D'autre part, l'ouverture de la formation par apprentissage (CDTI) m'a conduit à dispenser une part de mes cours vers cette formation. En moyenne depuis le début de ma carrière, la répartition par niveau de mes enseignements est présentée à droite sur la figure 2.2

2 THÉMATIQUES DES ENSEIGNEMENTS

D'un point de vue thématique, j'interviens sur des enseignements de deux natures :

- Thématique [Signal & Communications](#),
- Thématique [Électronique analogique](#)

J'apprécie particulièrement cette double facette de mes enseignements qui me permet bien souvent de décloisonner les approches, d'effectuer des parallèles ou des connexions entre concepts ou bien encore de proposer des exemples à caractère transverse.

Dans la suite, la liste des différents modules dont j'assume la responsabilité ou la co-responsabilité, puis ceux auxquels je participe, est donnée. Une responsabilité de module signifie la définition du programme, la gestion des supports de cours, la proposition de sujets d'exercices et de manipulations pour les TP, ainsi que la gestion de l'évaluation des étudiants. Ces responsabilités peuvent être partagées.

► Responsabilités de modules :

Depuis 2015 **Traitement du signal déterministe, 2e partie**, niveau L3

Volume : 8H de cours, entre 8H et 12H de TD

Contenu : Conversion analogique-numérique / outils d'analyse temps-fréquence des signaux discrets / Changements de cadence

Bases du traitement du signal déterministe, 2e partie, apprentissage

Volume : 12H mélangeant cours/TD et TP

Contenu : Outils d'analyse temps-fréquence des signaux discrets

Systèmes linéaires numériques, niveau L3

Volume : 20H mélangeant cours et TD

Contenu : Outils d'analyse des systèmes linéaires discrets / Filtrage numérique

Systèmes de communication, 1ere partie, niveau L3

Volume : 12 H de cours, 4H de TP

Contenu : Modèle de chaînes de communications / Transmissions sur fréquence porteuse / Modèle des signaux à bande étroite

2007–2015 Traitement numérique du signal, niveau M1

Volume : 24 H de cours

Contenu : Outils d'analyse des systèmes et signaux à temps discrets

Traitement du signal pour les communications analogiques, niveau L3

Volume : 14 H de cours

Contenu : Outils d'analyse des performances des modulations analogiques

► Autres implications :

Depuis 2011 Communications Numériques, niveau M1

Volume : variable entre 8 et 16 H de TD, entre 6H et 20H de TP

Contenu : Constellations, critères de Nyquist, calculs de performances, OFDM

Récepteurs avancés, niveau M2

Volume : variable entre 2H et 4H de TD, 6H de TP

Contenu : Techniques d'égalisation, filtrage adaptatif

Radiocommunications, niveau M1

Volume : 12H de TP

Contenu : Caractérisation des canaux de propagation, sondage de canal

Depuis 2007 Electronique analogique, niveau L3

Responsable des TP

Volume : variable entre 14 et 28 H de TP, 12H de projet

Contenu : lois de l'électronique linéaires, diodes et transistors

Systèmes linéaires analogiques, niveau L3

Responsable des TP

Volume : variable entre 10 et 20 H de TP, 24H de projet

Contenu : Amplificateur opérationnel, systèmes bouclés, filtrage, oscillations

Projets et bureaux d'étude, niveau M1/M2

Volume : variable selon les années, 15 H au maximum

Contenu : suivi de groupes d'étudiants sur des projets transversaux sur l'année ou le semestre, du cahier des charges à la réalisation finale.

3 INVESTISSEMENTS PÉDAGOGIQUES

Dans cette partie, je souhaite mettre en avant mon intérêt appuyé pour la pédagogie en montrant mon investissement pour la mise en place de nouveaux enseignements ou pour leur évolution. Il est bien évident que cet investissement va de soi pour un enseignant, mais la double vie de l'enseignant-chercheur peut parfois conduire à sur-favoriser une activité ou détrimenter l'autre. Je m'efforce donc de consacrer un temps suffisant à la réflexion (individuelle ou collective) dans le but de faire évoluer mon enseignement à la fois sur le fond (mise à jour du programme) et la forme (supports pédagogiques, façon d'enseigner). Sur ce dernier point, j'envisage d'ailleurs dès cette année d'expérimenter dans un de mes cours l'utilisation de la pédagogie dite par "classe inversée", dans laquelle certaines séances de cours (typiquement 2 sur 3) seront essentiellement le lieu de discussions et d'échanges autour des questions des étudiants et de problèmes posés, la théorie étant pour l'essentiel disponible en ligne ou sur documents ciblés que je mettrai à la disposition des étudiants pour qu'ils puissent travailler par avance.

3. Investissements pédagogiques

► Création/évolution des enseignements :

Sur les histogrammes présentés précédemment à la figure 2.1 sont indiquées les principales actions (numérotées de A1 à A12) que j'ai menées au fil des ans pour faire évoluer les différents enseignements dont j'ai eu la charge ou auxquels j'ai participé. Il a pu s'agir de la construction de nouveaux cours ou projets, ou bien du reformatage de certains.

A1 Construction d'un module dit de "sensibilisation"

Niveau L2, en collaboration avec 2 collègues

Actions menées : participation à la mise en oeuvre d'un mini-projet pour faire découvrir l'électronique fondamentale aux étudiants de 1er cycle universitaire. Application : mise en forme de signaux de télévision à partir de montages à composants discrets. Dimensionnement de l'ensemble des circuits et écriture d'un polycopié associé.

A2, A3 Reformatage d'un module de "traitement numérique du signal"

Niveau M1,

Actions menées : redéfinition d'un module complet sur les outils d'analyse et de traitement des signaux et systèmes à temps discret. Proposition de 6 séances de travaux pratiques associés au cours, avec manipulations sous Matlab.

A4, A5 Reformatage d'un module de "Modulations analogiques"

Niveau L3,

Actions menées : redéfinition d'un module complet sur les notions de transmissions de l'information sur onde porteuse. Proposition de 5 séances de travaux pratiques associés au cours, avec manipulations sous Matlab et sur analyseur de spectre.

A6, A7 Proposition de projets tutorés d' "électronique analogique"

Niveau L3, en collaboration avec 2 collègues

Actions menées : participation à la définition de deux projets de fin de semestre en électronique analogique regroupant l'ensemble des notions vues au cours. Définition des sujets, dimensionnement et mise en oeuvre et tests des circuits. Applications : observation automatique de caractéristiques de transistors à l'oscilloscope, réalisation d'un mini-analyseur de spectre.

A8 Proposition de nouveaux exercices en "communications numériques"

Niveau M1, en collaboration avec 1 collègue

Actions menées : participation à la définition de nouveaux sujets d'exercices suite à l'évolution du cours de communications numériques. Recherche de mises en situation pratique pour le dimensionnement système (problématiques de type ingénieur).

A9 Reformatage des TPs en "communications numériques"

Niveau M1, en collaboration avec 3 collègues

Actions menées : participation à la migration de l'ensemble des manipulations de TPs vers des plateformes radiologiques (USRP). Redéfinition complète du programme de TP, préparation des programmes, tests, rédaction des sujets.

A10, A11 Reformatage de deux modules de "traitement du signal"

Niveau L3, en collaboration avec 4 collègues

Actions menées : participation à la redéfinition complète du programme de traitement du signal sur 18 mois et reformatage des séances de cours/TD/TP associés. Mise à jour des supports, des exercices et des manipulations de TP.

A12 Nouveau cours de "traitement du signal" en formation par apprentissage

Niveau L3, en collaboration avec 2 collègues

Actions menées : participation à l'adaptation/redéfinition du programme de traitement du signal sur 12 mois pour des étudiants en apprentissage. Modification de la pédagogie : approche conjointe théorie, exercices et pratique sous Matlab.

► Supports pédagogiques :

Aux actions détaillées précédemment viennent s'ajouter au fil de l'eau la mise à jour régulière des supports pédagogiques. Ceux-ci diffèrent naturellement en fonction de la nature de l'enseignement, à savoir en cours ou en TP, et correspondent à un choix sur la pédagogie suivie :

- **Pour les cours magistraux**, je privilégie les cours au tableau pour leur côté plus interactif et spontané. Cela est possible dans la mesure où je fournis aux étudiants des photocopiés de cours volontairement très complets (cf. liste ci-dessous). La prise de notes reste donc à volume raisonnable et n'empêche pas la concentration sur le fond. Je peux donc ainsi consacrer l'essentiel du temps en cours pour expliciter et illustrer les principales notions du programme, pointer les aspects les plus techniques, mener les démonstrations les plus importantes et proposer les premiers exemples d'application. Il s'agit également d'attirer l'attention sur les pièges ou erreurs fréquemment rencontrés. Le cours magistral consiste donc en la prédigestion d'un contenu déjà disponible (le photocopié), censée faciliter l'assimilation finale qui reste évidemment du ressort de l'étudiant lui-même. Comme mentionné plus haut, j'envisage de tester d'autres formes de pédagogie où l'étudiant se montre plus acteur que spectateur du cours.
- **Pour les travaux pratiques**, au-delà de la fourniture d'un recueil de sujets à traiter en séance, je dispose pour chaque session de laboratoire d'un jeu de transparents (cf. liste ci-dessous) permettant de lancer les manipulations et de faire des points réguliers au tableau. Cela permet de pointer les principales observations et conclusions importantes de chaque manipulation, mais également de cadencer les séances en resynchronisant les différents binômes d'étudiants. Pour les simulations logicielles (ex : Matlab), je fournis sur Moodle l'ensemble des codes corrigés pour que les étudiants puissent travailler en dehors des séances encadrées.

P photocopiés **Module de "traitement du signal déterministe"**

de cours Niveau L3, chapitres 5 à 7, 40 pages

Module de "systèmes linéaires numériques"

Niveau L3, photocopié complet, 80 pages

Module de "systèmes de communications"

Niveau L3, chapitres 1 à 4, 80 pages

Module de "Traitement numérique du signal"

Niveau L3, photocopié complet, 150 pages

Supports **Module de "électronique analogique"**

de TP Niveau L3, sujets de TP (8 manipulations), transparents associés

Module de "systèmes linéaires numériques"

Niveau L3, sujets de TP (4 manipulations), codes Matlab associés

Module de "systèmes linéaires analogiques"

Niveau L3, sujets de TP (5 manipulations), transparents associés

Module de "Communications numériques"

Niveau M1, sujets de TP (6 manipulations), transparents associés

4 RESPONSABILITÉS ADMINISTRATIVES

Depuis ma nomination à l'INSA de Rennes en février 2007, je me suis impliqué comme chacun de mes collègues dans la prise en charge de responsabilités d'ordre administrative liées au fonctionnement du département d'enseignement. L'historique de ces responsabilités est donné ci-dessous.

Depuis février **Chargé de mission pour le département SRC**

2017 Missions : assistance au directeur de département pour la gestion globale de la formation pédagogique (suivi des maquettes d'enseignement, tenue des indicateurs de la formation, suivi du budget d'investissement), participation partielle aux réunions de co-direction au niveau de l'établissement INSA.

4. Responsabilités administratives

Depuis 2013 Membre élu au conseil de département

Département SRC

De 2009 à 2016 Responsable de la 3e année du département SRC

Missions : gestion des études et des étudiants en L3 au département SRC.

Suivi et mise à jour de la maquette pédagogique, construction des emplois du temps, suivi au quotidien des étudiants, préparation du jury d'année, liens avec le secrétariat.

De 2007 à 2011 Responsable du module de sensibilisation SRC

Missions : gestion du programme destiné aux étudiants de 1er cycle INSA, organisation des ateliers de découverte, des visites en entreprise et des tables rondes.

Cette partie est consacrée à la présentation synthétique de mes activités de recherche avec le but de faire ressortir les critères objectifs d'évaluation que sont l'encadrement de la recherche, la production scientifique, la participation à des projets collaboratifs ou la prise de responsabilités.

Mon laboratoire de rattachement est l'IETR (Institut d'Électronique et de Télécommunications de Rennes), et plus précisément l'équipe SYSCOM (Système de Communications) du département "Communications". Cette équipe, partagée géographiquement entre l'Université de Nantes et l'INSA Rennes est la plus importante du laboratoire en termes de nombre de personnes. Depuis janvier 2017, suite à la mise en place de la nouvelle organisation de l'IETR pour la période 2017-2020, je suis co-responsable de l'équipe pour la partie rennaise de l'équipe. Cette équipe compte environ 9 chercheurs et enseignant-chercheurs (aux pourcentages d'affectation prêt), dont 5 HDR parmi lesquels 3 professeurs des universités. Il faut également noter que je suis impliqué au sein de l'IRT B-Com à Rennes par le biais d'une mise à disposition à 20% de mon temps de travail, soient 40 jours par an. Une part de mes activités de recherche s'inscrit donc dans le cadre du laboratoire IR (Interfaces Réseaux) de l'IRT.

1 AXES DE RECHERCHE

Depuis mes débuts dans le monde de la recherche académique, mes activités ont eu pour dénominateur commun la [recherche d'efficacité dans les systèmes de communications numériques](#) en s'appuyant essentiellement sur [l'optimisation des couches physiques et d'accès des systèmes](#). Au fil des ans, différentes facettes de cette ligne se sont exprimées, au gré des opportunités et des envies, entre une approche système et des considérations plus algorithmiques et mathématiques. En faisant l'historique des principaux thèmes traités, il est possible de dégager deux phases dans mes activités :

- [La première phase, qui s'écoule de 2002 à 2010 environ](#) inclut mes travaux de thèse et ceux des premières années qui la suivirent. Durant cette période, mes activités se sont concentrées sur l'optimisation des schémas de modulation hybridant l'étalement de spectre et l'OFDM, encore appelées schémas de modulation à porteuses multiples à précodage linéaire. Mes travaux ont alors porté sur la recherche de solutions de synchronisation, d'estimation de canal et d'allocation des ressources dans différents contextes applicatifs, des liaisons filaires aux réseaux sans fil.
- [La seconde phase, qui a démarré vers 2009](#) a progressivement conduit à la structuration actuelle de mes activités, dans le prolongement des travaux effectués dans la première phase. Mes travaux de recherche actuels s'articulent donc autour de 3 thèmes principaux :
 1. Algorithmie et performances théoriques pour les systèmes de radiodiffusion,
 2. Algorithmie et performances théoriques pour le partage de la ressource dans les réseaux d'accès radio,
 3. Modélisation et analyse de performances des réseaux hybrides ou hétérogènes.

Une autre grille de lecture de mes activités de recherche peut-être celle des méthodes et outils utilisés et développés lors des différentes études. Les principales approches suivies, souvent de façon transverse aux thèmes listés ci-dessus, sont les suivantes :

- Estimation paramétrique,
- Optimisation sous contrainte,
- Modélisation stochastique de signaux et systèmes,
- Analyse analytique et semi-analytique de performances.

2. Encadrement de la recherche

Dans la suite de ce chapitre, l'ensemble des données et critères objectifs en lien avec mes activités de recherche seront exposées de façon synthétique, pour l'ensemble de mon parcours et pour les deux phases identifiées à l'instant. Dans la deuxième partie du document (cf. partie 2) consacrée à la synthèse de mes activités de recherche, seules les contributions associées à la seconde phase de mon parcours seront détaillées, celles de la première phase étant simplement rapidement décrites en guise de préambule dans le chapitre 5.

2 ENCADREMENT DE LA RECHERCHE

Depuis ma prise de poste en tant qu'ATER il y a 12 ans, j'ai effectué le **co-encadrement de 18 thèses, dont 15 soutenues**, avec un taux d'encadrement variant de 33% à 65% selon les cas. La figure 3.1 donne une vue globale de mon activité d'encadrement doctoral au fil des années, avec en légende la thématique associée à chaque thèse conformément aux axes identifiés dans le paragraphe précédent. En complément, sur ce diagramme sont indiqués les taux d'encadrement par thèse, ainsi que les thèses qui ont fait l'objet d'une co-tutelle ou/et d'une implication dans un projet collaboratif. Enfin, la durée moyenne des thèses, évaluée à **3 ans et 4 mois**, est mentionnée pour information sur cette figure. Cette figure met en évidence mon **implication continue et soutenue de l'encadrement de thèses**, avec en rythme souvent supérieur à 4 thèses en cours.

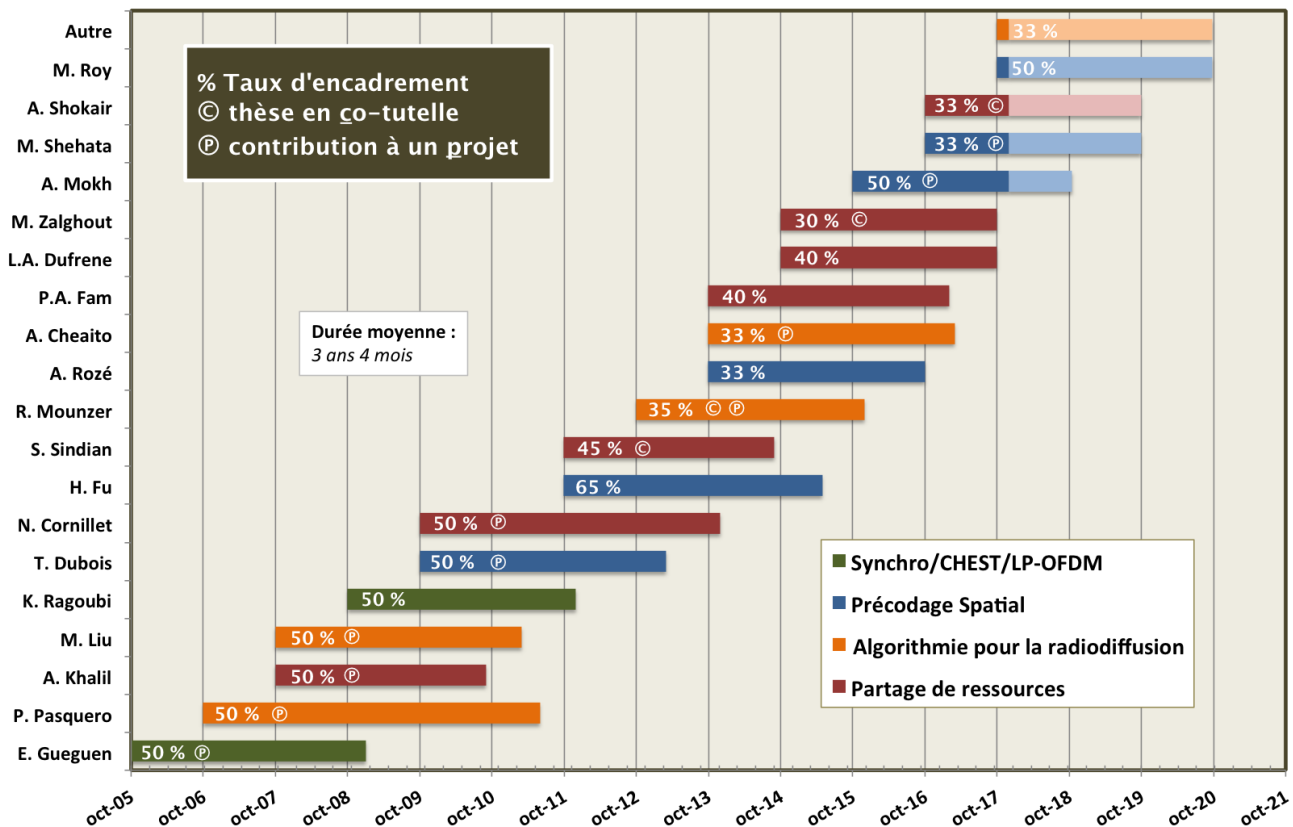


FIGURE 3.1– Déroulement chronologique des thèses co-encadrées et classification thématique.

Outre l'encadrement de thèses, j'ai également réalisé celui de **9 stages de Master** d'une durée de 4 à 5 mois chacun. Ces stages ont pour la plupart été menés en lien avec les travaux de thèse des doctorants, si bien que ces derniers en ont également été co-encadrants. Enfin, à ces activités d'encadrement s'ajoute également le **suivi de 5 post-doctorants**, même s'il est naturellement entendu dans ce cas que le travail de suivi s'apparente davantage à un **travail collaboratif**, étant donné l'autonomie et l'expérience de ce type de candidats.

Dans les sections qui suivent sont données les listes exhaustives et détaillées de l'ensemble des stagiaires et doctorants encadrés, ainsi que des post-doctorants avec qui j'ai travaillé.

► **Liste des thèses co-encadrées :**

Émeric GUEGUEN “Etude et optimisation des techniques UWB haut débit multibandes OFDM”
Soutenue le 14 janvier 2009
Directeur de Thèse : J.F. Hérald (50%)
Co-encadrant : M. Crussière (50%)
Position actuelle du Docteur : chargé d'affaires à EDF-TDG, France

Ayman KHALIL “Procédés inter-couches d'allocation de ressource pour les futurs systèmes UWB multiporteuse à haut-débit”
Soutenue le 13 septembre 2010
Directeur de Thèse : J.F. Hérald (50%)
Co-encadrant : M. Crussière (50%)
Position actuelle du Docteur : Enseignant-chercheur à l'UIL, Liban

Pierre-Oudomsack PASQUERO “Optimisation de Systèmes de télévision numérique terrestre : estimation de canal, synchronisation et schémas multi-antennes distribués”
Soutenue le 27 juin 2011
Directeur de Thèse : J.F. Hérald (50%)
Co-encadrant : M. Crussière (50%)
Position actuelle du Docteur : Ingénieur de recherche à DGA-MI, France

Ming LIU “Analyse et optimisation des systèmes asiatiques de diffusion de télévision numérique terrestre et mobile”
Soutenue le 30 mars 2011
Directeur de Thèse : J.F. Hérald (50%)
Co-encadrant : M. Crussière (50%)
Position actuelle du Docteur : Enseignant-chercheur à l'université de Pékin, Chine

Karima RAGOUBI “Techniques de raccourcissement de canal pour systèmes OFDM”
Soutenue le 8 décembre 2011
Directeur de Thèse : M. Hérald (50%)
Co-encadrant : M. Crussière (50%)
Position actuelle du Docteur : Chef de projet déploiement réseaux à ERDF, France

Samar SINDIAN “Optimisation de l'allocation de ressource pour les réseaux WPAN maillés à haut-débit”
Soutenue le 17 septembre 2014
Directeur de Thèse : J.F. Hérald (30%)
Co-encadrants : A. Khalil (25%), M. Crussière (45%)
Position actuelle du Docteur : chargée d'enseignement à l'IUL, Liban

Nicolas CORNILLET “Convergence des réseaux de télécommunications mobiles et de télédiffusion : modélisation et évaluation des performances d'un réseau hybride LTE/DVB-T2”
Soutenue le 18 décembre 2013
Directeur de Thèse : M. Hérald (50%)
Co-encadrant : M. Crussière (50%)
Position actuelle du Docteur : Ingénieur chez Nokia, France

Thierry DUBOIS “Application du retournement temporel aux systèmes multi-porteuses : propriétés et performances”
Soutenue le 12 février 2013
Directeur de Thèse : M. Hérald (50%)
Co-encadrants : M. Crussière (50%)
Position actuelle du Docteur : Chargé d'affaires chez ALTRAN, France

2. Encadrement de la recherche

Hua FU “Optimisation de la ressource spectrale dans les système multi-antennes multi-utilisateurs avec recouvrement partiel de bande”

Soutenue le 22 mai 2015

Directeur de Thèse : M. Hérald (35%)

Co-encadrant : M. Crussière (65%)

Position actuelle du Docteur : Post-Doc à l'université de Cherbrooke, Canada

Ralph MOUNZER “Nouveaux algorithmes de réservations de porteuses pour la réduction de PAPR des signaux multiporteuse”

Soutenue le 15 décembre 2015

Directeur de Thèse : J.F. Hérald (35%)

Co-encadrants : Y. Nasser (30%), M. Crussière (35%)

Position actuelle du Docteur : Ingénieur, USA

Antoine ROZÉ “Massive MIMO, une approche angulaire pour les futurs systèmes multi-utilisateurs aux longueurs d'onde millimétriques”

Soutenue le 17 octobre 2016

Directeur de Thèse : M. Hérald (33%)

Co-encadrants : C. Langlais (33%), M. Crussière (33%)

Position actuelle du Docteur : Ingénieur, Australie

Pape-Aboulaye FAM “Définition d'un système de diffusion hertzien de contenus multimédias convergent avec les réseaux broadcast et mobiles”

Soutenue le 9 février 2017

Directeur de Thèse : M. Hérald (40%)

Co-encadrants : P. Brétilon (20%), M. Crussière (40%)

Position actuelle du Docteur : Ingénieur de recherche à TDF, France

Ali CHEAITO “Recherche de solutions conjointes et adaptatives de réduction de PAPR et de prédistorsion pour les systèmes de radio intelligente utilisant les formes d'onde à porteuses multiples”

Soutenue le 10 mars 2017

Directeur de Thèse : M. Hérald (33%)

Co-encadrants : Y. Louët (33%), M. Crussière (33%)

Position actuelle du Docteur : Post-Doc à Supélec, France

Mohamad ZALGHOUT “Algorithmes d'attachements dans les réseaux hétérogènes WLAN et cellulaires”

Soutenance prévue le lundi 23 octobre 2017

Directeur de Thèse : J.F. Hérald (30%)

Co-encadrants : A. Khalil (20%), Samih Abdul-Nabi (20%), M. Crussière (30%)

Louis-Adrien DUFRENE “Recherche de solutions d'adaptation des réseaux GSM aux nouvelles contraintes des communications vers les objets”

À soutenir en novembre 2017

Directeur de Thèse : J.F. Hérald (40%)

Co-encadrants : J. Schwoerer (20%), M. Crussière (40%)

Ali MOKH “Optimisation des schémas de modulation spatiale”

Démarrée le 1 octobre 2015

Directeur de Thèse : M. Hérald (50%)

Co-encadrant : M. Crussière (50%)

Mohamed SHEHATA “Précodage spatial hybride analogique-numérique pour les communications en onde millimétrique”

Démarrée le 1 octobre 2016

Directeur de Thèse : M. Hérald (33%)

Co-encadrant : P. Pajusco (33%), M. Crussière (33%)

Ahmad SHOKAIR “Modélisation et optimisation de réseaux hybrides broadband/broadcast”
Démarrée le 1 octobre 2016
Directeur de Thèse : M. Hérald (33%)
Co-encadrants : Y. Nasser (33%), (M. Crussière (33%))

► Liste des Post-Doctorants suivis :

Youssef NASSER “Schémas MIMO pour les réseaux de diffusion”
octobre 2007 à septembre 2009
Projet : B21C

Ming LIU “Schémas MIMO pour les réseaux de diffusion”
janvier 2011 à janvier 2012
Projet : Engines

Jean-Christophe SIBEL “Modèles de statistique d’erreurs des codes LDPC DVB-S2”
octobre 2012 à octobre 2014
Projet : OptiSaT2

Ferdaouss MATTOUSSI “Modèles d’abstraction du protocole HbbTV2.0 sur couche PHY DVB-T2”
juin 2016 à décembre 2017
Projet : AdicTV

Krishna BULUSU “Optimisation des techniques de réduction de PAPR pour les normes DVB-T2 et ATSC3.0”
septembre 2016 à décembre 2017
Projet : GreenTEA

► Liste des stages de Master co-encadrés :

Eddy CHOLLET “ Etude de processus de synchronisation par la technique du pilote étalé”
septembre–décembre 2008
Encadrement : O.P. Pasquero, M. Crussière, J.F. Hérald

Elias NAJJAR “Allocation dynamique de ressources sous contrainte de qualité de service dans les réseaux UWB”
mars–juillet 2009
Encadrement : A. Khalil, M. Crussière, J.F. Hérald

Hassan ALI-AHMAD “Allocation de ressource et ordonnancement distribué dans les réseaux WPAN”
mars–juillet 2010
Encadrement : A. Khalil, M. Crussière, J.F. Hérald

Rana DIAB “Allocation de ressource temps-fréquence dans les réseaux WPAN”
mars–juillet 2011
Encadrement : A. Khalil, M. Crussière, J.F. Hérald

Imad JAMIL “Etude d’une architecture MESH pour les futurs réseaux WPAN”
mars–juillet 2012
Encadrement : S. Sindian, A. Khalil, M. Crussière, J.F. Hérald

Ali CHEAITO “Analyse conjointe des fonctions de prédistorsion et de réduction de facteur de crête sur les signaux OFDM”
mars–juillet 2013
Encadrement : M. Crussière, J.F. Hérald

3. Contrats et projets collaboratifs

Daniel KOBEISSI “Analyse des statistiques d’erreurs sur paquets MPEG-TS dans les réseaux DVB-T2”

mars-juillet 2016

Encadrement : F. Mattoussi, M. Crussière, J.F. Hérald

Syed-Muhammad FAHAD “Etude analytique du spectre des signaux multiporteuses dans un contexte d’amplification de puissance non-linéaire”

mars-juillet 2016

Encadrement : A. Cheaito, M. Crussière, J.F. Hérald

3 CONTRATS ET PROJETS COLLABORATIFS

L’équipe de recherche SYSCOM de l’IETR possède une activité contractuelle et partenariale soutenue. Aux côtés des collègues de l’équipe, une part importante de mon temps recherche est consacrée à la participation et au suivi des différents projets. Ainsi, j’ai donc eu une **implication conséquente dans les projets**, en prenant souvent des **responsabilités de lots (Work-Packages)**, **potentiellement importantes**, comme au sein des projets européens B21C et ANR MCube. Au total depuis 10 ans, j’ai **collaboré à 19 projets**, qu’ils soient de dimension régionale, **nationale, européenne ou encore industrielle** comme détaillé ci-après. Ces projets sont bien entendu un moyen d’entretenir des relations privilégiées avec le monde industriel et académique. Mais au-delà, il s’agit aujourd’hui d’un vecteur important du financement de la recherche pour l’équipe (cf. implication des doctorants dans les projets figure 3.1).

La liste des différents projets et les détails les concernant est donnée ci-après. En complément, une vue synthétique est proposée sur la figure 3.2 : répartition chronologique des différents projets/contrats, classement par type et signalétique de la nature de mon implication au plan administratif (montage, responsabilité, gestion).

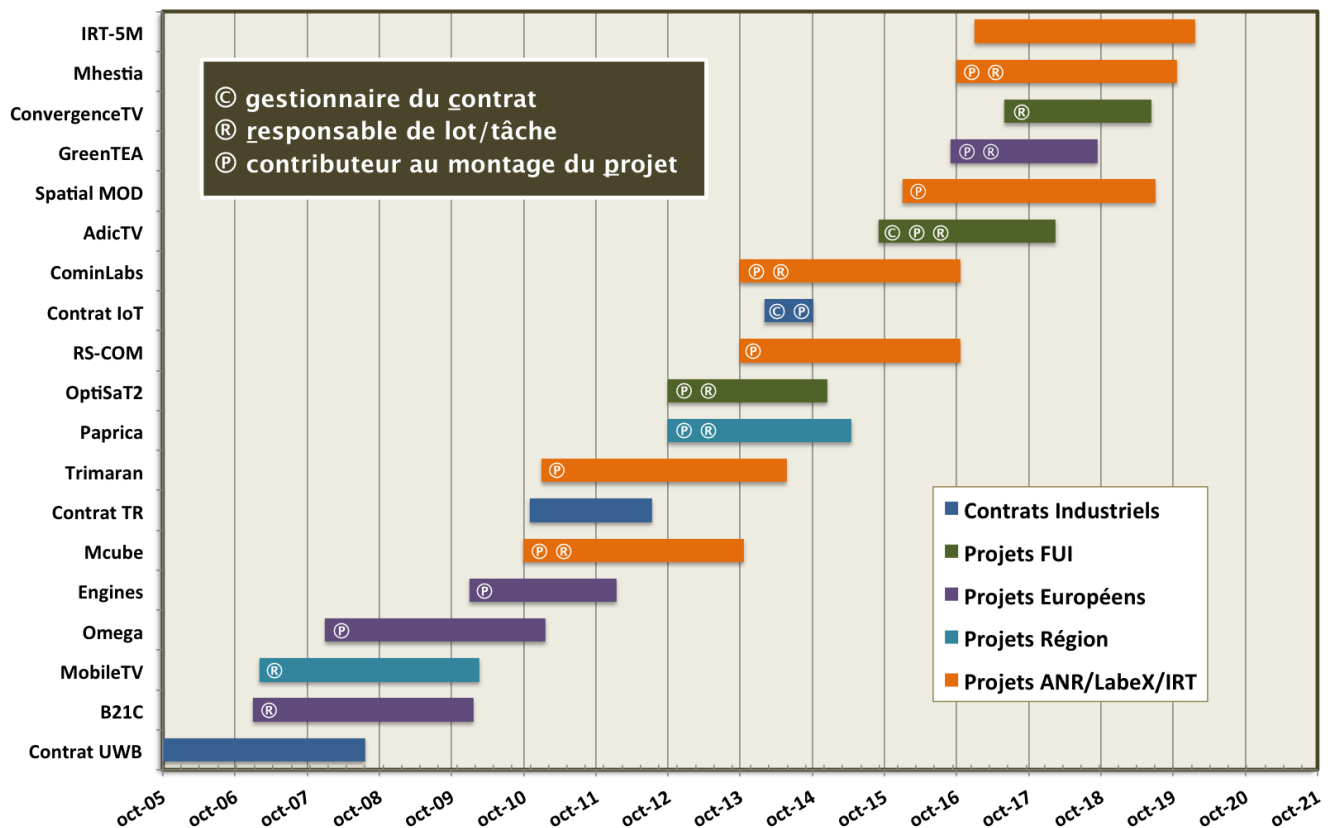


FIGURE 3.2– Chronologie et classification des différentes implications contractuelles et projets.

- Contrat d'étude** "Etude et optimisation de la combinaison des techniques UWB-MS et CDMA haut-débit et extension aux WLANs"
Type de client : opérateur de télécommunications, 2005–2007 (36 mois)
Implication personnelle : suivi des études
- OMEGA** "Home Gigabit Area, Converged, Ultra High Speed Home and Access Networks"
Projet Européen IST FP7, 2008–2010 (36 mois)
20 partenaires : hollandais, allemands, français, italiens, grecs, slovènes, etc.
Implication personnelle : contributeur au montage du projet, suivi des études
- B21C** "Broadcast for the 21st Century"
Projet Européen CELTIC, 2007–2009 (36 mois)
32 partenaires : allemands, italiens, anglais, suédois, finlandais, français, etc..
Implication personnelle : responsable de lot, suivi des études
- Mobile TV World** "Analyse des normes de télévision mobiles mondiales et optimisation des récepteurs associés"
Projet Région Bretagne du pôle "Image & Réseaux", 2007–2009 (36 mois)
Partenaires : Teamcast, Silembia, Bretagne International, BTIC.
Implication personnelle : suivi des études
- ENGINES** "Enabling Next Generation Networks for Broadcast Services"
Projet Européen CELTIC, 2010–2012 (36 mois)
32 partenaires : allemands, italiens, anglais, suédois, finlandais, français, etc..
Implication personnelle : contributeur au montage projet, suivi des études
- Mcube** "Mobile Multi Media"
Projet ANR, 2010–2013 (36 mois)
Partenaires : Orange Labs, CNES, ALU, MERCE, Telecom Bretagne, Teamcast, Parrot
Implication personnelle : contributeur au montage projet, responsable de lot, suivi des études
- TRIMARAN** "Time-Reversal for Green communications based on MicRo-structured ANtennas"
2011–2013, 40 mois
Projet ANR
Partenaires : Orange Labs, Inst. Langevin, Thalès, Telecom Bgne, TRcom.
Implication personnelle : contributeur au montage projet, suivi des études
- OptiSaT2** "Optimisation des Transmission Satellite de 2nd génération"
Projet FUI, 2012–2014 (26 mois)
Partenaires : Enensys Tech, TDF, SmartDTV, Telecom Paris Tech
Implication personnelle : contributeur au montage projet, suivi des études
- Contrat d'étude** "Etude de faisabilité d'exploitation des réseaux GSM pour l'intégration d'objets communicants au sein des réseaux de communications"
Type de client : opérateur de télécommunications, 2014 (8 mois)
Implication personnelle : proposition de l'étude, responsable de contrat, suivi des études
- PAPRICA** "PAPR Iterative Compression Algorithms"
Projet Région Bretagne du pôle "Images et Réseaux", 2012–2015 (30 mois)
Partenaires : Teamcast, Digidia
Implication personnelle : contributeur au montage projet, responsable de lot, suivi des études

4. Production et valorisation scientifique

Nombre de publications en revues internationales à comité de lecture (ACL)	24
Nombre de communications en conférences internationales (ACTI)	93
Nombre de communications en conférences nationales (ACTN)	6
Nombre de chapitres d'ouvrages scientifiques (OS)	4
Nombre de brevets	4
Nombre total de citations	689
H-Index	15

TABLE 3.1– Chiffres globaux de publications et citations 2003–2017 (source Google Scholar, septembre 2017)

RS-COM “Réseaux et Systèmes pour les Communications”

Projet ANR fléché IRT-BCOM, 2013–2016 (36 mois)

Partenaires : IRT-BCOM, UR1, Telecom Bgne, Orange Labs, TDF, Siradel

Implication personnelle : contributeur et suivi des études

AdicTV “Optimisation des transmissions non-linéaires sur les réseaux de diffusion”

Projet FUI, 2015–2019 (29 mois)

Partenaires : Enensys, TDF, HTTV, Quadrille, TelecomParisTech

Implication personnelle : contributeur au montage projet, responsable du contrat pour l'INSA, responsable de lot, suivi des études

Spatial Modulation “Spatial Modulation and reconfigurable antennas for high-rate connectivity to mobile and energy autonomous sensors”

Projet ANR, 2016–2019 (42 mois)

Partenaires : Orange Labs, IMT Atl., Inst. Langevin, Centrale Supélec, TR-COM

Implication personnelle : contributeur au montage du projet, suivi des études

GreenTEA “Green Transmission Efficiency Algorithms”

Projet Européen EUROSTAR, 2016–2018 (24 mois)

Partenaires : Teamcast, TRYO Communications

Implication personnelle : responsable de lot, suivi des études

Convergence TV “Algorithms for the convergence of worldwide Digital Television standards”

Projet FUI, 2017–2019 (24 mois)

Partenaires : Teamcast, TDF, BroadPeak, MotionSpell, ATEME, Canal+

Implication personnelle : suivi des études

4 PRODUCTION ET VALORISATION SCIENTIFIQUE

► Analyse bibliométrique de la production scientifique

La liste complète et détaillée de mes publications (revues, conférences, chapitres d'ouvrages et brevets) est donnée dans la partie 4 du document. Je fournis dans ce paragraphe une analyse synthétique de ma production scientifique sous la forme de diagrammes et tableaux.

Tout d'abord, le tableau 3.1 donne les chiffres globaux pour l'ensemble de mes publications et citations, ainsi qu'une évaluation du fameux H-index. L'ensemble de ces données sont issues de ma page Google Scholar accessible librement en consultation en ligne.

Ensuite, sur les figures 3.3 et 3.4 l'ensemble des données bibliométriques sont compilées et respectivement traduites sous la forme d'un histogramme temporel et d'un diagramme sectoriel, chacun tenant compte de la classification des publications par type.

► Actions de valorisation de la recherche

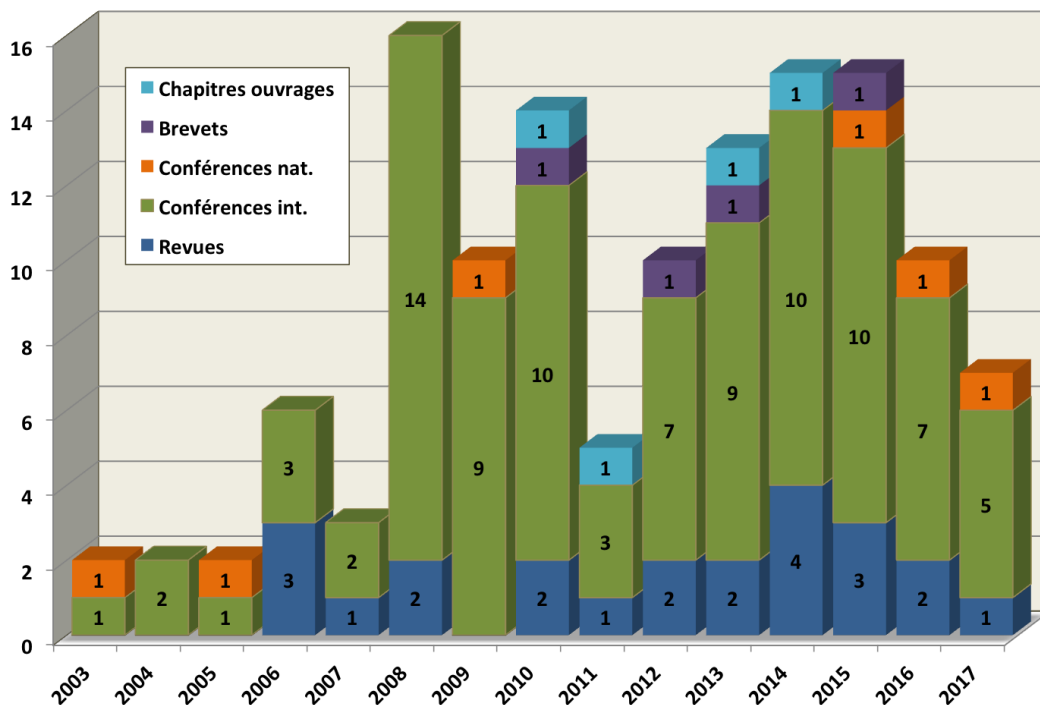


FIGURE 3.3– Évolution chronologique du nombre de publications et classification par type.

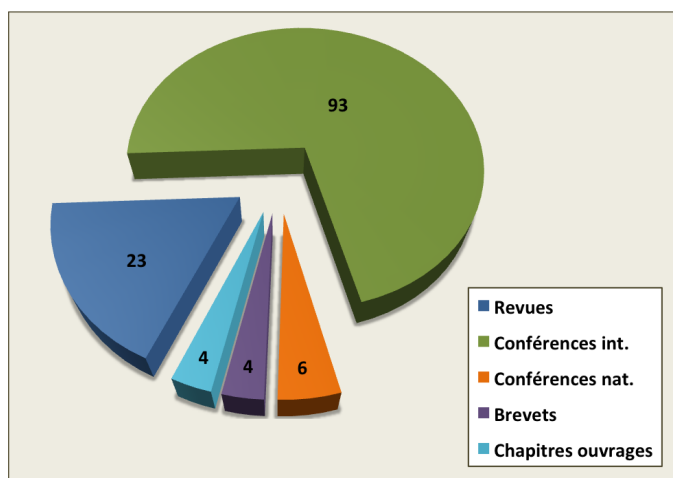


FIGURE 3.4– Répartition moyenne des publications par types sur la période 2003 à 2017.

4. Production et valorisation scientifique

Outre l'activité "classique" de publication en revues et conférences, j'ai mené, souvent en commun avec d'autres collègues, d'autres formes de dissémination et de valorisation des travaux listés ci-dessous. Ce type d'actions se sont intensifiées ces dernières années.

- Tutoriaux en conférences** **"The Time Reversal Paradigm : close relations with spatial filtering/beamforming and large-scale antenna systems"**
IEEE Asia Pacific Wireless and Mobile Conference (APWiMob'15), Bandung, Indonesia, août 2015.
M. Hérald, M. Crussière et Y. Kokar
- "Application of Time Reversal Principles to Wireless Communications : from SingleUser SISO to MultipleUser Large Scale MIMO Scenarios"**
International Conference on Software, Telecommunications and Computer Networks 2015 (SoftCom'15), Split, Croatie, sept. 2015.
M. Hérald, M. Crussière et J.C. Prévotet
- Papiers invités** **"Quantifying the Memory Effects of Power Amplifiers : EVM Closed-Form Derivations of Multicarrier Signals"**
IEEE International Globecom Conference 2017, Special WCL session, Singapore, dec. 2017
A. Cheaito, M. Crussière, J.F. Hérald et Y. Louët
- "Time Reversal Based Beamforming for Wireless Communications : A Theoretical Analysis from Moderate-Scale to Large-Scale Antenna Systems"**
5th IEEE International Conference on Communications and Networking (COMNET'15), Hammamet, Tunisie, nov. 2015
M. Crussière, H. Fu et M. Hérald
- Journées GDR** **"Retournement temporel pour des systèmes multi-antennes et multi-porteuses"**
journée scientifique conjointe des GDR ISIS et GDR ONDE "Développements récents en focalisation et communication par retournement temporel", 26 sept. 2013
M. Hérald, T. Dubois et M. Crussière
- "Optimisation de la ressource spectrale pour les systèmes MU-MIMO avec recouvrement fréquentiel partiel"**
journée scientifique conjointe du GDR ISIS "L'éco-radio", 6 mai 2015
H. Fu, M. Crussière et M. Hérald
- Séminaires industriels** **"Preuve de concept d'une transmission MISO à 2.4GHz utilisant le concept de retournement temporel"**
Salon de la recherche d'Orange Labs, Orange Gardens, Issy-les-Moulineaux, 9 déc. 2014
Y. Kokar, T. Dubois, M. Hérald et M. Crussière
- "Towards common broadcasting physical layer for future converged broadband/broadcast networks"**
Open Event du projet Mcube, Orange Gardens, Issy-les-Moulineaux, 16 mai 2013
M. Crussière
- Transfert de technologie** **"Procédé de réduction de facteur de crête pour les signaux DVB-T2"**
Technique brevetée, support à l'intégration sur plateforme matériel d'un partenaire industriel, 2015 et 2017
R. Mounzer, M. Crussière et J.F. Hérald

- Consortium de normalisation** “Potential of MIMO technologies for Next Generation Handheld broadcasting systems”
Présentation plénière, meeting du TM NGH du consortium DVB, 22 oct. 2009
M. Crussière

5 RESPONSABILITÉS SCIENTIFIQUES, RAYONNEMENT

► Comités de lecture et de programmes

- Membre de comités de lecture de revues** “IEEE Transactions on Broadcasting”
 “IEEE Transactions on Vehicular Technologies”
 “IEEE Wireless Communication Letters”
 “IEEE Communication Magazine”
 “EURASIP Journal of Wireless Communications and Networking (JWCN)”
 “Annals of Telecommunications”
Reviewer régulier depuis 2008, environ 5 papiers par an, toutes revues confondues.

- Membre de comités de programme** “IEEE Global Communication Conference (Globecom)”
TPC member depuis 2016
 “IEEE International Symposium on Power Line Communications (ISPLC)”
TPC member depuis 2015
 “IEEE International Symposium on Personal Indoor and Mobile Radio Communications (PIMRC)”
TPC member depuis 2013
 “IEEE International Wireless Communications and Networking Conference (WCNC)”
TPC member depuis 2011

- Responsable de comité de programme** “IEEE International Workshop on Cross-Layer Design (IWCLD)”
Responsable du programme technique (TPC Chair), 2011
3e Édition de la conférence organisée à Rennes.

- Comité de relecture de projets** “Programme ANR, appels à projets génériques”
Expert pour le comité d'évaluation CE25 (Infrastructures hautes performances, Sciences et Technologies Logicielles)
2016-2017

► Jurys de thèse

J'ai eu l'occasion de participer aux jurys de thèse mentionnés ci-après en tant qu'examinateur.

- Slim BEN-HALIMA** “Gestion des Interférences Pour les Réseaux de Femtocells en se basant sur les Techniques MIMO coopératives”
Soutenue le 29 nov. 2012
- Ahmad JABBAN** “Optimisation et analyse des réseaux intelligents et des réseaux hétérogènes”
Soutenue le 16 sept. 2013
- Dinh-Thuy PHAN-HUY** “Retournement temporel : application aux réseaux mobiles”
Soutenue le 14 déc. 2015

5. Responsabilités scientifiques, Rayonnement

► Responsabilités administratives et collectives

Enfin, depuis quelques années, je me suis impliqué dans la participation et la prise en charge de responsabilités d'ordre administratives sur le plan de la recherche, telles que celles données ci-dessous.

Depuis janvier 2017 **Responsable de l'équipe SYSCOM**
Missions : coordination/animation scientifique, gestion administrative, suivi des indicateurs et de la communications, représentation.

Membre nommé au conseil scientifique plénier de l'IETR

De 2014 à 2016 **Membre élu au conseil de laboratoire de l'IETR**
Représentant du collège MCF

Depuis 2010 **Membre nommé au comité de sélection section 63 de ENIB**
Membre externe, participation à la commission de recrutement d'un MCF en 2011
Membre nommé au comité de sélection section 63 de l'INSA de Rennes
Membre interne, participation à la commission de recrutement d'un MCF en 2009

Dans ce chapitre est répertoriée l'intégralité de mes publications classées par catégories : revues, conférences internationales et nationales, brevets et chapitres d'ouvrages.

► Revues internationales

- [R.1] Ali Cheaito, [Matthieu Crussière](#), Jean-François H elard, and Yves Lou et. "Quantifying the memory effects of power amplifiers : EVM closed-form derivations of multicarrier signals". *IEEE Wireless Communications Letters*, 6(1) :34–37, 2017.
- [R.2] Ali Cheaito, Jean-François H elard, [Matthieu Crussière](#), and Yves Lou et. "EVM derivation of multicarrier signals to determine the operating point of the power amplifier considering clipping and predistortion". *EURASIP Journal on Wireless Communications and Networking*, 2016(1) :281–292, 2016.
- [R.3] Pape Abdoulaye Fam, St ephane Paquelet, [Matthieu Crussière](#), Jean-François H elard, and Pierre Br etillon. "Analytical derivation and optimization of a hybrid unicast-broadcast network for linear services". *IEEE Transactions on Broadcasting*, 62(4) :890–902, 2016.
- [R.4] Hua Fu, [Matthieu Crussière](#), and Maryline H elard. "BER analysis for equal gain transmission in downlink multiuser MIMO systems". *Wireless Communications Letters, IEEE*, 4(5) :533–536, 2015.
- [R.5] Ming Liu, Jean-François H elard, Maryline H elard, and [Matthieu Crussière](#). "Towards the next generation video broadcasting : Improved performance using distributed MIMO". *Wireless Personal Communications*, 84(4) :2635–2649, 2015.
- [R.6] Samar Sindian, Jean-François H elard, Abed Ellatif Samhat, [Matthieu Crussière](#), and Ayman Khalil. "Resource allocation mechanism in IEEE 802.15.3 parent/child model". *Wireless Networks*, 21(6) :1863–1877, 2015.
- [R.7] Samar Sindian, [Matthieu Crussière](#), Jean-François H elard, Abed Ellatif Samhat, and Ayman Khalil. "Admission control and resource allocation strategies for IEEE 802.15.5". *EURASIP Journal on Wireless Communications and Networking*, 2014(1) :1–22, 2014.
- [R.8] [Matthieu Crussière](#), Catherine Douillard, Christian Gallard, Marie Le Bot, Benjamin Ros, Arnaud Bouter, and Alain Untersee. "A unified broadcast layer for horizon 2020 delivery of multimedia services". *Broadcasting, IEEE Transactions on*, 60(2) :193–207, 2014.
- [R.9] Ming Liu, [Matthieu Crussière](#), Maryline H elard, and Jean-François H elard. "Achieving low-complexity maximum-likelihood detection for the 3D-MIMO code". *EURASIP Journal on Wireless Communications and Networking*, 2014(1) :1–16, 2014.
- [R.10] Samar Sindian, Ayman Khalil, Abed Ellatif Samhat, [Matthieu Crussière](#), and Jean-François H elard. "Resource allocation in high data rate mesh WPAN : a survey paper". *Wireless personal communications*, 74(2) :909–932, 2014.
- [R.11] Thierry Dubois, Maryline H elard, [Matthieu Crussière](#), and C ecile Germond. "Performance of time reversal precoding technique for MISO-OFDM systems". *EURASIP Journal on wireless communications and networking*, 2013(1) :1–16, 2013.
- [R.12] Ayman Khalil, [Matthieu Crussière](#), and Jean-François H elard. "Cross-layer multiple-access optimization scheme for linear precoded OFDM UWB systems". *annals of telecommunications-Annales des t el ecomunications*, 68(5-6) :287–298, 2013.
- [R.13] Ming Liu, Maryline H elard, [Matthieu Crussière](#), and Jean-François H elard. "Distributed MIMO coding scheme with low decoding complexity for future mobile TV broadcasting". *Electronics letters*, 48(17) :1079–1081, 2012.

Bibliographie

- [R.14] Ming Liu, [Matthieu Crussière](#), and Jean-François Hélard. "A novel data-aided channel estimation with reduced complexity for TDS-OFDM systems". *Broadcasting, IEEE Transactions on*, 58(2) :247–260, 2012.
- [R.15] Ayman Khalil, [Matthieu Crussière](#), and Jean-François Hélard. "Adaptive self-learning resource allocation scheme for unlicensed users in high-rate uwb systems". *Wireless Personal Communications*, 56(3) :611–623, 2011.
- [R.16] Ayman Khalil, [Matthieu Crussière](#), and Jean-François Hélard. "Cross-layer resource allocation scheme under heterogeneous constraints for next generation high rate WPAN". *International Journal of Network Security & Its Applications (IJNSA)*, 2(3) :18–34, 2010.
- [R.17] Ayman Khalil, [Matthieu Crussière](#), and Jean-françois Hélard. "Time-frequency spectrum sharing scheme for next generation OFDM systems". *EURASIP Journal on Wireless Communications and Networking*, 2010 :116, 2010.
- [R.18] Antoine Stephan, Emeric Guéguen, [Matthieu Crussière](#), Jean-Yves Baudais, and Jean-François Hélard. "Optimization of linear precoded ofdm for high-data-rate UWB systems". *EURASIP Journal on Wireless Communications and Networking*, 2008 :10, 2008.
- [R.19] Youssef Nasser, J-F Hélard, and Matthieu Crussière. 3d mimo scheme for broadcasting future digital tv in single-frequency networks. *Electronics Letters*, 44(13) :829–830, 2008.
- [R.20] Youssef Nasser, J-F Hélard, and [Matthieu Crussière](#). "System level evaluation of innovative coded MIMO-OFDM systems for broadcasting digital TV". *International Journal of Digital Multimedia Broadcasting*, 2008, 2008.
- [R.21] Jean-Yves Baudais and [Matthieu Crussière](#). "Resource allocation with adaptive spread spectrum OFDM using 2D spreading for power line communications". *EURASIP Journal on Advances in Signal Processing*, 2007(1) :1–13, 2007.
- [R.22] Emeric Guéguen, Nadia Madaoui, Jean-François Hélard, and [Matthieu Crussière](#). "Combination of OFDM and CDMA for high data rate UWB". *Comptes Rendus Physique*, 7(7) :774–784, 2006.
- [R.23] [Matthieu Crussière](#), Jean-Yves Baudais, and Jean-François Hélard. "Adaptive spread-spectrum multicarrier multiple-access over wirelines". *Selected Areas in Communications, IEEE Journal on*, 24(7) :1377–1388, 2006.
- [R.24] [Matthieu Crussière](#), Jean-Yves Baudais, and Jean-François Hélard. "Loading algorithms for adaptive SS-MC-MA systems over wireline channels : comparison with DMT". *European transactions on telecommunications*, 17(6) :659–669, 2006.

► Conférences internationales

- [C.1] Pape-Abdoulaye Fam, [Matthieu Crussière](#), Stéphane Paquelet, Jean-François Hélard, and Pierre Brétilon. "Energy efficiency of hybrid unicast-broadcast networks for mobile TV services". In *Personal, Indoor, and Mobile Radio Communication (PIMRC), 2017 IEEE 28th Annual International Symposium on*, page 6. IEEE, 2017.
- [C.2] Ali Cheaito, Mohamed Saad-Farah, [Matthieu Crussière](#), Jean-François Hélard, and Yves Louët. "Spectral analysis of predistorted non-linear amplified multicarrier signals". In *Wireless Communications and Networking Conference (WCNC), 2017 IEEE*, page 6. IEEE, 2017.
- [C.3] Mohamad Zalgout, Samih Abdul-Nabi, Ayman Khalil, Maryline Hélard, and [Matthieu Crussière](#). "Optimizing context-aware resource and network assignment in heterogeneous wireless networks". In *Wireless Communications and Networking Conference (WCNC), 2017 IEEE*, page 6. IEEE, 2017.
- [C.4] Ferdaouss Mattoussi, Gheorghe Zaharia, Jean-François Hélard, and [Matthieu Crussière](#). "Analytical modeling of losses in FDP protocol of HbbTV based push-VOD services over DVB networks". In *Wireless Communications and Networking Conference (WCNC), 2017 IEEE*, page 6. IEEE, 2017.
- [C.5] Ali Mokh, Maryline Hélard, and [Matthieu Crussière](#). "Extended receive antenna shift keying". In *Telecommunications (ICT), 2017 International Conference on*, page 5. IEEE, 2017.

- [C.6] Mohamad Zalgout, Jean-François H elard, Ayman Khalil, Samih Abdul-Nabi, and Matthieu Cruss iere. "Load-aware power efficiency maximization in heterogeneous wireless networks". In *Telecommunications (ICT), 2017 International Conference on*, page 7. IEEE, 2017.
- [C.7] Ferdaouss Mattoussi, Jean-François H elard, Gheorghe Zaharia, and Matthieu Cruss iere. "A reliable delivery of HbbTV based push-VoD services over DVB networks using RS codes". In *Broadband Multimedia Systems and Broadcasting (BMSB), 2017 IEEE International Symposium on*, page 5. IEEE, 2017.
- [C.8] Krishna Chaitanya Bulusu Sri Satish, Matthieu Cruss iere, Jean-François H elard, Ralph Mounzer, and Youssef Nasser. "A low latency algorithm for efficient PAPR reduction for DVB-T2 and ATSC 3.0 broadcast". In *Broadband Multimedia Systems and Broadcasting (BMSB), 2017 IEEE International Symposium on*, page 5. IEEE, 2017.
- [C.9] Antoine Roz e, Matthieu Cruss iere, Maryline H elard, and Charlotte Langlais. "Comparison between a hybrid digital and analog beamforming system and a fully digital massive MIMO system with adaptive beamsteering receivers in millimeter-wave transmissions". In *Wireless Communication Systems (ISWCS), 2016 International Symposium on*, pages 86–91. IEEE, 2016.
- [C.10] Ferdaouss Mattoussi, Matthieu Cruss iere, and Jean-François H elard. "HbbTV based Push-VOD services over DVB networks : Analysis and AL-FEC code application". In *Ultra Modern Telecommunications and Control Systems and Workshops (ICUMT), 2016 8th International Congress on*, pages 414–419. IEEE, 2016.
- [C.11] Ali Cheaito, Yves Lou et, Matthieu Cruss iere, and Jean-François H elard. "Optimal operating point of the power amplifier with respect to the EVM for TV broadcasting applications". In *Broadband Multimedia Systems and Broadcasting (BMSB), 2016 IEEE International Symposium on*, pages 1–4. IEEE, 2016.
- [C.12] Ali Cheaito, Matthieu Cruss iere, Jean-François H elard, and Yves Lou et. "Energy-efficiency optimization of the high power amplifier for multicarrier systems : Analytical EVM derivation". In *Computer Communications Workshops (INFOCOM WKSHPS), 2016 IEEE Conference on*, pages 409–414. IEEE, 2016.
- [C.13] Louis-Adrien Dufrene, Ming Liu, Matthieu Cruss iere, Jean-François H elard, and Jean Schwoerer. "Blind repetitions for cellular-IoT : Performance analysis of combination mechanisms". In *Telecommunications (ICT), 2016 23rd International Conference on*, pages 1–6. IEEE, 2016.
- [C.14] Pape-Abdoulaye Fam, St ephane Paquetlet, Matthieu Cruss iere, Jean-François H elard, and Pierre Br etillon. "Optimal capacity of hybrid unicast-broadcast networks for mobile TV services". In *Broadband Multimedia Systems and Broadcasting (BMSB), 2016 IEEE International Symposium on*, pages 1–5. IEEE, 2016.
- [C.15] Mohamad Zalgout, Ayman Khalil, Matthieu Cruss iere, Samih Abdul-Nabi, and Maryline H elard. "SDRAN-based user association and resource allocation in heterogeneous wireless networks". In *Wireless Communications and Networking Conference Workshops (WCNCW), 2016 IEEE*, pages 296–302. IEEE, 2016.
- [C.16] Ming Liu, Matthieu Cruss iere, and Jean-François H elard. "Improved physical layer for energy-efficient M2M communications over cellular networks". In *Software, Telecommunications and Computer Networks (SoftCOM), 2015 23rd International Conference on*, pages 264–268. IEEE, 2015.
- [C.17] Pape-Abdoulaye Fam, Matthieu Cruss iere, Jean-François H elard, Pierre Br etillon, and St ephane Paquetlet. "Global throughput maximization of a hybrid unicast-broadcast network for linear services". In *Wireless Communication Systems (ISWCS), 2015 International Symposium on*, pages 146–150. IEEE, 2015.
- [C.18] Maryline H elard, Matthieu Cruss iere, Jean-Christophe Pr evotet, and Yvan Kokar. "Application of time reversal principles to wireless communications : from single user SISO to multiple-user large scale MIMO scenarios". In *Softcom 2015*, 2015.
- [C.19] Antoine Roz e, Maryline Helard, Matthieu Cruss iere, and Charlotte Langlais. "Millimeter-wave digital beamsteering in highly line-of-sight environments for massive MIMO systems". In *Wireless World Research Forum Meeting*, volume 35, 2015.
- [C.20] Matthieu Cruss iere, Hua Fu, and Maryline H elard. "Time reversal based beamforming for wireless communications : a theoretical analysis from moderate-scale to large-scale antenna systems". In *Communications and Networking (COMNET), 2015 5th International Conference on*, pages 1–6. IEEE, 2015.

Bibliographie

- [C.21] Antoine Rozé, Maryline H elard, [Matthieu Cruss iere](#), and Charlotte Langlais. "Linear precoder performance for massive MIMO systems in near LOS environments : Application to mmwave transmission". In *European Wireless 2015 ; 21th European Wireless Conference ; Proceedings of*, pages 1–6. VDE, 2015.
- [C.22] Ralph Mounzer, [Matthieu Cruss iere](#), Youssef Nasser, and J-F H elard. "Tone reservation based papr reduction technique with individual carrier power allocation for multiple peaks reduction". In *Vehicular Technology Conference (VTC Spring), 2015 IEEE 81st*, pages 1–6. IEEE, 2015.
- [C.23] Ali Cheaito, Jean-Fran ois H elard, Matthieu Cruss iere, and Yves Lou et. "Impact of clipping on evm of the predistorted non-linear amplified multicarrier signals". In *Wireless Communication Systems (ISWCS), 2015 International Symposium on*, pages 76–80. IEEE, 2015.
- [C.24] Ralph Mounzer, [Matthieu Cruss iere](#), Youssef Nasser, and Jean-Fran ois H elard. "Individual carrier multiple peaks tone reservation based PAPR reduction algorithms". In *VTC2015-Spring Proceedings of IEEE Vehicular Technology Conference*, pages 1–6, 2015.
- [C.25] Ali Cheaito, [Matthieu Cruss iere](#), Yves Lou et, and Jean-Fran ois H elard. "EVM derivation for multicarrier signals : Joint impact of non-linear amplification and predistortion". In *Vehicular Technology Conference (VTC Spring), 2015 IEEE 81st*, pages 1–6. IEEE, 2015.
- [C.26] Thierry Dubois, Maryline H elard, Pierre Siohan, [Matthieu Cruss iere](#), Laurent Chapelain, and Bruno Jahan. "Efficient MISO system combining time reversal and ofdm/oqam". In *European Wireless 2014 ; 20th European Wireless Conference ; Proceedings of*, pages 1–5. VDE, 2014.
- [C.27] Hua Fu, [Matthieu Cruss iere](#), and Maryline H elard. "Partial channel overlay in moderate-scale MIMO systems using WH precoded OFDM". In *Telecommunications (ICT), 2014 21st International Conference on*, pages 16–21. IEEE, 2014.
- [C.28] Jean-Christophe Sibel, [Matthieu Cruss iere](#), and Jean-Fran ois H elard. "Analysis of decoding failures of DVB-S2 LDPC codes". In *Vehicular Technology Conference (VTC Fall), 2014 IEEE 80th*, pages 1–6. IEEE, 2014.
- [C.29] Papa Moussa Ndao, Maryline H elard, [Matthieu Cruss iere](#), and Fran ois Yven. "Channel shortening for OFDM systems : An improved algorithm in noisy environments". In *Ultra-WideBand (ICUWB), 2014 IEEE International Conference on*, pages 228–233. IEEE, 2014.
- [C.30] Ralph Mounzer, Youssef Nasser, [Matthieu Cruss iere](#), and Jean-Fran ois H elard. "Power control optimization for tone reservation based PAPR reduction algorithms". In *Personal, Indoor, and Mobile Radio Communication (PIMRC), 2014 IEEE 25th Annual International Symposium on*, pages 97–102. IEEE, 2014.
- [C.31] Jean-Christophe Sibel, [Matthieu Cruss iere](#), and Jean-Fran ois H elard. "Modeling BP decoding error events with the LDPC codes of the DVB-S2 standard". In *Personal, Indoor, and Mobile Radio Communication (PIMRC), 2014 IEEE 25th Annual International Symposium on*, pages 902–907. IEEE, 2014.
- [C.32] Jean-Christophe Pr evotet, Yvan Kokar, Maryline H elard, and [Matthieu Cruss iere](#). "Implementation of a time relevel MISO OFDM test-bed". In *Wireless World Research Forum*, 2014.
- [C.33] Samar Sindian, Ayman Khalil, Abed Ellatif Samhat, [Matthieu Cruss iere](#), and Jean-Fran ois H elard. "Admission control and resource allocation in IEEE 802.15.5 HDR WPAN". In *Network of the Future (NOF), 2014 International Conference and Workshop on the*, pages 1–2. IEEE, 2014.
- [C.34] Samar Sindian, Ayman Khalil, Abed Ellatif Samhat, [Matthieu Cruss iere](#), and Jean-Fran ois H elard. "Resource allocation with differentiation between RT and NRT traffic in IEEE 802.15. 5". In *Mediterranean Electrotechnical Conference (MELECON), 2014 17th IEEE*, pages 39–44. IEEE, 2014.
- [C.35] Ming Liu, Jean-Fran ois H elard, [Matthieu Cruss iere](#), and Maryline H elard. "Cooperative distributed MIMO broadcasting : a promising solution to the 'mobile data tsunami' in 2020". In *Wireless World Research Forum WWRF# 31*, 2013.
- [C.36] Nicolas Cornillet, [Matthieu Cruss iere](#), and Jean-Fran ois H elard. "Optimization of the energy efficiency of a hybrid broadcast/unicast network". In *Wireless Communications and Networking Conference Workshops (WCNCW), 2013 IEEE*, pages 39–44. IEEE, 2013.
- [C.37] Hua Fu, [Matthieu Cruss iere](#), and Maryline H elard. "Spectral efficiency optimization in overlapping channels using TR-MISO systems". In *Wireless Communications and Networking Conference (WCNC), 2013 IEEE*, pages 3770–3775. IEEE, 2013.

- [C.38] Ming Liu, Jean-François Hélard, Matthieu Crussiere, and Maryline Hélard. "Reduced-complexity maximum-likelihood decoding for 3D MIMO code". In *Wireless Communications and Networking Conference (WCNC), 2013 IEEE*, pages 4015–4020. IEEE, 2013.
- [C.39] Imad Jamil, Samar Sindian, Ayman Khalil, [Matthieu Crussière](#), and Jean-François Hélard. "A new distributed decision making scheme for the IEEE 802.15.3 parent/child model". In *Communications and Information Technology (ICCIT), 2013 Third International Conference on*, pages 256–261. IEEE, 2013.
- [C.40] Samar Sindian, Abed Ellatif Samhat, Ayman Khalil, [Matthieu Crussière](#), and Jean-François Hélard. "Dynamic superframe size-based admission control in parent/child HR WPANs". In *Communications and Information Technology (ICCIT), 2013 Third International Conference on*, pages 314–319. IEEE, 2013.
- [C.41] Ming Liu, [Matthieu Crussière](#), Maryline Hélard, and Jean-François Hélard. "Distributed MIMO schemes for the future digital video broadcasting". In *Telecommunications (ICT), 2013 20th International Conference on*, pages 1–5. IEEE, 2013.
- [C.42] Ming Liu, Maryline Hélard, Jean-François Hélard, and [Matthieu Crussière](#). "A fast decodable full-rate STBC with high coding gain for 4×2 mimo systems". In *Personal Indoor and Mobile Radio Communications (PIMRC), 2013 IEEE 24th International Symposium on*, pages 677–681. IEEE, 2013.
- [C.43] Thierry Dubois, Maryline Hélard, [Matthieu Crussière](#), and Issam Maaz. "Time reversal applied to large MISO-OFDM systems". In *Personal Indoor and Mobile Radio Communications (PIMRC), 2013 IEEE 24th International Symposium on*, pages 896–901. IEEE, 2013.
- [C.44] Thierry Dubois, Maryline Hélard, and [Matthieu Crussière](#). "Time reversal in a MISO-OFDM system : Guard interval design, dimensioning and synchronisation aspects". In *WWRF29*, 2012.
- [C.45] Nicolas Cornillet, [Matthieu Crussière](#), and Jean-François Hélard. "On the hybrid use of unicast/broadcast networks under energy criterion". In *Personal Indoor and Mobile Radio Communications (PIMRC), 2012 IEEE 23rd International Symposium on*, pages 1256–1261. IEEE, 2012.
- [C.46] Ming Liu, [Matthieu Crussière](#), Maryline Hélard, Jean-François Hélard, and Youssef Nasser. "Enhanced mobile digital video broadcasting with distributed space-time coding". In *Communications (ICC), 2012 IEEE International Conference on*, pages 6971–6976. IEEE, 2012.
- [C.47] Ming Liu, Matthieu Crussiere, and Jean-François Hélard. "Improved channel estimation methods based on PN sequence for TDS-OFDM". In *Telecommunications (ICT), 2012 19th International Conference on*, pages 1–5. IEEE, 2012.
- [C.48] Roua Youssef, Maryline Hélard, [Matthieu Crussière](#), and Jean-François Hélard. "Effect of relaying on coverage in realistic deployment scenarios". In *Telecommunications (ICT), 2012 19th International Conference on*, pages 1–5. IEEE, 2012.
- [C.49] Ayman Khalil, [Matthieu Crussière](#), and Jean-François Hélard. "Spectrum sharing optimization model for OFDMA systems under joint time and frequency constraints". In *Telecommunications (ICT), 2012 19th International Conference on*, pages 1–5. IEEE, 2012.
- [C.50] Ayman Khalil, [Matthieu Crussière](#), and Jean-François Hélard. "Spectrum sharing optimization model for multiuser linear-precoded OFDM UWB systems". In *Wireless Communications and Networking Conference (WCNC), 2012 IEEE*, pages 1467–1472. IEEE, 2012.
- [C.51] Nicolas Cornillet, [Matthieu Crussière](#), and Jean-François Hélard. "Performance of the DVB-T2 system in a single frequency network : Analysis of the distributed alamouti scheme". In *Broadband Multimedia Systems and Broadcasting (BMSB), 2011 IEEE International Symposium on*, pages 1–4. IEEE, 2011.
- [C.52] Roua Youssef, Maryline Hélard, [Matthieu Crussière](#), and Jean-François Hélard. "Distributed coding for OFDM-based transmission in cooperative broadcast networks". In *Cross Layer Design (IWCLD), 2011 Third International Workshop on*, pages 1–5. IEEE, 2011.
- [C.53] Ayman Khalil, Rana Diab, [Matthieu Crussière](#), and Jean-François Hélard. "time-frequency resource allocation optimization model for OFDMA systems". In *Cross Layer Design (IWCLD), 2011 Third International Workshop on*, pages 1–5. IEEE, 2011.
- [C.54] Thierry Dubois, [Matthieu Crussière](#), and Maryline Hélard. "On the use of time reversal for digital communications with non-impulsive waveforms". In *Signal Processing and Communication Systems (ICSPCS), 2010 4th International Conference on*, pages 1–6. IEEE, 2010.

Bibliographie

- [C.55] Ayman Khalil, [Matthieu Crussière](#), and Jean-François Hélard. "Interference-aware prioritized spectrum scheduling for MB-OFDM systems". In *Personal Indoor and Mobile Radio Communications (PIMRC), 2010 IEEE 21st International Symposium on*, pages 1242–1247. IEEE, 2010.
- [C.56] Karima Ragoubi, Maryline Hélard, and [Matthieu Crussière](#). "Low complexity channel shortening technique applied to MB-OFDM UWB systems". In *Signal Processing and Communication Systems (ICSPCS), 2010 4th International Conference on*, pages 1–6. IEEE, 2010.
- [C.57] Ming Liu, [Matthieu Crussière](#), and Jean-François Hélard. "Enhanced two-dimensional data-aided channel estimation for TDS-OFDM". In *Signal Processing and Communication Systems (ICSPCS), 2010 4th International Conference on*, pages 1–7. IEEE, 2010.
- [C.58] Ayman Khalil, [Matthieu Crussière](#), and Jean-François Hélard. "Distributed coexistence-aware channel allocation for future unlicensed high-rate WPAN". In *Signal Processing and Communication Systems (ICSPCS), 2010 4th International Conference on*, pages 1–7. IEEE, 2010.
- [C.59] Hassan Ali-Ahmad, Ayman Khalil, [Matthieu Crussière](#), and Jean-François Hélard. "A joint distributed resource management and scheduling scheme for future UWB-based high-rate WPAN". In *Signal Processing and Communication Systems (ICSPCS), 2010 4th International Conference on*, pages 1–8. IEEE, 2010.
- [C.60] Karima Ragoubi, Maryline Hélard, and [Matthieu Crussière](#). "Channel shortening for bit rate maximization in DMT communication systems". In *Vehicular Technology Conference Fall (VTC 2010-Fall), 2010 IEEE 72nd*, pages 1–5. IEEE, 2010.
- [C.61] Iulia Ivan, Philippe Besnier, Xavier Bunlon, Loïs Le Danvic, [Matthieu Crussière](#), and M'hamed Drissi. "Influence of propagation channel modeling on V2X physical layer performance". In *Antennas and Propagation (EuCAP), 2010 Proceedings of the Fourth European Conference on*, pages 1–5. IEEE, 2010.
- [C.62] Ming Liu, [Matthieu Crussière](#), and Jean-François Hélard. "A combined time and frequency algorithm for improved channel estimation in TDS-OFDM". In *Communications (ICC), 2010 IEEE International Conference on*, pages 1–6. IEEE, 2010.
- [C.63] Ayman Khalil, [Matthieu Crussière](#), and Jean-François Hélard. "Multiuser service differentiated spectrum allocation scheme for high rate UWB systems". In *Wireless Communications and Networking Conference (WCNC), 2010 IEEE*, pages 1–6. IEEE, 2010.
- [C.64] Iulia Ivan, Philippe Besnier, [Matthieu Crussière](#), M'hamed Drissi, Loïs Le Danvic, Mickael Huard, and Eric Lardjane. "Physical layer performance analysis of V2V communications in high velocity context". In *Intelligent Transport Systems Telecommunications (ITST), 2009 9th International Conference on*, pages 409–414. IEEE, 2009.
- [C.65] Ayman Khalil, [Matthieu Crussière](#), and Jean-François Hélard. "Differentiated multiuser resource allocation scheme for multi-band UWB systems". In *Signal Processing Advances in Wireless Communications, 2009. SPAWC'09. IEEE 10th Workshop on*, pages 707–711. IEEE, 2009.
- [C.66] Ayman Khalil, [Matthieu Crussière](#), and Jean-François Hélard. "Dynamic cross-layer spectrum allocation for multi-band high-rate UWB systems". In *Multi-Carrier Systems & Solutions 2009*, pages 355–364. Springer Netherlands, 2009.
- [C.67] Oudomsack Pierre Pasquero, Youssef Nasser, [Matthieu Crussière](#), and Jean-François Hélard. "A joint channel and carrier frequency offset estimation based on spread pilot for future broadcasting systems". In *Multi-Carrier Systems & Solutions 2009*, pages 153–161. Springer Netherlands, 2009.
- [C.68] Oudomsack Pierre Pasquero, [Matthieu Crussière](#), Youssef Nasser, and Jean-François Hélard. "Efficient space code block code mimo channel estimation for future mobile video broadcasting". In *Wireless Communications and Networking Conference, 2009. WCNC 2009. IEEE*, pages 1–6. IEEE, 2009.
- [C.69] Oudomsack Pierre Pasquero, Eddy Chollet, [Matthieu Crussière](#), and Jean-François Hélard. "efficient spread pilot based synchronization method for linear precoded ofdm systems". In *Vehicular Technology Conference Fall (VTC 2009-Fall), 2009 IEEE 70th*, pages 1–5. IEEE, 2009.
- [C.70] Ayman Khalil, [Matthieu Crussière](#), and Jean-François Hélard. "Cross-layer resource allocation scheme for multi-band high rate UWB systems". In *Proceedings of the 2009 International Conference on Wireless Communications and Mobile Computing : Connecting the World Wirelessly*, pages 314–319. ACM, 2009.

- [C.71] Ming Liu, [Matthieu Crussière](#), and Jean-François H elard. "A novel iterative data-aided channel estimation for time domain synchronous OFDM". In *Signal Design and its Applications in Communications, 2009. IWSDA'09. Fourth International Workshop on*, pages 48–51. IEEE, 2009.
- [C.72] Ayman Khalil, [Matthieu Crussière](#), and Jean-François H elard. "Spectrum allocation optimization scheme for heterogeneous multiuser UWB systems". In *Cross Layer Design, 2009. IWCLD'09. Second International Workshop on*, pages 1–6. IEEE, 2009.
- [C.73] Ayman Khalil, Antoine Stephan, [Matthieu Crussière](#), and Jean-François H elard. "Multi-user cross-layer allocation design for LP-OFDM high data rate UWB systems". In *Wireless Communication Systems. 2008. ISWCS'08. IEEE International Symposium on*, pages 6–10. IEEE, 2008.
- [C.74] Fahad Syed Muhammad, Jean-Yves Baudais, Jean-François H elard, and [Matthieu Crussière](#). "A coded bit-loading linear precoded discrete multitone solution for power line communication". In *Signal Processing Advances in Wireless Communications, 2008. SPAWC 2008. IEEE 9th Workshop on*, pages 555–559. IEEE, 2008.
- [C.75] Fahad Syed Muhammad, Jean-Yves Baudais, Jean-François H elard, and [Matthieu Crussière](#). "Coded adaptive linear precoded discrete multitone over PLC channel". In *Power Line Communications and Its Applications, 2008. ISPLC 2008. IEEE International Symposium on*, pages 123–128. IEEE, 2008.
- [C.76] Oudomsack Pierre Pasquero, [Matthieu Crussière](#), Youssef Nasser, and Jean-François H elard. "2D linear precoded OFDM for future mobile digital video broadcasting". In *Signal Processing Advances in Wireless Communications, 2008. SPAWC 2008. IEEE 9th Workshop on*, pages 476–480. IEEE, 2008.
- [C.77] Youssef Nasser, Jean-François H elard, and [Matthieu Crussière](#). "Robustness of MIMO-OFDM schemes for future digital TV to carrier frequency offset". In *Broadband Multimedia Systems and Broadcasting, 2008 IEEE International Symposium on*, pages 1–4. IEEE, 2008.
- [C.78] Youssef Nasser, Jean-François H elard, and [Matthieu Crussière](#). "Bit error rate prediction of coded MIMO-OFDM systems". In *Signal Processing Advances in Wireless Communications, 2008. SPAWC 2008. IEEE 9th Workshop on*, pages 181–185. IEEE, 2008.
- [C.79] Oudomsack Pierre Pasquero, [Matthieu Crussière](#), Youssef Nasser, and Jean-François H elard. "A novel channel estimation based on spread pilots for terrestrial digital video broadcasting". In *Broadband Multimedia Systems and Broadcasting, 2008 IEEE International Symposium on*, pages 1–4. IEEE, 2008.
- [C.80] Ming Liu, [Matthieu Crussière](#), Jean-François H elard, and Oudomsack Pierre Pasquero. "Analysis and performance comparison of DVB-T and DTMB systems for terrestrial digital TV". In *Communication Systems, 2008. ICCS 2008. 11th IEEE Singapore International Conference on*, pages 1399–1404. IEEE, 2008.
- [C.81] Youssef Nasser, J-F H elard, [Matthieu Crussière](#), and Oudomsack Pasquero. "Efficient 3D space time space block code for future terrestrial digital TV". In *Signal Processing Advances in Wireless Communications, 2008. SPAWC 2008. IEEE 9th Workshop on*, pages 406–410. IEEE, 2008.
- [C.82] Youssef Nasser, Jean-François H elard, and [Matthieu Crussière](#). "On the influence of carrier frequency offset and sampling frequency offset in MIMO-OFDM systems for future digital TV". In *Wireless Pervasive Computing, 2008. ISWPC 2008. 3rd International Symposium on*, pages 93–96. IEEE, 2008.
- [C.83] Youssef Nasser, Jean-Fra  H elard, [Matthieu Crussière](#), and Oudomsack Pasquero. "Efficient MIMO-OFDM schemes for future terrestrial digital TV with unequal received powers". In *Communications, 2008. ICC'08. IEEE International Conference on*, pages 2021–2027. IEEE, 2008.
- [C.84] Jean-François H elard and [Matthieu Crussière](#). "Bit error rate prediction of coded MIMO-OFDM systems". In *IEEE Symposium on Signal Processing Advances in Wireless Communications*, page 5, 2008.
- [C.85] Jean-François H elard, [Matthieu Crussière](#), and Oudomsack Pierre Pasquero. "Efficient 3D space time space block code for future terrestrial digital TV". In *Symposium on Signal Processing Advances in Wireless Communications*, page 5, 2008.
- [C.86] Emeric Gu g en, [Matthieu Crussière](#), and Jean-François H elard. "An OFDM-CDMA scheme for high data rate UWB applications". In *Vehicular Technology Conference, 2007. VTC2007-Spring. IEEE 65th*, pages 2905–2909. IEEE, 2007.

Bibliographie

- [C.87] Emeric Guéguen, [Matthieu Crussière](#), and Jean-François Hérald. "Combination of OFDM and spread spectrum for high data rate UWB : optimization of the spreading length". In *Ultra-Wideband, 2007. ICUWB 2007. IEEE International Conference on*, pages 889–894. IEEE, 2007.
- [C.88] [Matthieu Crussière](#), Jean-yves Baudais, and Jean-françois Hérald. "Improved throughput over wirelines with adaptive MC-DS-CDMA". In *Spread Spectrum Techniques and Applications, 2006 IEEE Ninth International Symposium on*, pages 143–147. IEEE, 2006.
- [C.89] [Matthieu Crussière](#), Jean-Yves Baudais, and Jean-François Hérald. "Adaptive linear precoded DMT as an efficient resource allocation scheme for power-line communications". In *Global Telecommunications Conference, 2006. GLOBECOM'06. IEEE*, pages 1–5,. IEEE, 2006.
- [C.90] [Matthieu Crussière](#), Jean-Yves Baudais, and Jean-François Hérald. "New loading algorithms for adaptive SS-MC-MA systems over power line channels : Comparisons with DMT". *Multi-Carrier Spread-Spectrum*, pages 327–336, 2006.
- [C.91] [Matthieu Crussière](#), Jean-Yves Baudais, and Jean-François Hérald. "Robust and high-bit rate communications over PLC channels : a bit-loading multi-carrier spread-spectrum solution". In *Power Line Communications and Its Applications, 2005 International Symposium on*, pages 37–41. IEEE, 2005.
- [C.92] [Matthieu Crussière](#), Jean-Yves Baudais, and Jean-François Hérald. "A novel joint and iterative scheme for synchronization and channel estimation in MC-CDMA power line communications". In *Vehicular Technology Conference, 2004. VTC2004-Fall. 2004 IEEE 60th*, volume 3, pages 1723–1727. IEEE, 2004.
- [C.93] [Matthieu Crussière](#), Jean-Yves Baudais, and Jean-François Hérald. "New iterative time and frequency synchronization scheme for MC-CDMA systems over power line channels". In *Spread Spectrum Techniques and Applications, 2004 IEEE Eighth International Symposium on*, pages 315–319. IEEE, 2004.
- [C.94] [Matthieu Crussière](#), Jean-Marie Auffray, and Jean-François Hérald. "Comparison of STTCM over slow and fast rayleigh fading channels". In *Signal Processing Advances in Wireless Communications, 2003. SPAWC 2003. 4th IEEE Workshop on*, pages 249–253. IEEE, 2003.

► Conférences nationales

- [N.1] Ali Cheaito, Jean-François Hérald, Yves Louët, and [Matthieu Crussière](#). "expression analytique du spectre pour les signaux multiporteuses : Impact conjoint des non-linéarités de l'amplificateur de puissance et de la fonction de prédistorsion". In *GRETSI 2017*, 2015.
- [N.2] Pape Abdoulaye Fam, Stéphane Paquelet, [Matthieu Crussière](#), Jean-François Hérald, and Pierre Brétilon. "On the energy efficiency of hybrid unicast-broadcast networks for mobile TV services". In *Journée Scientifique URSI-France 2016 Energie et Radiosciences*, 2016.
- [N.3] Ali Cheaito, [Matthieu Crussière](#), Yves Louët, and Jean-François Hérald. "Expression analytique de l'EVM pour les signaux multiporteuses : Impact conjoint des non-linéarités de l'amplificateur de puissance et de la fonction de prédistorsion". In *GRETSI 2015*, 2015.
- [N.4] Elias Najjar, Ayman Khalil, [Matthieu Crussière](#), and Jean-François Hérald. Allocation dynamique de ressource dans les systèmes ULB sous contrainte de qualité de service. In *Conférence MajeSTIC 2009*, pages 1–5, 2009.
- [N.5] Jean-Yves Baudais and [Matthieu Crussière](#). "Allocation MC-CDMA : augmentation des débits sur les lignes de transmission". In *20e colloque GRETSI sur le traitement du signal et des images*, pages 735–738, 2005.
- [N.6] [Matthieu Crussière](#), Jean-Yves Baudais, and Jean-François Hérald. "Vers la transmission de données haut-débit par courant porteur en ligne". In *Journées thématiques TIC-CITE*, pages 423–432, 2003.

► Brevets

- [P.1] [Matthieu Crussière](#), Thierry Dubois, Maryline Hérald, and Dinh-Thuy Phan Huy. "Procédé et dispositif de communication radio pour antennes d'utilisateur multiples / radio communication method and device for multiple user antennas". Technical report, Orange Labs, Brevet français publié le 26.04.2012 (N° FR1058688) / Brevet US publié le 28 juin 2016 (Patent 9,379,797).

- [P.2] [Matthieu Crussière](#), Jean-François H elard, Rapha Mounzer, and Youssef Nasser. "Proc ed e et dispositif de transmission d'un signal multiporteuse, programme et signal correspondants". Technical report, INSA de Rennes, Brevet fran ais d epos e le 07.05.2015 (N  FR1554085).
- [P.3] Jean-Fran ois H elard, Maryline H elard, [Matthieu Crussière](#), and Roua Youssef. "Proc ed e d' mission coop erative, signal, entit  source, entit  relais, proc ed e de r ception, entit  destinataire, syst me et programme d'ordinateur correspondants / method of cooperative emission, signal, source entity, relay entity, method of reception, destination entity, system and computer program corresponding". Technical report, INSA de Rennes, Brevet fran ais publi e le 06.03.2014 (N  FR1258203) / Brevet US publi e le 3 sept. 2013 (Patent App. 14/425,555).
- [P.4] Maryline H elard, [Matthieu Crussière](#), and Karima Ragoubi. "Proc ed e de r duction de longueur de canal, filtre et signal correspondants/method for reducing channel length and corresponding filter and signal". Technical report, INSA de Rennes, Brevet fran ais publi e le 1 mars 2010 (N  FR1050656) / Brevet US Patent publi e le 2 juin 2015 (Patent App. 9,048,916).

► **Chapitres d'ouvrage**

- [B.1] Jean-Yves Baudais and [Matthieu Crussière](#). "*MIMO Powerline Communications : Narrow and Broad-band Standards, EMC, and Advanced Processing*", chapter 18 : 'Linear Precoding for Multicarrier and Multicast PLC', pages 493–530. CRC Press, 2014. ISBN : 978-146-6557-52-9.
- [B.2] Christian Gallard, Jean-Luc Sicre, [Matthieu Crussière](#), Catherine Douillard, and G erard Faria. "*Next Generation Mobile Broadcasting*", chapter 9 : 'Universal DVB-3GPP Broadcast Layer, an Enabler for new Business in Mobile Broadcasting Landscape', pages 253–291. CRC Press, 2013. ISBN : 978-143-9898-66-6.
- [B.3] Ayman Khalil, [Matthieu Crussière](#), and Jean-Fran ois H elard. "*Ultra Wideband Communications : Novel Trends-System, Architecture and Implementation*", chapter 14 : 'Cross-layer resource allocation for MB-OFDM UWB systems', pages 125–144. InTech, 2011. ISBN : 978-953-307-461-0.
- [B.4] Oudomsack Pierre Pasquero, [Matthieu Crussière](#), Youssef Nasser, Eddy Cholet, and Jean-Fran ois H elard. "*Digital Video*", chapter 7 : 'A new waveform based on linear precoded multicarrier modulation for future digital video broadcasting systems', pages 125–144. InTech, 2010. ISBN : 978-953-7619-70-1.

Partie



Synthesis of the Research Works

This second part of the manuscript provides the detailed description of my research activities from the beginning of my carrier. A particular classification of the work is proposed and explicitated to highlight the main fields of application I have been addressing during the last ten years. A first chapter presents the spirit of this classification and gives a broad view on the research programs I have co-supervised. The following three chapters focus on the main contributions within each of the identified fields of research. Finally, the last chapter of this part provides a structured view of the future envisaged studies. The whole of this part is written in english to give a more international scope to the document.

Outline

Chapter 5 : <i>Overview and classification of the research activities</i>	p.39
Chapter 6 : <i>Optimization of wireless broadcast transmissions</i>	p.43
Chapter 7 : <i>Optimization of the wireless broadband access</i>	p.75
Chapter 8 : <i>Broadband / Broadcast convergence studies</i>	p.113
Chapter 9 : <i>Research perspectives</i>	p.135

Overview of the Research Activities

Chap. 5

*Highly organized research
is guaranteed to produce nothing new.*

– Frank Herbert –

1 CLASSIFICATION

When starting writing such an activity overview document, one of the first question which quickly comes to mind of any researcher is undoubtedly : “what is the common denominator which is giving a sense to my work?”. Everyone knows that the answer to such a question is not so simple to give, honestly. As any researcher, I have been conditioned by my 3 years of PhD work. As many young assistant professor, I have been working (with pleasure) during my first years on subjects which main directions were essentially proposed or driven by the Professors who gave me the chance to work with. As any researchers, I have been influenced by my readings, my encounters with others during conferences, workshops and project meetings. But also, as any researcher, I have worked on subjects which could be funded. As such, finding a purely homogeneous common thread exhaustively linking all the contributions of several years research is almost impossible, and even undesirable unless yielding a very large but possibly unclear or fuzzy picture of the work.

Then comes the more appropriate possibility of research activity classification, which amounts to find several themes in the research, gathering close works into a given topic. However the question arises as to which kind of classification : “should the contributions be sorted by fields of application? by the used methodologies? by the exploited theoretical tools? or even chronologically?”. A unique classification is definitely not possible, and a given classification choice may have the inconvenients of another classification advantages and vice-versa. However, research activities classification should at least allow to highlight relationships between several studies thereby helping quickly perceiving the specificities of the research work.

From the above considerations, I have eventually chosen not to be exhaustive in the detailed description of my research activities. From a broad view, my research studies take place at the level of signal processing and system optimization applied to communication networks. To provide a more accurate description, I have selected the most representative contributions, organized in the following three main themes :

1. Wireless broadcast transmissions
2. Wireless broadband access
3. Broadcast/broadband convergent networks

Such a classification can be regarded as “application” kind but also implicitly allows differentiating between various problem statements, tools and methods used in each category.

The first theme on broadcast systems takes as a basic constraint that such systems sustain unidirectional downlink transmission without any knowledge or feedback from the receiver ends. Such systems can be viewed as “point-to-area” systems. The main related problematics we have addressed are then at the level of waveform optimization for diversity exploitation and energy efficiency.

The second theme on wireless access deals with adaptive systems able to embed flexible mechanisms due to the existence of feedback capability (partial or not) from the end terminals. Such systems are typically centralized

“point-to-multipoint” systems. The main studies we have led are the design of multiple access schemes and the optimization of radio resource management between users.

The third theme consists in system level rather than physical layer investigations, however taking basis on the radio system design potentially provided by the latter two themes. In this area of research, a major concern is the research for accurate models accounting for the joint usage of “heterogeneous radio technologies”. In our studies, we have specifically been interested in modeling hybrid networks made of dual broadcast/unicast modes and deriving the related performance metrics.

From 2007, I have progressively structured the major part of my research activities according to such a classification. In the following sections, a chronological overview of each topic is given while a more detailed scientific description is given in the following chapters upon selecting contributions.

2 OVERVIEW OF THE STUDIES

2.1 WIRELESS BROADCAST TRANSMISSIONS

► Synchronization and channel Estimation for next generation digital TV [2007-2011]

Our studies on broadcast systems started with our involvement in a large european Celtic project at the end of 2006 named B21C. At that time, the second version of the digital video broadcasting standard for terrestrial digital television (DVB-T2) had just been released. New investigations were needed in the perspective of the next generation for hand-held reception (DVB-NGH). Through the work of Pr. J.F. H elard, our research team was historically well recognized for its expertise in OFDM systems and MIMO systems which were central issues to address for DVB-NGH. We hence launched a PhD program (P.O. Pasquero) aiming at proposing novel robust and flexible synchronization and channel estimation algorithms for portable and mobile reception based on OFDM waveform combined with spread-spectrum techniques. We for instance proposed the concept of spread pilots, and showed its advantage in terms of flexibility and robustness in mobility scenarios.

Almost in parallel to this work, we built a regional project (MobileTVWorld) with industrial partners focusing on the optimization of mobile receivers for the chinese digital television standard (DTM-B). With this project, we launched a new PhD (M. Liu) to work on channel estimation aspects in the particular case of the TDS-OFDM (time-domain-synchronous OFDM) waveform used in the DTM-B standard. We especially proposed an original time-frequency turbo approach allowing for improved robustness against high mobility and long echoes, hereby solving one of the main limitation of the TDS-OFDM waveform. I incorporated in Appendix 3 the transaction paper we wrote to summarize our work on this topic.

► Space-time coding for broadcast networks [2009-2013]

In the same context as previously exposed, we also started new investigations on the potential upgrade of broadcast system with multiantenna capabilities. Our main concern was the design of new space-time codes well suited for single frequency network deployments which are typical of broadcast networks. This work was led during the second part of the PhD program of P.O Pasquero around and went on with two post-docs in the framework of the ENGINE Celtic project from 2009 to 2012 and partly of the MCube ANR project from 2010 to 2013. A major output of our works, further detailed in Chap. 6, was the proposal of various double-layer space-time codes robust to power imbalance coming from distant broadcast transmitters. We proposed various versions of such novel codes taking joint advantage of full-rank space-time codes such as Golden codes for intra-cell coding and orthogonal codes such as Alamouti code for inter-site coding. We also worked on simplified quasi-ML decoding strategies to optimized matrix code structures for moderate complexity receivers. I got the opportunity, as a responsible of the MIMO task force of the B21C project to expose the results of our work during a technical meeting of the DVB consortium in 2009.

► Energy efficiency of broadcast transmitters [2011-2017]

After the works achieved during the B21C and ENGINES projects, we decided to investigate an old but however not solved issue of OFDM systems, that is PAPR reduction. Indeed, the DVB-T2 standard turns out

2. Overview of the studies

to be the first standard enabling PAPR reduction through the reservation of dedicated subcarriers. However, no commercial use of such possibility was made due to poor performance and high complexity of the existing algorithms. Hence, in 2012 we launched a new study with the regional PAPRICA project on such topic. During the PhD of R. Mounzer which was launched in collaboration with Dr. Y. Nasser from the American University of Beirut (AUB) in Lebanon, we namely proposed new algorithms, one of which being patented and offering the best performance/complexity trade-off compared to the existing algorithms of the literature. This work was recently pursued with a new project (GreenTEA) which aim is to further optimize our algorithms in the perspective of an implementation in commercial products. A more deep description of this work is proposed in Chap. 6.

With our investigations about PAPR reduction optimization, we came up with new research ideas on the wide subject of power efficiency of high power transmitters. Indeed, from a theoretical point of view, no tools are available to accurately predict the performance of a transmission system equipped with a non-linear amplifier and some algorithms fighting against such non-linearities, such as PAPR reduction or predistortion functions. In 2013, we thus took the opportunity of the CominLabs LABEX in Rennes to participate to a project proposal dedicated to energy efficiency optimization in communication networks. We could then fund a PhD program (A. Cheaito) dedicated to the derivation of theoretical energy efficiency performance metrics. Many new closed-forms have been proposed as detailed in Chap. 6. A new PhD program starting in October 2017 is expected to push further the theoretical models we started to develop. This aspect will be developed as perspectives in Chap. 9.

2.2 WIRELESS BROADBAND ACCESS

This area of research is historically the one around which the SYSCOM research team developed its activities and expertise from its creation in the late 1990s. At that time, the central topic of interest driven by Pr. J.F. H elard, was the optimization of waveforms for spectral efficiency optimization and multiple access purpose, first using combined OFDM and CDMA techniques, and then extending them to space-time coding schemes. In particular, such expertise allowed the team to be involved in major European projects from 2002 to 2006 dealing with 4G and beyond 4G cellular system optimization such as the FP5-IST MATRICE and FP6-IST 4MORE project. During that period, I was myself leading my PhD work in the team on the optimization of spread-spectrum OFDM systems, but rather developing resource allocation mechanisms for wired transmission systems, namely Power Line Communications.

► **Waveform design and resource allocation for wireless personal area networks [2007-2014]**

As I joined the laboratory and the SYSCOM team as an assistant professor in 2007, I was already well integrated into the team and right in line with research activities. I could therefore rapidly take part in the supervising of PhD students. My first major involvements consisted in contributing to the set up of a new European FP7-IST project (OMEGA), dealing with the optimization of domestic networks based on multi-technology radio access. In parallel to this project, we also led system optimization studies for WPAN in collaboration with Orange Labs (Rennes). In this framework, I partly extended the work of my PhD on resource allocation optimization, however in the context of ultra-wide band communications applied to WPAN. Two PhD students, namely E. Gueguen and A. Khalil, were contributing to this study, at a pure physical layer level for the former and developing cross-layer resource allocation algorithms for the latter. With the work of E. Gueguen, we first proposed to incorporate a linear precoding component to the Multi-band OFDM physical layer of the IEEE 802.15.3a specifications. We hereby proved the advantage of the LP-OFDM (linear-precoded OFDM) solution in the WPAN context. With A. Khalil, we proposed various cross-layer allocation strategies and optimization problems aiming at judiciously assigning sub-bands to users, depending on QoS and priority indicators. A journal paper presenting our main results in this subject is available in Appendix 3. This work was then followed with a PhD program (S. Sindian) set up in collaboration with the International University of Lebanon (IUL). In this study, we extended the work of A. Khalil to integrate multi-hop capabilities of the 802.15.5a specifications for mesh WPAN.

► **Spatial filtering and beamforming strategies for multi-antenna systems [2009-2017]**

This topic of research started around 2009 as an evolution of the previous studies on multi-antenna systems in the team, however addressing the topic with the angle of spatial dimension multiple access (SDMA) relying on

closed (or almost closed) loop MIMO systems. The rising interest in the scientific community for such idea even in cellular systems in which channel knowledge at the transmitter is hard to guarantee, was promising numerous new investigations and theoretical studies.

Hence, Pr. M. H elard and me initiated a new research project, first starting with a Master Intership and then with the PhD program of T. Dubois. Our first studies were dedicated to time-reversal filters which can be viewed as the core foundation or basis of spatial filtering and beamforming schemes, as further explained in Chap. 7. We experimented time-reversal concepts applied to wireless communications and worked on the derivation of the theoretical performance of OFDM systems, mainly in single user scenarios. We thereby highlighted the frequency/spatial duality and green nature for such systems as more detailed in Chap. 7. This work was first funded through a collaborative work with Orange Labs (Issy-les-Moulineaux) and then pursued in the framework of the ANR Trimaran project from 2011 to 2014.

Encouraged by our first results, we also started a new PhD (H. FU) thanks to a ministerial grant obtained in 2011. In this study, we extended our work in the multiuser context and to other spatial filtering schemes, working on theoretical system capacity and bit error rate closed-form derivations. At that period was emerging the famous Massive MIMO paradigm, introduced by T. Marzetta around 2010, which can be easily connected with our investigations on time-reversal (see Chap. 7). In the PhD work of H. FU, we however chose to address realistic multiantenna system topologies with a reasonable number of antennas (hence not massive).

The raise of the number of antennas in our models came with the PhD of A. Roz e which started in 2013 in the framework of the launch of the IRT-Bcom in Rennes. Massive MIMO was identified within the IRT as a priority subject in the perspective of the future 5G system elaboration, which allowed us to initiate collaborations. By virtue of the win-win strategy of deploying massive MIMO systems at higher frequency bands than conventional ones, we focused our studies on mm-wave transmissions. We then proposed spatial filters and interference mitigation mechanisms more suited to such frequency bands, namely taking advantage of the quasi-stable angular structure of the propagation channels. All the work achieved in this field of research have actually opened the door to many new subjects for future investigations as further detailed in Chap. 9.

2.3

BROADCAST/BROADBAND CONVERGENT NETWORKS [2010 – 2017]

Around 2010 started to emerged the first views of what could be the future 5th generation wireless communication systems. Among many trends, the idea of making existing network converge, or at least cooperate, was assumed of being one of the key evolution at the horizon 2020. After several projects in the field of broadcast system optimization, we found interesting to investigate in what extent a cooperation between broadcast and broadband networks could enable overall improvement in system efficiency. Hence we started such new investigations, first in the framework of the ANR MCube project which was set up in 2010 with the collaboration of broadcast and broadband network operators (Orange Labs, TDF) but also with chip manufacturers (DibCom). Our first study relied on a collaborative contribution with the project partners to define a unified physical layer for a common broadcast/broadband network operation (see Appendix 3). Complementary to that, we put efforts on the modeling and the performance evaluation of such hybrid network during the PhD of N. Cornillet. We derived first theoretical results in terms of statistical performance metrics. This work was then pursued with the PhD of P.A. Fam through a collaboration between TDF and IRT-Bcom. As detailed in 8, we derived closed-form expressions in terms of service capacity and energy efficiency leading to optimal operating regimes of the network. Such research field, relying on our expertise in both the broadcast and wireless access systems calls for many further investigations as exposed in our research perspectives in Chap. 9.

*To regard old problems from a new angle,
requires creative imagination
and marks real advance in science.*

– Albert Einstein –

Selected Topics

As discussed in the previous chapter, a first major field of application of my research activities is related to the improvement of the performance of broadcast systems. Among the complete set of my contributions related to broadcast systems, I have chosen to highlight in this chapter the following three aspects of the work :

1. MIMO schemes for broadcast networks
2. Practical PAPR reduction design
3. Theoretical efficiency analysis of high power transmitters

1 MIMO SCHEMES FOR BROADCAST SYSTEMS

1.1 MOTIVATIONS

Since its formalization by Foschini and Telatar in the late 90s [Fos96, Tel99], the Multiple Input Multiple Output (MIMO) paradigm has been the subject of numerous researches and have known impressive advances during two decades of theoretical and technological studies from academia and industry. During the first 10 years following the V-Blast spatial multiplexing scheme demonstrated at Bell Labs in 1996, studies on MIMO concepts were almost exclusively dedicated to the optimization of space-time coding schemes with the idea of getting as much as possible from the promised spatial multiplexing and diversity gains [TSC98, TJC99, Ala98]. As a result, first space-time block codes (STBC) have been quite rapidly adopted in some first communication standards before 2010 for WiFi applications (802.11.n) and cellular networks (3G-HSPA). In the meantime, broadcast technologies were placing greater emphasis on the integration of multicarrier waveforms, high order constellations, powerful channel coding schemes and flexible specifications for multiple scenario network deployments. At that time, it was not clear within the broadcast community whether adopting MIMO technology would be a good strategy, since multiple antenna concepts are more suited for mobile receivers. Yet, the deployments of hand-held DVB applications (DVB-H) had been suffering a serious setback for about 10 years.

In this context, we took part in 2007 in the set up of a very large European project (B21C - Broadcast for the 21st Century). At that time, the second version of the DVB-T standard was in discussion and new investigations were asked concerning mobile broadcasting. The B21C project was actually constituting a contribution task force to the reflections engaged by the DVB consortium in the perspective of two new DVB standard releases, namely DVB-T2 and DVB-NGH (Next Generation Hand-held). The work done in the framework of this project should give a support for the conclusions and decisions within DVB. The aim was to study all the technological modules

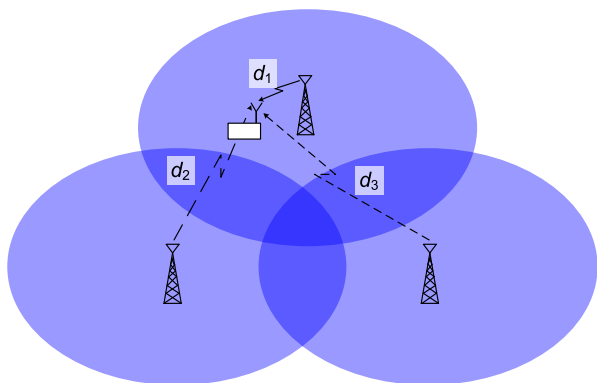


FIGURE 6.1– Single Frequency Network (SFN) area with three transmitters.

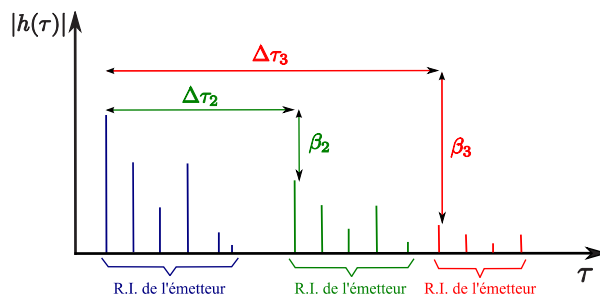


FIGURE 6.2– Composite channel impulse response in an SFN area with three transmitters.

which may compose a future system. Particularly, we were involved in the project to analyze the potential of MIMO schemes and propose new solutions adapted to broadcast scenarios. In the sequel, I present the problem we addressed and the solution we proposed. This work was initiated with the PhD of O.P. Pasquero and then pursued with two Post-Docs.

1.2 CAPACITY OF OFDM-MIMO SYSTEMS IN SFN

► Broadcast SFN

One major particularity of broadcast networks is the possibility to operate some specific coverage areas with several transmit towers using a unique frequency band. In such a case, a same signal is sent from several different transmitters at the same time on the same carrier frequency. This is the concept of signal frequency networks (SFN) which represents a spectrally efficient implementation of radio coverage. Operating an SFN in a broadcast transmission scenario is natively possible because the same signal is strictly transmitted from the different towers of the network. Theoretically, it however constraints the transmitters of a same SFN area to be tightly synchronized. If OFDM is used, synchronization constraints are somehow relaxed thanks to the guard interval commonly used to absorb the multipath effects of propagation channels. Let us for instance consider the SFN case of two transmitters, as represented in Fig. 6.1. The equivalent channel impulse response viewed by a receiver in the overall coverage area of the SFN is represented in Fig. 6.2. It is simply interpreted as the superposition of two independent impulse responses with some potentially different delays and gains. Hence, any OFDM receiver can accommodate such a channel response as soon as the used guard interval remains larger than the overall delay spread of such composite channel¹. When considering some MIMO upgrade of the network in the sequel, it is important to keep in mind the composite nature of the SFN channel.

► MIMO Capacity in SFN

From a system point of view, the SFN case implicitly poses the question of how to apply any space-time code across multiple antennas of the transmitters involved in the SFN area. As depicted in Fig. 6.3, one may think about a MIMO space-time code applied either at the level of the intra-cell antennas (co-localized STBC), or in a distributed fashion considering the inter-cell antennas (distributed STBC). Finally, a mixture of intra and inter-cell space-time code can also be envisaged. This idea, which we will refer to as 3D-MIMO, will be developed in the following section.

We addressed the capacity analysis question in [C.35] and provided some evaluation of the SFN system capacity for various MIMO configurations. The starting point of the evaluation was to restate the received signal taking into account the composite channel model and the way to exploit the MIMO channel, differentiating between the intra-cell and inter-cell channel links. In the general case of J transmission sites in the SFN area,

1. This means that the guard interval setting should strongly depend on the inter-site distance. For instance, in the 16K mode of DVB-T2, a guard interval of about 1.8 μs is used corresponding to an inter-site distance of about 133 km.

1. MIMO Schemes for Broadcast Systems

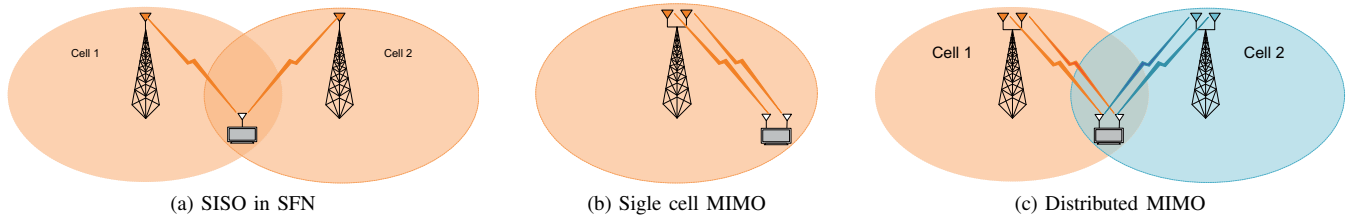


FIGURE 6.3– SISO and MIMO configurations and scenarios in an SFN.

each transmitter being equipped with N_T antennas and each receiver with N_R , we can write the received signal vector $\mathbf{Y}(k) \in \mathbb{C}^{N_R \times 1}$ on the k th subcarrier of the OFDM spectrum as,

$$\mathbf{Y}_k = \begin{bmatrix} \mathbf{H}_k^{(1)} & \cdots & \mathbf{H}_k^{(J)} \end{bmatrix} \begin{bmatrix} \Lambda^{(1)} \\ \vdots \\ \Lambda^{(J)} \end{bmatrix} \mathbf{X}_k \quad (6.1)$$

where $\mathbf{H}_k^{(j)}$ are the $N_R \times N_T$ channel matrices of flat fading coefficients for subcarrier k associated to each of the transmission sites, and $\Lambda^{(j)} = \sqrt{\lambda_j} \mathbf{I}_{N_T}$ are the power scale matrices taking into account the various levels of power associated to the signals received from different sites due to different propagation distances. Note that this system model considers a common signal $\mathbf{X}_k \in \mathbb{C}^{N_T \times 1}$ transmitted from each site, thus corresponding to the directly applying SFN concepts to MIMO signals.

We may rather take into consideration some distributed MIMO scheme, that is assuming that the transmitters collaborate and are responsible for the transmission of different information symbols. In that case, we have to rewrite Eq. (6.1) to differentiate between the transmitted signal from each site,

$$\mathbf{Y}_k = \begin{bmatrix} \mathbf{H}_k^{(1)} & \cdots & \mathbf{H}_k^{(J)} \end{bmatrix} \begin{bmatrix} \Lambda^{(1)} & & 0 \\ & \ddots & \\ 0 & & \Lambda^{(J)} \end{bmatrix} \begin{bmatrix} \mathbf{X}_k^{(1)} \\ \vdots \\ \mathbf{X}_k^{(J)} \end{bmatrix} \quad (6.2)$$

From these two signal models, the capacity of the MIMO SFN system can be easily derived as reported in the following contribution Contrib. II.1.

Contribution II.1 (Analytic Expression)

Ergodic capacity of a MIMO-OFDM system in SFN

Given an SFN of J transmitters of N_T antennas each, a receiver with N_R receive antennas, the OFDM-MIMO system capacities in the co-localized and distributed MIMO cases are

$$\text{Co-localized} \quad C = \mathbb{E} \left\{ \frac{1}{N} \sum_{k=1}^N \log_2 \left(\det \left[\mathbf{I}_{N_R} + \frac{P}{N N_T \sigma_n^2} \left(\sum_{j=1}^J \lambda_j \mathbf{H}_k^{(j)} \mathbf{H}_k^{(j)H} + \sum_{j \neq i} \sqrt{\lambda_i \lambda_j} \mathbf{H}_k^{(j)} \mathbf{H}_k^{(i)H} \right) \right] \right) \right\} \quad (6.3)$$

$$\text{Distributed} \quad C = \mathbb{E} \left\{ \frac{1}{N} \sum_{k=1}^N \sum_{j=1}^J \log_2 \left(\det \left[\mathbf{I}_{N_R} + \frac{P \lambda_j}{N N_T \sigma_n^2} \mathbf{H}_k^{(j)} \mathbf{H}_k^{(j)H} \right] \right) \right\} \quad (6.4)$$

where P is the transmit power of each site and $0 \leq \lambda_j \leq 1$ is the power scale factor due to path-loss from transmit site j such that $\sum_{j=1}^J \lambda_j \leq 1$.

From this result, it is highlighted that the distributed approach translates into a spatial multiplexing capability of the SFN network, whereas the co-localized strategy rather implies a higher spatial diversity exploitation. However, in this latter case, note that the obtained diversity is not fully constructive due to the second summation

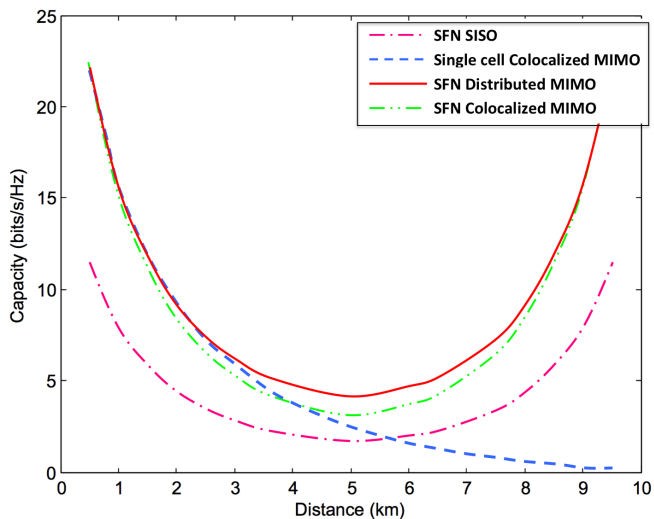


FIGURE 6.4– Channel capacity comparisons among several MIMO, SISO and SFN system strategies (Two transmitters).

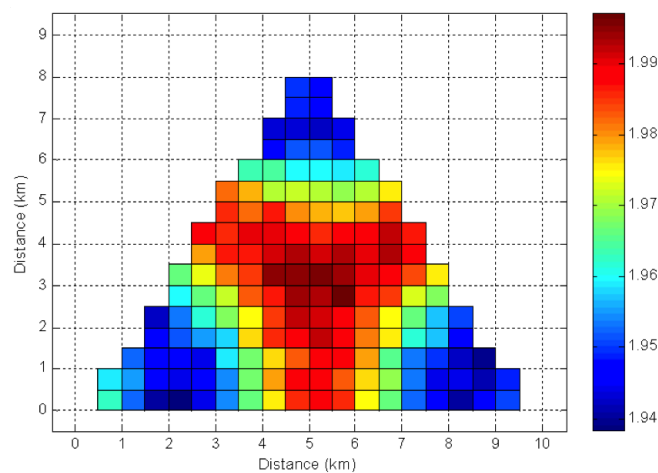


FIGURE 6.5– Channel capacity gain of MIMO-SFN systems over SISO-SFN (Three transmitters).

involving cross-talk terms (i.e. $jn^o i$) in the composite SFN channel. This exactly reflects the behaviour of a pure SFN strategy in which a same signal is transmitted from different transmitters : the energy of the arriving signals is gathered by the OFDM receiver but do not necessarily in a constructive manner, yielding a more frequency selective channel. The hope is that coded OFDM can accomodate with such selectivity, which is in principle its main asset.

Using Eq. (6.3) and (6.4) in Contrib. II.1, it is then possible to plot some capacity curves in different scenarios. Note that we can get the SISO SFN case (corresponding to the actual broadcast network configuration) by setting $N_R = N_T = 1$. Also, we can obtain the single cell MIMO case by choosing $J = 1$, which essentially yields the well-known results on MIMO capacity [BGP02]. Fig. 6.4 shows some example of results for an SFN area of two transmitters with an inter-site distance of 10 km (the first site is at distance 0 km and the second site is at 10 km). The channel coefficients are considered as independent complex Gaussian processes and a simple path-loss model is used. We plot the capacity curves as a function of the distance of the receiver to the first transmitter for various system configurations. These curves are interesting to highlight the SFN effect which gives some coverage continuity in space compared to the single cell case. Also, we clearly see the benefit of MIMO strategies over the SISO case. Nonetheless, it is observed that the distributed MIMO case achieves higher spectral efficiency for all the user locations compared to the co-localized case.

In both cases, maximum capacity is obtained on each side of the curves when path-loss is minimized for one transmitter (i.e. $\sum_j \lambda_j = 1$). Contrary to that, the worst capacity values are obtained (SFN case) when the user is located right in between the two towers. However, the MIMO gain is preserved in such a situation, namely for the distributed case. The loss observed for the co-located case is due to the higher selectivity of the composite SFN channel as stated before. It is interesting to translate these results into capacity gain (C_{MIMO}/C_{SISO}), as done in Fig. 6.5 for the distributed case. The obtained gain turns out to be almost constant for all receiver location, except some slight boost at the boundaries of the cells, where indeed it is the most difficult in practice to maintain the quality of service.

1.3 ROBUST DISTRIBUTED STBC FOR SFN

► Power Imbalance Criterion

From the previous results, we can conclude that the distributed MIMO strategy is a straightforward extension and effective enhancement of the classical SFN scheme. The question that remains to be answered is however : which STBC is the most suited for SFN ? We already know from the capacity considerations that a distributed strategy is the best approach to follow. However, we have also understood that the composite SFN channel is

1. MIMO Schemes for Broadcast Systems

strongly changing owing to high path-loss variations according to the distance of the terminal to the transmitters of the SFN area. In the sequel, we will be referring to such a behaviour as power imbalance. Eventually, our question can be restated as : which STBC is the most robust to power imbalance ?

The capacity considerations of previous section are far from being sufficient to answer that question. They have to be completed with a system point of view integrating power imbalance effects. Even if distributed MIMO seems to be the best strategy, capacity results do not exhibit the fact that the same service (data content) has to be delivered whatever the location of the user. In that sense, using for example a simple distributed spatial multiplexing strategy would lead to some catastrophic situations. For instance, only half of the throughput would be received by a user close to one site and far for the other and the only favorable situation would be for a user with intermediate position between two transmitters. However, in a broadcast scenario, no consideration about receiving conditions can be taken. Hence, the design of a SBTC in the SFN broadcast context has to integrate power imbalance effects.

From the literature, power imbalance is usually not taken as a constraint in the STBC code design. The criteria stated by Tarokh and Calderbank [TSC98] suggest optimal space-time code construction based on the pair wise error probability minimization, on the channel capacity maximization or on the spatial diversity maximization. Many proposals emerged from 1999 to 2008 [WFGV98, TJC99, ZG02, Ion03, GH03, LV07, ZHG08], among which the most popular ones for a 2x2 MIMO topology : the Alamouti Code [Ala98] and the Golden code proposed by Belfiore [BRV05]. The former is an orthogonal code of unit spatial rate but it can extract the entire spatial diversity with linear processing. The latter is a full rate and full diversity, quasi-orthogonal code which achieves the optimal diversity/multiplexing gain tradeoff.

No explicit criterion has been stated in case of power imbalance between the entries of the spatial channel matrix. However we can easily understand that full rate codes as Golden code are expected to perform poorly if one of the spatial link is lost. Such codes are designed to maximize the spatial diversity with channel matrices of statistically balanced power for each entry. Such codes would then dramatically suffer any power imbalance. Contrary to that, the orthogonality criterion can be interpreted as a good criterion. With orthogonal codes, the data symbols transmitted from one antenna are also transmitted from the other antennas, after applying a judicious linear combination such that if any spatial link associated to one antenna vanishes (due to strong fading, or in our case due to strong path loss) the other spatial links still allow the symbol to be propagated to the receiver, without interfering with the other symbols (owing to the orthogonality criterion) and can hence be still recovered by the receiver. Hence, we can intuitively formulate that a good criterion for distributed STBC in SFN is to ensure orthogonality between the symbols transmitted from distant sites. This criterion will be referred to as "inter-site orthogonality criterion". It has been highlighted in [R.19]

► Double Layer STBC Proposal

According to the inter-site orthogonality criterion, we went to the idea of designing hierarchical STBC which construction is based on two levels of coding, namely an intra-site coding and an inter-site coding level. The idea is to apply an orthogonal structure to the inter-site coding layer to make the overall code robust to power imbalance. For the intra-site coding layer, any classical criterion can then be used because no power imbalance is experienced. Among the various possibilities we investigated, one of the most interesting one is the hierarchical Golden/Alamouti code introduced in [R.19]. This code, referred to as 3D-MIMO code, is specifically optimized for an SFN of two sites with two antennas per site and a receiver also equipped with two antennas. A corresponding illustration is given Fig. 6.6 highlighting the inter-cell coding based on Alamouti code and intra-cell coding based on Golden code.

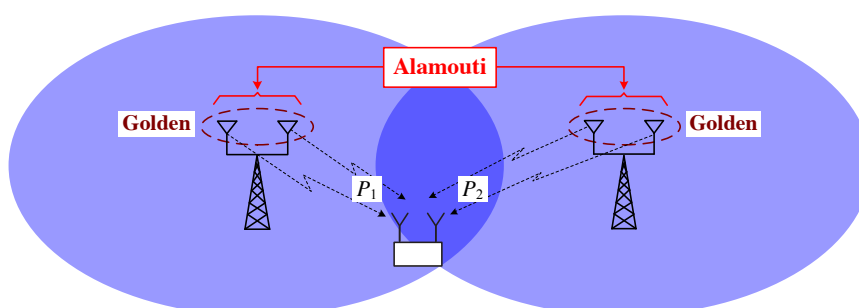


FIGURE 6.6– Principle of the 3D-MIMO code as a 4x2 distributed STBC for an SFN with two transmitters.

Contribution II.2 (System Design)

3D-MIMO code robust to power imbalance

Given an SFN of 2 transmitters with $N_T = 2$ antennas each antennas, a robust distributed STBC of rate $R = 2$ is achieved with the following two-layer construction

$$\text{Inter-site STBC} \quad \mathbf{X} = \begin{bmatrix} \mathbf{X}_1 & -\mathbf{X}_2^* \\ \mathbf{X}_2 & \mathbf{X}_1^* \end{bmatrix} \quad (6.5)$$

$$\begin{aligned} \text{Intra-site STBC} \quad \mathbf{X}_1 &= \frac{1}{\sqrt{5}} \begin{bmatrix} \beta(s_1 + \theta s_2) & \beta(s_3 + \theta s_4) \\ j\bar{\beta}(s_3 + \bar{\theta} s_4) & \bar{\beta}(s_1 + \theta s_2) \end{bmatrix} \\ \mathbf{X}_2 &= \frac{1}{\sqrt{5}} \begin{bmatrix} \beta(s_5 + \theta s_6) & \beta(s_7 + \theta s_8) \\ j\bar{\beta}(s_7 + \bar{\theta} s_8) & \bar{\beta}(s_5 + \theta s_6) \end{bmatrix} \end{aligned} \quad (6.6)$$

with s_i the input data symbols, $\theta = \frac{1+\sqrt{5}}{2}$, $\bar{\theta} = 1 - \theta$, $\beta = 1 + j(1 - \theta)$ and $\bar{\beta} = 1 + j(1 - \bar{\theta})$.

By applying such a code, we ensure a full-diversity and non-vanishing coding gain if strong power imbalance occurs, while maximizing the rate for the intracell coding. Indeed, from a capacity point of view, the inter-site orthogonal structure leads to a constructive combination of the branches of the composite SFN channel. If we were able to build a 3D code with an orthogonal inter-site layer whatever the number of transmitters in the SFN, Eq. (6.4) would be transformed into,

$$C = \mathbb{E} \left\{ \frac{1}{N} R_{inter} \sum_{k=1}^N \log_2 \left(\det \left[\mathbf{I}_{N_R} + \frac{P}{NN_T \sigma_n^2} \frac{1}{R_{inter}} \left(\sum_{j=1}^J \lambda_j \mathbf{H}_k^{(j)} \mathbf{H}_k^{(j)H} \right) \right] \right) \right\} \quad (6.7)$$

where R_{inter} is the rate of the inter-site STBC. In this capacity expression, we can note that the SFN diversity is fully exploited since the cross-talk terms in Eq. (6.4) are no more considered. This is an essential indication about power imbalance robustness. The cost to pay for such robustness is the global spatial rate limitation due to the orthogonality criterion which imposes $R_{inter} \leq 1$ [TJC99, JH05]. Since 2x2 Alamouti is of rate $R_{inter} = 1$ and 2x2 Golden code is of rate $R_{intra} = 2$, the proposed 3D-MIMO code has a global spatial rate of $R = 2$. Assuming a receiver with two antennas, the 3D-MIMO code is thus of maximal rate.

However, in a more general perspective of SFN areas composed of more than two transmitters, it becomes impossible to build a two-layer STBC of rate $R = 2$ since there exist no orthogonal codes of rate $R_{inter} = 1$ for $N_T > 2$. In the PhD of P. Pasquero, we studied various configurations with three transmitters and went to the conclusion that the best deployment scenario was to keep the 3D-MIMO code. For the intra-site coding however, many solutions are possible to address higher order MIMO topologies using 3x3 or 4x4 non-orthogonal STBC as those proposed in [LC08] [SR13].

► Performance Analysis

In [R.19] and [C.41] we provided the main simulation results showing the superiority of the proposed code compared to other classical codes of the literature. We first identified the most important codes and MIMO strategies and established a list of these solutions as in Tab. 6.1. With the two-layer approach in mind, it is possible to understand the structure of many codes distinguishing between the intra-cell and the inter-cell coding, as done in the table. For example, it is seen that the Jafarkhani code [Jaf01] hierarchically encodes two Alamouti codes. Also, the L2 code [HH02] is seen as a variant.

Simulations have been launched using the complete DVB-NGH specifications using the DVB-NGH MIMO outdoor channel model [MPB11]. Such a model emulates a cross-polarized 2x2 MIMO transmission in UHF band and includes many propagation factors (multipath effects, Doppler shift, correlation among channel links). Fig. 6.7 first gives the obtained results when no power imbalance is considered for the different codes listed in Tab. 6.1. It clearly appears that the proposed 3D-MIMO codes outperforms all the other codes. Note that the SM 4x2 code corresponds to a special case of SFN co-localized MIMO (combining SFN for inter-cell and spatial multiplexing for intra-cell). Interestingly such a code is not giving satisfying results as it could be expected from

1. MIMO Schemes for Broadcast Systems

TABLE 6.1– Summary of different space-time coding schemes applied to SFN.

Category	ST scheme	Nb. of cells	N_T	N_R	Nb. of info. symb.	Nb. of time slots	Intra-cell ST coding	Inter-cell ST coding	ST decoding complexity ^a
Classical solutions	SISO SFN	2	2	1	1	1	–	SFN	$\mathcal{O}(N)$
	MISO	2	2	1	2	2	–	Alamouti 2×1	$\mathcal{O}(N)$
	SIMO MRC	1	1	2	1	1	–	–	$\mathcal{O}(N)$
	MIMO	1 (or 2)	2	2	2	2	Alamouti (–)	– (Alamouti)	$\mathcal{O}(N)$
Rate one	Jafarkhani	2	4	2	4	4	Alamouti	Alamouti	$\mathcal{O}(M^4)$
	L_2 code	2	4	2	4	4	Alamouti-like	Alamouti	$\mathcal{O}(2M^2)$
	Rate 1 Alamouti	2	4	2	2	2	Alamouti	SFN	$\mathcal{O}(M^2)$
Rate two	3D code	2	4	2	8	4	Golden	Alamouti	$\mathcal{O}(M^8)$
	SM 4×2	2	4	2	2	1	SM 2×2	SFN	$\mathcal{O}(M^2)$
	Rate 2 Alamouti	2	4	2	4	2	Alamouti	SM 2×2	$\mathcal{O}(M^4)$

^a The computational complexities required by the rate one and rate two ST coding schemes are the worst case searching times for each received symbol using sphere decoder. The searching space is associated to a given constellation size M .

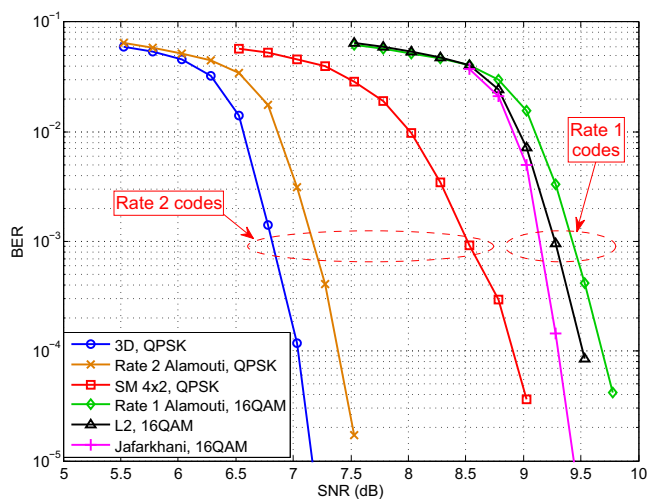


FIGURE 6.7– Performance of distributed STBC schemes in the DVB-NGH outdoor MIMO channel without power imbalance. Doppler frequency is set to 33.3 Hz.

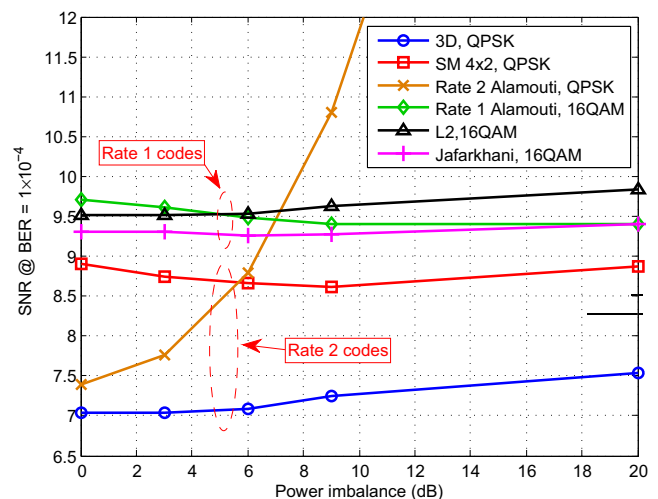


FIGURE 6.8– Performance of distributed STBC schemes in the DVB-NGH outdoor MIMO channel with power imbalance. Doppler frequency is set to 33.3 Hz.

the capacity analysis in Fig. 6.4 when the receiver is at intermediate distance from the two transmitters. Then, Fig. 6.8 shows how the performance degrades when power imbalance occurs. The superiority and the robustness of the 3D-MIMO code is clearly confirmed against such power imbalance. Equivalent robustness is also noticed for all the other codes which are built upon orthogonal or SFN inter-cell strategy. Yet, as it could be expected, the code built upon inter-cell spatial multiplexing is dramatically degraded under the effect of power imbalance.

1.4 FAST DECODABLE DISTRIBUTED STBC

► Decoding Complexity Analysis

As demonstrated, the 3D-MIMO code outperforms all the other code of the literature considering an SFN system setting with two antennas per site and two antennas at the receiver. However, performance is not the only criterion to take into account for a solution to be chosen for practical implementation. Indeed, even if the inter-cell coding layer of our 3D-MIMO code is built upon an orthogonal structure, the overall resulting code is no more orthogonal. This means that optimal ML decoding can not be obtained through linear processing. The complexity of ML decoding is then directly depending upon the size of the search tree. The way to exhibit the complexity order of ML decoding of STBC is to rewrite the received signal following the approach in [BHV09]. The idea is to separate the real and imaginary parts of matrices and stacking them into vector forms,

$$Y = HX + W \quad \longrightarrow \quad \tilde{y} = H_{eq} \tilde{s} + \tilde{w} \quad (6.8)$$

with \mathbf{H}_{eq} an equivalent channel matrix directly conditioned by the STBC structure. The equivalent channel matrix can then be QR decomposed, i.e. $\mathbf{H}_{eq} = \mathbf{QR}$, in order to get the ML solution of the transmitted symbols as,

$$\hat{\mathbf{s}} = \arg \min_{\mathbf{s} \in \Theta^S} \|\mathbf{Q}^T \hat{\mathbf{y}} - \mathbf{R}\mathbf{s}\|^2 \quad (6.9)$$

with Θ the set of constellation symbols, and S the number of symbols involved in a STBC codeword. Hence, the ML solution is a joint search of S information symbols of size M resulting in a complexity of $\mathcal{O}(M^S)$ ². As 8 information symbols are involved in the structure of the proposed 3D-MIMO code, the obtained complexity becomes of order $\mathcal{O}(M^8)$. The last column in Tab. 6.1 gives the related complexity orders for the other tested codes. As evident from these figures, our code exhibits the highest decoding complexity.

► Lowering the decoding complexity of the 3D-MIMO STBC

A first simple idea to work out the decoding complexity problem of the proposed code is to modify its structure in order to minimize the number of involved symbols. In other words, the aim was to obtain a more compact coding matrix. Hence, we built a new double layer STBC by re-arranging the Golden codewords following the Alamouti structure, but not proceeding to an hierarchical structure as made before. We finally went to a new version of the 3D-MIMO code viewed as a shorten one. Such code proposal has been introduced in [R.13] and is reported below.

Contribution II.3 (System Design)

Shorten 3D-MIMO code

Given an SFN of 2 transmitters with $N_T = 2$ antennas each antennas, a robust distributed STBC of rate $R = 2$ is achieved with the following two-layer construction

$$\text{Inter-site STBC} \quad \mathbf{X} = \frac{1}{\sqrt{2}} \begin{bmatrix} \mathbf{X}_1 & -\mathbf{X}_2^* \\ \mathbf{X}_2 & \mathbf{X}_1^* \end{bmatrix} \quad (6.10)$$

$$\text{Intra-site STBC} \quad \mathbf{X}_1 = \frac{1}{\sqrt{5}} \begin{bmatrix} \beta(s_1 + \theta s_2) \\ j\bar{\beta}(s_3 + \bar{\theta} s_4) \end{bmatrix} \quad \mathbf{X}_2 = \frac{1}{\sqrt{5}} \begin{bmatrix} \beta(s_3 + \theta s_4) \\ j\bar{\beta}(s_1 + \bar{\theta} s_2) \end{bmatrix} \quad (6.11)$$

with s_i the input data symbols, $\theta = \frac{1+\sqrt{5}}{2}$, $\bar{\theta} = 1 - \theta$, $\beta = 1 + j(1 - \theta)$ and $\bar{\beta} = 1 + j(1 - \bar{\theta})$.

Since the Alamouti and the Golden code structures have been kept, the shorten version of the 3D-MIMO code is expected to provide good performance. But in addition to this, a straightforward complexity reduction from $\mathcal{O}(M^8)$ to $\mathcal{O}(M^4)$ is obtained. Furthermore, the Alamouti structure of the code allows for some further reduction of decoding complexity. Indeed, stacking the four transmitted and received complex symbols in a vector yields

$$\underbrace{\begin{bmatrix} Y_1(1) \\ Y_2(1) \\ Y_1^*(2) \\ Y_2^*(2) \end{bmatrix}}_{\mathbf{y}} = \underbrace{\begin{bmatrix} h_{11} & h_{14} & \vdots & h_{13} & h_{12} \\ h_{21} & h_{24} & \vdots & h_{23} & h_{22} \\ h_{13}^* & -h_{12}^* & \vdots & h_{11}^* & h_{14}^* \\ h_{23}^* & -h_{22}^* & \vdots & -h_{21}^* & h_{24}^* \end{bmatrix}}_{\mathbf{H}} \underbrace{\begin{bmatrix} X_1(1) \\ X_2(1) \\ X_1(2) \\ X_2(2) \end{bmatrix}}_{\mathbf{x}} + \underbrace{\begin{bmatrix} W_1(1) \\ W_2(1) \\ W_1^*(2) \\ W_2^*(2) \end{bmatrix}}_{\mathbf{w}} = \quad (6.12)$$

where $X_k(n)$ denotes the coding symbol transmitted at antenna k during symbol interval n . Hence, it clearly appears that the received symbols are generated through a channel matrix composed of two blocks. As the generator matrix of the Golden code is a block diagonal matrix [BRV05], we can show that the received symbol vector takes the following general form

$$\mathbf{y} = \mathbf{F}_1 \mathbf{u} + \mathbf{F}_2 \mathbf{v} + \mathbf{w} \quad (6.13)$$

2. Note that lower decoding complexity may be achieved in practice through sphere decoding. Also some parallelisation can be processed by exploiting the orthogonality between information symbols. A correlation analysis between the information symbols can actually be acquired identifying the zero entries of matrix \mathbf{R} [IFS13, SR09].

1. MIMO Schemes for Broadcast Systems

with $\mathbf{u} = [s_1, s_2]^T$ and $\mathbf{v} = [s_3, s_4]^T$ and $\mathbf{F}_{1/2}$ some matrices depending on the channel coefficients and the Golden code generator matrix. From this equation, we can then think of applying some conditional ML algorithm. This is what we showed in more details in [R.13] and is summarized in the following algorithm.

Contribution II.4 (Algorithm)

Mixed ZF/ML decoding of the shorten 3D-MIMO code

A conditional ML solution to Eq. (6.13) is obtained as

$$\hat{\mathbf{u}} = \arg \min_{\mathbf{u} \in \Theta^2} \|\mathbf{y} - \mathbf{F}_1 \mathbf{u} - \mathbf{F}_2 \hat{\mathbf{v}}(\mathbf{u})\|^2 \quad (6.14)$$

with, $\hat{\mathbf{v}} = \mathcal{Q}(\tilde{\mathbf{v}}(\hat{\mathbf{u}}))$

$$\tilde{\mathbf{v}}(\mathbf{u}) = (\mathbf{F}_2^H \mathbf{F}_2)^{-1} \mathbf{F}_2^H (\mathbf{y} - \mathbf{F}_1 \mathbf{u})$$

with \mathcal{Q} the hard decision function over the set of constellation symbols Θ .

As a consequence to this proposal, the estimation of \mathbf{v} is achieved through linear processing (ZF detection) and the \mathbf{u} is decoded through a search over M^2 combinations of information symbols leading to an overall complexity of $\mathcal{O}(M^2)$ instead of $\mathcal{O}(M^4)$ for the optimal ML algorithm. Hence, this conditional ML searching offers a trade-off between the ML and linear decoding methods.

► Performance and complexity trade-off analysis

A summary table of complexity evaluation is given in Tab. 6.2 for the proposed shorten 3D-MIMO with the ML and the conditional ML decoding strategies. Other promising codes of the literature are given for comparison purpose. It turns out that the proposed code needs the lowest decoding complexity among all rate-two codes to obtain ML solution. Note that the rate-one codes should use M^2 -QAM to achieve the same throughput as the rate-two ones with M -QAM. Therefore, the proposed code requires the same decoding complexity as rate-one codes to support the same system throughputs. Moreover, it needs least complexity among all STBCs considered if the conditional ML searching is employed.

Then moving to the performance results obtained in a DVB-NGH system setting, we give the curves of Fig. 6.9. As expected the proposed code exhibits a strong resistance to the power imbalance, even if about 0.5 dB performance degradation loss is experienced compared to the original 3D-MIMO code equal reception power

STBC	Rate	Complexity
Short 3D-MIMO (ML)	2	$\mathcal{O}(M^4)$
Short 3D-MIMO (Cond. ML)	2	$\mathcal{O}(M^2)$
3D-MIMO	2	$\mathcal{O}(M^8)$
DjABBA [AHW07]	2	$\mathcal{O}(M^7)$
BHV [BHV09]	2	$\mathcal{O}(M^6)$
Srinath-Rajan [SR13]	2	$\mathcal{O}(M^{4.5})$
Jafarkhani [JH05]	1	$\mathcal{O}(M^2)$
L2 [HH02]	1	$\mathcal{O}(M^2)$

TABLE 6.2– Worst case decoding complexity of STBC.

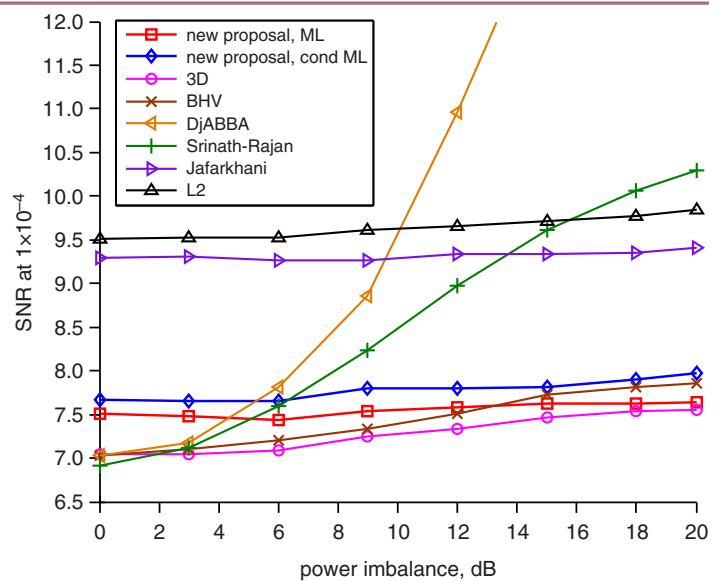


FIGURE 6.9– Performance of distributed STBC schemes in the DVB-NGH outdoor MIMO channel with power imbalance. Doppler frequency is set to 33.3 Hz.

between the transmitters of the SFN. Interestingly, the two codes have similar performance with high power imbalance. Then, the conditional ML solution suffers around 0.2 dB performance loss regarding the optimal ML decoding. We can also note that the BHV code has similar performance as the long 3D-MIMO code without power imbalance, but converges to the shorten 3D-MIMO performance when a transmission site is lost. We can then conclude that the proposed low complexity solution gives the best performance/complexity trade-off among the existing codes.

1.5 CONCLUSION

From 2007 to 2012, an important contribution of my work was at the level of the optimization of distributed STBC in the context of broadcast SFN. The 3D-MIMO and Shorten 3D-MIMO proposals have been two major outputs of this work. We participated during the B21C project to promote the idea of using Alamouti code structures for distributed coding in a SFN. Actually, a simple case of distributed MISO Alamouti (not detailed here) was part of the proposals made by different partners of DVB. The distributed MISO Alamouti code actually represents the first layer of the proposed 3D-MIMO code. Hence, in collaboration with other partners, we put some efforts providing some simulation results and analysis on this simple case, in order to prepare the promotion of the 3D-MIMO structure. As responsible of the MIMO task force within the B21C project, I had the opportunity to present the results of this work during a plenary DVB meeting in october 2009.

The simple distributed MISO solution has finally been confirmed as an option in the actual DVB-T2 specifications. Some field trials led by broadcast operators have recently shown the advantage of such simple technique. As far as the 3D-MIMO code is concerned, we tried to promote its concept during the ENGINES project in the perspective of the DVB-NGH elaboration. Due to complexity reasons, the solution finally retained for NGH is a simple mixture of localized Alamouti used in an SFN fashion. However, the basis of the 3D-MIMO code (first layer) is embedded in DVB. It is also the case for the newly released ATSC3.0 in USA. So, for these two actual standards, it might be a chance of possible extension to 3D-MIMO concepts for a future release.

Summary (PhD/Dissemination/Projects)

- 1 PhD (P. Pasquero) and 2 Post-Doc (Y. Nasser, M. Liu)
- 4 international journal papers [R.5][R.9][R.13][R.19]
- 6 communications in internat. conf. and worksh. [C.35][C.38][C.41][C.42][C.81][C.82]
- 1 Contribution to DVB forum
- 2 projects (B21C, ENGINES)

2 PRACTICAL DESIGN OF PAPR REDUCTION ALGORITHMS

2.1 MOTIVATIONS

The last two decades have witnessed the generalization of multicarrier modulations in almost every communication standards, with in a pole position the world of TV broadcasting. It is however well-known that one of the main drawback of OFDM systems remains the high peak-to-average power ratio (PAPR) of the time domain signal which raises distortion and power efficiency issues at the amplification stage. It is indeed difficult to amplify OFDM signals without introducing any distortions (in band or out of band) using RF amplifiers since these latter are non-linear by nature, especially close to the saturation region. Also, limiting such distortions by backing off the signal power at the input of the amplifier in order to exploit the most linear region of its characteristics (far from the saturation region) leads to a dramatic loss of power efficiency (since it is maximum around the saturation point). Hence, for a given statistical distribution of the signal amplitude and for a given power

2. Practical design of PAPR reduction algorithms

amplifier characteristics, distortion mitigation and power efficiency increase appear as two adversarial problems. This situation is particularly critical in the case of high power amplifiers such as those used in broadcast networks which energy consumption is huge (in the order of several Megawatts for countries like France or Spain) and evaluated as being due to the power amplification of the signal for a ratio of about 80%.

Hence, a important field of my research of these last years at the level of broadcast systems was to find some solutions for the improvement of the energy efficiency of transmitters. Two well-known complementary strategies to counteract the above mentioned antagonism are on the one hand to work on the OFDM signal amplitude statistics modification, namely using PAPR reduction techniques, and on the other hand to compensate for the non-linearities of the power amplifier by means of linearization and predistortion techniques.

In the work described in this section, we have investigated the question of PAPR reduction. The objective of PAPR reduction is to decrease the fluctuations of the transmitted signal in order to exploit the PA at an operating point closer to the saturation region where its power efficiency is maximized. [A huge amount of PAPR reduction algorithms have actually been proposed since 1990s \(around 3500 hits in the IEEE Xplore database\).](#) Even though, it turns out that there exist today no practical algorithms able to offer a sufficient performance-complexity trade-off to be implemented in today's modulators. Hence, even if the topic of PAPR reduction in OFDM can be considered as an old subject widely addressed for years in the scientific community (and even at IETR), we decided to go a step further in the studies trying to understand the reasons of such a situation. During the european Celtic project B21C, some first studies allowed us to deal with the asymptotic performance it was possible to reach applying the TR concepts with infinite complexity. At the end of this project, we decided to set up a new project (PAPRICA) with one of the involved SME to specifically study and propose practical algorithms with implementation constraints. We naturally focused our attention upon tone reservation concept as it is already included in some digital broadcast standards (DVB-T2/NGH and ATSC3.0).

2.2 PAPR REDUCTION AND TONE RESERVATION ALGORITHMS

► State of the art

The objective of PAPR reduction is to decrease the fluctuations of the transmitted signal in order to exploit the PA at an operating point closer to the saturation region where its power efficiency is maximized. Various approaches and strategies have been suggested and studied as for example summarized in [HL05] [GEPB06] [KBP⁺12]. Clipping and filtering [LC98], coding [JWB94], partial transmit sequence [MH97] or selected mapping [BFH96], are the most popular reduction techniques. The main drawback of these methods is their high complexity with limited gain and the necessity to transmit, for some of them, side information to the receiver. In recent years, active constellation extension (ACE) [KJ03] and tone reservation (TR) techniques [TMoEE99] have been studied by many researchers because they are expected to offer the highest potential and do not need to transmit any side information. In particular, these two PAPR reduction techniques have been selected in various standards such as digital video broadcasting - second generation DVB-T2 [DT09], DVB for next generation handheld (DVB-NGH) and more recently the American digital video broadcasting standard ATSC 3.0 [ATS16].

► Tone Reservation Concept

The TR concept introduced by Tellado in [TMoEE99] relies on the dedicated usage of a subset of subcarriers for PAPR reduction purposes. This subset of so-called peak reduction tones (PRT) is used to generate a kernel signal in the time domain, added to the original one, and yielding a transmitted signal which has a lower PAPR than the original one³. To better understand the difficulty behind practical TR principles implementation, let us consider that we allocate R tones for PAPR reduction of the OFDM system of N subcarriers. We define \mathcal{B} as the PRT subset of these R locations and \mathbf{C} as the vector of R peak reduction symbols transmitted on these positions and zeros elsewhere. Similarly, let the complement set \mathcal{B}^c be the data tone subset of the useful data positions and \mathbf{D} the vector of the $N - R$ associated transmitted data symbols and zeros elsewhere. The resulting

3. Clearly, tone reservation does not degrade the BER performance of the system (at fixed E_b/N_0), since data subcarriers and PRT are orthogonal and can be naturally separated in the frequency domain at the receiver. Thus TR algorithms can be categorized as a downward compatible method [LP08].

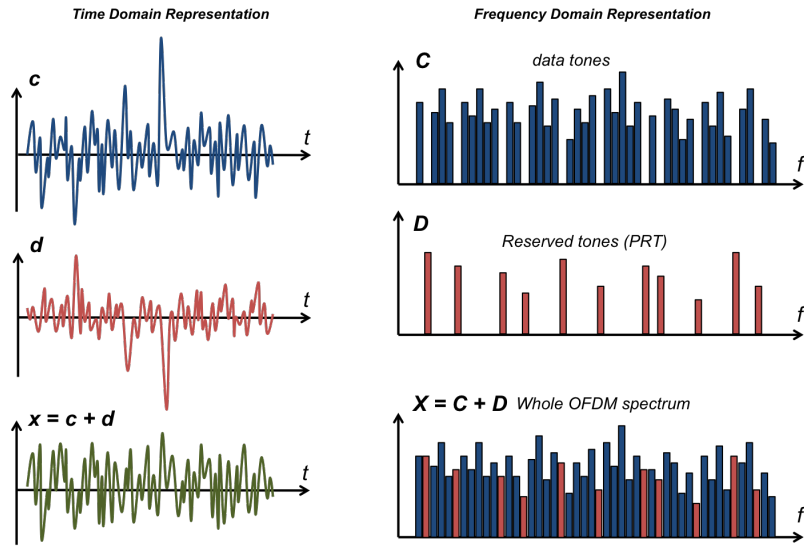


FIGURE 6.10– Typical illustration of a TR scheme.

signal to be transmitted can be represented in frequency and time domains as

$$\begin{aligned}
 \mathbf{X} = \mathbf{C} + \mathbf{D} & \xleftrightarrow{\mathcal{F}} x = c + d & (6.15) \\
 \text{where, } \mathbf{C} = \begin{cases} C_k \neq 0, & \forall k \in \mathcal{B}, \\ C_k = 0, & \forall k \in \mathcal{B}^c, \end{cases} & \text{ and, } \mathbf{D} = \begin{cases} D_k \neq 0, & \forall k \in \mathcal{B}^c, \\ D_k = 0, & \forall k \in \mathcal{B}, \end{cases}
 \end{aligned}$$

and with \mathcal{F} standing for the discrete Fourier Transform. The illustration of such a model is given in Fig. 6.10. From this signal model, the PAPR of the baseband signal x , defined over a duration window corresponding to the OFDM symbol size, is then defined as follows,

$$\text{PAPR}_x = \frac{\|\mathbf{x}\|_\infty^2}{\frac{1}{N} \|\mathbf{x}\|_2^2} = N \frac{\|\mathbf{c} + \mathbf{d}\|_\infty^2}{\|\mathbf{c}\|_2^2 + \|\mathbf{d}\|_2^2}, \quad (6.16)$$

where $\|\cdot\|_\infty$ and $\|\cdot\|_2$ denote infinity and Euclidean norms, respectively.

From Eq. (6.15) and (6.16), we understand that the central issue is to design efficient algorithms able to compute, at each new symbol, the adequate c (or equivalently the adequate values C_k to load on the reserved tones) so as to efficiently reduce the PAPR. In addition, it can be understood that the power allocated to c has to be limited in practice not to reduce the PAPR to the detriment of the useful power assigned to d . Hence, the search of the adequate c shall respect some predefined power constraint.

► Theoretical optimization problem formulation

It is possible to state the TR optimization problem as a quadratically constrained quadratic program (QCQP) [TC98].

$$\begin{aligned}
 \mathcal{P}_0: \quad & \min_{\mathbf{C}} \quad \|\mathbf{d} + \mathbf{F}^H\{\mathbf{C}\}\|_\infty^2 & (6.17) \\
 & \text{subject to, } \|\mathbf{C}\|_\infty^2 \leq \frac{\Gamma}{N-R} \|\mathbf{D}\|_2^2.
 \end{aligned}$$

with \mathbf{F} the Fourier matrix. This problem essentially finds the optimal vector \mathbf{C} of complex values to associate to the PRTs so as to minimize the maximum peak value Λ of the output signal. Note that the power constraint imposed on the reserved tones is a peak power constraint defined with respect to the power level associated to data tones. This corresponds to the case of DVB-T2/NGH and ATSC3.0 specifications, where the PRTs power boost Γ shall be set to 10 dB maximum.

Indeed, Problem \mathcal{P}_0 can also be viewed as a special case of second order cone program (SOCP) [ZPLL06], which is a convex optimization problem class that minimizes a linear function over the intersection of an affine set and the product of second-order (quadratic) cones. Finding the optimal solution to \mathcal{P}_0 using SOCP requires very high computational complexity which completely prevents to implement such algorithm in practical transmitter.

2. Practical design of PAPR reduction algorithms

2.3 EXISTING PRACTICAL SOLUTIONS

Alternatively, the computation of the complex values C_k assigned to the reserved tones can be computed iteratively. For instance, the DVB-T2, DVB-NGH and ATSC 3.0 broadcasting specifications include a gradient-based iterative algorithm for TR PAPR reduction. This solution, initially proposed in [JKE08] is based upon iteratively cancelling out the signal peaks by a set of impulse-like kernels. The reference kernel signal denoted as κ , is a Dirac-like pulse obtained by letting $C_k = 1, \forall k \in \mathcal{B}$, that is

$$\kappa = \mathbf{F}^H\{\mathbf{1}_{\text{TR}}\}, \quad \text{where, } \mathbf{1}_{\text{TR}} = \begin{cases} 1, & k \in \mathcal{B}, \\ 0, & k \in \mathcal{B}^c. \end{cases} \quad (6.18)$$

From this kernel definition, one may understand that each peak of the time-domain signal can be mitigated or even cancelled by adequately shifting the original kernel κ to make its peak position coincide with the detected one, and then scaling and subtracting the shifted kernel to reduce the signal peak amplitude⁴. Hence, the QCQP optimization problem can be restated as follows,

$$\mathcal{P}_1 : \quad \min_{\rho_i, \tau_i} \left\| \mathbf{d} + \kappa \otimes \sum_{i=1}^{N_i} \rho_i \delta_N[n - \tau_i] \right\|_{\infty}^2 \quad (6.19)$$

subject to, $\|\mathbf{C}\|_{\infty}^2 \leq \frac{\Gamma}{N-R} \|\mathbf{D}\|_2^2$.

in which \otimes stands for circular convolution and $\delta_N[n]$ is the Dirac delta discrete sequence vector of size N . In \mathcal{P}_1 , the search of the optimal solution translates into finding the optimal time delays τ_i and weighting factors ρ_i , for a sufficient number of iterations N_i . The optimal resolution of \mathcal{P}_1 leads to the same final solution as solving \mathcal{P}_0 . However, a suboptimal approach can be followed, by fixing Λ to a fixed reference value $\tilde{\Lambda}$ corresponding to the average value obtained in simulation by running the optimal resolution. Then, an iterative process can be established consisting in detecting the first highest peak, cancelling it, and then iteratively repeating the process for the other peaks. This iterative algorithm is schematically represented in fig. 6.11. The algorithm exits as soon as the power constraint is violated or when a predefined maximum number of iterations is reached.

As shown later on and published in [C.30][C.8], the gradient-based TR algorithm does not offer a sufficient performance-complexity trade-off to be implemented in today's DVB-T2 modulators. The major issue of this algorithm is its very slow convergence yielding a high number of iterations. A second issue is that it is inefficient in properly exploiting the available amount of power granted to the reserved tones. These last years, multiple researches have been focusing on enhancing the performance of TR gradient-based algorithms (e.g. [MNP⁺10a, MNP10b]). However, even if some improvements have been achieved, the proposed solutions does not sufficiently alleviate the convergence and power constraint issues for practical implementation.

2.4 PROPOSED ALGORITHM BASED ON NEW KERNEL DEFINITION

► Comb-like kernel

The techniques introduced in this section are based on a new kernel definition and allocate power to the PRTs in order to benefit from all the amount of power available for PAPR reduction. We present a first algorithm referred to as Individual Carrier allocation for Multiple Peaks reduction (ICMP) and which offers a good performance/complexity tradeoff. Then, a second algorithm named Grouped ICMP (GICMP) is proposed in order to lower the latency of the previous one. Instead of a Dirac-type kernel as suggested by the DVB-T2 specifications, during the PhD of R. Mounzer [C.24], we came up with the idea of generating a comb-like kernel, associated to the activation of a single reserved tone at each iteration of the algorithm. The proposed kernel is then defined for each iteration i as,

$$\mathbf{v}_i = \mathbf{F}^H\{\Upsilon^{(i)}\} \quad \text{with, } \Upsilon^{(i)} = \begin{cases} \Upsilon_k^{(i)} = 1, & k \in \mathcal{B}(i) \\ \Upsilon_k^{(i)} = 0, & \text{otherwise} \end{cases} \quad (6.20)$$

4. This essentially amounts to modify the phase and the amplitude of the frequency domain complex values associated to the reserved tones.

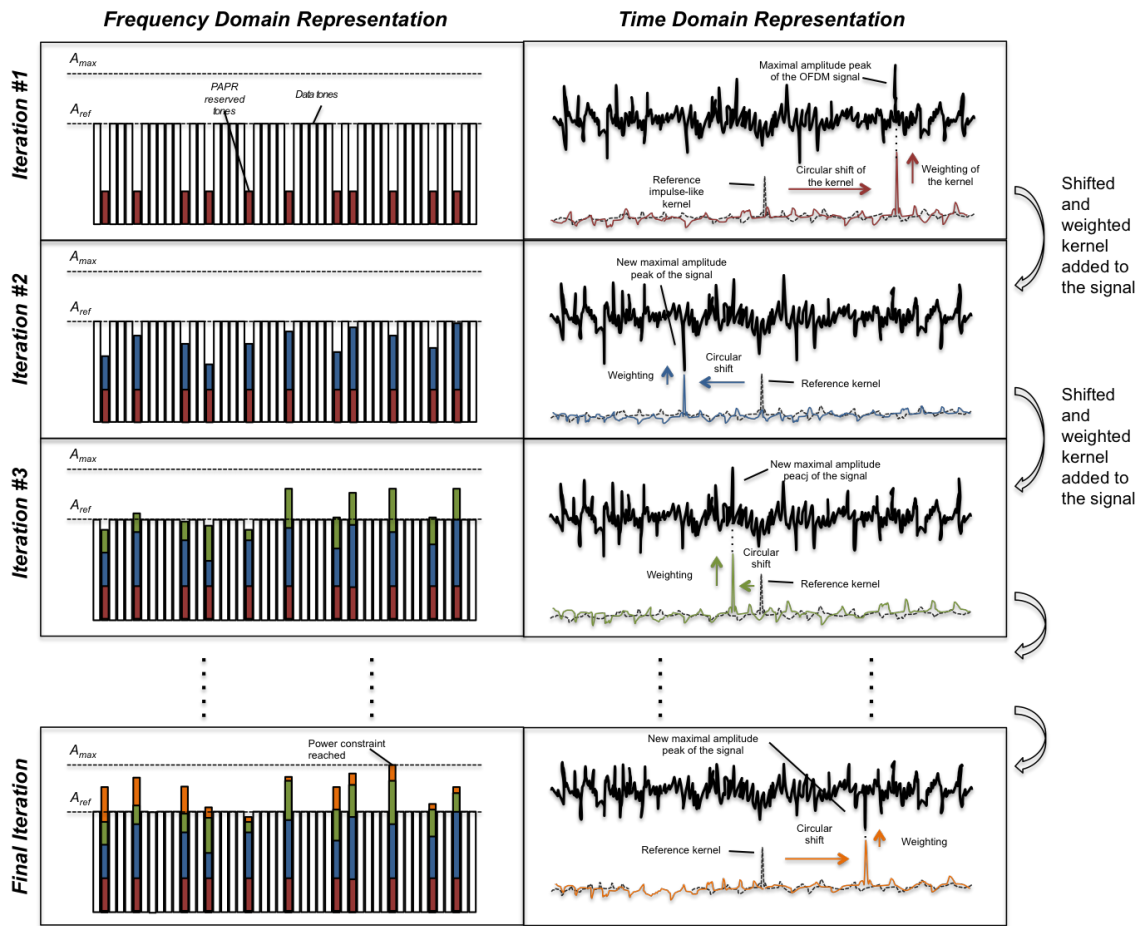


FIGURE 6.11– Schematic representation of the TR gradient algorithm.

The reason for such a choice is threefold. At first, allocating each reserved tone one by one allows to perfectly and implicitly control the power allocated to the tones. Then, the comb-like structure of the time domain kernel is expected to be able to reduce multiple peaks at a time since its energy is spread all over the OFDM symbol duration. The condition for that is to compute adequate phase-shift of the kernel as detailed hereafter. Last but not least, the kernel computation can directly be processed in time domain, without the use of any IFFT, since it is easily computed as follows

$$v_i(n) = \frac{1}{N} e^{-j\phi} e^{-j\frac{2\pi B(i)n}{N}}, \quad 0 \leq k < N. \quad (6.21)$$

► Related Optimization Problem

From this new kernel definition, we can state the modified optimization problem \mathcal{P}_2 as follows,

$$\mathcal{P}_2 : \quad \min_{\forall \rho_i, \forall \phi_i} \left\| \mathbf{d} + \sum_{i=1}^{N_i} \rho_i e^{j\phi_i} \mathbf{v}_i \right\|_{\infty}^2 \quad (6.22)$$

subject to, $\rho_i \leq \frac{\Gamma}{N-R} \|\mathbf{D}\|_2^2$.

where it becomes obvious that the power constraint is easily controlled. Optimal resolution of problem \mathcal{P}_2 involves an intensive search of the optimal values ρ_i and ϕ_i . However, after thorough analysis of the optimal values obtained in simulations running the original QCQP algorithm on \mathcal{P}_0 , it turns out that almost all reserved tones are loaded at the maximum allowed power level. Hence, a simplified sub-optimal problem can be obtained by fixing $\rho_i = A_{max}, \forall i$. Also, the search on the optimal ϕ_i values can be simplified by converting the infinite norm into a quadratic norm, but restricting the computation upon a given subset of time samples corresponding to the highest peak values of the OFDM signal. Hence, instead of minimizing the maximum peak amplitude (infinite

2. Practical design of PAPR reduction algorithms

norm criterion), we rather minimize the energy carried by multiple peaks above a given amplitude threshold (quadratic norm criterion). The corresponding optimization problem we have thus proposed states as,

$$\begin{aligned} \mathcal{P}_3 : \quad & \min_{\forall \phi_i} \left\| \mathbf{d}(\mathcal{S}) + \sum_{i=1}^R A_{\max} e^{j\phi_i} \mathbf{v}_i(\mathcal{S}) \right\|_2^2 \\ & \text{subject to, } \left\| \mathbf{d}(\mathcal{S}^c) + \sum_{i=1}^R A_{\max} e^{j\phi_i} \mathbf{v}_i(\mathcal{S}^c) \right\|_\infty^2 \leq \tilde{\lambda} \\ & \text{and, } \mathcal{S} = \{k : |d(k)| > \tilde{\lambda}\}. \end{aligned} \quad (6.23)$$

where the threshold value $\tilde{\lambda}$ to use can be determined through simulations as in the gradient-based case.

► ICMP Algorithm

The crucial step in the resolution of Problem \mathcal{P}_3 is then the computation of the optimal phase ϕ_i of each comb-like Kernel \mathbf{v}_i , which takes into account several peak positions (hence the name of the algorithm). As in the gradient-based case, a sub-optimal solution is used to solve the problem iteratively, i.e. computing the optimal phases ϕ_i sequentially. In such a case, the number of iterations equals the number R of available pilots. For one particular iteration i , assuming a given subset \mathcal{S}_i of detected peaks and a kernel \mathbf{v}_i the optimal phase ϕ_i^* is obtained solving the following sub-problem,

$$\mathcal{SP}_3 : \quad \min_{\phi} \left\| \mathbf{d}(\mathcal{S}_i) + \mathbf{c}(\mathcal{S}_i) \cdot A_{\max} e^{-j\phi} \right\|_2^2. \quad (6.24)$$

Such a sub-problem involves a differential quadratic form which minimization is easy to obtain. After classical mathematical manipulations, the optimal phase $\phi_i^*(\mathcal{S}_i)$ can then be expressed as,

$$\phi_i^*(\mathcal{S}_i) = \text{atan} \left(\frac{\text{Im} \left\{ \mathbf{d}^H(\mathcal{S}_i) \mathbf{v}_i(\mathcal{S}_i) \right\}}{\text{Re} \left\{ \mathbf{d}^H(\mathcal{S}_i) \mathbf{v}_i(\mathcal{S}_i) \right\}} \right) - \frac{\pi}{2} \quad (6.25)$$

Eventually, the new tone reservation method we have proposed for reducing the PAPR of an OFDM signal is summarized hereafter and illustrated in Fig. 6.12. It has to be noticed that the proposed algorithm relies on quite low computation complexity. The $\tilde{\lambda}_i$ threshold may be adapted at each iteration to take into account the progressive PAPR reduction which is expected to occur along the iterations. These threshold values can be optimized in advanced through simulations.

Contribution II.5 (Algorithm)

Individual Carrier allocation for Multiple Peaks reduction (ICMP)

From an initial time-domain OFDM symbol vector \mathbf{d} , the ICMP TR-based PAPR reduction algorithm applied on R reserved tones yields the following symbol vector :

$$\mathbf{x} = \mathbf{d} + \mathbf{c} \quad \text{with, } \mathbf{c} = A_{\max} \sum_{i=1}^R \mathbf{v}_i e^{j\phi_i^*(\mathcal{S}_i)} \quad (6.26)$$

where \mathbf{v}_i is obtained from (6.21) and $\phi_i^*(\mathcal{S}_i)$ is iteratively computed from (6.25) with \mathcal{S}_i the instantaneous subset of time-domain samples to consider at each iteration such that :

$$\mathcal{S}_i = \left\{ k : \left| d(k) + A_{\max} \sum_{j=1}^{i-1} \mathbf{v}_j(k) e^{j\phi_j^*(\mathcal{S}_i)} \right| > \tilde{\lambda}_i \right\}.$$

with $\tilde{\lambda}_i$ a predefined amplitude threshold.

► GICMP Algorithm

With the proposed algorithm, the global latency, which is the most important criterion in PAPR reduction algorithm, is however proportional to the number of iterations and then to the number of PRTs. Since DVB-T2

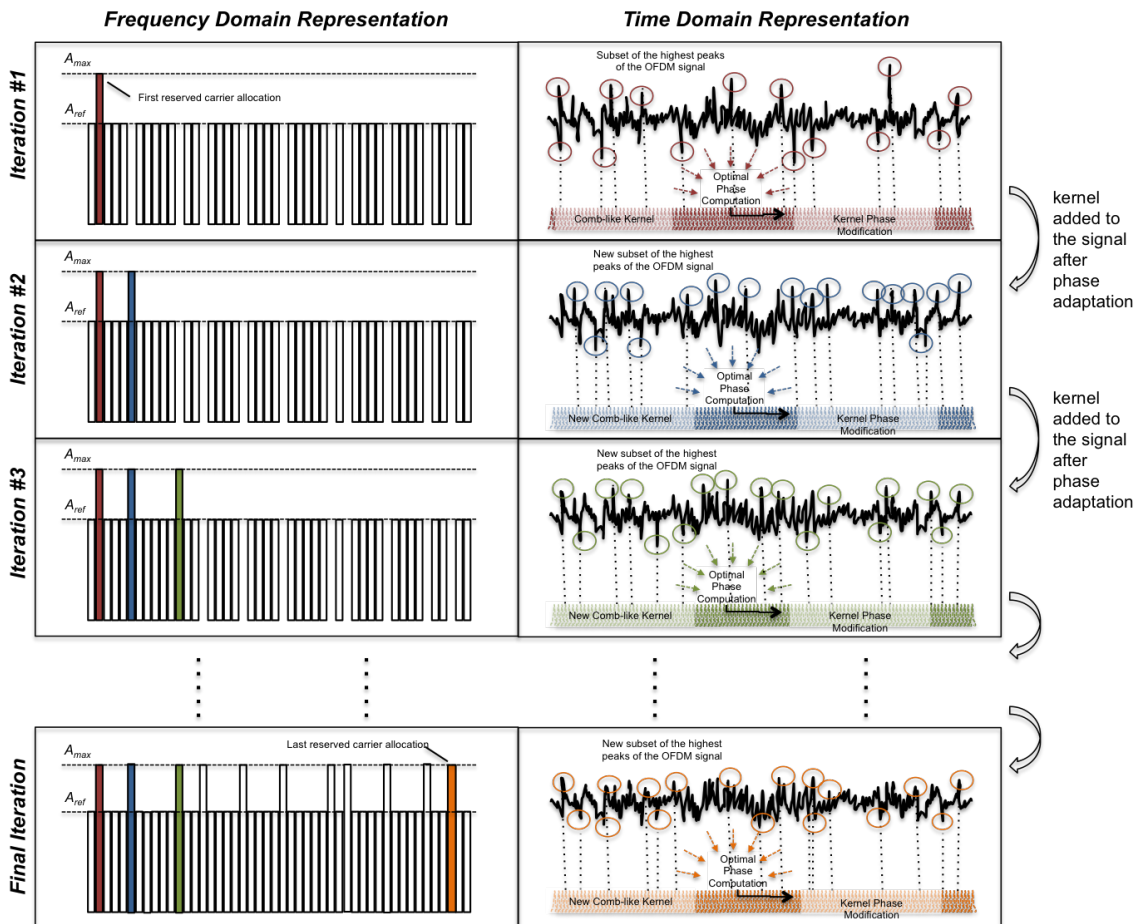


FIGURE 6.12– Iterative power allocation of the PRTs with ICMP in the frequency domain.

and ATSC3.0 reserves 1% of the subcarriers for PAPR reduction, this would lead to a number of iterations raising from $R = 9$ in 2K mode to $R = 288$ in 32K mode. Since the latter mode it most likely to be deployment for terrestrial broadcast networks, ICMP it not yet suited to such a situation. To address this latency issue of the ICMP algorithm, we proposed a new algorithm, namely GICMP, based on a grouping strategy of the PRTs. More precisely, the reserved pilots are grouped into G groups as follows

$$\mathcal{B} = \{\mathcal{B}_1, \dots, \mathcal{B}_G\}, \tag{6.27}$$

$$\mathcal{B}_i = \left\{ P_{1 + \frac{(i-1)R}{G}}, \dots, P_{1 + \frac{iR}{G}} \right\}, \text{ for } 1 \leq i \leq G. \tag{6.28}$$

Then, one peaks search is executed per group with GICMP, instead of one per PRT with ICMP. The latency becomes then proportionnal to the number G of groups. The resulting GICMP algorithm is presented in the next contribution section on top of next page. With this final algorithm, the optimal phases associated to the PRTs of a same group are different but are computed in a parallel fashion based on a common peaks search to produce an aggregated kernel \underline{v}_g at each iteration. Hence, the latency, which is essentially driven by the peaks search process, can be substantially lowered since it becomes proportional to the number of groups⁵. One first counterpart of the parallel processing is the increase of the computation complexity of each iteration. A second one is the potential performance degradation, since the parallel phase computations avoid the possibility of taking into account any mutual effects occuring when summing up the kernels \underline{v}_{g+i} to form the aggregated kernel. Finally, a tradeoff between latency, performance and computational complexity has to be studied as addressed in the performance analysis of next section.

5. For instance, in the 32K OFDM mode of the DVB-T2 standard for which the number of PRTs is 288, one can use $G = 8$ groups of 36 PRTs.

2. Practical design of PAPR reduction algorithms

Contribution II.6 (Algorithm)

Grouped Individual Carrier allocation for Multiple Peaks reduction (GICMP)

From an initial time-domain OFDM symbol vector \mathbf{d} , the GICMP TR-based PAPR reduction algorithm applied on G groups of R/G reserved tones yields the following symbol vector :

$$\mathbf{x} = \mathbf{d} + \mathbf{c} \quad \text{with, } \mathbf{c} = A_{\max} \sum_{g=1}^G \underline{\mathbf{v}}_g \quad (6.29)$$

$$\text{and, } \underline{\mathbf{v}}_g = \sum_{i=0}^{\frac{R}{G}-1} \mathbf{v}_{g+i} e^{j\phi_{g+i}^*(\mathcal{S}_g)}$$

where \mathbf{v}_{g+i} is obtained from (6.21) and $\phi_{g+i}^*(\mathcal{S}_g)$ is iteratively computed from (6.25) however using \mathcal{S}_g the subset of time-domain samples constituted at each grouped iteration (i.e. for each group g) as :

$$\mathcal{S}_g = \left\{ k : \left| d(k) + A_{\max} \sum_{h=1}^{g-1} \mathbf{v}_h(k) \right| > \tilde{\lambda}_g \right\}.$$

2.5 PERFORMANCE RESULTS AND ANALYSIS

The proposed ICMP and GICMP algorithms have been patented in 2015 [P.2]. By then, many results on the proposed algorithms have been published, namely in [C.22], [C.24], and a journal paper has recently been submitted to IEEE Transactions on Broadcasting aiming at summarizing our work on new PAPR reduction algorithms including the measurement obtained on testbeds in the framework of the PAPRICA collaborative project led in collaboration with a device manufacturer.

In the following we give the main results in terms of performance and complexity of the proposed ICMP and GICMP algorithms. As QCQP yields optimal performance (at the price of huge computational complexity), it will be considered as the upper-bound in all the presented results. On the other hand, Gradient-based algorithm suggested by the DVB-T2 standard will be used as a benchmark for state-of-the art performance. Finally the original situation without any PAPR reduction will be given as lower-bound.

► Simulation conditions

The different simulations have been obtained using a baseband physical layer simulation chain which main parameters respect the DVB-T2 system specifications, namely at the level of the OFDM waveform [DT09]. More importantly, the location of the data and reserved tones have been set regarding the standard.

The different curves that will be providing in the sequel correspond to either CCDF (complementary cumulative distribution function) curves of the PAPR value, or MER (modulation error ratio) curves of the output signal after amplification. The definition of these two metrics are introduced hereafter.

CCDF of PAPR is actually the most commonly used metrics in the academic literature. However, a more practical figure of merit used in practice by device manufacturers and network operators is MER. MER quantifies the performance of a digital radio transmitter or receiver in a communication system using digital modulation. It is a direct measure of the signal quality taking into account the imperfections regarding practical implementation⁶. The MER computation consists in comparing the actual location of a received symbol vector to its ideal location.

6. The European Telecommunications Standards Institute (ETSI) defines the MER as one of the measurement guidelines for DVB systems [V1.01].

It is defined in dB as⁷,

$$\text{MER}\{\mathbf{X}, \widehat{\mathbf{X}}\} = 10 \log_{10} \left(\frac{\|\mathbf{X}\|_2^2}{\|\mathbf{X} - \widehat{\mathbf{X}}\|_2^2} \right). \quad (6.30)$$

Focusing on the degradation due to non-linear amplification, \mathbf{X} is the ideal symbol vector measured at the input of the amplifier and $\widehat{\mathbf{X}}$ is measured at its output. Thus, MER gives an indication of the ability of the receiver to correctly decode the signal. Indeed, the MER metric gives additional insights compared to CCDF since it directly integrates the impact of the non-linearity of the power amplifier. Hence, we propose to widely consider the MER as the main parameter in quantifying the performance of PAPR reduction techniques. In addition, unlike CCDF of PAPR, MER is independent of the symbol length and then of the number of subcarriers [V1.01].

Measuring the MER however depends on both the power amplifier behavior and the power back-off applied to the signal at the input of the amplifier. As for the power amplifier we will consider in simulations the well-known Rapp model which is commonly used for solid-state HPAs which do not apply any phase change to the input signal [Rap91]. Such a model is governed by a so-called knee factor b revealing the smoothness of transition from the linear region to the saturation region (the lower b , the smoother the transition). In all the presented results, a knee factor $b = 10$ will be used, corresponding to a quite good predistorted amplifier approaching the so-called soft envelope limiter [OI02b]. This choice is reasonable since practical implementations often embed predistortion techniques. In particular, this will be the case of the later introduced testbed used to validate our algorithms.

Using this model, we will measure the MER considering variable Input power Back-Off (IBO) values, yielding MER versus IBO curves. Since a larger IBO leads to a higher MER, these MER curves will be monotonously increasing with the IBO. Therefore, using these curves for performance comparison purpose will be easy : the upper the better the MER curves.

► ICMP and GICMP optimal settings

In this paragraph, we seek how to set the parameters of the proposed algorithms which still remain as degrees of freedom. As for the ICMP algorithm first, we have to find through simulations the optimal thresholds $\tilde{\lambda}_i$ to use at each iteration i to select the highest peaks in the time domain signal further used for the optimal phase computation ϕ_i^* . After thorough analysis of the algorithm behaviour, we went to the conclusion that a constant threshold could be used across the iterations. Also, as the number of detected peaks directly impacts the computational complexity of the optimal phase computation, we led our simulations rather using parameter S defined as the number of selected peaks, i.e. $S = \text{Card}\{S\}$. Hence, by varying the size of S , the threshold level $\tilde{\lambda}$ is indirectly adjusted, but the impact on complexity is directly caught.

Fig. 6.13 gives the MER for a varying number S of selected peaks, and comparing the ICMP results with the reference curves previously identified. The power level of the PRTs is set to $\Gamma = 10$ dB above that of the data tones. It first turns out that the proposed algorithm clearly outperforms the state-of-the art gradient-based algorithm, even if the latter is run over a large number $N_i = 30$ of iterations. Then, making S vary, we are able to approach the optimal QCQP performance. As increasing S amounts to increase the computational complexity, an acceptable trade-off for the sequel will be to set $S = 100$ in 32K mode. In that case, targeting an MER of 34 dB, the proposed algorithm leads to a IBO reduction of about 0.5 dB compared to the original situation without PAPR reduction, and of about 0.3 dB compared to the gradient-based algorithm. The IBO could be further reduced of about 0.1 dB only if implementing the QCQP optimal solution were possible. On the other hand, with an IBO of 6.4 dB, the ICMP algorithm yields an MER gain of 2 dB compared to the gradient-based solution and almost 3 dB compared to the non PAPR reduction case.

Leading the same analysis for other OFDM modes yields the general conclusion that using between 2% and 3% of the samples (the highest peaks) is a good performance/complexity trade-off. Complementary results in terms of CCDF in 2K mode are given in Fig. 6.14 with $S = 5$ proving the superiority of the proposed algorithm compared to the gradient-based approach.

As ICMP is not adapted for the highest OFDM modes, let us now get the optimal settings for the GICMP algorithm. As ICMP and GICMP are based on the same concept, we will be using the same approach for the peak detection in the GICMP case as in the ICMP case. Hence, the rest of the simulations will be obtained with a fixed threshold, i.e. a fixed maximum peaks set size S , along the iterations. The particular parameter that has

7. Note that MER is closely related to the error vector magnitude, where the later can be defined as the square root of the former.

2. Practical design of PAPR reduction algorithms

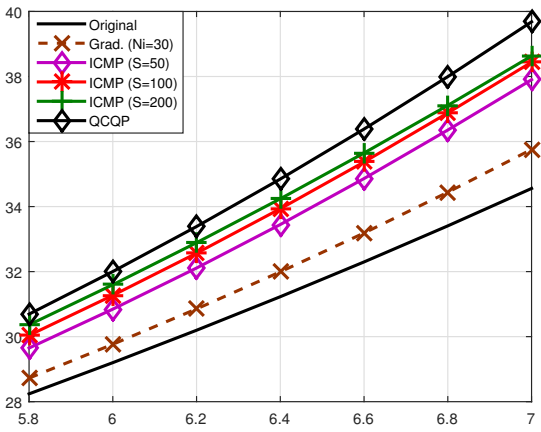


FIGURE 6.13– MER for a DVB-T2 system in 32K mode with ICMP : choice of the peaks subset size $S = \text{card}S$. Power constraint is set to $\Gamma=10$ dB.

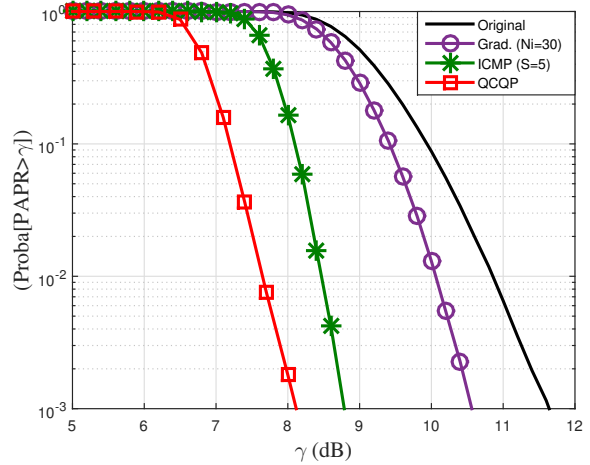


FIGURE 6.14– CCDF of PAPR for DVB-T2 system in 2K mode. Comparison between QCQP, ICMP and Gradient-based algorithms. Power constraint is set to $\Gamma=10$ dB.

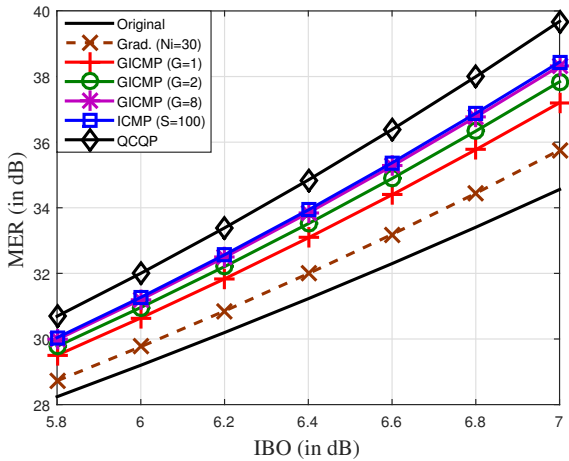


FIGURE 6.15– MER for a DVB-T2 system in 32K mode with GICMP : choice of the number of groups G . Power constraint is set to $\Gamma=10$ dB

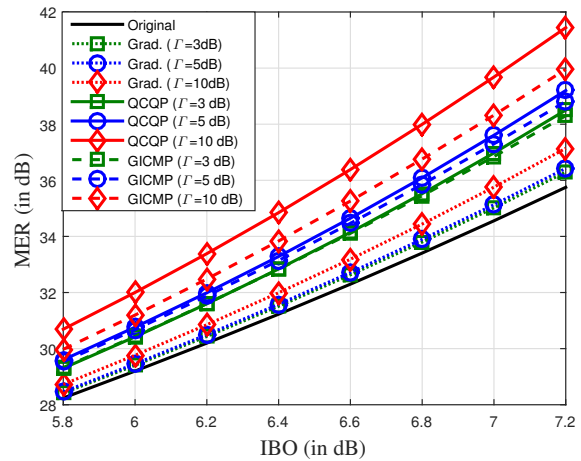


FIGURE 6.16– MER for a DVB-T2 system in 32K mode with GICMP : influence of the power constraint Γ . GICMP parameters are $S = 100$ and $G = 8$.

to be optimized is however the number G of PRTs groups. In that perspective, Fig. 6.15 gives the MER plots when G varies from $G = 1$ (i.e. considering all the 288 PRTs once) to $G = 8$ (i.e. considering 8 iterations of 36 PRTs). It appears that GICMP almost converges to ICMP at $G = 8$ meaning that the performance degradation expected from the grouping and kernel aggregation approach becomes negligible. Then, the choice of G only relies on complexity and latency considerations. In any case, we conclude that the proposed algorithm solves the latency issue identified as one of the major drawback of the gradient-based solution.

We finally provide provided additional results obtained when changing the power constraint Γ applied to the PRTs. Fig. 6.16 gives the MER curves for the different algorithms for Γ varying from 3 to 10 dB. Interestingly, the proposed GICMP algorithm yields quasi-optimal results at very tough power constraint, i.e. for 5 and 3 dB. This proves the ability of the proposed algorithm to accomodate for the power constraint contrary to the gradient-based solution.

► complexity/latency/performance analysis

In this paragraph, we give a synthetic view of the studied and proposed algorithms comparing their respective complexity, latency and performance. Table 6.3 summarized the main concluding points extracted from the simulations and preceding analyses.

TABLE 6.3– Comparison analysis of different TR algorithms for DVB-T2 and ATSC 3.0.

Criteria	DVB-T2 TR	QCQP	ICMP	GICMP
Performance	Poor --	Optimal +++	Quasi-optimal ++	Quasi-optimal ++
Complexity	Very low +++	Very high ---	Low ++	Medium +
Latency	high --	Very high ---	Medium [†] -/+	Low +++
Real time kernel generation	No -	No -	Yes ^{††} +	Yes ^{††} +
Efficient power use	No -	Yes ++	Yes +	Yes +

† : depends on the number of reserved tones

†† : Can be done with simple phase shift operations

TABLE 6.4– Average MER gain vs power levels.

	Class AB MER	Doherty MER
No PAPR reduction	35.9 dB	37.0 dB
GICMP, PC=3 dB	37.5 dB (+ 1.6)	38.6 dB (+1.6)
GICMP, PC=5 dB	38.0 dB (+ 2.1)	39.0 dB (+2)
GICMP, PC=10 dB	38.2 dB (+ 2.3)	39.2 dB (+2.2)

For all the algorithms, latency is essentially due to the number of iterations needed to reach the optimal (QCQP) or yield satisfying results (gradient, ICMP, GICMP). It has to be understood that each iteration of each of the algorithms needs a complete scanning of the OFDM symbol under process (i.e. N clock cycles) for the detection of the maximum or set of maximum peaks. As a new OFDM symbol frame is expected to be output also every N clock cycles, PAPR reduction can be accommodated by the processing platform only if an overclock factor roughly equivalent to the number of iterations is used. Hence, the gradient-based algorithm leads to either a prohibitive number of iterations, or to very poor results. In classical ICMP, the number of iterations is equal to the total number of reserved subcarriers, while in GICMP it is equal to the number of groups. This explains the substantial decrease in the implementation latency.

As for the complexity, ICMP and GICMP algorithms turn out to be more complex than the gradient-based algorithm due to the optimal phase computation of Eq. (6.25) involving S complex values. This complexity is even increased with GICMP owing to the parallel computing of R/G phase values in parallel. However, ICMP and GICMP algorithms trade complexity for substantial performance improvement, which makes them much more promising algorithms.

► Testbed measurements

To go further in the performance analysis of the proposed algorithms, we took the opportunity of a the PAPRICA project to lead MER measurements on a real testbed hosted by an industrial partner. The goal was to evaluate the impact of the PAPR reduction on the system as a whole. The platform was equipped with a complete DVB-T2 modulator set integrating the GICMP algorithm, a digital predistortion stage and a radio front-end embedding a Class AB or a Doherty amplifier.

Many measurements have been led among which the MER performance evaluation using different power constraints $\Gamma = \{3, 5, 10\}$ dB. As an example, the MER vs time measurements for the Doherty amplifier have been plotted in Fig. 6.17. The figure exhibits the MER evolution during the transmission of 8 successive DVB-T2 superframes of about 250ms, with some null signal between each superframe. In each case, the total output power and the IBO are fixed for all the tested configurations. As evident from the plots, it is confirmed that the used of the GICMP algorithm leads to a clear improvement of the MER. The long term measurements have been reported in Table 6.4 for both amplifiers. We then conclude that 2 dB improvement can be expected with the algorithm as soon as the power boost exceeds 5 dB.

As PAPR reduction is expected to yield power efficiency improvement of the transmission chain, further tests

2. Practical design of PAPR reduction algorithms

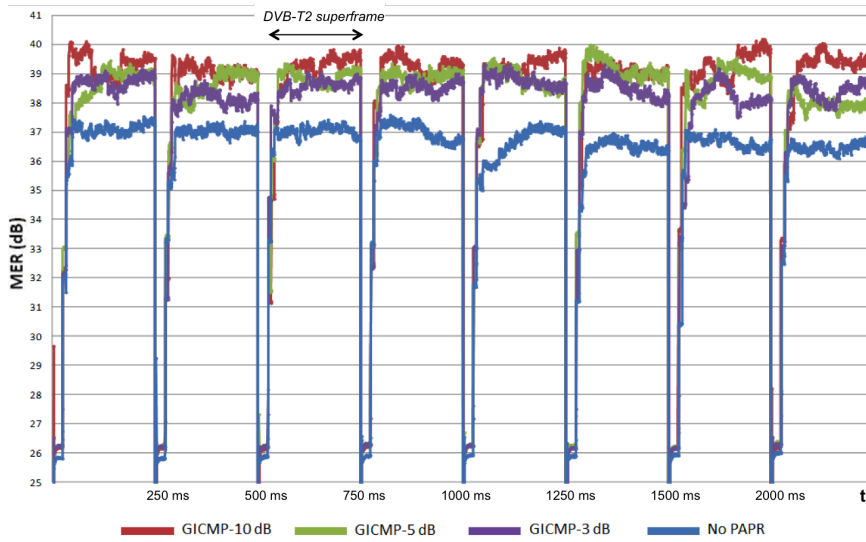


FIGURE 6.17– MER vs time measurements with Doherty test amplifier at output power 210 W.

TABLE 6.5– Average power consumption at a target MER of 36 dB

	No PAPR reduction	GICMP, PC=5 dB
Power consumption	313 W	284 W

were conducted at the level of the power consumption of the amplifier. More precisely, when PAPR algorithm was activated, we tried to reduce the power supply of the amplifier to modify the power consumption until achieving a target MER at constant output power. As shown in table 6.5, we managed to reduce the consumption of the amplifier of about 10% only constraining the power boost of the reserved tones to 5 dB. This reduction in energy consumption confirms the “green” benefit of the proposed algorithm at a time when all transmitter manufacturers are working at improving the energy efficiency of their systems.

2.6 CONCLUSION

Even if PAPR reduction has been a widely studied topic for more than 20 years, no practical implementation of any algorithm have been adopted in commercial products by now. As we worked in some collaborative projects with device manufacturers in the field of TV transmitters, we had the opportunity to better understand the major constraints and issues to address for practical implementation of PAPR reduction algorithms. From the good performance/latency/complexity trade-off shown in the foregoing sections, the proposed ICMP but especially GICMP algorithm, can be considered as a good candidate for future implementations of DVB-T2 and ATSC3.0 green transmitters.

Further works on PAPR reduction and green transmitter design have still to be conducted, especially trying to integrate in a unified model the whole transmission chain characteristics. This is the aim of the subject introduced in the following section.

Summary (PhD/Dissemination/Projects)

- 1 PhD (R. Mounzer) and 1 Post-Doc (K. Bulusu)
- 1 submitted publication to IEEE Transactions on Broadcasting
- 1 patent [P.2]
- 4 communications in international conferences and workshops [C.8][C.22][C.24][C.30]
- 1 regional project (PAPRICA) and 1 Eurostar project (GreenTEA)

3 THEORETICAL ANALYSIS OF JOINT PAPR REDUCTION AND PREDISTORTION

3.1 MOTIVATION

As previously explained, the two main methods usually advocated in literature to mitigate the effects of power amplifier non-linearity are the PAPR reduction and linearization techniques, respectively. Hence, complementary to the PAPR reduction techniques discussed in the previous section, the optimization of the overall performance of a transmitter can be improved by means of linearization techniques which try to compensate for the power amplifier non-linearities

Two approaches can then be followed for the combination of the PAPR reduction and linearization techniques : non-collaborative approach and joint approach. The non-collaborative approach simply consists in cascading a PAPR reduction module and a linearization one, letting them operate independently. Indeed, the PAPR reduction parameters are optimized and adjusted independently from the linearization and vice versa. However, many studies focusing on the performance results associating PAPR reduction and linearization techniques have highlighted some opposite effects due to mutual interactions between the two functions [SPCK04, KC06, HCVG09, RL03, RHL⁺04, BAT⁺11, CY09]. As a result, the non-collaborative approach appears as being simple however sub-optimal. To avoid this, it makes sense to envisage a collaborative or joint treatment guaranteeing the global optimal usage of the power amplifier.

Numerous simulation results exist in the literature concerning these two approaches. Yet, only few contributions have been made on the analytical aspects, for example providing expressions of in-band or out-of-band distortions of the transmitted signals [GOU13, KHNSL12, H⁺13]. Having a complete and unified analytical model would however be beneficial to predict the overall performance of the system depending on the implemented algorithms for PAPR reduction and linearization. Besides, such a model would allow for a better understanding of the abovementioned mutual effects and provide useful analytical tools towards a global transmitter optimization.

During the TEPN project (Towards Energy Proportional Networks) taking part of the CominLab LabeX framework, we launched a PhD program with the aim of providing new contributions on the analytical level for the performance evaluation of transmitter architectures embedding PAPR reduction and linearization modules.

3.2 TRANSMITTER ARCHITECTURE MODEL

Our studies have been based on a generic block diagram of the transmission chain with clipping and predistortion stages preceding the PA, as depicted Fig. 6.18. The multicarrier signal $x_1(t)$ becomes $x_2(t)$ after clipping, and $x_3(t)$ after the predistortion operation. The output of the PA is $z(t)$. Such a model can then be particularized specifying the effectively used algorithms or components as detailed hereafter. From such an architecture, the idea will be then to derive the analytical expressions for some commonly used figures of merit revealing the level of signal distortions at the output of the power amplifier, e.g. EVM (Error Vector Magnitude) or ACPR (Adjacent Channels Power Ratio).

► PAPR effects modeling

Thanks to the central limit theorem, it is well accepted that OFDM signals with a large number of subcarriers can be approximated by a complex Gaussian random process with zero mean [BLG02]. However, after PAPR reduction, the distribution of the signal may change, or at least its parameters. Although numerous PAPR algorithms are available in the literature, there have been very few studies at the level of the theoretical modeling of such algorithms to understand their effect on the signal statistics modification before and after PAPR reduction. The only contributions concern the probabilistic PAPR reduction methods [BFH96, MH97, BP08] which are however not downward compatible. As far as tone reservation methods are concerned, the distribution of the signal after PAPR reduction is likely to be different for each method depending on the additive signal $c(t)$. Therefore, it is not straightforward to provide a unified framework on this aspect. Such a question is indeed part of the research topics I propose to address as perspectives in Chap. 9. However, in the work done these

3. Theoretical Analysis of Joint PAPR Reduction and Predistortion

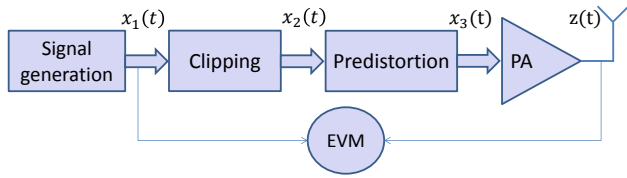


FIGURE 6.18– Generic block diagram model of a transmitter equipped with PAPR and predistortion functions.

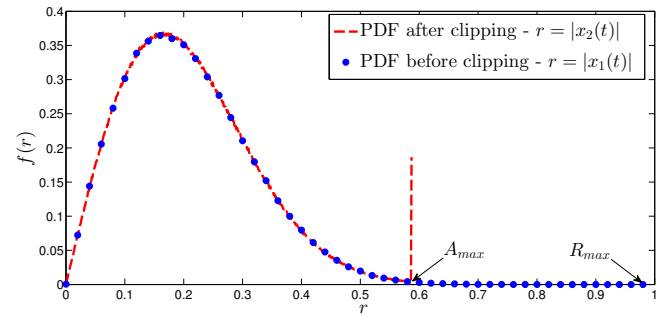


FIGURE 6.19– Probability density function of the signal amplitude before and after Clipping.

last years, we have focused our attention on the clipping technique due to its popularity and its straightforward reduction gain. It is then rather simple to predict the probability density function (PDF) of the amplitude of the output signal.

Let us consider the clipping function using the following relationship between the input and the clipped signal

$$x_2(t) = \begin{cases} x_1(t) & \text{if } |x_1(t)| \leq A_{max} \\ A_{max} e^{j\phi(x)} & \text{if } |x_1(t)| > A_{max} \end{cases} \quad (6.31)$$

with A_{max} the amplitude of the clipping threshold. The amplitude PDF f_{x_2} of the clipped signal can then be simply written as

$$f_{x_2}(r) = \begin{cases} \frac{2r}{P_{x_1}} e^{-\frac{r^2}{P_{x_1}}} & \text{if } r < A_{max} \\ e^{-\Lambda} & \text{if } r = A_{max} \end{cases} \quad (6.32)$$

where r is the magnitude of the signal, P_{x_1} the average power of the input signal $x_1(t)$ and Λ is defined as the clipping power ratio, i.e. $\Lambda = \frac{A_{max}^2}{P_{x_1}}$. The second line ($r = A_{max}$) is simply obtained integrating the Rayleigh PDF from A_{max} to $r \rightarrow \infty$. Fig. 6.19 presents the amplitude distribution of the input signal $x_1(t)$, and the clipped signal $x_2(t)$. In our study, we have thus assumed that PAPR reduction could be modeled as obtaining a signal $x_2(t)$ which amplitude follows the PDF given by (6.32) controlled by a single parameter Λ .

► Power Amplifier Models

One central aspect of the proposed work is to integrate accurate models for the power amplifier since it is the key element which brings distortions on the signal. Conventional static power amplifier models, such as AM/AM and AM/PM characteristics, can represent, with reasonable accuracy, the power amplifier behavior driven by narrowband input signals. However, in practice the actual amplitude and phase of the high PA output voltage are not only determined by the current input voltage. In reality, the output of high power amplifiers such as those used in wireless base stations depend on the instantaneous inputs, but also on the previous inputs too. This kind of phenomenon is described as memory effects and it is illustrated in Fig. 6.21. Besides, wideband signals also tend to induce memory effects in the PA. In such cases, memoryless models can be ineffective. Thus, accurate representation of the memory effects is crucial as further detailed in [VRM01].

During the past few decades, various models have been proposed trying to reflect with more or less accuracy the true behaviour of power amplifiers. A broad view on the subject can be given by distinguishing three types of models : memoryless and quasi-memoryless models, and models with memory. As already introduced in section 2.5, the most popular but simple model were proposed by Rapp [Rap91] for amplifiers based on semiconductors (SSPA). This Rapp model is memoryless, i.e. its output at a determined time instant does not depend on the previous entries. In addition, it does not present any phase distortions. The AM/AM transfer curve of the PA is then given by

$$H_{PA}(r) = \frac{r}{\left(1 + \left(\frac{r}{A}\right)^{2b}\right)^{\frac{1}{2b}}}, \quad (6.33)$$

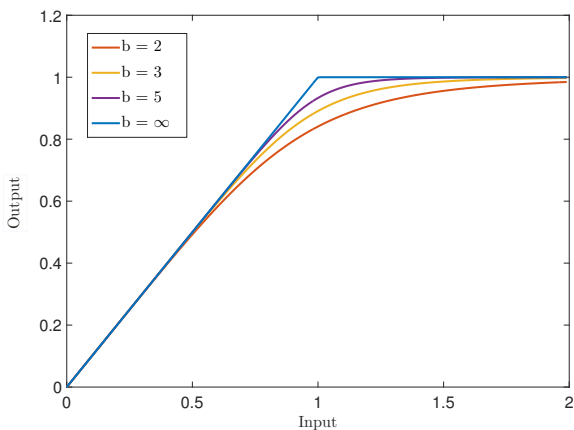


FIGURE 6.20– AM/AM power amplifier characteristics following the Rapp Model

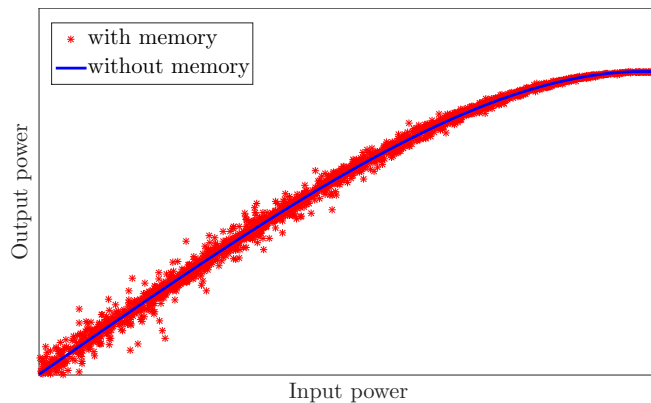


FIGURE 6.21– Example of AM/AM power amplifier characteristics with memory effects

where r is the magnitude of the input voltage, A is the amplitude of the saturation output voltage of the amplifier and b is the ‘knee factor’ parameter which controls the smoothness of the transition between the linear and the saturation zones of the characteristics. Fig. 6.20 presents the AM/AM characteristic of the Rapp model for different knee factor values with a unitary amplification gain. It has to be noted that as the value of b increases, the Rapp model approaches to a soft envelope limiter model.

Another popular and useful PA model is the memoryless polynomial model which principle relies on a parametric Taylor series expansion of the true AM/AM characteristics of a given PA [JBS00]. The PA output is then expressed in baseband by the following odd order polynomial :

$$H_{PA}(r) = \sum_{l=0}^{L_p} b_{2l+1} r^{2l+1} \tag{6.34}$$

where L_p denotes the nonlinear model order and b_{2l-1} are the polynomial coefficients⁸. Making the coefficients complex will result in a quasi memoryless polynomial model. Other models have been proposed for various amplifiers technologies as for instance the Saleh model [Sal81] for memoryless Traveling Wave Tube Amplifiers.

Finally, in the category of memory amplifier models, the most accurate model is the one based on Volterra series. A Volterra series is a combination of linear convolution and a nonlinear power series so that it can be used to describe any nonlinear stable system with fading memory. The Volterra series model can achieve higher accuracy than other memory models at the cost of very high computational complexity. More practical models have thus been proposed [BF82, GMB05, NG66], which can essentially be viewed as simplified special cases of the Volterra model. In our study, we chose to use the very popular memory polynomial model [KK01] which is also a truncation of the general Volterra series, by only keeping the diagonal terms in the Volterra kernels. Thus, the number of parameters is significantly reduced compared to conventional Volterra model, and the computational complexity of the coefficients identification is remarkably decreased. The memory polynomial model can be viewed as parallel connected memoryless nonlinear models, each with individually delayed input signal so that the outputs of the nonlinear sub-models would be summed up.

Hence, the relationship between the input and output of the memory polynomial model is given by the following equation

$$z(t) = \sum_{q=0}^Q \sum_{l=1}^L b_{lq} x(t-q\tau) |x(t-q\tau)|^{2(l-1)}, \tag{6.35}$$

where Q is the memory depth, τ is a delay parameter, L is the polynomial order and b_{lq} are complex coefficients. All these parameters reflect the nonlinearities and memory effects of the PA and can be obtained through measurements and estimation algorithms for a particular amplifier [MMK+06].

► Linearization model

8. Note that the odd order comes from the bandpass assumption of power amplifier transfer function.

3. Theoretical Analysis of Joint PAPR Reduction and Predistortion

Among the large variety of linearization techniques, digital predistortion is by far the one the most popular [Fra16, Din04, Was04]. The main principle of this technique is to apply the inverse function of the PA transfer function to cancel the nonlinearities at the PA output [INM89, SC92]. Therefore, the cascade of the predistorter and the PA gives a linear response. Letting H_{PA} and H_{PD} be the PA and predistortion baseband transfer functions, ideal computation of H_{PD} through digital predistortion theoretically leads to

$$H_{PA} \circ H_{PD} = I_d, \quad (6.36)$$

where \circ is the composite function and the I_d is the identity. The advantage of predistortion is that it is relatively easy to implement at a low cost. As such, predistortion is frequently applied, not also in research, but also in commercially available products [SSS03].

Even though the predistortion modeling and PA modeling are two different applications, the working principles of both are almost identical to each other. In fact, the PA modeling aims at finding the exact PA transfer function, while the intention of the predistortion is to estimate the inverse transfer function of PA characteristics. Nonetheless, both the PA characteristics and its inverse transfer function can be based on the same mathematical models. That is why most of PA models previously mentioned can be used in the predistortion modeling such as the Rapp model or the polynomial model for example. Hence, in the case of Rapp model, the transfer function of the predistortion module can be expressed as,

$$H_{PD}(r) = \frac{r}{\left(1 + \left(\frac{r}{A}\right)^{2a}\right)^{\frac{1}{2a}}}, \quad (6.37)$$

which has exactly the same form as (6.37), except the use of a predistortion knee factor a instead of the exact knee factor b of the amplifier⁹.

On the other hand, it is also possible to adopt the polynomial model to model the predistortion function which is a good compromise between compensation performance and complexity. Thus, the predistorted signal can be expressed as follows

$$x_{PD}(t) = \sum_{k=0}^{K_p-1} a_{2k+1} x(t)^{2k+1}, \quad (6.38)$$

with a_{2k+1} the nonlinear polynomial coefficients and K_p the parameter which determine the nonlinear model order. Note that the objective of the conventional DPD modeling is to find the inverse transfer characteristics of PA to compensate the static nonlinearity of PAs without consideration of memory effects. In practice, one is able to estimate the inverse PA characteristic using a special training signal. Consequently, the resulted DPD transfer function does not need to be adapted since the PA characteristics are assumed to be unchanged during the operating time. Many solutions exist to handle the estimation process and get the polynomial parameters a_{2k+1} , with various pros and cons in terms of stability, bandwidth capacities and complexity [MMK⁺06].

3.3 ANALYTICAL DERIVATIONS OF THE EVM

Various closed-forms of the EVM have been derived during the PhD of A. Cheaito and published namely in [R.1][R.2][C.12], taking into account the activation or not of the different modules of the system (PAPR reduction through clipping and linearization through predistortion) and the model of the power amplifier (Rapp model, polynomial model, memory polynomial model). All these contributions have consisted in leading the mathematical derivations of the EVM from the following definition,

$$EVM = \sqrt{\frac{\mathbb{E}\{|\epsilon(t)|^2\}}{\mathbb{E}\{|x_1(t)|^2\}}} \quad (6.39)$$

$$\text{with, } \epsilon(t) = z(t) - x_1(t) \quad (6.40)$$

9. Perfect linearization would be performed with $a = b$.

While it is obvious that the denominator of the EVM is simply representing the input signal power P_{x_1} , we also understand that the computation of the numerator needs some efforts. Given that $\epsilon(t)$ can be seen as a complex random variable $\epsilon(r, \theta)$ with uniformly distributed phase θ , the derivation that should be led can be stated as :

$$\mathbb{E}\{|\epsilon|^2\} = \int_0^{2\pi} \int_0^\infty |\epsilon(r, \theta)|^2 \frac{1}{2\pi} f_R(r) dr d\theta \quad (6.41)$$

with $f_R(r)$ the PDF of the amplitude of ϵ which results from the activation of the clipping function or not (according to (6.31)) but also on the power amplifier and predistortion models. The computation can then take various forms. The results obtained in the cases of the Rapp model and the polynomial model are briefly summarized in the following paragraphs.

► **Rapp model amplifier case**

In the Rapp model case, let us recall that the non linearities only affect the amplitude of the input signal. In the most general case when considering a clipping threshold of A_{max} and combining the transfer functions of the predistortion and the power amplifier, Eq. (6.41) can be restated as,

$$\mathbb{E}\{|\epsilon|^2\} = \underbrace{\int_0^{A_{max}} |r - H_{EQ}(r)|^2 f_r dr}_{I_1} + \underbrace{\int_{A_{max}}^\infty |r - H_{EQ}(A_{max})|^2 f_r dr}_{I_2} \quad (6.42)$$

where,
$$H_{EQ}(r) = \frac{r}{\left(\left(1 - \left(\frac{r}{A}\right)^{2a}\right)^{\frac{b}{a}} + \left(\frac{r}{A}\right)^{2b} \right)^{\frac{1}{2b}}}$$

The first integral form I_1 corresponds to the distortion term due to the amplification non-linear effects which remains when imperfect predistortion is used (i.e. $b \neq a$). The second term is essentially coming from the clipping effect. After some manipulations, these two integral forms can be derived and an analytic expression of the EVM is obtained as stated below. The proof yielding this general result is given in [R.2].

Contribution II.7 (Analytic Expression)

EVM – Rapp model The EVM of a clipped and amplified multicarrier signal assuming a Rapp model for the power amplifier and the predistortion module is

$$\begin{aligned} \text{EVM} = & \left[1 + G_{clip} \left(1 - \frac{2\Gamma\left(\frac{3}{2}, \Lambda\right)}{\sqrt{G_{clip}}} \right) \Lambda e^{-\Lambda} \right. \\ & \left. + \sum_{i=0}^{+\infty} \left[\binom{-\frac{1}{b}}{i} - 2 \binom{-\frac{1}{2b}}{i} \right] \sum_{j=0}^{+\infty} \binom{-\frac{b}{a} \left(\frac{1}{2b} + i\right)}{j} \times (-1)^j \frac{\gamma(a j + b i + 2, \Lambda)}{\left((1 - e^{-\Lambda}) \text{IBO} \right)^{a j + b i}} \right]^{1/2}. \end{aligned} \quad (6.43)$$

with IBO the power back-off applied to the input signal, Λ the clipping ratio defined in (6.32) and G_{clip} the gain of the predistorted amplifier at the clipping threshold,

$$G_{clip} = \left| H_{EQ} \left(\sqrt{\frac{\Lambda}{(1 - e^{-\Lambda}) \text{IBO}}} \right) \right|^2 \quad (6.44)$$

The obtained EVM expression only depends on the IBO, clipping ratio Λ and the power amplifier and predistortion parameters (knee factors a and b). Also, the form can be particularized in the case when no clipping is operated, taking $\Lambda \rightarrow \infty$. In that case, the first term of the expression tends to unity and the incomplete lower Gamma function $\gamma(x, \Lambda)$ tends to the complete Gamma function $\Gamma(x)$ in the second term. Also, if no predistortion is used, it can be proven that the same expression is obtained simply discarding the terms involving the a knee factor [R.1].

3. Theoretical Analysis of Joint PAPR Reduction and Predistortion

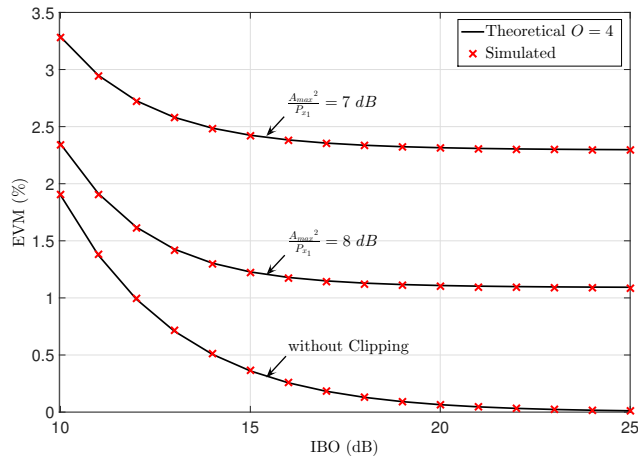


FIGURE 6.22– Theoretical and simulated EVM versus IBO without predistortion. Knee factor is $b = 1.6$

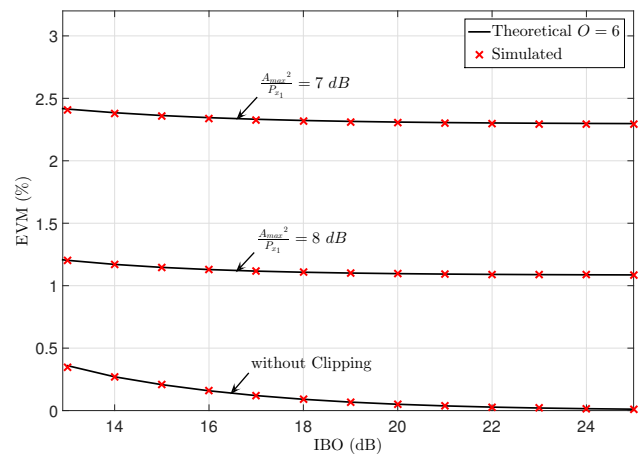


FIGURE 6.23– Theoretical and simulated EVM versus IBO with predistortion. Knee factors are $a = 1.5$ and $b = 1.6$.

Even if the obtained formula can not be considered as a closed-form due to the infinite series expansion, we verified that an evaluation at a reasonable order is sufficient to get a very good accuracy of the EVM. This can be observed in Fig. 6.22 and Fig. 6.23 which gives some EVM curves obtained in simulation and applying the theoretical expressions at finite order, namely $\mathcal{O} = 4$ without predistortion and $\mathcal{O} = 6$ with predistortion. The fact that a higher order is needed in the predistortion case is due to the two non-linear functions involved in the computation (amplifier and predistortion gains) instead of a single one when no predistortion is used.

Above all, these curves reflect the two main expected effects owing to clipping and predistortion. On one hand, when clipping is activated, we observe that the threshold Λ directly affects the EVM floor. As commonly known, the lower the clipping threshold, the larger the EVM. However, the proposed analytical expressions provide numerical prediction of the degradation. On the other hand, when predistortion is used, the EVM values at low IBO are significantly reduced while their floor values are not changed. This reflects the linearity improvement of the predistorted power amplifier which can directly be forecast through the proposed expressions.

► Polynomial model case

In the polynomial model case, $|\epsilon|$ is obtained using the polynomial expression given in Eq. (6.34) for $z(t)$. In the general case, the polynomial coefficients are complex and the non linearities now affect the amplitude and the phase of the input samples, which means that the complete computation of Eq. (6.41) has to be led. After some manipulations detailed in [R.2], it is possible to extract from Eq. (6.41) four integral forms leading to complete and incomplete Gamma functions. The final obtained result is given in Contrib. II.8.

The EVM expression in (6.45) only depends on the input back-off, clipping ratio Λ and on the polynomial coefficients. Note that the predistortion effect is simply taken into account through these coefficients, since a predistorted non-linear amplifier can be represented by an equivalent polynomial with new coefficients. Indeed, the residual non linearity effects are reflected by the two summations over k and k' . In particular, it is verified that EVM equals zero when $b_1 = 1$ and $\forall k > 1, b_k = 0$, i.e. for a perfectly linear normalized amplifier. This will be namely obtained with a perfect predistortion. As in the case of the Rapp model, it is also possible to get the EVM expression when no clipping is applied, by letting $\Lambda \rightarrow \infty$. In that case, the exponential terms disappears and the incomplete Gamma functions simply tend to factorial functions (since their arguments are integers).

Interestingly, contrary to the Rapp model, the obtained expression here is a closed-form. As most of power amplifiers can be accurately approximated with polynomial representation of sufficient order, this gives a high importance to the proposed result. Note that even a Rapp amplifier can be modeled using polynomial formulation. In Fig. 6.24 for example, we give the EVM versus IBO curves obtained with our closed form, but modeling the Rapp amplifier with a polynomial form of order $K = 6$. The very good match between the simulated and theoretical results confirm the validity and accuracy of the closed-form. In Fig. 6.25, the same kind of results are given but now using a true amplifier used for DVB-T2 applications [NXP10] and for which a polynomial form of order $K = 6$ has been used. Again we conclude that our closed-form is valid.

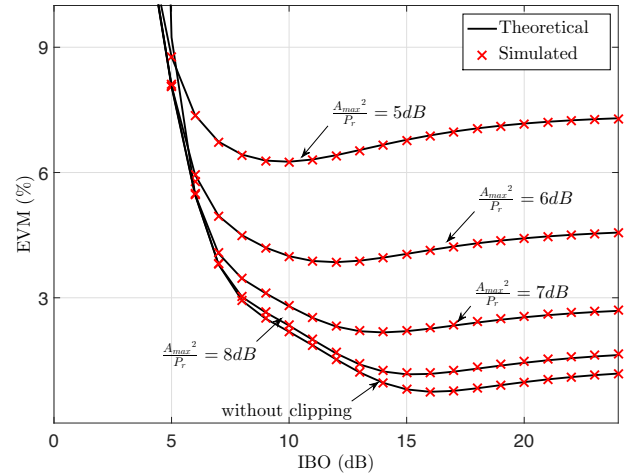
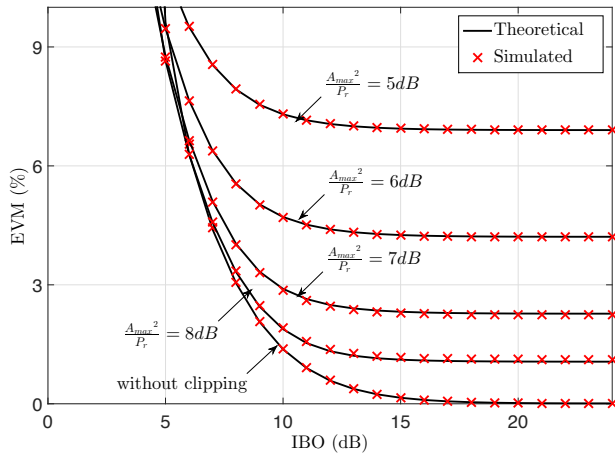


FIGURE 6.24– Theoretical and simulated EVM versus IBO for a Rapp amplifier without predistortion. Polynomial representation of order $K = 6$ is used, for an original knee factor of the Rapp model of $b = 2$.

FIGURE 6.25– Theoretical and simulated EVM versus IBO for a DVB-T amplifier [NXP10] without predistortion. Polynomial representation of order $K = 6$ is used.

Contribution II.8 (Analytic Expression)

EVM - Polynomial model

The EVM of a clipped and amplified multicarrier signal assuming a polynomial model for the power amplifier and the predistortion module is

$$EVM = \left[1 + \sum_{k=1}^K \sum_{k'=1}^K v_{kk'} \left(\gamma(k+k', \Lambda) + \Lambda^{k+k'-1} e^{-\Lambda} \right) - u_k \left(\gamma(k+1, \Lambda) + \Lambda^{k-\frac{1}{2}} \Gamma\left(\frac{3}{2}, \Lambda\right) \right) \right]^{\frac{1}{2}} \quad (6.45)$$

where u_k and $v_{kk'}$ are defined as,

$$u_k = 2 \frac{\Re\{b_k\}}{\left((1 - e^{-\Lambda}) IBO \right)^{k-1}} \quad \text{and,} \quad v_{kk'} = \frac{b_k b_{k'}^*}{\left((1 - e^{-\Lambda}) IBO \right)^{k+k'-2}} \quad (6.46)$$

with $\{b_k\}_{1 \leq k \leq K}$ the coefficients of the polynomial model of order K .

► Memory Polynomial model case

The last case of our study was to take into consideration memory effects which are known to have a strong influence on signal distortion. This case can be seen as a generalization of the polynomial case discussed before. Derivations are quite similar as in the non-memory polynomial case, but a bit trickier because of the refined model of Eq. 6.35. The complete derivations have been published in [R.1] and the final result is provided in Contrib. II.9 hereafter.

Eventually, when memory effects are taken into consideration, the EVM closed-form is similar to that obtained with the memoryless polynomial model except in the definition of parameter $v_{kk'}$ which now integrates the contribution of memory coefficients, i.e. with index $q > 0$. From this closed-form, it is then possible to analyze the impact of memory on the EVM. In Fig. 6.26, we give the EVM curves using a power amplifier with fifth odd-order nonlinearity ($K = 5$) and memory depth of $Q = 0$ or $Q = 2$. The values of the polynomial coefficients b_{kq} , which are taken from [D⁺04], were extracted from an actual Class AB PA.

3. Theoretical Analysis of Joint PAPR Reduction and Predistortion

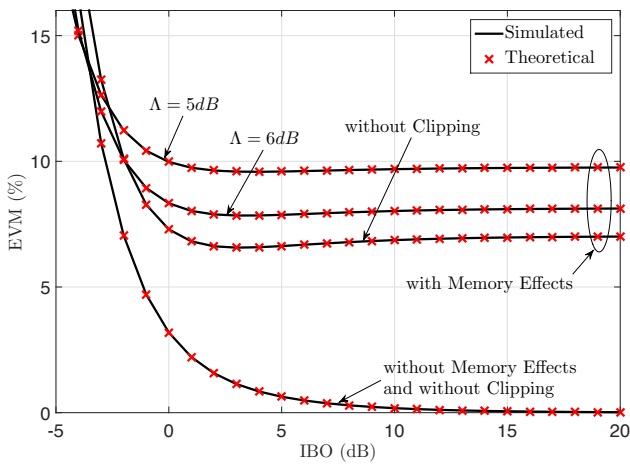


FIGURE 6.26– Theoretical and simulated EVM as a function of the IBO, with and without clipping, with and without memory effects ($Q = 2, K = 5$).

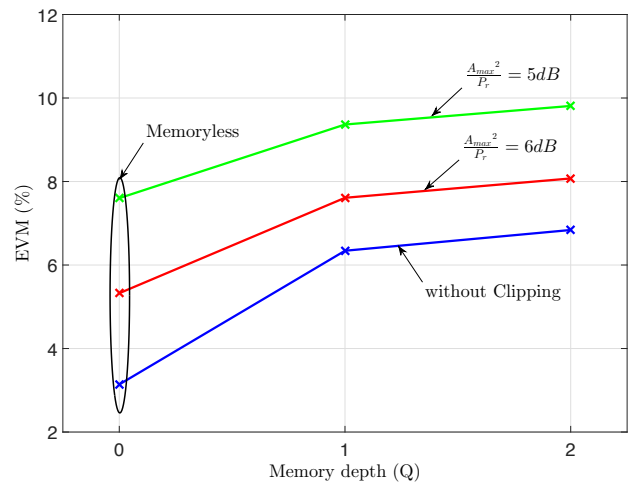


FIGURE 6.27– EVM as a function of the memory depth at IBO=10 dB.

Contribution II.9 (Analytic Expression)

EVM - Memory Polynomial model The EVM of a clipped and amplified multicarrier signal assuming a memory polynomial model for the power amplifier and the predistortion module is given by Eq. (6.45) where u_k and $v_{kk'}$ are restated as,

$$u_k = 2 \frac{\Re\{b_{k0}\}}{\left((1 - e^{-\Lambda})\text{IBO}\right)^{k-1}} \quad \text{and,} \quad v_{kk'} = \sum_{q=0}^Q \frac{b_{kq} b_{k'q}^*}{\left((1 - e^{-\Lambda})\text{IBO}\right)^{k+k'-2}} \quad (6.47)$$

with $\{b_k\}_{1 \leq k \leq K, 0 \leq q \leq Q}$ the coefficients of the polynomial model of order K and memory depth Q .

From the comparison between the theoretical (star markers) and simulated (continuous lines) results, we first conclude that our analytical evaluations perfectly match the simulated EVM. Besides, these results allow us to highlight the significant difference between the EVM of the amplified signal using memory and memoryless PA models. In particular, EVM curves reach a floor at high IBO when memory effects are taken into account. Indeed, a strong performance loss is obtained at large IBO values, however corresponding to expected linear regions of the PA characteristics. This proves that the memory effects can not be ignored in practice and may even become predominant compared to non-linearity effects. In addition, it appears that clipping leads to smaller performance degradations than the memory effect, once again proving the necessity of introducing the memory effects in analytical models.

To further quantify the weight of the memory effects on EVM results, Fig. 6.27 depicts the EVM as a function of the memory depth, for an IBO of 10 dB and different clipping thresholds. These curves are obtained from the proposed closed-form. As expected, the deeper the memory of the amplifier, the stronger the EVM. Hence the memoryless polynomial model ($Q = 0$) is not sufficient for modeling the power amplifier behavior when the memory effects are present. For example, when clipping is deactivated, the EVM of amplified signals using memoryless polynomial model is 2.5%. However, using memory polynomial model with memory depth of 2, the EVM increases to 6.8% which is quite significant.

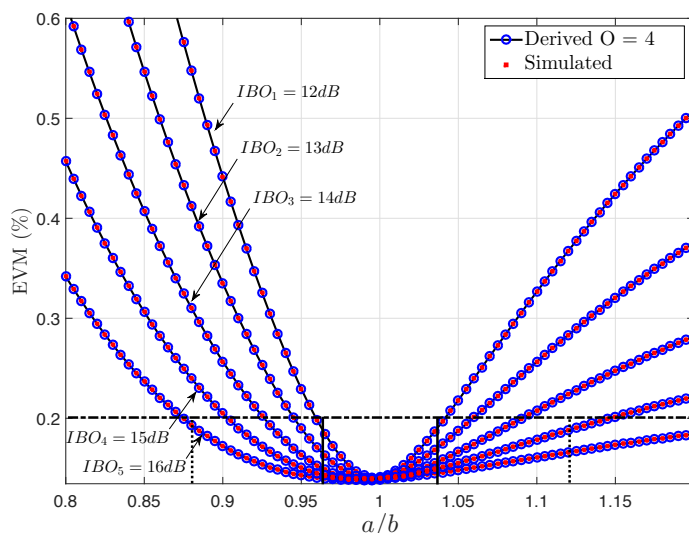


FIGURE 6.28– EVM chart for the Rapp model. EVM is given versus predistortion accuracy for variable IBO. Clipping ratio is 10 dB.

3.4 APPLICATION TO OPTIMAL SETTING OF THE TRANSMITTER

From the obtained analytical expressions of the EVM, it is now possible to carry out thorough analyses of the global behavior of a transmitter depending on the various identified parameters. The aim is to find optimality behavior regimes of the transmitter regarding some signal quality constraints. For instance, given a particular power amplifier, a major question that arises in practice is how to control both the clipping ratio and the predistortion accuracy to respect some target EVM according to standard specifications, while maximizing the power efficiency of the amplifier.

In the case of the Rapp model for example, it is possible to build some EVM chart gathering several EVM curves versus the quality of the predistortion function for various IBO values. The predistortion accuracy can be simply represented by the ratio between the knee factors of the amplifier and the predistortion functions, i.e. a/b . An example of such chart is given Fig. 6.28, for a clipping ratio of 10 dB. The optimal operating point is when $a = b$ but means high complexity is spent to estimate the amplifier response and have tight predistortion. But we note that some degree of freedom can be exploited considering some target EVM, (for instance 2% represented here which corresponds to the average EVM in the DVB-T2 requirements). Namely, the chart shows how some less accurate predistortion can be tolerated if some IBO margin is taken. Conversely, maximizing the power efficiency and thus reducing the IBO as much as possible, imposes a minimum accuracy of the predistortion function. Hence, such chart can be useful in the perspective of finding some adequate trade-off between power efficiency and complexity.

In the case of the polynomial model, it is even possible to go a bit further in the analysis. Let us consider the chart of Fig. 6.29 consisting of EVM curves versus IBO for various clipping ratios Λ . The power amplifier considered here is of order $K = 6$, with coefficients extracted from [NXP10]. The predistortion complexity is represented by the order of the polynomial used for the linearization ($K_p = 5$). The optimal operating regime of the transmitter is easily identified as being the curve corresponding to the lower limit of the network of curves, i.e. for which EVM is minimized at each IBO. Then plotting such optimal curves for various orders of the predistortion polynomial yields the results of Fig. 6.30. This final chart allows to find the adequate IBO to use for a given predistortion complexity for a given target EVM. Thanks to the proposed closed-forms, these charts are easy to build and only need the knowledge of the polynomial coefficients of the power amplifier.

3. Theoretical Analysis of Joint PAPR Reduction and Predistortion

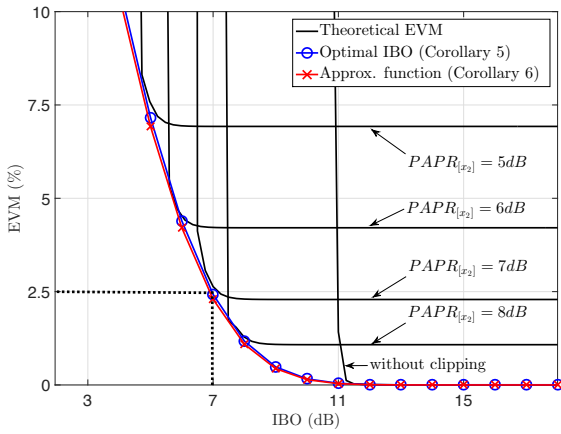


FIGURE 6.29– EVM chart for the Polynomial model. EVM is given versus IBO for variable clipping ratios. Power amplifier is of order $K = 5$ and predistortion of order $K_p = 5$.

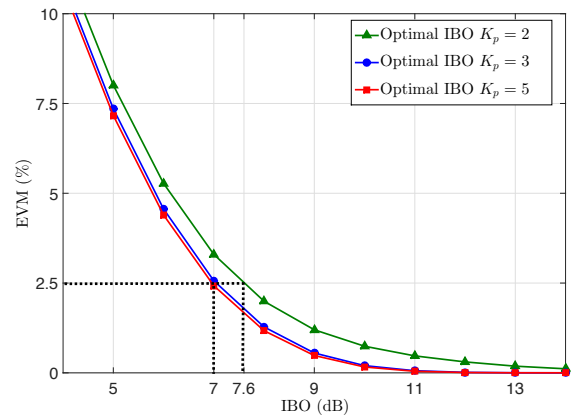


FIGURE 6.30– Final EVM chart for the polynomial model. EVM is given versus IBO for variable predistortion orders. Power amplifier is of order $K = 5$.

3.5 CONCLUSION

This study comes at a complement to the algorithmic studies on PAPR reduction detailed before, with a more theoretical approach and wide scope. Our aim was to provide new analytical tools for the overall optimization of transmitters. On this subject, only upper-bounds or approximated expressions were available in the literature, which was not bringing sufficient insight into the performance and interactions between the various modules of transmitters. The derived analytic forms are a first attempt towards the elaboration of a complete set of analytic laws that are expected to help designing and properly setting the different modules of a transmitter. The first provided charts already show how it is possible to play with many degrees of freedom, address some performance/efficiency/complexity trade-off and evaluate their impact. However, as it will be detailed in my research perspectives, additional efforts are still needed to have a complete set of tools.

Summary (PhD/Dissemination/Projects)

- 1 PhD (A. Cheaito) and 1 Master Internship (S.M. Fahad)
- 2 international journal papers [R.1][R.2]
- 5 communications in international conferences and workshops [C.2][C.11][C.12][C.23][C.25]
- 2 communications in national conferences [N.1][N.3]
- 1 Best paper award [C.12]
- 1 invited talk at IEEE Globecom 2017, Special session on selected Wireless Communications Letters
- 1 project LabeX project (CominLab TEPN)

Optimization of the Wireless Broadband Access

Chap. 7

There is no science in this world like physics. Nothing comes close to the precision with which physics enables you to understand the world around you.

– Neil de Grasse Tyson –

Selected Topics

In this chapter, I will present the main contributions of my research at the level of wireless broadband communication systems, with a special focus on the general idea of spatial filtering. During the last years, spatial filtering concepts, also commonly referred to as beamforming or spatial precoding, have progressively been introduced in many communication models hereby revealing some new paradigm we have been trying to appropriate and exploit for new system optimizations. To highlight our contributions on this topic, I have selected the three following aspects of the work :

1. Time Reversal Based Communications : Performance Analysis for Single-User Transmission
2. Spatial Filtering for MU-MIMO : Spectral Resource Optimization in Moderate-Scale Antenna regime
3. Practical Spatial filtering Strategies for massive MIMO mmWave Communications

1 ANALYSIS OF TIME-REVERSAL BASED COMMUNICATIONS

1.1 MOTIVATIONS

As already reminded in section 6, multiple antenna concepts have brought about a real revolution in the field of wireless communications. Looking back to the late 1990s, the seminal works of Foschini, Telatar, Calderbank, Tarokh and others [Fos96, Tel99, TSC98] were promising impressive capacity gains behind the ever-considered single link Shannon limit. MIMO has thus rapidly been viewed as a goldmine of researches and developments, not solely for academics but also for system designers and network operators who were already facing exponential bitrate demands. Therefrom, MIMO has become a key technology in the evolution of wireless systems.

In the early years of its existence, MIMO was essentially considered as a new degree of freedom upon which some additional channel diversity (spatial) could be reaped to fight against selectivity and multipath effects. MIMO integration in system models were thus carried out following the same general approach as that used when dealing with frequency and time diversities. The main first contributions on MIMO systems were hence at the level of space-time code design (in addition to the essential synchronization and channel estimation issues) [TJC99, ZG02, GH03, LV07].

Around 2005, a new vision of MIMO attracted interest through the multiuser dimension of many communication system models. Multiuser downlink scenarios were considered with the idea of using a set of single antenna users as a virtual antenna array [SSH04, CM04]. Spatial multiuser diversity could then be exploited to send data streams in parallel targeting different users. Hence was introduced the concept of MU-MIMO, and accordingly the idea of spatial division multiple access (SDMA). In 2003 Caire and Shamai had already shown in [CS03] that Dirty Paper Coding strategies could succeed in achieving the capacity region of the downlink broadcast channel¹. However, the design of optimal Dirty Paper Coding turns out to be a hard non-linear problem, and, more importantly, the fundamental assumption that channel state information should be available at the transmitter (CSIT) was not convincing practical system designers. CSIT was historically an advantage reserved to static transmission systems, as for example wired communications.

Hence, in the late 2010s, one major question that arose in the optimization of MIMO systems (and that has not found a definite answer until today) was mainly related to the practical design of MU-MIMO schemes, using linear spatial treatments at the transmitter and that could accommodate limited channel feedback from the users. Such spatial domain linear operations can be called **spatial filters** as they act on the spatial branches and modify their complex gains. Such filters have to be continuously adapted to the propagation conditions to make the communication to multiple users well established, and possibly be non-interferent. With this spatial filtering perspective, time-reversal techniques appeared to us as a potentially well suited candidate as it will be further explained. We therefore started some preliminary studies in 2008 and launched a PhD program (T. Dubois) on that subject in 2009 in parallel with an ANR project (TRIMARAN). Hereby, we first focused on single user scenarios (SU-MIMO). In 2011, a second PhD started (H. Fu) to work on complementary analyses in the SU-MIMO case and extend them to the MU-MIMO context. In parallel to this, important hardware developments were led within the research team with other colleagues to provide proof of concepts of our studies [C.32]. These latter aspects will be further discussed in the proposed perspective works in section 9.

1.2 TIME REVERSAL FILTER CONCEPT

► Origin

The time-reversal concept takes its origin from the research works of Fink *et al.* on ultra-sound and underwater acoustic waves in the 1990s [Fin92, DTF99]. Based on the acoustic wave propagation equation, Fink demonstrated that it was possible to re-create an acoustic impulse at a precise source location, by generating adequate waves from an infinite number of transducers surrounding that source in a closed contour. The waves to generate for this should exactly correspond to the time-reversed versions of those measured by the transducers during a first step, called sounding phase, when the source emits an impulse. Fink based his proof of the time-reversal concept on the Green function of the non-dissipating propagation environment,

$$G(r_1, r_2, w) = G(r_2, r_1, w) \tag{7.1}$$

which represents the generalization of the channel impulse response taking into account of the overall propagation environment and in particular the location r_1 and r_2 in space of the reference input/output. The symmetry of the Green function with respect to space variables yields the fundamental reciprocity property which essentially says that the roles of the transmitter and receiver can be interchanged in harmonic propagation regime. Fink realized many experiments on acoustics wave as the one depicted in Fig. 7.1 to prove the concept of time-reversal and particularly the back-focusing effects of propagation waves in the form of focal spots at the target location. Fink introduced the idea of **time-reversal** filters used at the transducers which make the overall generated wave propagates back through the same environment in a reverse way, hereby retracing its former paths and eventually focusing its power in space at the receiver. This phenomenon is called spatial focusing and is observed in practice in the form of a focal spot. Other experiments tended to show that efficient focusing effects could also be obtained with a limited number of transducers not necessarily surrounding the target location, assuming a sufficiently dispersive propagation environment. This is the idea of time-reversal mirror as illustrated in Fig. 7.2.

1. Such channel is referred to as Broadcast Channel using the information theory terminology, which has not to be confused with the broadcast transmission mode we have been considering in this document.

1. Analysis of Time-Reversal Based Communications

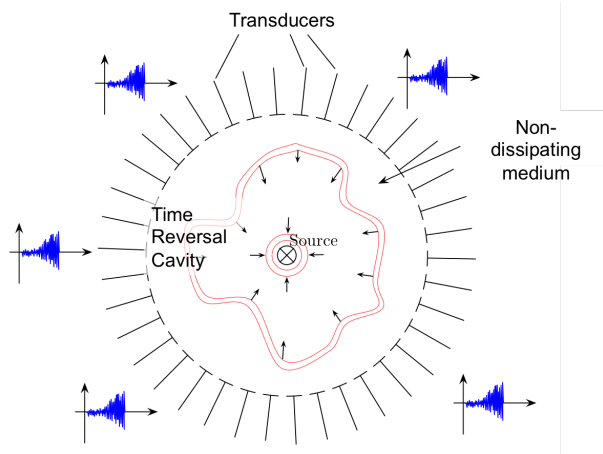


FIGURE 7.1– Time Reversal experiment using a Time Reversal Cavity (non-dissipating medium).

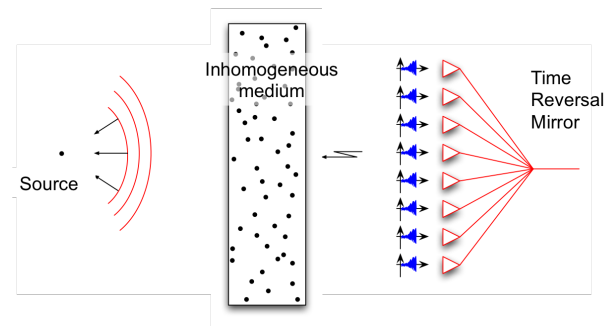


FIGURE 7.2– Time Reversal experiment using a Time Reversal Mirror (inhomogeneous medium).

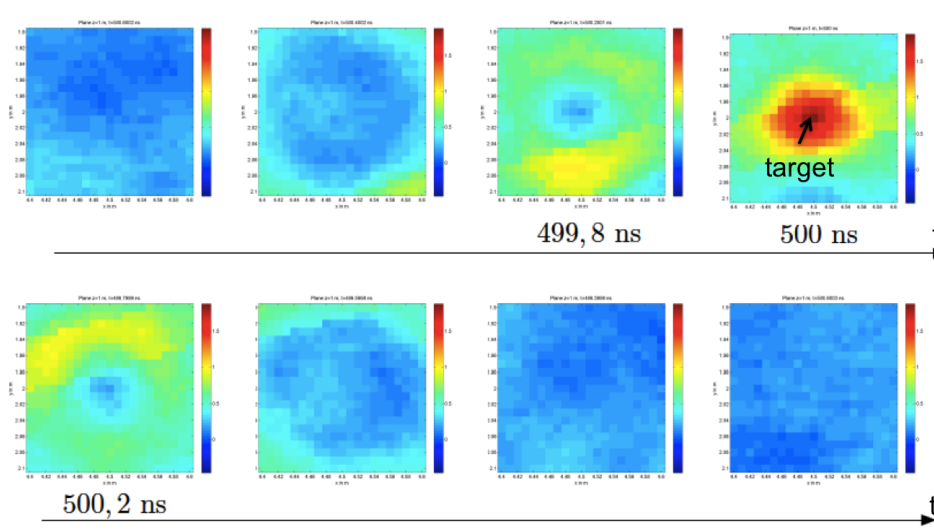


FIGURE 7.3– Time Reversal experiment with electromagnetic waves in a reverberant chamber

During the 2000s, time-reversal was further applied to electromagnetic waves for many system configurations [LdRT⁺04, OHE⁺04, LdT⁺06]. Time-reversal refocusing properties are today well understood mathematically. Many works have in particular analyzed subwavelength spatial focusing effects in highly dispersive media [OKPP05, LdTF07].

► Application to Wireless Communications

The time-reversal concepts theoretically studied and demonstrated by physicians can actually be translated into communication terminology. Embedding time-reversal concepts in a communication chain amounts to equip a transmitter with a time-domain pre-filter built from the knowledge of the CSI. Provided sufficient richness of the scattering environment hence, time-reversal filters are capable of confining electromagnetic energy to narrow beams. This strong property makes it a promising solution for energy efficient transmissions [WWH⁺11], allowing for spatial discrimination between multiple users [HYW⁺12] but also leading to low-complexity receivers [EVH⁺04b].

In the field of wireless communications, TR was initially studied for Ultra WideBand (UWB) systems, i.e. considering signals spreading over large bandwidths [NBEZ09, NZZK09]. In such a case, efficient focusing effect is expected from the highly time-dispersive nature of the channel response resulting from the high temporal resolution used to observe the propagation environment. Indeed, the larger the bandwidth, the better the resolution for resolving multipaths, and the thinner the focal spot. Applying TR to IR-UWB signals is straightforward, by directly using the reversed channel impulse response as the pulse-shaping function at the transmitter. First studied as a pre-RAKE transmission solution leading to low-complexity UWB receivers [SEH⁺04, PFDB09], TR

was also proposed for multiple-user UWB communications [NKE07].

More recently, TR was applied to multiple antenna transmitters with the idea of enriching the propagation channel through the exploitation of the spatial dimension, hereby improving the focusing effects without increasing the bandwidth [NZZK09]. In that case, one TR filter is used for each antenna element of the transmitter according to the spatial link between this antenna and the receiver antenna. Thus, the transmit antenna array plays the role of the so-called time-reversal mirror (TRM) as experienced with acoustic waves and optics [DTF99]. The larger the antenna array, the more accurate the time reversal effect regarding the overall propagation environment, and the better the spatial focusing.

We actually started our work on time-reversal by leading proof of concept studies from realistic measurements or embedded in electromagnetic reverberation chambers to characterize the focusing effects obtained with TR-based multiple-input-multiple-output (MIMO) wireless systems [C.54]. Some examples of obtained focusing effects is depicted in Fig. 7.3. The wave focusing is clearly obtained in space around the target, but also in time. From this starting point, our aim was to apply the concept to OFDM multiple antenna systems and to lead some system design and theoretical studies for such systems.

► Generic TR-based System Model

Let us consider a general system model as depicted in Fig. 7.4 made of one transmitter equipped with M antennas and K single antenna receivers. Denoting $\mathbf{h}_{m,k} \in \mathbb{C}^{L \times 1}$ the sampled L -tapped impulse response of the baseband channel from antenna m to receiver k , the TR filter associated to this channel consists in the following :

$$\mathbf{g}_{m,k} = \frac{1}{\sqrt{M}} \cdot [h_{m,k}(L-1), \dots, h_{m,k}(2), h_{m,k}(0)]^H \quad (7.2)$$

with $h_{m,k}(i)$ being the i th entry of $\mathbf{h}_{m,k}$. Hence, $\mathbf{g}_{m,k}$ is a FIR filter of the same size as $\mathbf{h}_{m,k}$, but whose tap values are conjugated and arranged in a reverse chronological order compared to $\mathbf{h}_{m,k}$. Clearly, $\mathbf{g}_{m,k}$ is the temporal matched filter of $\mathbf{h}_{m,k}$. Note that factor $\frac{1}{\sqrt{M}}$ is used for power normalization purpose along the antenna dimension. As evident from Fig. 7.4, there are as many TR filters as the number of antennas and targeted users, i.e. a total of $M \times K$ filters. Note that the knowledge of the channel state is theoretically needed at the transmitter side to feed these filters, which means that TR is applicable to closed loop systems. However, the idea behind time-reversal filters is that they can be refreshed periodically by simply storing the impinging signals coming from simple short impulses sent by the users. This is expected to be a quite quick and low-complex process.

Let $\mathbf{s}_k \in \mathbb{C}^{N \times 1}$ be a frame of N complex symbols intended to user k . By modeling the convolution operation by Toeplitz matrix multiplication, the signal transmitted by each antenna can then be expressed as,

$$\mathbf{x}_m = \frac{1}{\sqrt{K}} \cdot \sum_{k=1}^K \mathbf{T}(\mathbf{g}_{m,k}) \cdot \mathbf{s}_k \quad (7.3)$$

where $\frac{1}{\sqrt{K}}$ guarantees a unity power factor whatever the number of users. In this equation, $\mathbf{T}(\mathbf{v})$ means that vector \mathbf{v} is converted into a Toeplitz matrix² which first column is $[\mathbf{v}^T, 0, \dots, 0]^T$ and first row is $[v(1), 0, \dots, 0]$. From Eq. (7.3) and Fig. 7.4, it is important to see that in a TR-MIMO system, each antenna branch sends the same data symbols \mathbf{s}_k , the spatial dimension being exploited for beamforming purpose rather than for space diversity and multiplexing as in conventional MIMO systems. However, multiuser multiplexing is obtained if $K > 1$ since data symbols of various users k are accumulated after TR filtering and then sent simultaneously.

In the single user case, a unique data frame \mathbf{s}_k is transmitted at a time. After classical manipulations, we can express the received signal as,

$$\mathbf{y}_k = \frac{1}{\sqrt{K}} \cdot \mathbf{T}(\tilde{\mathbf{W}}_k) \cdot \mathbf{s}_k + \mathbf{n}_k \quad \text{with, } \tilde{\mathbf{W}}_k = \sum_{m=1}^M \mathbf{w}_{m,k} \quad (7.4)$$

and defining $\mathbf{w}_{m,k}$ as

$$\mathbf{w}_{m,k}(l) = \frac{1}{\sqrt{M}} \cdot \sum_{i=-L+1}^{L-1} \mathbf{h}_{m,k}^*(i) \mathbf{h}_{m,k}(i+l-L) \quad (7.5)$$

2. Note that the size of \mathbf{T} is determined by that of the vector used for right multiplication. In the present case, $\mathbf{T}(\mathbf{g}_{m,k})$ is of size $(L+N-1) \times N$.

1. Analysis of Time-Reversal Based Communications

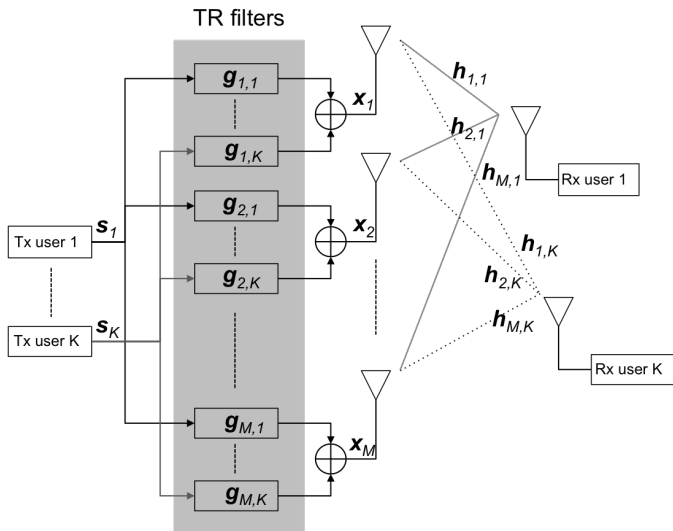


FIGURE 7.4– Generic multiple user multiple antenna system model using Time Reversal filters.

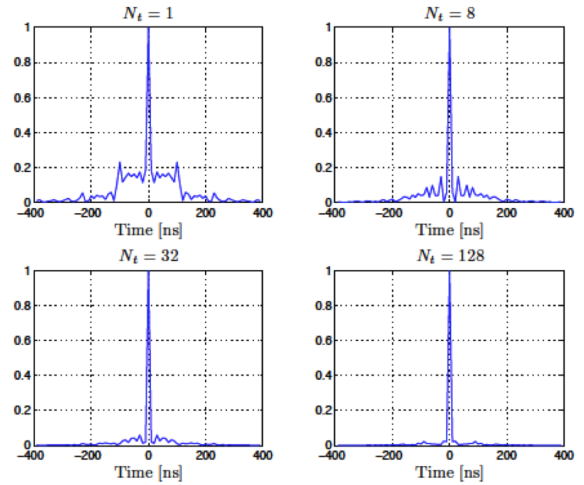


FIGURE 7.5– Equivalent propagation channels obtain with TR filtering with $M \in [1, 8, 32, 64]$. Indoor environment, central frequency is 2.4 GHz, bandwidth is 20 MHz.

the equivalent MISO channel response experienced by the data symbols, including TR precoding. Vector $w_{m,k}$ turns out to be the autocorrelation of channel vector $h_{m,k}$, which is at the fundamental basis of TR concept. Due to TR precoding thus, symbols s_k pass through an equivalent channel which impulse response is the autocorrelation of the initial channel. More precisely, \tilde{W}_k is a sum of autocorrelation functions and represents the baseband equivalent model for the radio propagation channel, including TR precoding, from the M -element transmit array to the receive antenna k . In the time domain, these autocorrelation functions consist of a central peak and some side lobes. Some examples of these autocorrelation functions measured in an Indoor office environment are given Fig. 7.5. Owing to the TR effect, the peaks add up constructively at the receive antenna location, whereas the side lobes are likely to recombine destructively by virtue of random phases. With sufficiently rich channel responses then, equivalent channel \tilde{W}_k may converge to a Dirac delta function revealing a Gaussian channel response. Such an effect is expected to be obtained in case of a large frequency bandwidth, but also with a high number M of decorrelated channel responses as observed in Fig. 7.5. One may understand that the transmission becomes then easy to handle using simple threshold detectors at the receiver side. However, if autocorrelation functions are not sufficiently thin due to a lack of scattering richness in the MISO channel, the receiver will have to treat residual ISI and compensate for channel distortions by means of equalization.

Let us now extend the received signal expression in a multiple user scenario, that is when various symbol vectors are transmitted simultaneously. In that case, let $k = j$ be the user of interest, Eq. (7.4) rewrites as :

$$y_j = \underbrace{\frac{1}{\sqrt{K}} \cdot T(\tilde{W}_j) \cdot s_j}_{\text{useful term}} + \underbrace{\frac{1}{\sqrt{K}} \cdot \sum_{k \neq j} T(\tilde{\omega}_{kj}) \cdot s_k + n_j}_{\text{Interference term}} \quad (7.6)$$

where we now have to introduce $\tilde{W}_{kj} = \sum_{m=1}^M w_{m,kj}$ as,

$$w_{m,kj} = \frac{1}{\sqrt{M}} \cdot \sum_{i=-L+1}^M \sum_{i=-L+1}^{L-1} h_{m,k}^*(i) h_{m,j}(i+n-L) \quad (7.7)$$

These latter functions are the MISO equivalent cross-correlation functions due to the combined effect of TR filtering for user k and channel response from the transmit station to user j . These functions are responsible for the multiuser interference (MUI) term and models the recombination of waves intended to competing users. In the ideal case of fully decorrelated channel responses between users, cross-correlation functions $w_{m,kj}$ are cancelled and Eq. (7.6) becomes equivalent to Eq. (7.4). This can be interpreted as a consequence of the spatial focusing effect. As in the SU-MIMO case, decorrelation properties are strongly related to the bandwidth and the number of antennas. The larger the bandwidth and the higher the number of antennas, the weaker the cross-correlation functions.

► Frequency domain Time Reversal

In practice, as the combination of MIMO and OFDM is often considered in many systems, it is interesting to pose the problem of TR precoding in MIMO-OFDM. Namely, combination with OFDM is an simple and efficient solution to get rid of residual ISI as a consequence of imperfect autocorrelation functions. One simple approach for this is the use of the famous guard interval (GI) as a cyclic extension in preamble of the time-domain OFDM symbols. Taking this mechanism as reference, it is well known that every linear convolution function occurring between the OFDM modulator and demodulator is translated into circular convolution. This also means that the related Toeplitz matrices in Eq. (7.6) become circulant. Hence, it is very easy to get the equivalent expression of Eq. (7.6) but for OFDM waveform as,

$$Y_j = \frac{1}{\sqrt{K}} \cdot \underbrace{\tilde{W}_j \cdot S_j}_{\text{useful term}} + \frac{1}{\sqrt{K}} \cdot \underbrace{\sum_{k \neq j} \tilde{W}_{kj} \cdot S_k}_{\text{Interference term}} + N_j \quad (7.8)$$

in which $Y_j = F_N y_j$, $S_k = F_N s_k$ are the frequency domain symbol vectors with $F_N \in \mathbb{C}^{N \times N}$ the N -point Digital Fourier Transform (DFT) matrix. The equivalent channel and interferent diagonal matrices \tilde{W}_j and \tilde{W}_{kj} such that

$$\begin{cases} \tilde{W}_j = \frac{1}{\sqrt{M}} \cdot \sum_{m=1}^M \text{Diag}\{H_{m,j}\} \text{Diag}\{G_{m,j}\} \\ \tilde{W}_{kj} = \frac{1}{\sqrt{M}} \cdot \sum_{m=1}^M \text{Diag}\{H_{m,j}\} \text{Diag}\{G_{m,k}\} \end{cases} \quad (7.9)$$

with $H_{m,k} = F_N h_{m,k}$. This result simply confirms that the time-domain TR FIR filter can be implemented as a point-wise multiplication with the data symbols before OFDM modulation by using the frequency domain coefficients $G_{m,k} = F_N g_{m,k}$ of the TR filter obtained through DFT. From the TR filter definition in Eq. (7.2), it is straightforward to write

$$G_{m,k} = \frac{1}{\sqrt{M}} \cdot H_{m,k}^* \quad (7.10)$$

which indicates that the frequency domain TR filter essentially amounts to applying to each subcarrier n of the OFDM spectrum a complex weighting factors $H_{m,k}^*(n)$ being the conjugate of the frequency domain channel gain. Eq. (7.10) can be viewed as a matched filter, applied to each subcarrier n and each antenna m , i.e. to the overall space-time channel. The corresponding transmitter is depicted in Fig. 7.6, highlighting the frequency domain TR precoding stage.

Some interesting interpretations can be done from this result, in comparison to the expression obtained in Eq. (7.6). First, the frequency domain equivalent channel \tilde{W}_j appears as a summation of real coefficients. More precisely, the n th entry of \tilde{W}_j , corresponding to the n th subcarrier of the OFDM signal, is $\tilde{W}_j(n) = \frac{1}{\sqrt{M}} \sum_m |H_{m,j}(n)|^2$. This pure real value has to be understood as the effect of the constructive recombinations of waves as already discussed in the previous section. Thus, the larger the M , the better the equivalent channel gain $\tilde{W}_j(n)$ on each subcarrier n and the stronger the resulting useful term. Equivalently, the better the time focusing. On the other hand, the interfering component k on subcarrier n experiences the following equivalent channel $\tilde{W}_{kj}(n) = \sum_m H_{m,j}(n) H_{m,k}^*(n)$. Hence, the interfering symbols are weighted by a sum of complex numbers with independent amplitudes and phases. As such, the interfering power tends to be naturally reduced, namely with large M , which consists in another interpretation of the spatial focusing concept. Eventually, this comes in favor of the MU multiplexing ability of the TR-based precoded system. TR filters can thus be used for SDMA purpose.

Such important interpretations of time-reversal filtering behaviour with large M coincides with the initial postulate relying on wave propagation and which was telling that wave focusing could be theoretically obtained with a sufficiently large number of transducers. Interestingly, this point of view which is known for many years from the studies of Fink is another interpretation of the famous massive MIMO paradigm introduced by Marzetta in 2010 [Mar10a]. Some connections with massive MIMO and MU-MIMO literature will thus be regularly established in the sequel.

1. Analysis of Time-Reversal Based Communications

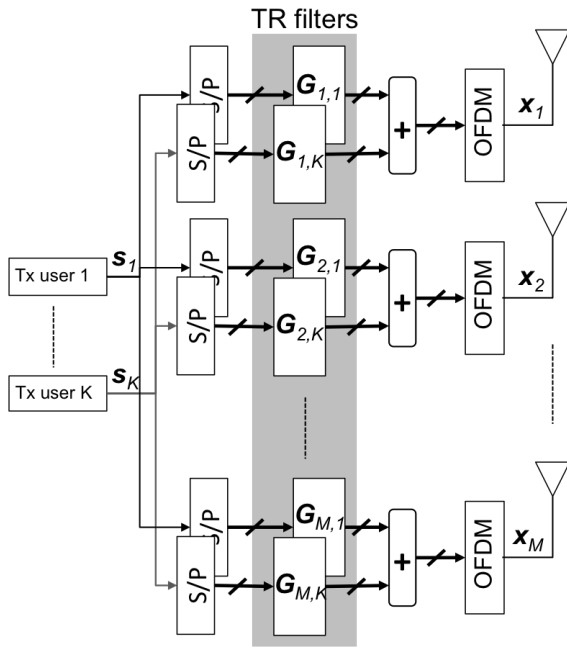


FIGURE 7.6– TR-OFDM system model with Time Reversal applied in frequency domain.

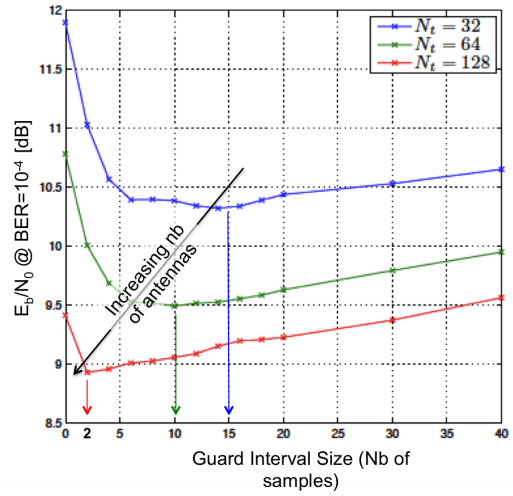


FIGURE 7.7– Optimal guard interval setting in TR-OFDM with variable number of antennas.

► Guard Interval Settings

One first parameter to correctly set when carrying out OFDM communications is the guard interval. Yet, as time-reversal is originally processed through a time domain FIR filter, it leads to a straightforward time dispersion of the symbols which comes in addition to the dispersion produced by the channel itself. In other words, the equivalent channel experienced by the filtered OFDM symbols is of theoretical length $2L - 1$, if L is the original channel length. However, when implementing the time reversal filter in frequency domain, linear convolution translates into circular one, and the additional time dispersion disappears.

Nonetheless, in both cases, the resulting channel impulse response will benefit from the properties of autocorrelation functions. In particular, the equivalent channel will have a symmetric power delay profile, with the highest tap in the middle of the response. Hence, it can be shown that **a judicious choice to ease the synchronization stage at the receiver is to circularly extend the OFDM symbols with a prefix and a suffix**, as summarized in Contrib. III.1 and shown in [C.44].

Contribution III.1 (System Design)

CPCS Guard Interval Setting for a TR-OFDM system

Consider an TR-OFDM system of order N . A conventional OFDM receiver correctly recovers the OFDM frame synchronization if each OFDM symbol is prepended and appended with a cyclic extension (Cyclic Prefix Cyclic Suffix - CPCS) of $\nu = \frac{\Delta}{2}$ samples. Hence, the l th OFDM symbol s_l is,

$$s_l = \mathbf{G}_{\text{CPCS}} \mathbf{F}_N^H \mathbf{X}_l \quad \text{with, } \mathbf{G}_{\text{CPCS}} = \begin{bmatrix} \mathbf{O}_{\nu \times (N-\nu)} & \mathbf{I}_\nu \\ \mathbf{I}_\nu & \mathbf{O}_{\nu \times (N-\nu)} \end{bmatrix} \quad (7.11)$$

where $\mathbf{0}$ and \mathbf{I} are zero-entry and identity matrices, \mathbf{F}_N is the square Fourier matrix and \mathbf{X}_l is the vector of data symbols.

In addition, depending on the time-domain (TD) or frequency-domain (FD) implementation of the time reversal filter, we have,

$$\Delta_{\text{FD}} = \frac{\Delta_{\text{TD}}}{2} \quad (7.12)$$

Complementary to this analysis, owing to the time focusing effects, guard interval durations are expected to be less using a TR filter than in common OFDM. We led simulations using measured channel responses in order to identify the reduction of the guard interval when increasing the number of antennas. Our results, as presented in Fig. 7.7 confirm the expected behaviour.

► Receiver Synchronization

As above mentioned, using TR filtering results in an equivalent channel response with linear phase. We showed that this particular feature can be advantageously exploited to derive a very simple ML estimation of the OFDM symbol synchronisation error at the receiver. Hence we proved that **time reversal filtering can also be leveraged to ease the OFDM symbol timing recovery and lead to a very simple algorithm which can be processed with the help of few pilots, and even blindly if the number of transmit antennas and subcarriers high sufficiently high**. The main principle of this simple algorithm is based on a least-square estimation, as summarized hereafter and argued in [C.44].

Contribution III.2 (Algorithm)

Multiple Antenna RT-OFDM Synchronization

Given a MIMO TR-OFDM system, ML symbol offset estimation ϵ_j at receiver j can be obtained using a subset \mathcal{P} of pilot subcarriers as,

$$\hat{\epsilon}_j = \left[\frac{1}{2\pi} \cdot \frac{\sum_{n \in \mathcal{P}} n |Y_j(n)| \arctan \left(\frac{\text{Im} \{Y_j(n)X^*(n)\}}{\text{Re} \{Y_j(n)X^*(n)\}} \right)}{\sum_{n \in \mathcal{P}} n^2} \right] \quad (7.13)$$

Also, when $M \gg 1$, and assuming a sufficient number N of subcarriers a blind algorithm can be processed as,

$$\hat{\epsilon}_j = \left[\frac{1}{2\pi} \cdot \frac{3}{N^3} \cdot \sum_{n=0}^{N-1} n \arctan \left(\frac{\text{Im} \{Y_j(n)\}}{\text{Re} \{Y_j(n)\}} \right) \right] \quad (7.14)$$

► Comparison with other spatial filters

From the previous considerations, it appears that time-reversal filtering can be viewed as a particular multi-antenna linear precoding function. Hence, some commonalities with classical MU-MIMO precoding schemes may be identified. Having a look back to the literature of MU-MIMO systems, and in especially regarding linear precoders, matched-filter-like solutions have already been proposed for the design of MIMO systems using CSI at the transmitter. The main two ones are Maximum Ratio Transmission (MRT) [Lo99] and Equal Gain Transmission (EGT) [LH03]. Considering the same OFDM-MIMO system model as previously introduced, we can restate such precoders for a particular user k as

$$\text{EGT : } \quad \mathbf{G}_{m,k} = \frac{1}{\sqrt{M}} \mathbf{\Phi}_{m,k}^* \quad \text{with, } \Phi_{m,k}(n) = \frac{H_{m,k}}{|H_{m,k}|} \quad (7.15)$$

$$\text{MRT : } \quad \mathbf{G}_{m,k} = \text{Diag} \{ \Lambda_k \} \mathbf{H}_{m,k}^* \quad \text{with, } \Lambda_k(n) = \frac{1}{\sqrt{\sum_{m=1}^M |H_{m,k}(n)|^2}} \quad (7.16)$$

Compared to time-reversal, the EGT precoding scheme yields a transmission with a unitary gain on every link, in frequency and space domains. It consists in a simple phase rotation and thus avoids any power imbalance between the signals propagated by each antenna. This can be a positive aspect regarding the power amplification efficiency as discussed in 6.

1. Analysis of Time-Reversal Based Communications

On the other hand, comparing Eq. (7.16) with Eq. (7.10), it is concluded that TR and MRT precoding follow the same overall approach by applying the conjugate of the frequency domain channel responses, thus leading to similar (but not strictly equivalent) conclusion in terms of time and spatial focusing properties. The difference between them merely comes from power normalization. Indeed, TR precoding is based on a simple equal power allocation across the antennas, whilst being strictly identical whatever the subcarrier index and the user. With MRT, the power normalization can be rather interpreted as a spatial normalization which may differ from one subcarrier to another as well as between users. It can easily be shown that the power factor Λ_k simply corresponds to the singular value of the MISO channel on subcarrier n [R.11].

We will analyze the difference between these two schemes in terms of capacity and performance the next two sections. Let us first try to identify for each technique the focusing gain we obtained, i.e. the average useful power that is transferred to the receiver. Focusing gain can be understood as the array gain obtained at the antenna level when a particular precoding scheme is used. The obtained results, published in [R.11] are reported in the following contribution.

Contribution III.3 (Analytic Expression)

Focusing gain of matched filter like spatial filters

Assuming independent normalized complex Gaussian fading per antenna, the ergodic power array gain obtained for the TR, MRT and EGT spatial filtering schemes in an MIMO-OFDM system with M antennas are,

$$\text{TR} \quad \mathcal{G}_{\text{TR}} = M + 1 \quad (7.17)$$

$$\text{MRT} \quad \mathcal{G}_{\text{MRT}} = M \quad (7.18)$$

$$\text{EGT} \quad \mathcal{G}_{\text{EGT}} = 1 + \frac{\pi}{4}(M - 1) \quad (7.19)$$

This results already show that MRT and TR become equivalent when $M \gg 1$. On the other hand, EGT gives the lowest focusing gain, since such spatial filter only plays with the phases of the channel complex gains, hereby loosing one degree of freedom. We conclude that TR is the best choice in terms of average SNR maximization, which makes it the best strategy for green communications.

Last but not least, as it has been noticed that the MRT precoding vector applied on each subcarrier n is taking into account the gains of the spatial links for all the antennas, it turns out that MRT precoding has to be computed in a centralized way. Indeed, the channel responses of different transmit antenna pairs need to be gathered to compute the normalization factor $\lambda_k(n)$, which is required for each subcarrier of each user. With TR or EGT filtering, each precoding vector can rather be processed independently at each transmit antenna. Hence, TR and EGT could easily be envisaged in systems with distributed antennas. This is not the case of MRT.

After the system level analysis discussed so far, the aim of our work during the first years of studies on time-reversal (i.e. 2009–2011), was to establish new results from a green communication point of view. We then targeted single user downlink scenarios, considering the spatial filters as promising solutions for link budget enhancement rather than for multiuser management. In the previous section, we have already classified the matched-like filters in terms of focusing gains. In the following ones, we give the results of our investigations in terms of theoretical ergodic capacity and BER performance of the SU-MIMO precoded systems.

1.4 ACHIEVABLE RATE IN SINGLE USER SCENARIOS

From the introduced system model in 1.3, and focusing on a particular subcarrier n , getting the achievable rate of the system in the SU case amounts to developing the following expression depending on the used precoding scheme,

$$\mathcal{R} = \mathbb{E} \left\{ \frac{1}{N} \sum_{n=0}^{N-1} \log_2 \left(1 + |\tilde{W}_k(n)|^2 \gamma \right) \right\} \quad (7.20)$$

where γ is the reference ratio between data symbol and noise variances, i.e. $\gamma = \sigma_s^2/\sigma_n^2$, and where \tilde{W}_n is the equivalent channel for one particular subcarrier embedding the normalization factor per antenna. The problem is then a derivation of achievable rate for SISO link, but involving a dedicated statistical fading model. Boosted by the introduction of the Massive MIMO context around 2010, numerous results about achievable rates have been produced regarding precoded MIMO schemes during our own studies on time-reversal. Most of the contributions were however focusing on the asymptotical results with infinite number of antennas M . As we were more interested in practical system design, we first tried to provide contributions in a moderate-scale antenna regime.

► Equivalent Channel Statistical Analysis

A first step towards the derivation of closed-forms of the achievable capacity was to identify the statistical law that could properly model the equivalent channel fading. Without loss of generality, we assume independent and identically distributed variables across the subcarriers. In [R.11], we provided an analysis on this subject which can be summarized as follows.

Contribution III.4 (Analytic Expression)

Statistical Model of the Spatially Filtered MISO Channel

Assuming independent normalized complex Gaussian fading per antenna, the equivalent fading channel models of a precoded MISO system with M antennas are,

$$\text{TR} \quad \tilde{W}_{\text{TR}} \sim \text{Gamma} \left(k = M, \theta = \frac{1}{\sqrt{M}} \right) \tag{7.21}$$

$$\text{MRT} \quad \tilde{W}_{\text{MRT}} \sim \text{Nakagami} (\mu = M, w = M) \tag{7.22}$$

$$\text{EGT} \quad \tilde{W}_{\text{EGT}} \sim \text{Nakagami} \left(\mu = M, w = 1 + \frac{\pi}{4}(M - 1) \right) \tag{7.23}$$

where k and θ are the shape and scale parameters of the Gamma distribution, and μ and w are the shape and spread parameters of the Nakagami distribution.

This first analysis tells us that the EGT and MRT schemes yield the same statistical behaviour of their equivalent channel. They namely present the same shape parameter and only differs on their spread values. As the shape parameter corresponds to the number of degrees of freedom of the law, we conclude that EGT and MRT can theoretically exploit the same channel diversity order. As for the spread parameter, it is directly equal to the average power of the distribution, hence indicating that MRT will benefit from highest average SNR than EGT. This latter coincides with the previous analysis on the focusing gain in Eq. (7.17). On the other hand, the TR equivalent channel is governed by a Gamma distribution with also M degrees of freedom. By comparing the Gamma and Nakagami CDF with identical shape parameters, it turns that the Gamma distribution is much more spread but exhibits a higher average value. This means that a higher average SNR can be expected however with a higher probability of deep fades. As the log is a concave function, this will positively influence the expectation in Eq. 7.20 for low SNR values, but negatively for high SNR values.

These considerations, published in [R.11] can be easily verified through simulations as proposed in Fig. 7.8. As expected, the capacity curves of MRT and EGT follow exactly the same trend with some outperformance of the EGT scheme. However, the TR curve crosses the MRT curve for some SNR, hence outperforming the MRT for low SNR range while suffering from degradation at high SNR. Hence we conclude that the TR filter is the optimal solution at low SNR. Instead, MRT is optimal at high SNR. The former follows the matched filter criterion, hence maximizing the SNR. The latter relies on the singular value $\Lambda_k(n)$ of each MISO channel, hence maximizing the rate at high SNR.

Overall, since the number of degrees of freedom is the same for the three cases, the capacity curve exhibit the same slope at high SNR. Fig. 7.8 also gives the achievable rates when combining spatial filtering and OSTBC. We indeed studied this combination since matched-type prefilters yield an equivalent channel with real values (i.e. fading coefficients are real numbers), which enables easy combination with OSTBC of rate one for an arbitrary number of antennas [WC09a]. However, leading the same approach in terms of statistical analysis leads to the

1. Analysis of Time-Reversal Based Communications

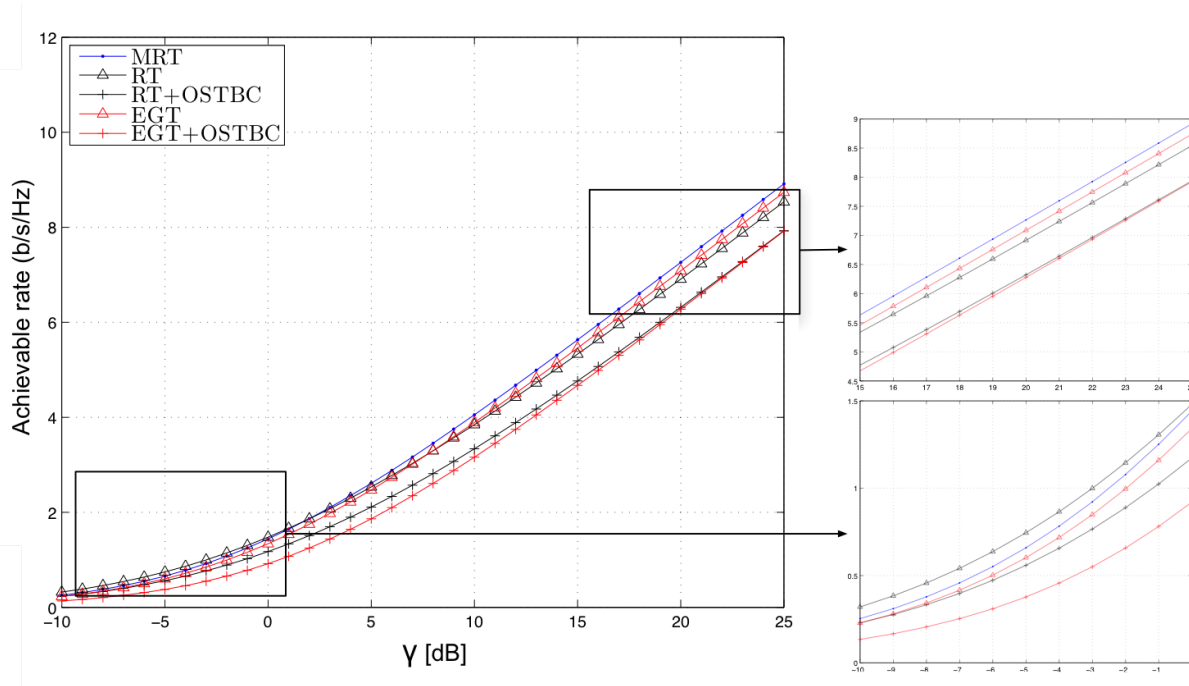


FIGURE 7.8– Achievable Rate comparison between various spatial filtering methods with $M = 2$ antennas.

conclusion that achievable rates are dramatically reduced in that case. More insights on this aspect have been given in [R.11]

► Closed-forms and bounds

To go a step beyond, we also worked on the theoretical derivation of the expectation in Eq. (7.20), aiming at providing new closed-forms for a moderate number of antennas. We succeeded for the MRT and EGT cases for which the integral forms are the same and are tractable identifying some special functions as stated in the following closed-form expression.

Contribution III.5 (Analytic Expression)

Closed-Form of the achievable rate in SU MRT/EGT MISO

Assuming independent normalized complex Gaussian fading per antenna, a precoded MISO system with M antennas yields an achievable rate expressed as,

$$\mathcal{R}_{\text{MRT,EGT}} = \frac{e^{\kappa^{-1}}}{(M-1)! \kappa^M \log 2} \sum_{m=0}^{M-1} \binom{M-1}{m} (-1)^{M-1-m} \left[\kappa^{m+1} m! (\Psi(m+1) + \log \kappa) + \frac{1}{(m+1)^2} {}_2F_2\left(m+1, m+1; m+2, m+2; -\frac{1}{\kappa}\right) \right] \quad (7.24)$$

where $\kappa = \frac{\mathcal{G}_{\text{MRT,EGT}}}{M} \times \gamma$ is a so-called normalized SNR taking into account the focusing gains as given in Contrib. III.3.

The obtained closed-form involves the Euler Digamma function $\Psi(x)$ and the generalized hypergeometric function ${}_pF_q(\cdot, \cdot; \cdot; x)$. Note that this closed-form is valid whatever the SNR and whatever the number M of antennas. Similar closed-forms can actually be found in the literature for the MRT case, but following another approach to lead the derivation [NMDL13]. Our approach allows to generalize the result to the EGT case. We partially published this result in an invited paper [C.20]. As far as time-reversal filtering is concerned, the integral form becomes untractable. Instead we thus derived some capacity lower bounds for the high SNR regime, but still without any assumption on the number of antennas.

Contribution III.6 (Analytic Expression)

Achievable rate lower bounds (high SNR) for TR, MRT and EGT

Assuming independent normalized complex Gaussian fading per antenna, achievable rates at high SNR for TR/MRT/EGT precoded MISO system with M antennas are,

$$\text{TR} \quad \mathcal{R}_{\text{TR}}^{\text{low}} = 2 \frac{\Psi(M)}{\log 2} + \log_2 \left(\frac{1}{M} \gamma \right) \quad (7.25)$$

$$\text{MRT} \quad \mathcal{R}_{\text{MRT}}^{\text{low}} = \frac{\Psi(M)}{\log 2} + \log_2 \left(\frac{\mathcal{G}_{\text{MRT}}}{M} \gamma \right) \quad (7.26)$$

$$\text{EGT} \quad \mathcal{R}_{\text{EGT}}^{\text{low}} = \frac{\Psi(M)}{\log 2} + \log_2 \left(\frac{\mathcal{G}_{\text{EGT}}}{M} \gamma \right) \quad (7.27)$$

On the other hand classical Jensen's inequality can be used to obtain some upper-bounds. Interestingly, the obtained bounds are equivalent to those obtained in the massive MIMO asymptotic regime. This can be understood from the so-called channel hardening effect which occurs when M increases to infinity. From 2010 to 2015, many publications have provided such kind of upper-bounds using the theory of large random matrices. In the case of TR precoding, following either the Jensen's inequality or the large matrix assumption, we find the following upper-bound. It can be proved that this result holds for MRT and EGT precoding using the appropriate focusing gain \mathcal{G} .

Contribution III.7 (Analytic Expression)

Achievable rate upper bounds (large M) for TR

Assuming independent normalized complex Gaussian fading per antenna, achievable rates at high SNR for a TR precoded MISO system with M antennas is,

$$\mathcal{R}_{\text{TR}}^{\text{up}} = \log_2 (1 + \mathcal{G}_{\text{TR}} \gamma) \quad (7.28)$$

► Simulations

In order to show the accuracy of these bounds and closed forms, we give in Fig. 7.9 and 7.10 two examples of achievable rate plots in the TR and EGT cases. For the EGT case, the closed-form is given in comparison to simulated results for validation. For EGT and TR, lower and upper-bounds can be compared to the simulations. We conclude that the provided lower-bounds are more tight in a moderate-scale antenna regime than the upper-bounds, as soon as the SNR is of at least 5 dB. In addition, they turn out to be also very accurate if M is large, which can be explained by the fact that at large M the focusing gain makes the SNR substantially increase. Hereby, the convergence to the high SNR regime is faster. Hence, the proposed lower-bounds can be preferred than other existing bounds to approach the achievable rate of precoded MISO systems without any assumption upon the size of the antenna array.

1.5 BIT ERROR RATE PERFORMANCE ANALYSIS

In the same way we had been working on the derivation of achievable rates, we also tried to obtain the closed form expressions of the BER performance in the case of TR filtering, but also for the other precoders. Our main results have been published in [R.11]. The derivation merely consists in averaging the Q-function $\mathcal{Q}(\cdot)$ over the PDF of the equivalent channels, as identified in Eq. (7.21). For QPSK modulation for example, the theoretical

1. Analysis of Time-Reversal Based Communications

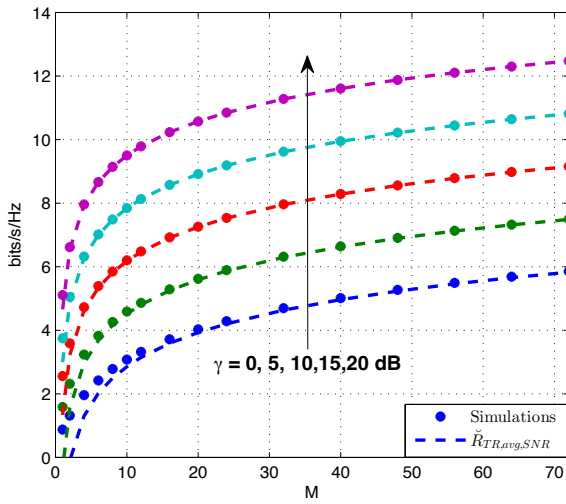


FIGURE 7.9– Achievable rate of the TR-OFDM system (Simulation and lower bound at high SNR).

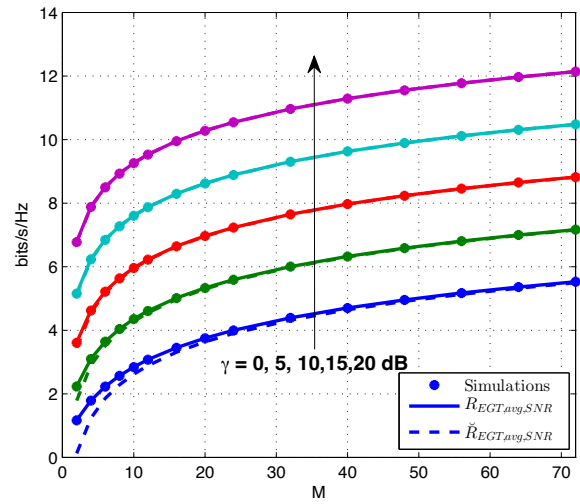


FIGURE 7.10– Achievable rate of the EGT-OFDM system (simulation, closed-form and lower bound at high SNR).

average BER in the TR case is obtained by deriving the following integral,

$$\mathcal{P}_e(\gamma, M) = \int_0^\infty \underbrace{\mathcal{Q}(r\sqrt{\gamma}) \times \frac{(M^2 + M)^{\frac{M}{2}}}{(M-1)!} r^{M-1} e^{-(M^2+M)\frac{1}{2}r}}_{f_T(r, M)} dr \quad (7.29)$$

in which one may recognize the PDF of the Gamma distribution which models the equivalent channel in the TR case. Similar forms are obtained with EGT and MRT precoding, simply modifying the involved PDF. Using particular integral results of the literature, namely [GRJ⁺65], it is possible to get a closed-form for each precoding case. For example, we give hereafter the obtained result for the TR case which is the most challenging case in terms of mathematical derivations. Note that this result is valid whatever the number of antennas and for all positive SNR in dB. For the MRT and EGT cases, computations need slightly less effort as they can be viewed as a particular case of BER derivations over Nakagami channels for which one can find already published material as for example in [HB06].

Contribution III.8 (Analytic Expression)

BER Closed-form for TR filtering

Assuming independent normalized complex Gaussian fading per antenna and QPSK constellations, the BER performance of a TR precoded MISO system with M antennas is,

$$\mathcal{P}_e = \frac{1}{2} - \sqrt{\frac{1}{2\pi}} \sum_{m=0}^{M-1} \kappa^{\frac{m+1-M}{2}} e^{\frac{1}{4\kappa}} \mathcal{D}_{m-M}\left(\frac{1}{\sqrt{\rho}}\right) \quad (7.30)$$

with $\kappa = \frac{G_{TR}}{M} \gamma$ the normalized SNR, and \mathcal{D}_p the p th order parabolic cylinder function.

This closed-form will be further exploited in section 2 for MU-MIMO system optimization with the concept of partial frequency re-use. However, additional insights can be brought from their series development, namely getting the asymptotic behaviour at high SNR. Doing this for each scheme leads us to the following results given here as an example for QPSK modulation [R.11].

Contribution III.9 (Analytic Expression)

Asymptotic (high SNR) QPSK performance in TR/MRT/EGT SU-MISO

Assuming independent normalized complex Gaussian fading per antenna and QPSK constellations, the asymptotic BER performances at high SNR of a precoded MISO system with M antennas are,

$$\text{TR} \quad \lim_{\gamma \rightarrow \infty} \mathcal{P}_e^{\text{TR}} = \frac{1}{2^{M+1}} \frac{(M+1)^{\frac{M}{2}}}{\left(\frac{M}{2}\right)!} \left(\frac{1}{\kappa}\right)^{\frac{M}{2}} \quad (7.31)$$

$$\text{MRT} \quad \lim_{\gamma \rightarrow \infty} \mathcal{P}_e^{\text{MRT}} = \frac{1}{2^{M+1}} \frac{(2M)!}{(M!)^2} \left(\frac{1}{\kappa}\right)^M \quad (7.32)$$

$$\text{EGT} \quad \lim_{\gamma \rightarrow \infty} \mathcal{P}_e^{\text{EGT}} = \frac{1}{2^{M+1}} \frac{(2M)!}{(M!)^2} \left(\frac{1}{\kappa}\right)^M \quad (7.33)$$

with $\kappa = \frac{\mathcal{G}_{\text{TR,MRT,EGT}}}{M} \gamma$ the normalized SNR.

As already expected from the study of the equivalent channel statistics, we notice that MRT and EGT have the same asymptotic behaviour, the only difference being at the level of the normalized SNR, once again resulting from the weaker focusing gain of EGT compared to MRT. As far as TR is concerned, the closed-form exhibits some differences compared to the other two. **The most important thing we can learn from these forms is the fact that MRT and EGT exploit the full diversity of the channel, i.e. the number M of spatial branches. Instead, TR exploits half of this diversity, which could appear as a bit surprising. The simulated results given in Fig. 7.11 and 7.12 for QPSK modulation confirm these theoretical analysis. MRT and EGT BER curves follow the same slope straightforwardly given by the number M of antennas, whereas the TR results suffer a loss of half the diversity order.**

This particular trend however results from the simple fact that a Gamma distribution is roughly equivalent to the square of a Nakagami. This indeed yields that the QPSK symbols transmitted through a TR filter experience deep fades with higher probability than in the case of EGT or MRT precoding. Conversely, they also experience favorable channel gains with higher probability. These latter can however not compensate the former since the concavity of the Q-function. **Eventually, we can interpret that the TR filter boosts the spatial links already exhibiting favorable gains to the detriment of the links with poor gains. This leads us to the conclusion that TR filtering can be viewed as a spatial matched filter but also including some implicit power allocation mechanism across the frequency spectrum. Contrary to that, EGT does not imply any amplitude modification, and hence does not produce any kind of power allocation. Also, MRT involves power factor corrections (namely matrix Λ in Eq. (7.16)) to compensate for the natural power boost of its time-reversal filter part.**

1.6 CONCLUSION

This first part of our studies on spatial filters has been dedicated to time-reversal filtering. This has made us learn many important points about the characteristics of time-reversal in comparison to its EGT and MRT counterparts. A major difference is that TR can be implemented in time or frequency domain, whereas EGT and MRT are applicable only in frequency (or at least by means of two DFTs). A first important corollary to this property is that time-reversal is waveform-agnostic. A second corollary is its ability to be implemented in a pure distributed antenna scenario since no data exchange is needed to compute the filter applied to each antenna. Interestingly, this latter property is also true for EGT since no centralized gain control has to be computed with this scheme.

Then, we have identified the fact that time-reversal have to be viewed as a space-time matched filter to the propagation channel, whereas MRT is a matched filter in the frequency domain only. This means that time-reversal maximizes the power transfer through the space-time channel hence maximizing the receive SNR globally over the considered frequency band. As a pure flat fading precoding approach instead, MRT maximizes the power transfer along the spatial axis only, independently from one narrow band to another, i.e. without

2. Spatial Filtering for MU-MIMO in Moderate-Scale Antenna regime

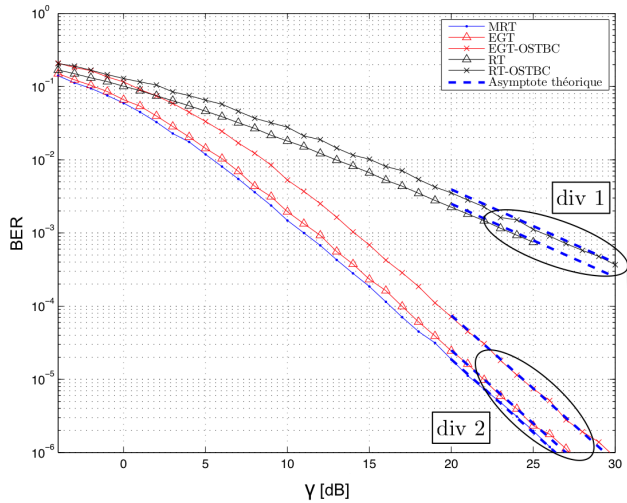


FIGURE 7.11– Bit error rate performance of SU OFDM-MISO systems using various precoding schemes with $M = 2$ transmit antennas.

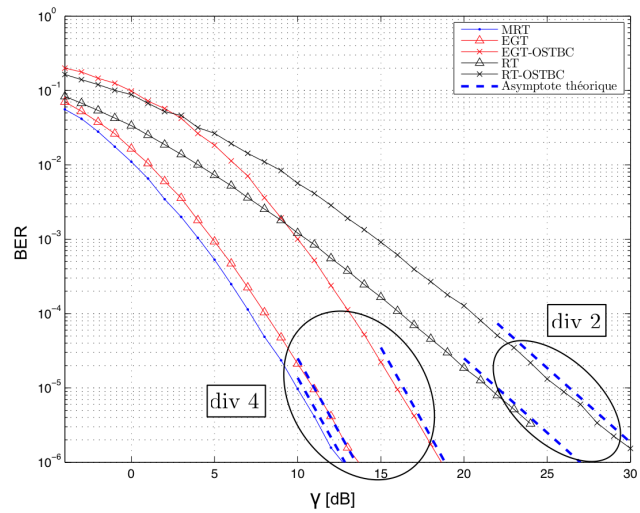


FIGURE 7.12– Bit error rate performance of SU OFDM-MISO systems using various precoding schemes with $M = 4$ transmit antennas.

accounting for the channel characteristics along the frequency axis. As a result, time-reversal performance both depend on the bandwidth and the number of antennas, whereas MRT is solely depending on the antenna scale.

From a theoretical point of view, time-reversal is the optimal solution at low SNR, by virtue of the matched filter criterion. Instead, MRT uses a power adjustment based on the singular value of the channel. Thus, it represents the optimal solution at high SNR, by virtue of the maximum capacity criterion. As for EGT, it can be viewed as an optimal precoding scheme at high SNR and low SNR, but under the constraint of strict equal power allocation across the antennas.

Eventually, it is worth remembering that the time-reversal concept comes propagation wave considerations and naturally leads to the concept of large-scale antenna systems. Massive MIMO systems have been introduced from a different perspective, judiciously applying random matrix theory to MIMO systems described by channel matrices of high dimension. This brilliant idea came in 2010 thanks to T. Marzetta, whereas the concept of time-reversal mirrors and cavity which embodies all the main concepts of spatial focusing was already existing since 1990 with the works of M. Fink.

Summary (PhD/Dissemination/Projects)

- 1 PhD (T. Dubois)
- 1 international journal paper [R.11]
- 4 communications in international conferences and workshops [C.26][C.43][C.44][C.54]
- 1 GDR workshop
- 1 Brevet [P.1]
- 1 ANR project (TRIMARAN)

2 SPATIAL FILTERING FOR MU-MIMO IN MODERATE-SCALE ANTENNA REGIME

2.1 MOTIVATIONS

The first part of our studies on spatial filters has somehow allowed to bridge the two concepts of time-reversal and massive MIMO. Many issues have however not been addressed in this first part, among which the spatial

focusing properties of the precoding filter in a multiuser context, i.e. their ability to efficiently separate the users in spatial domain (SDMA). These aspects are investigated in the present section under the constraint of a reasonable number of antennas. Indeed, as we started our studies on time-reversal, we were ourselves not that aware of being working on massive MIMO which was just being emerging at this period. Hence, our first feeling around 2011 was to investigate spatial filtering concepts when using not so large antenna arrays, what we call here the moderate-scale antenna regime.

To validate the Massive MIMO concept, theoretical lower bounds when $M \rightarrow \infty$ had already been derived in the early 2010s and show a promising increase of the network capacity of order of M [JAMV11]. For a constrained M however, spatial separation between multiple signals may become imperfect or be obtained at the cost of decreased useful power, hereby degrading the global system performance. This is commonly reflected in most of the works through the evaluation of multiuser interference (MUI) and signal to interference and noise ratio (SINR). Based on this, it is possible to find the critical M needed to approach the capacity bounds as done by Caire or Hoydis around 2012 [HCPR12b, HTBD⁺13a]. At the time of our studies hence, we could find various contributions dealing with SINR maximization through resource allocation mechanisms taking benefit of the beamforming gains [BSHD13a, ZDPC13], or also looking into user clustering strategies and playing with spatial, frequency or even time dimensions (e.g. [JCS14]). Our complementary idea was to tackle the problem of inter-user interference following two aspects :

- Study the interference term when M is moderately large, not to use strong assumption on channel hardening as done in many papers
- Investigate partial frequency or sub-band reuse between users to control the MUI term, i.e. allowing some adaptive frequency overlap between several user signals

Even if there is an abundant literature regarding SINR-based investigations, no analytical study had been provided on these aspects. As we were working on time-reversal, we proposed to combine time-reversal filtering with the partial frequency reuse concept as subject of a new PhD program (Hua FU), that started in 2011 in a complementary way with the studies previously presented. This program was partially included in the framework of the ANR TRIMARAN project and with contractual studies with Orange Labs.

2.2 MU-MIMO ACHIEVABLE RATE IN THE MODERATE-SCALE ANTENNA REGIME

► Matched filters vs min-Interference filters

A first step in our studies was to extend the theoretical achievable rate results from the SU-MIMO case to the MU-MIMO case. When dealing with MUI, instead of using the matched filtering approaches studied before (TR, MRT, EGT), one may prefer null-steering strategies such as zero-forcing (ZF) [YM13b] or Regularized ZF [NE08]. ZF spatial filtering is a simple method to guarantee strict absence of the MUI terms by exciting orthogonal propagation modes of the channel. Using a classical flat fading matrix representation of the MU-MIMO system, the vector of the received symbols at each of the K receivers $\mathbf{Y}(n)$ for a particular subcarrier index n can be stated as,

$$\mathbf{Y}(n) = \underbrace{\mathbf{H}(n)\mathbf{G}(n)}_{\mathbf{W}(n)}\mathbf{S}(n) + \mathbf{N}(n) \quad (7.34)$$

where $\mathbf{G}(n)$ is the $M \times K$ spatial precoding matrix and $\mathbf{H}(n)$ the MU-MIMO channel matrix of size $K \times M$. Using ZF precoding means forcing the equivalent channel matrix $\mathbf{W}(n)$ to be an identity matrix. This is simply obtained imposing

$$\mathbf{G} = \frac{1}{\eta} \mathbf{H}^H (\mathbf{H}\mathbf{H}^H)^{-1} \quad (7.35)$$

where η is the power normalization factor of the filter. We understand that such a power normalization factor is directly influenced by the structure of the channel matrix, depending on the number of spatial links. Especially, if the channel matrix is ill-conditioned, the inversion will lead to a high value, and hence a dramatic degradation of the SNR. If the entries of channel matrix \mathbf{H} follow unit variance i.i.d complex Gaussian processes, it can be shown that the focusing gain \mathcal{G}_{ZF} of the ZF scheme tends to $\frac{M-K}{K}$ [WCDS12a]. This means that ZF precoding can not accommodate a two important increase of the number of users, unless the number of transmit antennas is sufficient, as in the large-scale antenna regime. This behaviour is illustrated in Fig. 7.13.

2. Spatial Filtering for MU-MIMO in Moderate-Scale Antenna regime

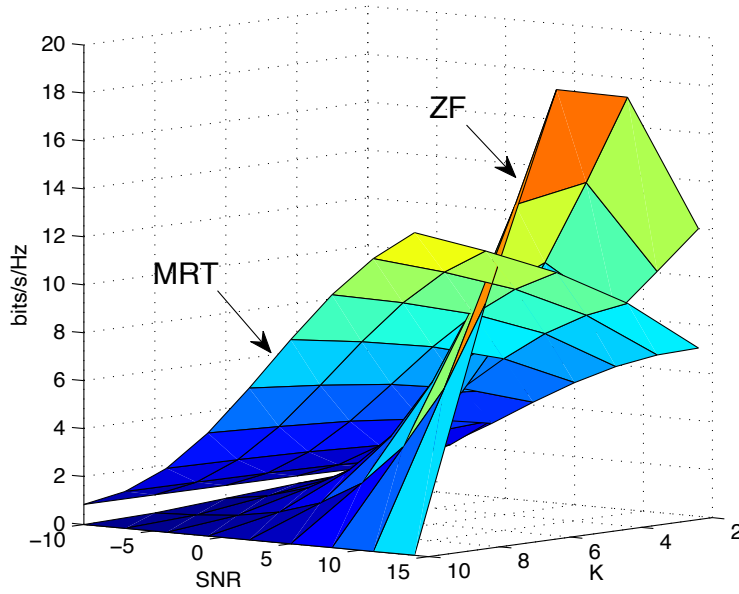


FIGURE 7.13– Comparative achievable rates MU-MIMO systems using ZF and MRT precoding schemes with $M = 8$ transmit antennas.

From these considerations, and adding the complexity fact of matrix inversion, we chose to pursue our studies preferring matched-filtering approaches to deal with multi-user configurations. Then, the key aspect of the study was the evaluation of the impact of the MUI terms on the performance. We first led the analysis through the derivation of the achievable rate as explained in the sequel.

► Achievable rate analysis

The generalization of Eq. (7.20) to the case of a MU-MIMO system leads to the following expression,

$$\mathcal{R}_{\text{MU-MIMO}} = \mathbb{E} \left\{ \frac{1}{N} \sum_{n=0}^{N-1} \log_2 \left(1 + \frac{|\tilde{W}_k(n)|^2 \gamma}{\sum_{j \neq k} |\tilde{W}_{kj}(n)|^2 \gamma + 1} \right) \right\} \quad (7.36)$$

with the definitions of \tilde{W} taken from the system model introduced in section 1.3. The derivation of this equation is not straightforward since the useful and interference terms may not be independent. Indeed equivalent channels \tilde{W}_{kj} embed the channel fading coefficients of the spatial links also involved in \tilde{W}_k . A capacity lower bound can be derived as proposed in [JAMV11], based on the common worst-case of uncorrelated additive interference modeled as a complex Gaussian distribution of the same variance [HH03]. Even if such assumption can be accepted for asymptotically high M , it turns out to be very inaccurate in a moderate-scale antenna regime. The other common approach used by many authors since the introduction of the Massive MIMO concept is to invoke the channel hardening effect which occurs at large M [YM13b]. This roughly consists in stating that the interference and useful terms become somehow deterministic if $M \rightarrow \infty$. In that case, we get a much simpler expression for the achievable rate,

$$\mathcal{R}_{\text{MU-MIMO}} \xrightarrow{M \gg 1} \frac{1}{N} \sum_{n=0}^{N-1} \log_2 \left(1 + \frac{\mathbb{E}\{\tilde{W}_k^2(n)\} \gamma}{\sum_{j \neq k} \mathbb{E}\{\tilde{W}_{kj}^2(n)\} \gamma + 1} \right) \quad (7.37)$$

which can also be almost viewed as the convergence of the achievable rate to its upper-bound based on Jensen's inequality. However, at moderate scale antenna regime, this strong assumption does not hold. One of our contributions was then to work out the initial achievable rate derivation of Eq. (7.37), i.e. without assuming channel hardening considerations. Our first investigations led us to study in details the distributions of the useful and interference terms up to the conclusion that these terms can eventually be modeled by two independent random processes. In other words, although the useful term and the interference term are both function of a

common random process, they can be considered as independent. This result essentially holds because of the uniformly distributed phase of the common random process. From this fact, the useful term can be modeled as proposed in Contrib. III.4. As for the interference terms, they do not follow a Gaussian distribution but rather a Gamma distribution. This first result is formally stated in the following contribution.

Contribution III.10 (Analytic Expression)

Approximated Average Achievable Rate of TR/MRT/EGT MU-MIMO Systems

Assuming independent normalized complex Gaussian fading per antenna link, the achievable rate of a MU-MIMO system with K users based on TR/MRT/EGT precoding is accurately approximated as

$$\tilde{\mathcal{R}} \approx \int_{X \in \mathbb{R}^+} \int_{Y \in \mathbb{R}^+} \log_2 \left(1 + \frac{x^2}{y+1} \right) p_X(x) p_Y(y) dx dy \quad (7.38)$$

where X and Y are two independent random processes with X following the laws given in Contrib. III.4 for each spatial filter, and $Y \sim \text{Gamma}(1, K - 1)$.

It is interesting to note that the distribution of the interference term in Contrib. III.10 is not changing from one spatial filter scheme to another, whereas the distribution of the useful term does (according to already established results in Contribution II.8). As an example in Fig. 7.14, it is verified that the proposed random processes provide a tight model for the achievable rate computation in the TR precoding case. The model is valid whatever the number of antennas and for all SNR range. From the above contribution, it is even possible to go a step further in the EGT and MRT cases, for which it is possible to gather the two random processes X and Y into a single one which directly models the SINR, as proposed hereafter.

Contribution III.11 (Analytic Expression)

Approximated Average Achievable Rate of MRT/EGT MU-MIMO Systems

Assuming independent normalized complex Gaussian fading per antenna link, the achievable rate of a MU-MIMO system with K users based on MRT and EGT precoding is accurately approximated as

$$\tilde{\mathcal{R}} \approx \int_{Z \in \mathbb{R}^+} \log_2(1+z) p_Z(z) dz \quad (7.39)$$

where Z is a random processes with PDF,

$$p_Z(z) = \frac{\theta e^{\frac{1}{(K-1)\gamma}}}{(K-1)(M-1)!} \frac{z^{M-1}}{\left(z + \frac{\theta}{K-1}\right)^{M+1}} \Gamma\left(M+1, \frac{1}{\gamma} \left(\frac{1}{\theta} + \frac{1}{(K-1)}\right)\right) \quad (7.40)$$

with $\theta = 1$ for MRT and $\theta = \frac{1 + \frac{\pi}{4}(M-1)}{M}$ for EGT, and $\Gamma(x, s)$ the upper incomplete Gamma function.

However, it turns out that no closed-form solutions to the ergodic capacity can be established due to the high complexity of the statistical law. In the literature, one can find closed-forms only in the massive MIMO regime [HCPR12b]. Nonetheless it is possible to get some lower and upper bounds as in the SU-MIMO case, without invoking the asymptotic regime. These bounds have partly been proposed in [C.20] and are still being worked out for future publications. As an example, the lower bounds are summarized in the following contribution.

2. Spatial Filtering for MU-MIMO in Moderate-Scale Antenna regime

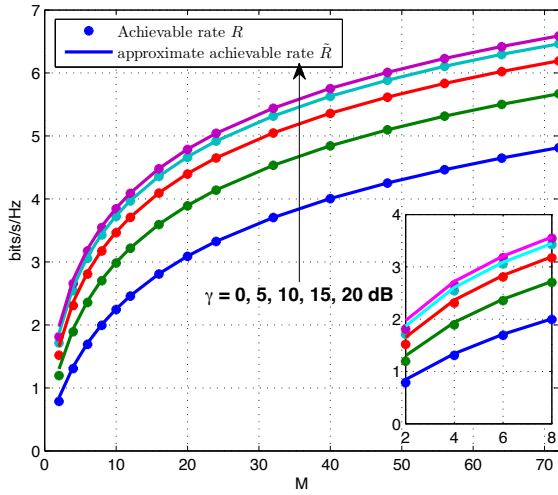


FIGURE 7.14– Exact and approximated achievable rate of the TR MU-MIMO system. Approximation is obtained from the random processes proposed in Contrib. III.10.

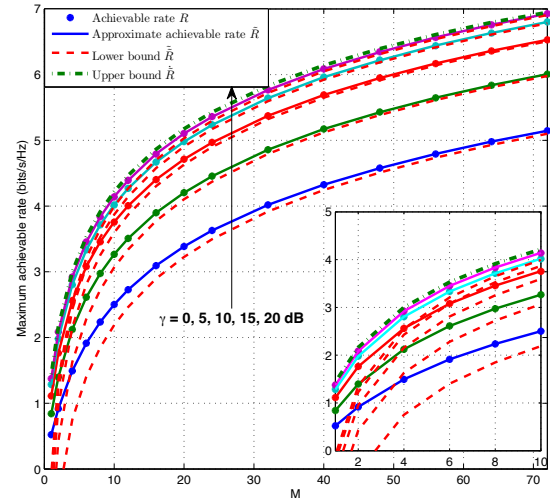


FIGURE 7.15– Achievable rate of the MRT MU-MIMO OFDM system (Simulation, Approximation, Lower-bound at high SINR, and Upper-bound at high SINR).

Contribution III.12 (Analytic Expression)

Lower Bounds of the Average Achievable Rate of MRT/EGT MU-MIMO Systems

Assuming independent normalized complex Gaussian fading per antenna link, the lower bounds of the achievable rate at high SINR regime of a MU-MIMO system with K users based on TR/MRT/EGT precoding are

$$\mathcal{R}_{\text{MU-MIMO}}^{\text{low}} = \mathcal{R}_{\text{SU-MIMO}}^{\text{low}} + \frac{e^{\frac{1}{(K-1)\gamma}}}{\log 2} \text{Ei}\left(-\frac{1}{(K-1)\gamma}\right) \quad (7.41)$$

with $\mathcal{R}_{\text{MU-MIMO}}^{\text{low}}$ given in Contrib. III.6 for TR/EGT/MRT, and $\text{Ei}(x)$ the exponential integral function.

Corresponding simulation results are given in Fig. 7.15 in the case of the MRT filters. It appears that the obtained bounds are less accurate in the MU case than in the SU case, unless M or SNR is sufficiently large. Hence, the derivation of closed-forms or approximated closed-forms for the theoretical achievable rate in MU-MIMO systems without particular assumption on the antenna scale is still an open problem. Since the end of our work in 2015 on this subject, massive MIMO concepts have been so largely accepted that the new contributions about average achievable rate have always been considering the channel hardening effect as a basic assumption, thereby not considering the case when M remains moderate.

2.3 BER PERFORMANCE WITH PARTIAL BANDWIDTH OVERLAP

After our work on average achievable rate, we have been interested in practical performance using conventional modulation constellations. As already discussed at the beginning of section 2.2, using MRT/TR/EGT filters is expected to lead to potentially strong MAI terms. Instead of reducing such MAI level by means of orthogonalization methods as with ZF and thus losing at the level of the focusing gain, we have proposed some partial frequency reuse mechanisms to control the MUI as detailed hereafter. The reason for excluding ZF of the scope of our study was also because we were focusing on system designs adapted to decentralized scenarios, i.e.

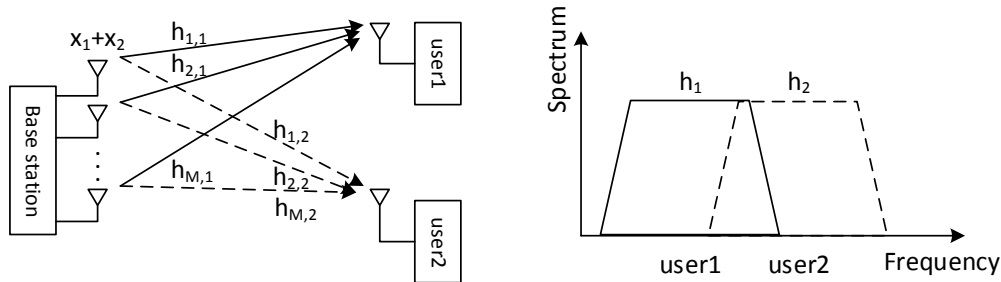


FIGURE 7.16– Simple illustration of the two-user partial frequency band overlapping (PFBO) scheme.

in the case of cooperative spatial filtering between distant stations. For the same reason, MRT precoding could not be considered in our scenario. Hence only EGT and TR are the selected filters for the rest of the study.

► Partial frequency bandwidth overlapping system model

From the system model introduced in 1.3, spatial matched filters such as TR and EGT are not initially designed to cancel the inter-user interference in MU-MIMO systems. The interference term is only asymptotically zeroed or can at least be neglected compared to noise thanks to the tight focusing effect at large M . In a moderate-scale antenna regime however, the system performance is expected to be directly resulting from the SINR level due to imperfect spatial focusing. The idea behind the proposed partial frequency reuse scheme is to control such SINR level by constraining the inter-user interference to appear in some frequency subband only. Accordingly, instead of reusing the whole available bandwidth for each user as in the classical MU-MIMO approach, two particular users would only share a common subband, or a common subset of subcarriers in the multicarrier case. The principle is depicted in Fig. 7.16 for a two-user scenario. Applying the sub-band reuse concept to the system model in 1.3 leads to the following received signal for one particular user j considered as the user of interest,

$$Y_j = \frac{1}{\sqrt{K}} \cdot \underbrace{\tilde{W}_j \cdot S_j}_{\text{useful term}} + \frac{1}{\sqrt{K}} \cdot \underbrace{\sum_{k \neq j} \tilde{W}_{kj} \cdot B_k \cdot S_k}_{\text{Interference term}} + N_j \tag{7.42}$$

in which we introduce the diagonal sub-band assignment matrices B_k which diagonal entries are $B_k(n) = 1$ if the n th subcarrier is assigned to user k , and 0 otherwise. Accordingly, we may define the frequency overlap ratio of the system as,

$$\tau = \frac{1}{K} \sum_{k=1}^K \tau_k \quad \text{with, } \tau_k = \frac{1}{N} \text{Tr} \left(\sum_{j \neq k} B_j \right) \tag{7.43}$$

with τ_k is the overlap ratio of user k . An overlap ratio τ_k means that user k shares τ_k % of its subcarriers with others users³. If all assignment matrices B_k are identity, the overlap ratio reaches $K \times 100\%$ and the MAI term is maximized. This latter case is the typical situation of conventional MU-MIMO systems.

From a general perspective, the optimal setting of such a system is highly complex, since it can be viewed as a mixed integer programming problem, albeit some greedy or iterative solutions can be found. However, our aim was rather to evaluate the system BER degradation regarding the overlap ratio and then understand how such a degree of freedom can be exploited regarding some quality of service constraints. Indeed, any sub-band assignment algorithm would need some evaluation of the performance degradation to decide how to share the spectrum between several users. SINR based measurements could be used in a first approach, but we will see that more precise performance estimation can be obtained.

Eventually, the underlying issue to address is the evaluation of the BER of a MU-MIMO system with a variable number of users, a variable number of antennas and using a finite symbol alphabet according to a particular constellation. Under the massive MIMO assumption again, the answer is almost straightforward since

3. Note that random assignment matrices could also be used to target a particular overlap ratio without changing the rest of the study.

2. Spatial Filtering for MU-MIMO in Moderate-Scale Antenna regime

the interference terms can be reasonably approximated as extra additive Gaussian noise [R.4]. Yet, in the moderate-scale antenna regime, further investigations are needed as developed during the work of H. Fu and summarized in the sequel.

► BSPK Constellation with two competing users

The simplest model to start with is the case of Binary Phase Shift Keying (BPSK) modulation with only two users assigned to a same sub-band. We derived the theoretical BER of such a situation, when EGT filtering is used⁴. Beyond the obtained BER closed-form, the developed analysis gives new insights into how fading effects and MUI terms behave in a MU-MIMO system with not so large M values. Indeed, on the subject of interfering systems, one can find some problems with close formulations in the literature, for example about cochannel interference in cellular systems [BC04] or in jamming situations [LAZ07]. However, in the papers dealing with theoretical derivations (and not simulations) interfering signals are mostly considered as Gaussian process. In multiuser MIMO systems however, the MUI term experiences the same channel fading as the useful signal, which introduces correlation in the received signal and makes the Gaussian approximation inappropriate. During the PhD of H. Fu, we experimented a new way of modeling the interfering signal as directly taking part of the fading effect of the channel. We proposed our method and published our results in [R.4]. The main points are summarized below.

Let us first give the simplified expression of the received signal $y^{(1)}$ (for the user of interest) as,

$$y^{(1)} = \frac{1}{\sqrt{M}} \sum_{m=1}^M |H_m^{(1)}| x^{(1)} + \frac{1}{\sqrt{M}} \sum_{m=1}^M |H_m^{(1)}| e^{j\theta_m} X^{(2)} + n \quad (7.44)$$

with θ_m a phase rotation due to EGT. This model involves the desired symbol $x^{(1)}$ and the interfering symbol $x^{(2)}$. Since x belong to a finite alphabet of reduced dimension common models based on the classical Gaussian approximation of the interfering term or on other RV assumed independent of the useful term are likely to yield poor BER estimates [JAMV11]. One may rather try to get the joint p.d.f. for the useful and interference terms. To circumvent such a hard task, we rather proposed in our study to treat the MUI term as an additional distortion factor applied to the useful term. This is obtained letting $x^{(2)} = \rho e^{j\phi} x^{(1)}$, with ρ and ϕ depending on the constellation point coordinates. This leads to the modified model,

$$y^{(1)} = \underbrace{\frac{1}{\sqrt{M}} \sum_{m=1}^M |H_m^{(1)}|}_{\xi} (1 + \rho e^{j\psi_m}) x^{(1)} + n \quad (7.45)$$

where $\psi_m = \theta_m + \phi$ such that $\psi_m \sim \text{Unif}(0, 2\pi)$. This expression highlights the fact that the system can be viewed as a particular fading model governed by the complex weighting factor ξ . Our idea was to find some statistical model to ξ and then derive the average BER. In the simple case of BPSK constellation, finding the convenient PDF of ξ is tractable under some reasonable assumptions and approximations. The first result we obtained, considering BSPK and two users, is stated in the following Contrib. III.14 and detailed in [R.4].

It is noticed that the statistic law that is obtained in Eq. (7.46) of Contrib. III.14 is the same as that of the EGT SU-MIMO system (see Contrib. III.4), with however different parameter expressions. The proposed model is controlled by parameters \tilde{m} and $\tilde{\omega}$ which can be simplified if M is sufficiently high, in practice as soon as $M > 8$. The former reveals the intrinsic (inverse) fading amplitude of the MISO Rayleigh channel, while the latter represents a kind of “overfading” effect due to interference. The equivalent channel can hence be viewed as a global fading model for the interfered Rayleigh MISO channel.

In Fig. 7.17, the typical scatter plot obtained at the receiver for one of the two possible BPSK symbols is represented. As evident from the shape of the cloud of points, the interference could not been considered as Gaussian additive. In Fig. 7.18, the comparison between the empirical PDF and the theoretical Nakagami PDF is given, confirming the accuracy of the proposed model for various M.

4. It turned out that TR precoding led to much more complex derivations which were in most of the case even not tractable.

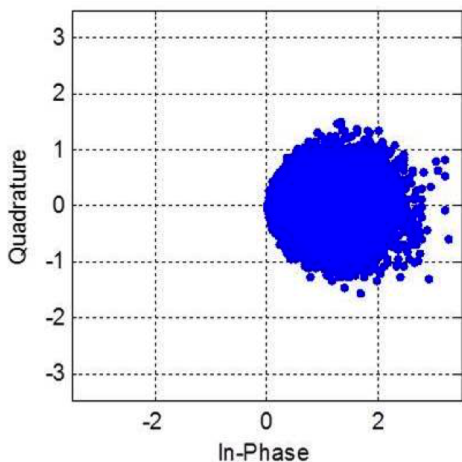


FIGURE 7.17– Received BPSK scatter plot without noise with EGT precoding and two competing two users.

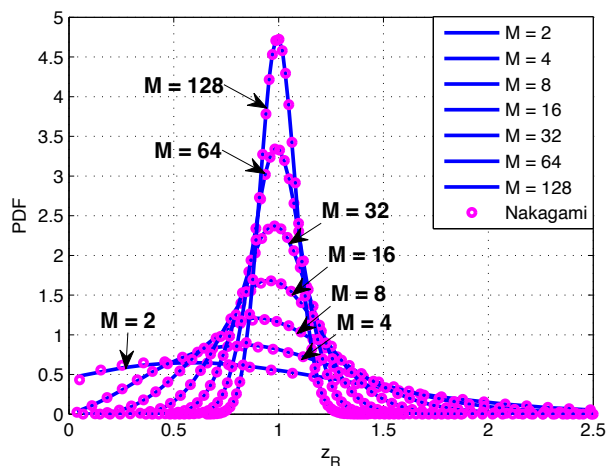


FIGURE 7.18– PDF of the amplitude of the received In-phase component with BPSK, EGT precoding and two competing users.

Contribution III.13 (Analytic Expression)

Nakagami equivalent fading model of a two-user BPSK EGT MU-MIMO System

Assuming independent normalized complex Gaussian fading per antenna link, the equivalent fading model of a two-user BPSK EGT MU-MIMO transmission can be approximated as,

$$y = \xi x + n \quad \text{where, } \xi \sim \text{Nakagami}(\tilde{\mu}, \tilde{\omega}) \tag{7.46}$$

with n the Gaussian noise sample, and ξ an equivalent Nakagami fading model such that,

$$\tilde{\mu} \left[\frac{\Gamma(\tilde{\mu})}{\Gamma(\tilde{\mu} + \frac{1}{2})} \right]^2 = 1 + \frac{\frac{6}{\pi} - 1}{M} \quad \text{and, } \tilde{\mu} \xrightarrow{M \gg 1} \bar{\mu} = \frac{\pi}{24 - 4\pi} M + \frac{1}{8} \tag{7.47}$$

$$\tilde{\omega} = \frac{\pi(M - 1) + 6}{\pi(M - 1) + 4} \quad \text{and, } \tilde{\omega} \xrightarrow{M \gg 1} \bar{\omega} = 1 \tag{7.48}$$

► Extension to QSPK Constellation and to multiple users

From Eq. (7.45), it is possible to apply the proposed method to the QPSK case and it can be shown that the Nakagami distribution can be used as a good equivalent fading model again. However, as illustrated by the scatter plot of Fig. 7.19, the cloud of points is crossing the real and imaginary axes, which translates into a PDF with non-zero values for $x < 0$. Yet, the Nakagami distribution is strictly positive definite. As the global shape of the PDF seems convenient, we proposed to modify the Nakagami distribution into a so-called translated Nakagami distribution. The shifted version of the PDF is such that it can be defined for positive values only. Many values of translation Δ may be used in practice. A convenient choice, obtained through extensive simulations, is to take $\Delta = 1$. Finally, extension to higher order modulations, e.g. 16QAM, becomes harder to study, albeit possible. Hopefully, the need to treat such cases is questionable since the Gaussian approximation becomes progressively acceptable as the order the constellation increases.

It is also possible to extend our model to the multiple user case, i.e. for more than two users. In such a case, the translated Nakagami solution turns out to be a good approximation to the equivalent fading channel as illustrated in Fig. 7.20 where a translation factor of $\Delta = 1$ is used to make the Nakagami PDF be defined over $[-1, +\infty)$. The proposed translated Nakagami model is summarized in the following contribution. A journal paper is in preparation for the unified approach exposed here.

2. Spatial Filtering for MU-MIMO in Moderate-Scale Antenna regime

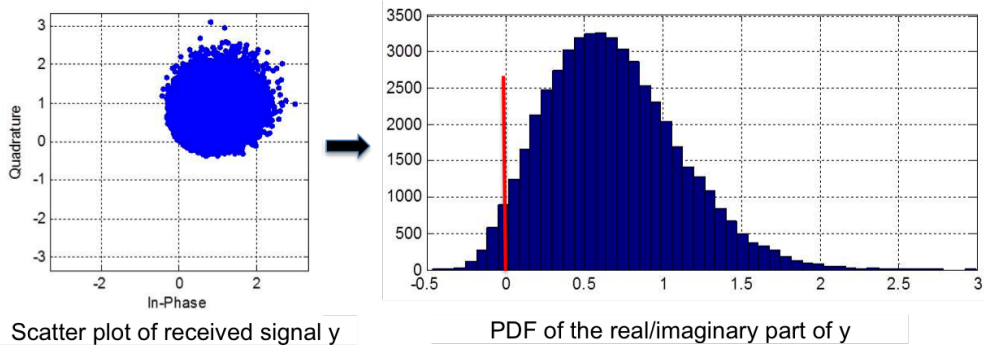


FIGURE 7.19– Received QPSK scatter plot with EGT precoding with two competing two users, and empirical PDF of the amplitude on the real and imaginary parts.

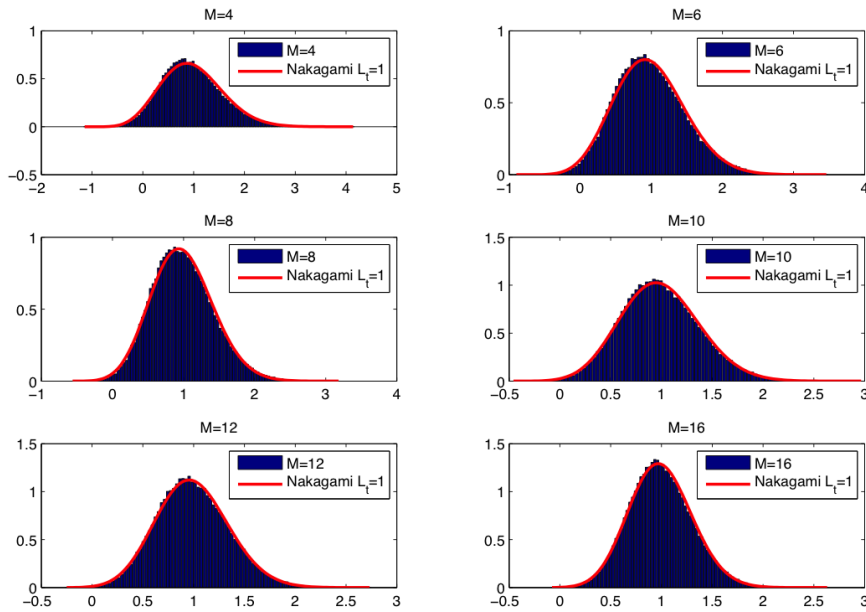


FIGURE 7.20– PDF of the amplitude of the received In-phase component with BPSK, EGT precoding and 3 competing users.

Contribution III.14 (Analytic Expression)

Translated-Nakagami equivalent fading model of a K-user BPSK EGT MU-MIMO System

Assuming independent normalized complex Gaussian fading per antenna link, the equivalent fading model of a K-user QPSK EGT MU-MIMO transmission can be approximated as,

$$y = v_I x_I + j v_Q x_Q + \Delta + n \quad \text{where, } v_{I,Q} \sim \text{Nakagami}(\tilde{\mu}, \tilde{\omega}) \quad (7.49)$$

with n the Gaussian noise sample, and $v_{I,Q}$ two independent Nakagami processes defined as,

$$\tilde{\mu} = \frac{\alpha \pi M + \Delta^2 (4 - \pi)}{8(K+1) - 4\pi} + \frac{1}{8} \quad \text{with, } \alpha = 1 + 2\Delta^2 + 2\Delta \sqrt{\frac{\pi(M-1) + 4}{\pi M}} \quad (7.50)$$

$$\tilde{\omega} = \frac{\pi(M-1) + 2(K+1)}{\pi(M-1) + 4} + 2\Delta \sqrt{\frac{\pi M}{\pi(M-1) + 4}} + \Delta^2 \quad (7.51)$$

in which Δ is a translation factor adjusted through simulations.

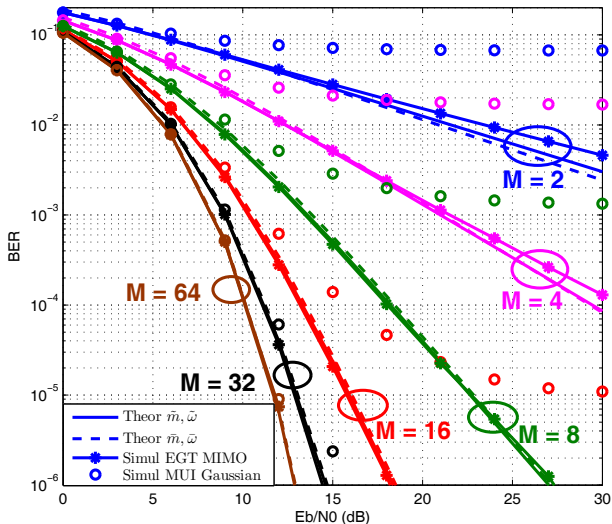


FIGURE 7.21– Average BER of the EGT MU-MIMO system with two competing users using BPSK modulation and 100% bandwidth overlap.

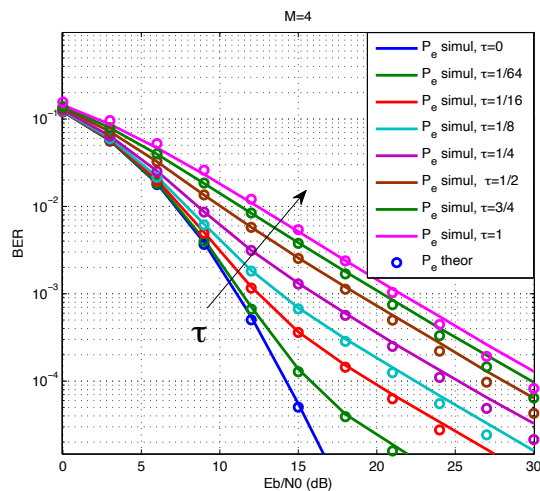


FIGURE 7.22– Average BER of the EGT MU-MIMO system with two competing users using BPSK modulation and variable overlap ratios τ .

► Simulation results

From the developed statistical models, it is then possible to derive some closed-forms of the average BER. As an example, using the parameters $\tilde{\mu}$ and $\tilde{\omega}$ of the equivalent Nakagami fading channel, the closed-form obtained with BPSK/QPSK writes,

$$P_e(\gamma_b) = \frac{\Gamma_B(\tilde{\mu} + \frac{1}{2})}{\Gamma_B(\tilde{\mu} + 1)} \cdot \frac{[\frac{\tilde{m}}{\tilde{\omega}}]^\mu \gamma_b^{\frac{1}{2}}}{[\gamma_b + \frac{\tilde{\mu}}{\tilde{\omega}}]^{\tilde{\mu} + \frac{1}{2}}} \times {}_2F_1\left(1, \tilde{\mu} + \frac{1}{2}, \tilde{\mu} + 1, \frac{\frac{\tilde{\mu}}{\tilde{\omega}}}{\frac{\tilde{\mu}}{\tilde{\omega}} + \gamma_b}\right) \tag{7.52}$$

where $\gamma_b = \frac{\sigma_b^2}{N_0}$. This last result gives us a formula to predict the BER of a MU-MIMO system with an arbitrary number of antennas and an arbitrary number of users utilizing the same sub-band. Fig. 7.21 gives an example of the obtained results with BPSK modulation for the two-user case. Comparison is made between the proposed Nakagami model and the common Gaussian approximation. It is clearly concluded that the proposed model is much more accurate in predicting the BER than the Gaussian approach.

Finally, it is possible to run performance simulations of the proposed partial frequency overlap system. Depending on the overlap ratio τ , the global BER is obtained through a weighted average between the BER in the single user case for the non-overlapped sub-bands and in the multi-user case when the sub-band is used by more than one user. Hence, the system BER is computed using both the theoretical BER formula obtained in SU-MIMO case (see Eq. 7.30) and the above formula for the MU-MIMO case (Eq. (7.52)). In Fig. 7.22, an example of BPSK BER curves is given for various overlap ratios, in the case of two competing users with $M = 4$ antennas. It is noticed that the Gaussian approximation becomes acceptable from $M = 32$ antennas and almost equivalent to our model for $M = 64$ antennas. This is due to the Nakagami distribution which tends to a Gaussian one as the scale parameter $\mu \rightarrow \infty$. Hence, the proposed Nakagami model can be viewed as a general statistical model for MU-MIMO interfering channels, also valid for low M .

Finally, in Fig. 7.23, a synthetic performance chart is given allowing to identify which overlap ratio can be tolerated for a target BER performance of 5×10^{-3} depending on the number of available antennas. We clearly see the progressive beneficial effect of increasing the number of antennas. Using our closed-forms, it is then possible to obtain such kind of system level analysis for any number of antennas and not solely in the massive MIMO regime.

2. Spatial Filtering for MU-MIMO in Moderate-Scale Antenna regime

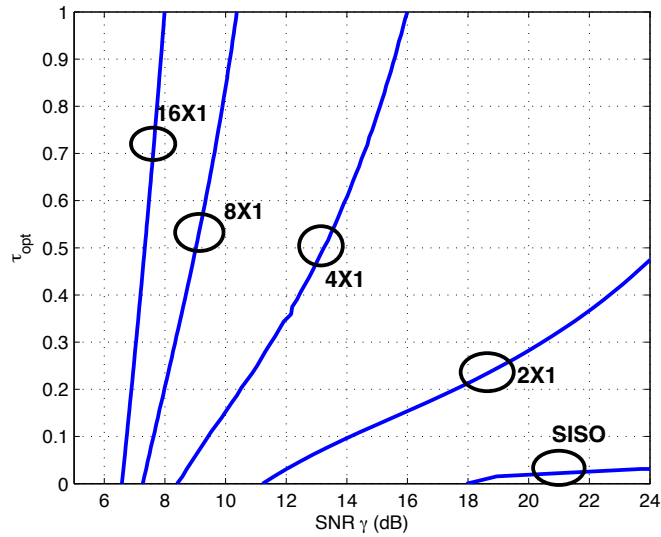


FIGURE 7.23– Maximal overlap ratio τ for a target BER of 5×10^{-3} and for variable number M of antennas.

2.4 EXTENSION TO SS-OFDM WAVEFORM

In the same general study on MU-MIMO systems with partial sub-band overlap, we also try to study the influence of a spread-spectrum (SS) component added to the OFDM waveform. As SS-OFDM is known to be robust to narrow-band interference, the MU-MIMO SS-OFDM system with sub-band overlap is expected to outperform the OFDM system, at least in some situations that have to be identified. Following the same approach as previously, we analyzed the BER performance of the SS-OFDM system based on an inter-channel interference model and then compared the robustness of the SS-OFDM and OFDM waveforms to the overlap ratio, depending on the number of antennas.

► SS-OFDM system model

The combination of SS with OFDM, yielding so-called linear precoded OFDM (LP-OFDM) [Kai02], has been widely studied and demonstrated to offer an additional multipath diversity gain to conventional OFDM [DJ98, Pop99]. In addition, spread-spectrum techniques are well-known to increase the resistance of a system to the interference and jamming. Hence, in our context of sub-band reuse, a competing user can be viewed as a possibly narrow-band interference which negative impact could be advantageously mitigated using spreading sequences. SS can easily be associated to OFDM by applying the spreading sequences to the symbols conveyed by the OFDM subcarriers, in the form of a linear precoding function applied to the frequency domain symbol vector before OFDM modulation through DFT. To accommodate various transmission constraints, many spreading code families have been proposed in the literature [Gol67]. As we are in a synchronous communication system, we have been using the classical orthogonal Walsh-Hadamard spreading sequences [TZ06]. Formally, the transmitted signal, including spatial filtering can be stated as,

$$Y_j = \frac{1}{\sqrt{K}} \underbrace{\tilde{W}_j P S_j}_{\text{useful term}} + \frac{1}{\sqrt{K}} \underbrace{\sum_{k \neq j} \tilde{W}_{kj} B_k P S_k}_{\text{Interference term}} + N_j \quad (7.53)$$

with the spreading code matrix P introduced to model the SS-OFDM waveform in the form of a linear precoding. Note that the same spreading matrix is used for all the users. However, looking at the interference term, it is observed that the sub-band allocation matrix B_k acts as a puncturing process applied to the spreading matrix P of the interfering users. Hence, unless a 100% overlap ratio is used, the only user who receives the totality of the code chips is the user of interest j . Therefore, a partial frequency overlap translates into a partial sequence overlap, as simply illustrated in Fig. 7.24 in a two-user scenario. It is finally noticed that each user in a full-load

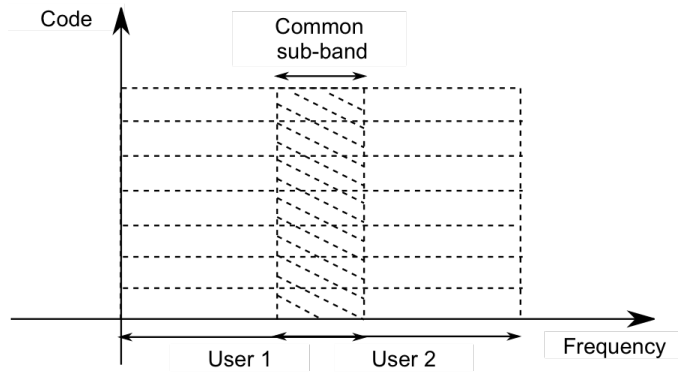


FIGURE 7.24– Illustration of a two-user partial frequency overlap model with SS-OFDM waveform.

SS-OFDM situation, i.e. each user makes use of all the available sequences to spread its own data symbols over the spectrum. This means that the spreading sequences are not used for code division multiple access (CDMA) but rather to whiten the interference terms.

At the receiver side, despreading has to be process to sum up all the code chips of all sequences hence retrieving the data symbols. Due to the fading channel effects, the orthogonality (or pseudo-orthogonality) between the spreading sequences is lost. In practice, it is then convenient to equalize the receive frequency domain signals before despreading. It is well-known that the MMSE equalizer gives the best results in terms of BER performance [HLGHB01]. In such a case, the output symbol vector at the receiver side, after equalization and despreading can be expressed and decomposed as,

$$\begin{aligned}\hat{S}_j &= \frac{1}{\sqrt{K}} \mathbf{P}^H \mathbf{E}_j \tilde{\mathbf{W}}_j \mathbf{P} \mathbf{S}_j + \frac{1}{\sqrt{K}} \sum_{k \neq j} \mathbf{P}^H \mathbf{E}_j \tilde{\mathbf{W}}_{kj} \mathbf{B}_k \mathbf{P} \mathbf{S}_k + \tilde{\mathbf{N}}_j \\ &= \mathbf{Z}_j \mathbf{S}_j + \underbrace{\mathbf{I}}_{\text{ICI}} + \underbrace{\mathbf{J}(\tau)}_{\text{MAI}} + \tilde{\mathbf{N}}_j\end{aligned}\quad (7.54)$$

where matrix \mathbf{E}_j accounts for equalization at the j th receiver. Compared to the OFDM case, an additional Inter-code Interference term (ICI) has to be considered owing to the imperfect orthogonality among the spreading sequences after MMSE equalization.

► Approximate BER

The general study of each of these terms have to be led in the perspective of some BER theoretical derivation. In the literature, some coarse estimation of the performance degradation in case of partial sub-band reuse can be found, defining the so-called jammer-to-signal ratio [PKH+03, LAZ07]. As it will be highlighted later on, this approach is far from being accurate in the BER prediction. **Paying particular attention to our system model, it is noticed that each signal component results from an averaging over all the subcarriers owing to the spreading function. In this way, the coloured narrow band interference responsible of the MAI term turns out to be transformed into a white noise over the whole bandwidth.** This common assumption can be verified in our case and is shown to be a sufficient approximation at high SNR range, (typically above 10 dB), and for a high, albeit moderated, number of antennas (typically $M > 8$). Similar conclusion can be drawn for the ICI term, hence leading to an homogeneous expression of the received symbols, whatever the subcarrier index n , as

$$\hat{S}(n) = \rho S(n) + \omega_{\text{ICI}} + \omega_{\text{MAI}} + \omega_{\text{N}} \quad (7.55)$$

where ω_{ICI} , ω_{MAI} and ω_{N} follow independent complex Gaussian processes, and ρ is a real random variable driving the average fading due to the combined effects of spreading/despreading, spatial filtering, channel propagation and equalization. From this fact, we have finally showed that a good approximation of the BER could be obtained simply taking into account second order statistics of the random processes, as summarized in the following contribution. **Note that the result remains valid for other fading models than the theoretical complex Gaussian model. This means that the proposed approximate BER formula can be used for any channel model, as soon as the second order statistics of the involved random variable can be extracted.** Some further results at this level have been published in [C.27].

Contribution III.15 (Analytic Expression)

Approximated Average BER for a MU-MIMO SS-OFDM System

Assuming independent fading per antenna link, the average BER performance of a MU-MIMO SS-OFDM system using EGT/MRT/TR precoding can be approximated through,

$$BER \approx Q \left(\sqrt{\frac{\mathbb{E} [|\rho|^2] \sigma_s^2}{\mathbb{E} [|\omega_{ICI}|^2] + \mathbb{E} [|\omega_{MAI}|^2] + \mathbb{E} [|\omega_N|^2]}} \right) \quad (7.56)$$

with the variance of ρ , ω_{ICI} , ω_{MAI} and ω_N specifically computed from the system model of Eq. (7.54) taking into account the precoding scheme and the channel model.

► Performance results

Using the proposed approximate BER formula, we give in Fig. 7.25 the BER curves obtained with SS-OFDM over BRAN-A channels [Med98]. A comparison is made between the simulated results, the theoretical results extracted from our approximation and the results obtained applying the partial-jamming approach found in literature, e.g. in [LAZ07]. The given curves represent various settings of the overlap ratio, from $\tau = 1\%$ to 100% , with a number of antennas set to $M = 4$. It is clearly concluded that the proposed strategy gives the best prediction of the BER, namely concerning the level of the error floor at high SNR.

In addition, using the BER expressions obtained with OFDM and SS-OFDM systems, it is also possible to lead comparative simulations in the context of MU-MIMO transmissions with partial sub-band reuse. In particular, it is interesting to study in what extent SS-OFDM can be more robust to MAI and tolerate a higher overlap ratio compared to OFDM. As already discussed, SS-OFDM is expected to offer better immunity in a moderate-scale antenna regime. First results showing the superiority of the SS-OFDM waveform are given in Fig. 7.26 in the case of $M = 10$ when the overlap ratio τ varies from 1% to 12% . The robustness of the SS-OFDM waveform over the OFDM waveform is clearly observed, since the former can better accommodate an increasing overlap ratio than the latter. However, it can be understood that the resistance of SS-OFDM to the interference starts failing from a given overlap ratio value. In addition, as SS-OFDM also suffers some ICI, its performance may even become worse than that offered by OFDM. To highlight this, Fig. 7.27 gives the maximum overlap ratio tolerated by each waveform for a target BER depending on the number of antennas. Interestingly, the SS-OFDM waveform maintains its advantage if $M < 10$, that is in the moderate-scale antenna regime.

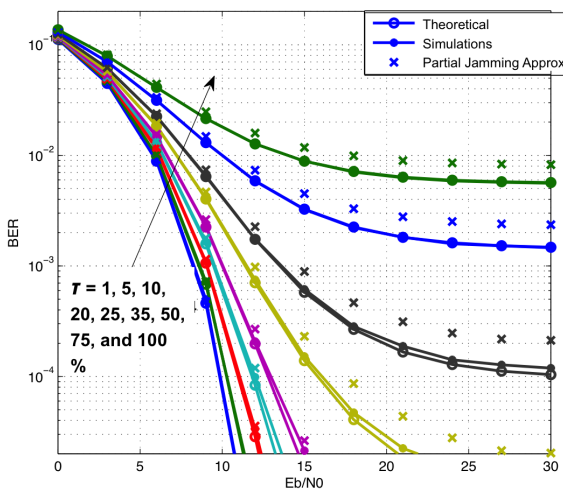


FIGURE 7.25– Average BER of the EGT MU-MIMO system based on SS-OFDM. QPSK modulation, $M = 4$ antennas, two competing users with variable overlap ratio τ .

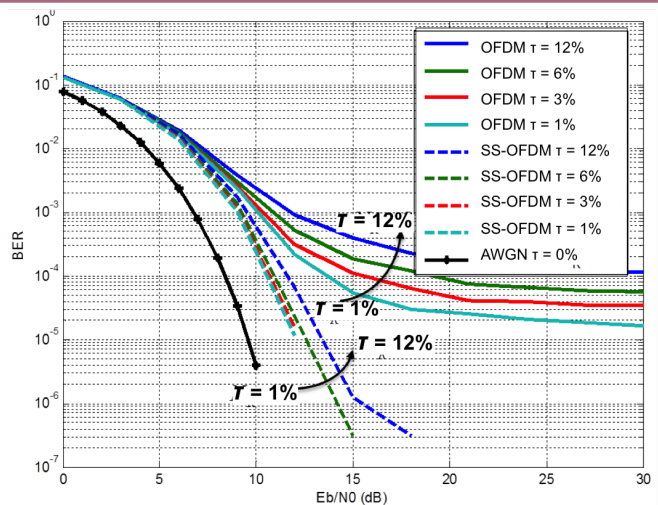


FIGURE 7.26– Comparison of average BER between OFDM and SS-OFDM in a EGT MU-MIMO system. QPSK modulation, $M = 8$ antennas, two competing users with variable overlap ratio τ .

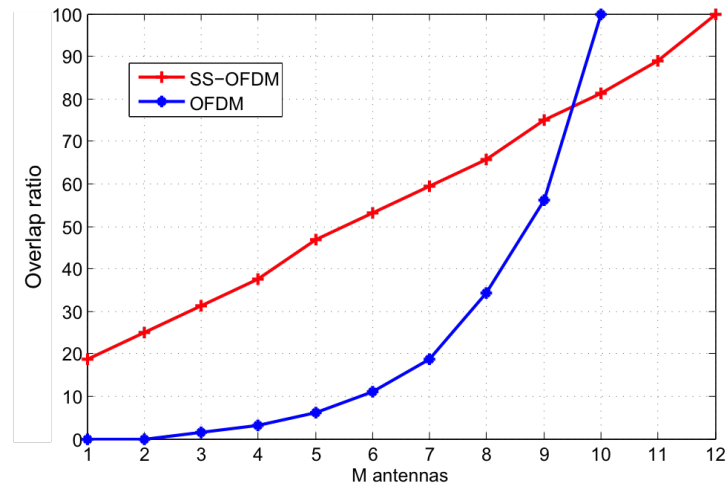


FIGURE 7.27– Achievable bandwidth reuse rate versus the number M of antennas at target $BER=10^{-3}$.

2.5 CONCLUSION

In this work, we have chosen to investigate the MU-MIMO system performance under the constraint of a moderate number of antennas at the central station, typically between 8 and 16. We did definitely not assume in our work any asymptotic regime of the MU-MIMO system, hence trying to tackle the problem of achievable rate and BER theoretical derivations with more general perspective. This has allowed us to bring some complementary insights in the very fertile period that had started since the introduction of the massive MIMO paradigm.

Our approach has been based on a thorough statistical analysis and modeling of the so-called equivalent channel resulting from the combined effect of spatial filtering and wireless propagation. As a result, we have been able to highlight the progressive focusing effects of matched-type spatial filters when increasing the number of cooperative antennas, providing some new analytical expressions of the achievable rate and BER. However, most of the closed-forms were obtained with MRT and EGT filters, the TR filter generally leading to much more complex expressions. Therefore, closed-form expressions for TR-based MU-MIMO systems are still to be solved.

On one other hand, most of our derivations have been based upon i.i.d complex Gaussian MIMO channel models. Even if this strong assumption allows for general system behaviour prediction, it may be far from describing the reality of the propagation conditions for practical systems. Nonetheless, the developed methodology based on statistical equivalent channel models may be easily extended to any propagation characteristics. Such analyses may even become essential since large-scale MIMO systems are expected to be deployed in mmWave bands, where i.i.d complex Gaussian models lack consistency.

Summary (PhD/Dissemination/Projects)

- 1 PhD (H. Fu)
- 1 international journal paper [R.4]
- 3 communications in international conferences and workshops [C.20][C.27][C.37]
- 1 GDR workshop
- 2 Tutorial in conferences (APWiMob'15, Softcom'15)

3 PRACTICAL BEAMFORMING STRATEGY FOR MMWAVE COMMUNICATIONS

3.1 MOTIVATIONS

The studies led during the PhD of Hua FU and summarized in the previous section were essentially focused on theoretical aspects based upon the common i.i.d. complex Gaussian model of the spatial links. The obtained results have a general scope and allows to understand the main trends in terms of MU-MIMO system performance, namely without particular assumption on the antenna array size. Yet, the translation of such results in practical propagation environments remains questionable, which encouraged us to start complementary studies with a more system-level view.

Four years after our first investigations about time-reversal and spatial filters, the concept of massive MIMO was already initiating deep changes in the way of envisaging the evolution of future communication systems [LETM13]. Firstly, the scientific community enthusiastically took up this new subject which was offering numerous new optimization opportunities. In parallel, industrials involved in the strategic reflexions of the future generation of wireless networks (5G) were starting considering Massive MIMO techniques as a key enabler to support higher achievable data rates [KPR12] [NNB⁺13]. A general trend that was also progressing at that period was the natural evolution towards higher frequency bands, namely the so-called mmWave usage. People were hence understanding that a joint use of millimeter waves and massive MIMO schemes could be viewed as a win-win scenario [EAHAS⁺12]. Indeed, MmWave regime enabled antenna arrays to be deployed with reasonable array form factors at such frequencies, which makes the large-scale antenna assumption become more conceivable.

Last but not least, network densification was a general idea which was also starting to be seriously considered as an additional degree of freedom for future wireless communication networks to achieve better coverage and higher data rates [BLM⁺14a] [JMZ⁺14]. Densely deploying small cells with high data rate requirements and small per cell coverage area encourages using new solutions adapted to Line-of-Sight (LOS) channels which are indeed favourable well adapted to mmWave frequencies [KPR12].

At that period started the IRT (Institute for Research and Technology) initiatives in France, with namely in Rennes IRT Bcom which was launched in 2013. I was involved in this new research structure to take part in new prospective works, and in particular in Massive MIMO studies. We then had the opportunity to launch a new PhD program on the topic of large-scale antenna systems in mmWaves. Our aim was to investigate the specificities of mmWave propagation conditions in the perperspective of designing adequate spatial filters. The results discussed hereafter have been provided in the framework of the RS-COM project within Bcom, under ANR and regional financial supports.

3.2 SYSTEM MODEL WITH GEOMETRIC-BASED CHANNEL DESCRIPTION

► Channel angular spectrum

The basic system model considered in this work is similar to that of the previous sections, except that the used channel matrix is of particular structure resulting from the specificities of the propagation channel in mmW. More precisely, as the carrier frequency increases, it can be shown that the propagation channel becomes sparser in the sense that less propagation rays can survive than in lower frequency bands due to higher losses when waves interact with obstacles. As a consequence, the channel matrix is mainly governed by the specular components of the propagation environment, corresponding to the most significative propagation rays. Adding the fact that off course the higher the operating frequency, the more accurate the ray-optics approximations, the MU-MIMO channel matrix can accurately be obtained from a pure geometrical representation of the propagation environment. From such a geometrical approach, a straightforward correlation between the antenna links is naturally obtained, giving more consistency to the MIMO channel model than using i.i.d. random fading processes.

To go further with this idea it becomes possible to provide an angular visualization of the channel as proposed in Fig. 7.28. The propagation channel can indeed be described through its angular spectrum, i.e. the collection

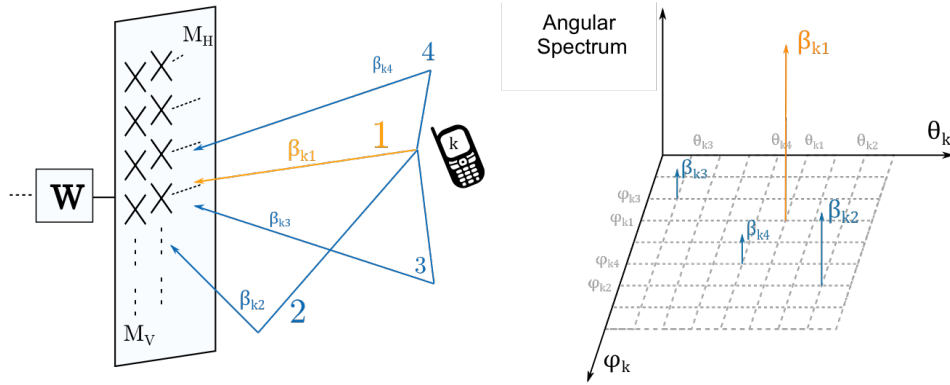


FIGURE 7.28– Representation of the MIMO channel from its angular spectrum.

of complex components associated to angles of arrival (or departure) of the impinging rays, in the horizontal (azimuth) and vertical (elevation) planes. Using an infinite size antenna array, each ray can be perfectly isolated and discriminated and the channel can be represented by a sum of specular components (angle-based Dirac delta functions). Hence, the specular angular spectrum can be stated as,

$$S(\theta, \varphi) = \sum_i \sum_j \sqrt{\beta_{ij}} e^{j\phi_{ij}} \delta(\theta - \theta_i, \varphi - \varphi_j) \quad (7.57)$$

with θ and φ the azimuth and elevation angles, respectively.

Yet, observing the propagation environment through an antenna array of limited size translates into some spatial filtering effect of the angular spectrum. Each impinging ray is then viewed through the antenna array angular response, commonly referred to as array factor $F(\theta, \varphi)$. Therefore, the angular spectrum taking into account the finite antenna array size writes,

$$S(\theta, \varphi) = \sum_i \sum_j \sqrt{\beta_{ij}} e^{j\phi_{ij}} F(\theta - \theta_i, \varphi - \varphi_j) \quad (7.58)$$

The well-known examples of linear or planar arrays yield Dirichlet functions for the array factor expressions [Chr00].

► Geometrical MIMO Channel Representation

From the above considerations, it is then possible to imagine a ray-based MIMO channel matrix description taking into account the angles of arrival of the propagation paths and the geometrical structure of the antenna array. Indeed, from the antenna array geometry it is possible to define the so-called steering vectors representing the phase deviations which occurs at each radiating element of the antenna array when a plane wave impinges with a particular angle of arrival. For a planar antenna array made of $M = M_H \times M_V$ horizontal and vertical elements as represented in Fig. 7.30 for example, such steering vector states as,

$$\mathbf{a}_{\theta, \varphi} = [1, e^{jv}, \dots, e^{j(M_H-1)v}]^T \otimes [1, e^{ju}, \dots, e^{j(M_V-1)u}]^T \quad (7.59)$$

with \otimes the kronecker product, and

$$u = \frac{2\pi}{\lambda} d_V \sin(\varphi) \quad v = \frac{2\pi}{\lambda} d_H \sin(\theta) \cos(\varphi) \quad (7.60)$$

where θ and φ are the azimuth and elevation angles of the considered impinging ray (see Fig. 7.30), while d_v and d_H represent the distance between two vertical antennas and between two horizontal antennas of the planar antenna array. These expressions are easily found from the phase shifts at each antenna of the array, as illustrated in Fig. 7.29.

Then, considering the MISO channel between the antenna array and a single antenna terminal, each geometrical path between both ends yields one impinging ray to the antenna array which itself translates into one

3. Practical Beamforming Strategy for mmWave Communications

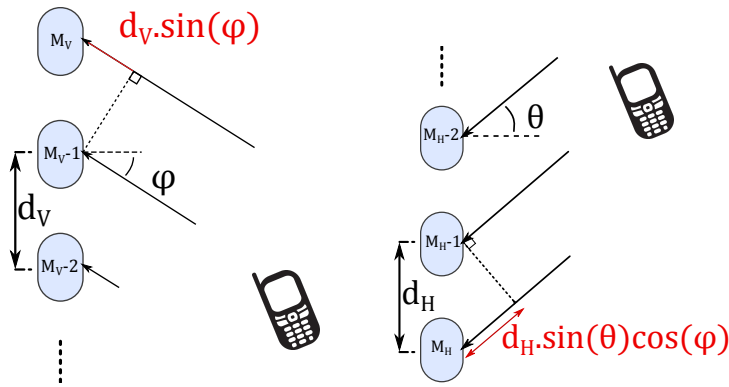


FIGURE 7.29– Relative phase shifts experienced at each antenna of a linear array (vertical and horizontal).

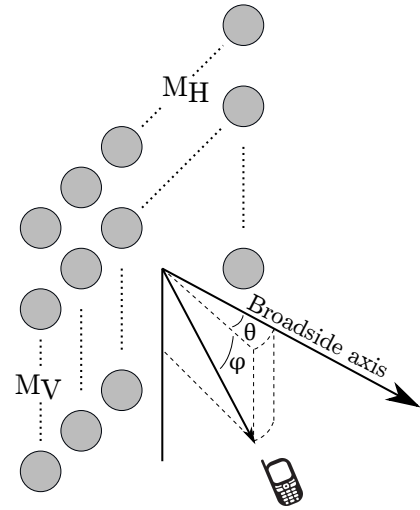


FIGURE 7.30– Planar antenna array with azimuth and elevation angles of arrival.

steering vector with the corresponding angle of arrival. Gathering all the geometrical paths for one terminal user k thus leads to the following channel vector,

$$\mathbf{h}_k = \sum_{l=1}^{L_k} \sqrt{\beta_{k,l}} e^{j\phi_{k,l}} \mathbf{a}_{k,l} \quad (7.61)$$

with $\mathbf{a}_{k,l}$ the steering vector corresponding to angle of arrival $\theta_{k,l}$, $\varphi_{k,l}$. From such a model, the MU-MIMO channel matrix with K users and M antennas at the central station finally writes,

$$\mathbf{H} = \sum_{l=1}^L \mathbf{D}_l^{1/2} \Phi_l \mathbf{A}_l \quad (7.62)$$

where $\mathbf{A}_l = [\mathbf{a}_{1,l}, \mathbf{a}_{2,l}, \dots, \mathbf{a}_{K,l}]^T \in \mathbb{C}^{K \times M}$ is the steering matrix of path l and $\mathbf{D}_l \in \mathbb{C}^{K \times K}$ (resp. Ψ_l) is the diagonal complex matrix describing path attenuation (resp. phase shifts) with their k th diagonal entries calculated as :

$$(\mathbf{D}_l^{1/2})_k = \sqrt{\beta_{k,l}} \quad (\Psi_l)_k = e^{j\phi_{k,l}} \quad \forall k \in [1, K] \quad (7.63)$$

As in a mm-wave scenario, the propagation environment can be described from its macro-structure by a few geometrical rays, it is essential to make use of such channel model based on steering vectors. Differentiating between the small-scale and large-scale propagation effects (typically the path-losses), the overall geometrical based channel model at the level of a whole coverage area can be written as,

$$\mathbf{H} = \underline{\mathbf{D}}^{1/2} \sum_{l=1}^L \tilde{\mathbf{D}}_l^{1/2} \Phi_l \mathbf{A}_l \quad (7.64)$$

with $\tilde{\mathbf{D}}_l^{1/2} = \underline{\mathbf{D}}^{1/2} \tilde{\mathbf{D}}_l^{1/2}$ meaning that the large-scale path-loss associated to each user is factored. This model can be applied for each subcarrier of an OFDM signal.

► MU-MIMO system model

The MU-MIMO system model introduced in the previous sections can then integrate the geometrical ray-based model. Considering a downlink Massive MIMO system with M transmit antennas at the central station and a set of K single antenna users, the received signal vector for one particular flat fading channel writes,

$$\mathbf{Y} = \underline{\mathbf{D}}^{1/2} \sum_{l=1}^L \tilde{\mathbf{D}}_l^{1/2} \Phi_l \mathbf{A}_l \cdot \underbrace{\mathbf{G}\mathbf{S}}_{\mathbf{X}} + \mathbf{N} \quad (7.65)$$

with \mathbf{X} the vector of precoded symbols and \mathbf{G} is the normalized multiuser spatial filtering matrix, i.e. $\mathbb{E}[\text{Tr}(\mathbf{G}^H \mathbf{G})]$. In the following, we will consider that spatial filtering is applied at the transmit side in a pure SDMA mode allowing for transmitting different data to each user at the same time and in the same bandwidth.

3.3 DIGITAL BEAMSTEERING STRATEGIES

► Beamsteering approach of conventional spatial filters

From the aforementioned system model, one can re-express the most common spatial filters of the literature already introduced in the previous sections, namely MRT, EGT, TR and ZF. In the case of matched-filter like schemes, it is even possible to find a direct expression of the filters from the steering matrices \mathbf{A}_l , hence obtaining filters in the form of a sum of beamsteering precoders. As described in more details in [C.19], this leads to the following result.

Contribution III.16 (Analytic Expression)

Beamsteering based MU-MIMO spatial matched filters

Assuming the geometrical model of the MU-MIMO channel of Eq. (7.65), the TR and EGT spatial filter matrices can be expressed as a combination of digital beamsteering matrices as,

$$\text{EGT : } \mathbf{G} = \frac{1}{\sqrt{M}} \sum_{l=1}^L \mathbf{B}_l \Phi_l^H \tag{7.66}$$

$$\text{TR : } \mathbf{G} = \frac{1}{\sqrt{M}} \sum_{l=1}^L \mathbf{B}_l \Phi_l^H \mathbf{D}_l^{1/2} \tag{7.67}$$

$$\text{MRT : } \mathbf{G} = \frac{1}{\sqrt{M}} \sum_{l=1}^L \mathbf{B}_l \Phi_l^H \mathbf{D}_l^{1/2} \mathbf{\Lambda} \quad \text{where, } (\mathbf{\Lambda})_k = \frac{1}{\sum_{l=1}^L \beta_{k,l}} \tag{7.68}$$

with the digital beamsteering matrix \mathbf{B}_l enclosing the hermitian transpose of the steering vectors of the K users for their l th path as,

$$\mathbf{B} = \mathbf{A}_l^H \tag{7.69}$$

This contribution essentially tells us that conventional spatial matched filters can be interpreted as linear combinations of unitary beamsteering beamformers associated to the angle of arrival of the geometrical paths of each user. As an example, one unitary beamsteering vector of , i.e. one column of the beamsteering matrix \mathbf{B}_l , applies the adequate phase shifts to the input signal such that the antenna array exhibits a radiation pattern with a maximum gain steered in the direction of the angle of arrival of the treated path. This idea, inherited from the traditionnal analog beamforming theory, is illustrated in Fig. 7.31 for a single steered beam. Eventually, can be simply interpreted as the formation of multiple beams so as to produce the waves propagating along the geometrical rays that will reach and recombine constructively at each intended user. MRT and TR does form the same beams but modify their amplitude to maximize the SNR of each user. Hence, the latters can be viewed as spatial Rake pre-filters expressed in the angular domain.

An interesting consequence of such geometrical decomposition of the channel is the reduced number of parameters to estimate to build the spatial filters. Hence, instead of estimating the $M \times K$ entries of the initial channel matrix, as commonly defined in MU-MIMO systems, only $L \times K$ angles of arrival and the related complex coefficients have to be estimated. In the context of massive MIMO systems in which $M \rightarrow \infty$, we understand that the geometrical description of the channel becomes highly advantageous. In addition, another interest of the geometrical basis representation is its inherent reciprocity, whatever the sub-band used. More precisely, the purely geometrical structure of the channel is not varying with the subcarrier index or between two adjacent sub-bands. Hence, putting apart the phase terms in matrices $\mathbf{\Phi}_i$, all the other components remains unchanged in uplink or downlink, even in an FDD duplexing mode. This characteristic is of high interest according to channel state information feedback mechanisms in FDD mode, which is identified of one of the major issues in massive MIMO systems.

3. Practical Beamforming Strategy for mmWave Communications

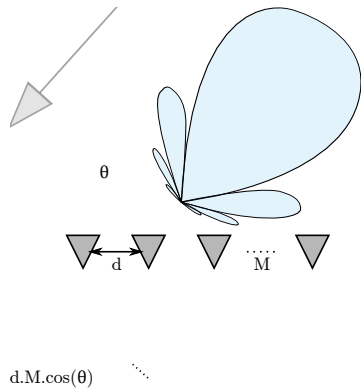


FIGURE 7.31– Steerable array beam through phase shifters.

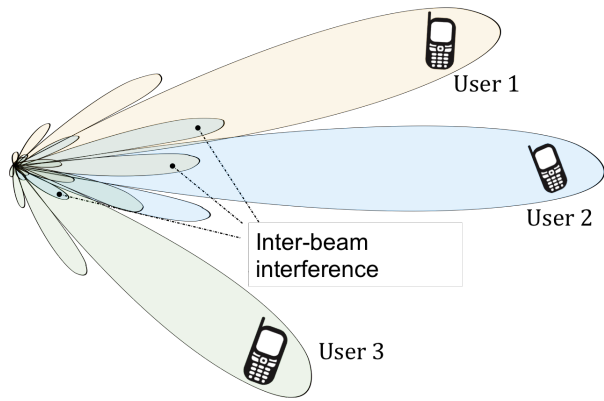


FIGURE 7.32– Example of multi-user digital Beamforming based on the LOS component of three users.

► Digital Beamsteering for LOS environments

From a general point of view, the received signal carried by the $\tilde{\mathbf{W}} = \mathbf{H}\mathbf{G}$ equivalent channel can be decomposed in order to separate the direct path components from the reflected ones. For a particular user k , the equivalent channel vector can be written as,

$$\tilde{\mathbf{w}}_k = \underbrace{\sqrt{\beta_{k,1}} e^{j\phi_{k,1}} \mathbf{a}_{k,1}^T \mathbf{g}_k}_{\text{Direct path}} + \underbrace{\sum_{l=2}^{L_k} \sqrt{\beta_{k,l}} e^{j\phi_{k,l}} \mathbf{a}_{k,l}^T \mathbf{g}_k}_{\text{Reflections}} \quad (7.70)$$

where \mathbf{g}_k is the k th row of the spatial precoding matrix \mathbf{G} . Due to the strong path-losses in a mm-waves, it is expected that the propagation channel is mainly governed by the line-of-sight components for each user link and that the reflected paths remain of low amplitude. In addition, at mm-wave frequencies, it is appropriate to use small cells within which the LOS connectivity between transmitter and receiver is very probable. It is then possible to envisage suboptimal spatial filters by relaxing the constraint on the complete knowledge of the channel. Hence, we proposed to build beamsteering filters only based on the main path component of each user. If we assume a purely LOS channel, i.e. only considering the direct path from each user to the central station, the channel matrix simplifies to,

$$\mathbf{H}_{\text{LOS}} = \mathbf{D}_1^{\frac{1}{2}} \Phi_1 \mathbf{A}_1 \quad (7.71)$$

Hence a very simple multi-user digital beamsteering (DBS) scheme can be used, as proposed in [C.19], consisting of forming only one beam per user steered in the direction of the main path of that user as illustrated in Fig. 7.32. In that case, no particular attention has to be paid to the phase component of the unique propagation ray of each user since no constructive combination between multiple beams has to be obtained. Hence, the only pieces of information about the channel that have to be known by the transmitter to build the DBS filter are reduced to the angles of arrival of the LOS rays for each user. Interestingly, this channel parameters are intrinsically reciprocal, in TDD and FDD modes. This important result, summarized in Contrib. III.18 on top of next page, has been detailed in [C.21].

The proposed beamformer leads to maximizing the emitted power only in the main direction of each user. It can be visualized as a filter adapted to the channel described by its main steering vector (angles $\theta_{k,1}$ and $\varphi_{k,1}$).

► Simulation results and analysis

The proposed DBS filter has been experimented and compared to other approaches through simulations. A practical propagation environment as illustrated in Fig. 7.33 has been created and simulated using ray-tracing methods to produce the channel matrices of the MU-MIMO system. Two types of channel responses can be obtained : the purely LOS channel, only retaining the direct path between the central station and each user, and the complete multipath channel made of the LOS and NLOS components.

Contribution III.17 (System Design)

TDD/FDD suboptimal Multiuser Digital Beamsteering (DBS)

In a MU-MIMO system with K users which channels each exhibit one strong propagation ray with an angle of arrival (θ_k, φ_k) at the central station, can be multiplexed over the space dimension using the following digital beamsteering (DBS) matrix,

$$\mathbf{G} = \frac{1}{\sqrt{M}} \mathbf{A}^H \quad (7.72)$$

with the digital beamsteering matrix \mathbf{A} enclosing the steering vectors of the K users for their strongest path as,

$$\mathbf{A} = [\mathbf{a}_{\theta_1, \varphi_1}, \dots, \mathbf{a}_{\theta_K, \varphi_K}]^T \quad (7.73)$$

where $\mathbf{a}_{\theta_k, \varphi_k}$ is defined in Eq. (7.59).

In Fig. 7.34, we give the synthetic results obtained for the proposed simple DBS solution opposed to the ZF and MRT filters, in the case of the LOS and LOS+NLOS channels at 60 GHz and using a square 6 antenna array. It is first verified that the DBS and MRT results converge in the purely LOS channel, as expected from the previous analysis on the geometrical channel representation. Then, the ZF filter exhibits contrasted performance depending on K . Indeed, the ZF filter hardly succeeds in accommodating more than 10 users and even fails compared to MRT and DBS schemes when K becomes to large. As already discussed, ZF relies on channel matrix inversion which can properly be achieved only if the matrix is well conditioned. Practically, with K users, the channel matrix shall be of rank K at least to be invertible. Yet, with K users in the street area, we showed in [C.21] and proved that the channel rank is essentially of the order of the horizontal size M_H of the antenna array in purely LOS channels, and slightly more if some multipaths occur. Hence, in our example, as $M_H = 6$, the optimum number of users to address in parallel with ZF is $K \approx 6$, otherwise experiencing some performance drop. For the two other filters, the increase of the number of users yields higher interbeam/interuser interference and hence a sum capacity saturation. The interference terms are of higher amplitude when more propagation modes are present, i.e. when multipaths are activated, which explains the better results in LOS compared to LOS+NLOS. However, this effect remains of limited impact on performance since multipaths components vanish rapidly in mm-waves. Finally, since DBS only exploits the knowledge of the LOS component, its performance is slightly degraded compared to the MRT filter. However, as it requires only two angles per user to be produced, the DBS filter can be viewed as a interesting performance/complexity trade-off.

3.4 LEAKAGE BASED POWER ALLOCATION

In the following of the work on spatial filtering for mm-waves based on DoA, we investigated power allocation techniques to enhance the previously presented results on achievable rate. It is well known from the literature that power allocation in Multi User (MU) MIMO [FSY11, WWGY10, WYZD13, JLL03] is an additional processing layer that can be utilized separately or jointly with other blocks in order to optimize the system spectral or energy efficiency. However most of the contributions available for MU-MIMO systems are based on iterative procedures than can hardly be scaled to massive MIMO system topologies. As for massive MIMO systems, it was already shown around 2015 that low complexity linear precoders such as MRT can achieve considerable gains when coupled together with an interference wise power allocation [ZZZ13, CL14]. However, no practical low-complexity algorithms were available at that time. After the proposal of the previously introduced DoA-based spatial filters, our idea was to extend such filters with power allocation solutions of low complexity. Due to the fact that MRT/EGT/TR or DBS strategies only aims at maximizing the received signal and doesn't consider the interference, we focused on adapting these kinds of spatial filters taking into account the inter-beam interference, or more exactly what we will call the beam leakage in the sequel. This can be done with extra processing layer

3. Practical Beamforming Strategy for mmWave Communications

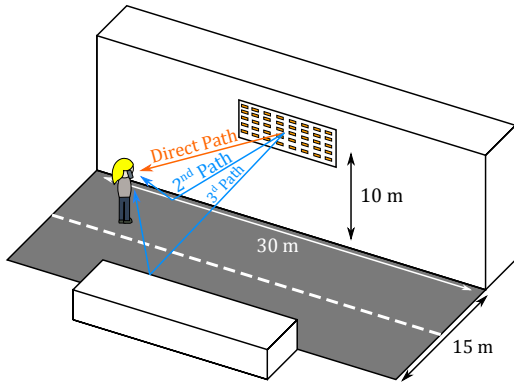


FIGURE 7.33– Simulation scenario as a street canyon area with a planar antenna array at the central station. Channel response is obtained through LOS and reflected rays.

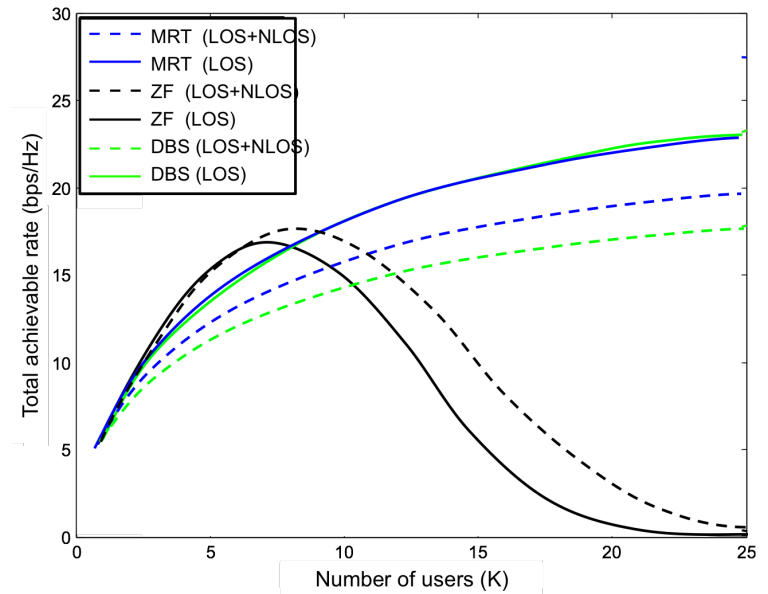


FIGURE 7.34– Total achievable rate using ZF, MRT and DBS spatial filters in purely LOS and LOS+NLOS channels. Planar antenna array with $M = 6 \times 6$ elements.

referred to as LB-PA (Leakage-based Power Allocation) aiming at mitigating the interference power produced by competing users, but not following the strict nulling strategy of ZF. Contrary to all the proposed algorithms in the literature, the LB-PA solution is a closed-form non iterative one as long as partial or complete channel information is known at the central station.

► Beam leakage

Let us introduce the beam leakage metric which will be considered as the main building block of our power allocation algorithm. The leakage has to be understood from a central station perspective as a measure of how the formation of a beam to a given user will harm its neighbours. In other words the leakage effect, translates the propensity to impact neighbouring transmissions, as simply illustrated in Fig. 7.35. Note that leakage differs from interference. The latter is a measure for one given user k of the signal power perceived from the signals transmitted to other users, while the former measures the nuisance level that one transmission to a user k creates upon other users. The leakage L_k created by the transmission to user k is expressed as,

$$L_k = \sum_{j \neq k=1}^K |\mathbf{h}_j^T \mathbf{g}_k|^2 \quad (7.74)$$

where \mathbf{g}_k is the precoding vector constructed to target user k .

Since the leakage is an evaluation of the power emitted in the direction of the other users, it is possible to assess its level exploiting the angular model of the channel introduced in Eq. (7.65). The leakage can hence be restated using the channel steering vectors as,

$$L_k = \sum_{j \neq k}^K \sum_{l=1}^{L_j} \beta_{j,l} |\mathbf{a}_{j,l}^T \mathbf{g}_k|^2 \quad (7.75)$$

where $\beta_{j,l}$ and $\mathbf{a}_{j,l}$ are the path-losses and steering vectors describing the propagation channel for user j as reminded in Fig. 7.36. Note that both expressions in Eq. (7.74) and (7.75) are valid for a given flat fading channel. The leakage evaluation is thus depending on the subcarrier in case of an OFDM waveform.

► Leakage with reduced channel knowledge

From the above expression, it is clear that the calculation of the leakage level requires a complete knowledge of the channel response, however reduced to some particular angles of arrival if using the geometrical channel

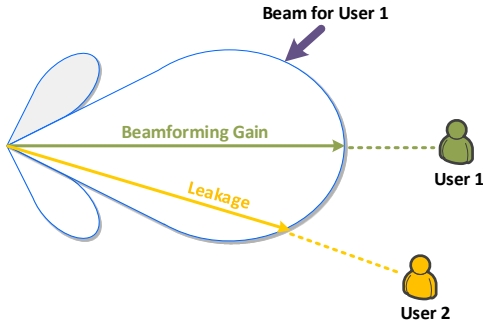


FIGURE 7.35– Illustrating the effect of the leakage

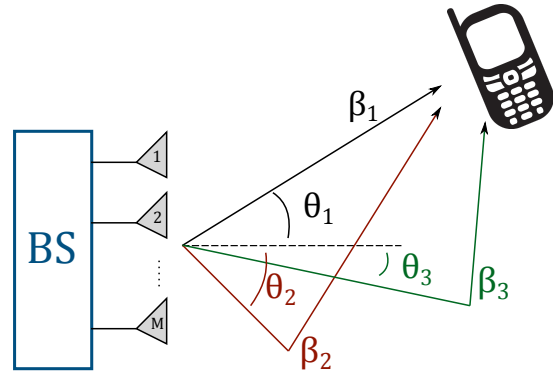


FIGURE 7.36– Angle-based channel knowledge for one user.

description. In the case of a propagation scenario strongly conditioned by the LOS component of the channel, as is the case in mmWave and/or in the small-cell environment, it is favorable to implement a spatial filters based on the main angles of arrival of the propagated rays such as those introduced in Contrib. III.18). In that case, a simpler expression of the leakage can be formulated depending only on the steering vectors of the users. In addition, the aforementioned properties of mm-waves make it possible to provide an approximate expression of the leakage focusing on the main path of each user, leading to

$$\tilde{L}_k = \sum_{j=1 \neq k}^K \beta_{j,1} |a_{j,1}^H a_{k,1}|^2 \tag{7.76}$$

This expressions assumes that the leakage level is mainly governed by the emitted power in the main direction of each user, i.e. by the LOS components of the MU-MIMO channel. Interestingly, in contrast to the former expressions given by Eq. (7.74) or Eq. (7.75), the expression we propose here does not depend on the frequency response H , impulse response of the channel, nor the number of subcarriers N but only the geometric structure of the channel. It is even possible to push further the simplification of the leakage evaluation by removing this path-loss parameter β , hence only measuring the amount of interfering energy that is radiated toward the other users from an angular point of view, regardless of their distance to the central station. Then a basic, albeit consistent, leakage definition can be provided as,

$$\tilde{\tilde{L}}_k = \sum_{j=1 \neq k}^K |a_{j,1}^H a_{k,1}|^2 \tag{7.77}$$

which means that only the angles of arrival of the LOS rays are exploited to evaluate the leakage level.

The use of both reduced channel knowledge solutions aforementioned in a realistic environment allows the BS to approximately assess the interference that each transmission produces on each user in a common coverage area. The leakage can be evaluated in any system with a channel estimation process, but the simple definitions given here allows for a very economic parameter estimation for each user, since only $2K$ values have to be obtained (2 angles per user). In addition to the extremely simple expression of the leakage in that case (low complexity and low overhead), such a definition allows for greater fairness of power allocation between users as it will not hinder cell edge users more than other users.

3.5 LEAKAGE BASED POWER ALLOCATION

From the latter definitions of leakage, it is now possible to envisage leakage minimization power allocation strategies and then act on the individual power weights per user in order to minimize the interbeam interference effects. In case the power distribution is uniform among all users, $P_k = \frac{P_T}{K}$ with P_T the total power emitted and K the number of users. On this basis, a situation of equity between users in terms of leakage level is to guarantee

3. Practical Beamforming Strategy for mmWave Communications

that any user does not produces more leakage than another. Hence, the optimization problem can be stated as,

$$\begin{aligned} \mathcal{P}: \quad & \min_{P_k, \forall k} \max P_k L_k & (7.78) \\ \text{w.r.t.} \quad & \sum_{k=1}^K P_k = P_T \end{aligned}$$

with P_T the total transmit power to be shared between users. The resolution of such a problem leads to the following power allocation algorithm, proposed in [C.9].

Contribution III.18 (Algorithm)

Leakage-Based Power Allocation for MRT/DBS spatial filters

In a MU-MIMO system with K users and a total transmit power P_T , MRT or DBS spatial filters yield uniform leakage if the power allocated to each user is such that,

$$P_k = \frac{P_T}{1 + \sum_{j \neq k} \frac{L_k}{L_j}} \quad (7.79)$$

with L_k the leakage level of user k evaluated from Eq. (7.75) (perfect Leakage estimation), from Eq. (7.76) (LOS component approximation) or from Eq. (7.77) (LOS angle-based approximation).

► Simulation results

The various simplifications proposed for the leakage level evaluation will naturally lead to a sub-optimality of the precoding and power-weighting processes. However, the simulation results provided in Fig. 7.37 show that the performance degradation remains minimal in practical situations. It is indeed observed that the accuracy of the leakage evaluation yields negligible effect on the performance results, hence concluding that the underlying complexity reduction is worth interest. Interestingly, it is also noticed that using the proposed power allocation algorithm makes the simple digital beamsteering and the MRT filters perform similarly, whereas MRT is out-performing DBS with uniform power allocation. Last but not least, the power allocation algorithm succeeds in decreasing the gap significantly between MRT/DBS and ZF. These results unleash the main advantage of the proposed algorithm, which is reducing the benefit of using a high complexity-high overhead signal processing techniques.

3.6 CONCLUSION

Between the beginning and the end of this study, massive MIMO mmWave systems have clearly evolved as key enablers for the future generation of wireless networks (5G) [TvWA⁺16, XMH⁺17] to support higher achievable data rates. Due to the wide bandwidth and high antenna gains, it is today recognized that massive MIMO mmWave systems are able to achieve very high per user peak data rates of tens of Gigabits per second (Gbps) [SAHC14a].

In our study, we have started investigating spatial filter concepts in the context of mm-waves propagation environments exploiting the sparse nature of the channel mainly governed by its geometrical structure as suggested by the works of Rappaport [RRE14]. On this basis, we have shown that angle based precoders could provide almost optimal performance, however using a limited number of information parameters about the channel state, namely as many azimuth and elevation angles as there are users. This contributes to the growing conviction that DoA estimation and angle based precoders are simple and effective solutions for high frequency small cell systems.

However, working at such high frequencies imposes a lot of hardware and channel implications that need to be tackled in order to unleash the high potentials of Massive MIMO. Such questions will be part of the perspective works detailed in 9.

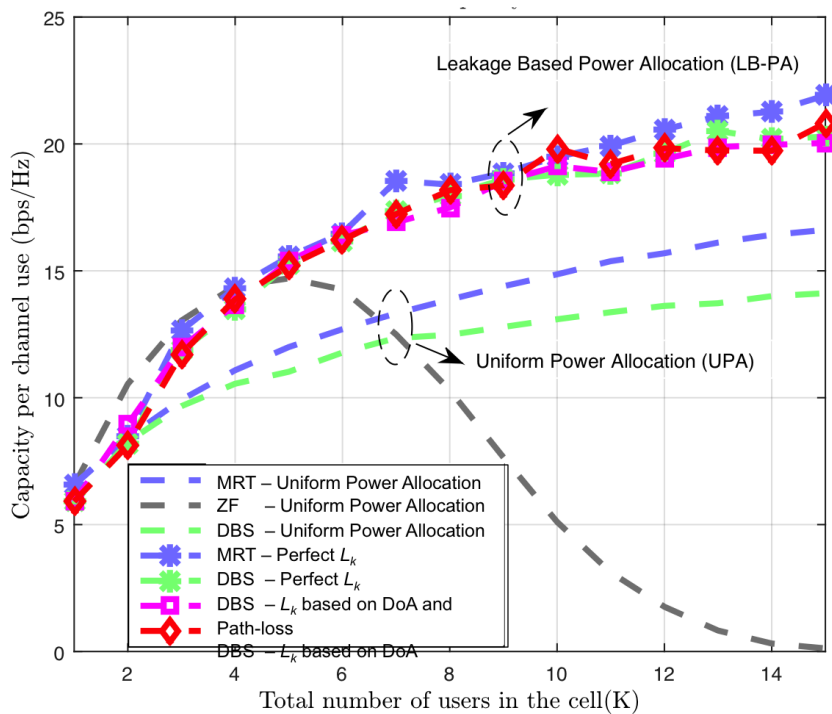


FIGURE 7.37– Total achievable rate of a MU-MIMO system using MRT/DBS/ZF spatial filters with and without leakage-based power allocation. Planar antenna array of 16 elements.

Summary (PhD/Dissemination/Projects)

- 1 PhD (A. Rozé)
- 1 submitted international journal paper
- 3 communications in international conferences and workshops [C.9][C.19][C.21]
- 1 IRT-Bcom Project (RS-COM)

*Great discoveries and improvements
invariably involve
the cooperation of many minds.
– Alexander Graham Bell –*

Selected Topics

This chapter introduces the last field of research I have been developing during these last years on the hybridization between wireless broadcast and broadband networks. Contrary to the previous two topics which were mainly concentrating on physical layer aspects, this research field takes place at an upper-layer stage aiming at assessing the leverage of making two different networks cooperate and interwork. The selected aspects of our work are :

1. Semi-analytic analysis of dual mode broadcast/unicast networks
2. Wireless hybrid broadcast/broadband network optimization

1 SEMI-ANALYTIC ANALYSIS OF DUAL MODE BROADCAST/UNICAST NETWORKS

1.1 MOTIVATION

From 2000 to 2010, the progressive disappearance of the analogue television throughout the world have released large amounts of spectrum in the UHF and VHF bands. This so-called digital dividend have coincided with the beginning of the tremendous growth in the area of mobile telecommunications following the arrival of smart phones, and has motivated the assignment of the newly available frequencies to mobile oriented services, namely the 791–821 MHz and 832–862 MHz bandwidths for the deployment of the LTE standard [Rep14]. Even if this new spectrum opportunity has been a windfall for mobile network operators, it can not be considered as the unique long term solution to the data tsunami. Indeed, new trends of data consumption over wireless broadband networks have started to be witnessed around 2010 with the generalization of the mobile Internet access. On the one hand, consumer needs have become more and more user-specific because of the growing demand for surfing the Internet and making use of social networks on mobile terminals. On the other hand, the number of downloaded/streamed popular multimedia contents and the usage of handheld terminals for watching TV programmes have known a constant inscrease. As a matter of fact, users are more and more watching linear services (such as live TV) on their tablets and smartphones which are connected to a mobile broadband network relying on a unicast transmission system.

Hence, mobile network operators have to accomodate these two antagonist phenomena : content individualization and massive consumption of popular contents among which an increased proportion of linear services. The former issue can partially be solved using larger bandwidths, reducing the size of the cells in dense environments (femtocells), or even taking advantage of local area networks, namely WiFi, as soon as they are available to each

user. To address the latter yet, multicast or broadcast instead of the by-default unicast transmission mode may be more adapted owing to their user factorization nature. Indeed, delivering identical pieces of data to different users in a unicast manner duplicates the bandwidth consumption and becomes a greedy strategy when the number of users increases. Meanwhile the broadcast approach provides service access to multiple users with a constant spectrum utilization. The complementarity between unicast and broadcast modes has already been addressed by the last 3GPP-LTE specifications that define a broadcast component called E-MBMS (evolved multimedia broadcasting multicast service). E-MBMS can be activated in some situations to optimize the spectrum use in cellular networks [1].

Nevertheless, broadcast transmission mode is expected to provide more benefit in case of large coverage areas in which the factorization effect is higher, which is typically the case with the high-power high-tower (HPHT) network topology of conventional TV broadcast networks. Hence, one new idea which emerged around 2010 was consisting in a cooperation between cellular network and terrestrial broadcast network infrastructures for the exploitation of the VHF/UHF frequencies in a more efficient way. The cooperation would rely on a complementary exploitation of terrestrial digital TV transmitters to broadcast selected multimedia contents within a large coverage area. The objective is to reduce the multimedia unicast traffic on the cellular networks by enabling the off-load of some contents from one unicast network to a broadcast one. The dual unicast/broadcast modes of the 3GPP-LTE can be viewed as a cooperation between two virtual networks, however based on the same cellular infrastructure. In the case of the broadcast/broadband network hybridization, the cooperation concept is pushed a step further.

We decided to put some efforts on this topic as we were working in parallel with mobile networks operators and broadcast networks operators, trying to find some new approach to face the famous data tsunami. Our study, which has been led in the framework of the ANR MCube project, dealt both on the definition of a common physical layer suited for the overall hybrid network, and on the performance evaluation methodology of the hybrid network depending on various application scenarios. The work on the common physical layer are not detailed in this manuscript but has been published in [R.8] and [B.2] as a collaborative study with other academic and industrial partners involved in the ANR MCube project. In the following, we rather focus on our contributions concerning the cooperative aspects between unicast and broadcast networks. Such a global hybrid network approach raises the question of how to define some unified model and to how decide which sub-network to exploit between the cellular unicast one and the terrestrial broadcast one, to deliver a service to a given number of end users. These aspects have been addressed in the PhD work of Nicolas Cornillet summarized in the sequel.

1.2

SYSTEM LEVEL HYBRID BROADBAND/BROADCAST WIRELESS NETWORK MODEL

► Hybrid Network System Model

The hybrid network considered in our study is the combination of two components. The first component is a classical cellular network made of a great number of relatively small hexagonal cells of side c with low power base stations providing unicast broadband signals according to a mobile communication standard such as LTE. The second component is a broadcast network of coverage radius R_B based upon one single high-power transmitter emitting a broadcast signal such as DVB-T2 for instance. Each component is assumed to use distinct frequency bands so that no inter-component interference can occur. Typically, the broadcast component uses a VHF carrier frequency, e.g. around 800 MHz, while the unicast component is operated around 2-3 GHz. The coverage area of the broadcast network is circular and completely overlaps the cellular network as depicted in Fig. 8.1. The overall coverage area of the hybrid network corresponds to that of the broadcast network and the broadcast transmitter is used as the coordinate reference, i.e. it is considered as the center of the hybrid network. Typical value for the broadcast network coverage radius is $R_B = 100$ km, while hexagonal cells have a side length of about $c = 1$ km.

The users are supposed to have dual-system receiver capabilities such that they can receive the proposed service from either the broadcasting system or the unicast system. According to such a hybrid network, various user location patterns can be considered and have strong influence on the overall system performance. In our study, we used a uniform distribution of the users within the overall coverage area, but also a two-dimensional Gaussian distribution (centered or not) for instance representing the situation of a coverage area at the scale of a whole city which center coincides with the center of the Gaussian distribution.

1. Semi-analytic analysis of dual mode Broadcast/Unicast Networks

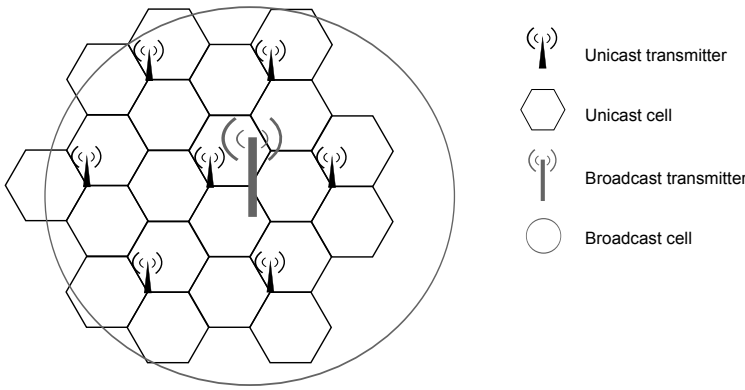


FIGURE 8.1– Proposed hybrid unicast/broadcast network

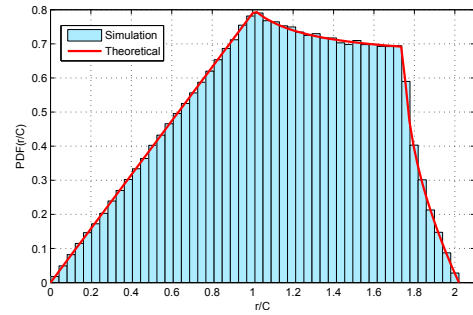


FIGURE 8.2– PDF of the distance within a unicast cell : comparison between the simulation and theoretical results assuming a Gaussian user distribution.

Such topology fixes the spatial pattern of the hybrid network from which it will then be possible to compute some performance metrics for example in terms of average spectral efficiency, achievable rate, energy consumption or service success rate. Even if they can be computed building a system level simulator, we were mostly interested in deriving some analytical or semi-analytical expressions for such metrics, as detailed further. In that perspective, some statistical functions have to be defined such as the probability density function (PDF) of the distance between users and transmit stations, and then the probability density function of the achievable rate per user for each component of the network. Classical derivations based on the geometrical properties of the hybrid coverage model are used in the sequel to obtain the desired PDF.

► PDF of the user distance to transmit stations

A key step to derive statistical performance metrics of the hybrid network is to compute the PDF of the user distance to the nearest transmit station, in the broadcast and unicast cases. Such PDF is needed to further derive the statistical properties of the spectral efficiency attained within the region of interest, depending on the used component (unicast or broadcast). Our first contributions have then been to provide the PDF of the user distance to the cellular and broadcast stations for various spatial user distributions, e.g. uniform or Gaussian. We give in Contrib. IV.1 hereafter the result for a two-dimensional Gaussian distribution of the user, in the general case when the Gaussian function is not necessarily centered regarding the hybrid network.

Contribution IV.1 (Analytic Expression)

PDF of the user distance to transmitter in the hybrid network with Gaussian user distribution

Given a hybrid network made of a single transmitter broadcast network of coverage radius R_B and a cellular network with hexagonal cells of side length c , the probability density function $p_R(r)$ of the distance r between a user and a transmit station of each component assuming a Gaussian distribution of the users across the overall coverage area are

$$\text{Broadcast} \quad p_R(r) = \frac{1}{1 - Q_1\left(\frac{\Delta}{\sigma}, \frac{R_B}{\sigma}\right)} \frac{r}{\sigma^2} e^{-\frac{\Delta^2 + r^2}{2\sigma^2}} I_0\left(\frac{\Delta r}{\sigma^2}\right) \quad 0 \leq r \leq R_B \quad (8.1)$$

$$\text{Unicast} \quad p_R(r) = \begin{cases} \frac{2\pi r}{3A} & 0 \leq r \leq c \\ \frac{2r}{A} \arcsin\left(\frac{c\sqrt{3}}{2r}\right) & c < r \leq c\sqrt{3} \\ \frac{2r}{A} \arcsin\left(\frac{c\sqrt{3}}{2r}\right) - \frac{2\pi r}{3A} & c\sqrt{3} < r \leq 2c \end{cases} \quad \text{with, } A = \frac{3\sqrt{3}}{2} c^2 \quad (8.2)$$

where σ is the standard deviation of the Gaussian distribution such that $\sigma \gg c$ and Δ is the distance between the center of the Gaussian distribution and the center of the hybrid network. (i.e. broadcast transmitter location). $Q_1(\cdot, \cdot)$ and $I_0(\cdot)$ are the Marcum Q -function and the modified Bessel function of the first kind and order 0, respectively.

The proof yielding the expressions of (8.1) and (8.2) have been published in [C.45]. With this first result, one may observe that the distribution of the distance between the users and the nearest unicast station does not depend on the Gaussian function parameter σ governing the spatial distribution of the users in the hybrid network. This fact is valid under the mentioned assumption that $\sigma \gg c$, indicating that the spread of the Gaussian distribution is sufficiently wide compared to the hexagonal cell dimension. Indeed, it can be shown in that case that the user distribution within a cell is almost uniform [C.36]. This is for example verified through Monte-Carlo simulation as illustrated in Fig. 8.2. The histogram of the simulation results is obtained considering a Gaussian distribution of the users at the scale of the broadcast coverage area, while the theoretical plot is obtained from Eq. (8.2). Hence, from one unicast cell to another, the expression of the PDF is valid and will remain the same. Then, the only difference between cells rather comes from the number of users per cell depending on the cell location within the hybrid network. This can be reflected by the probability that a particular user falls within the coverage area of a particular cell in the hybrid network. Such result summarized in the Contrib. IV.2 was also part of the study published in [C.36].

Contribution IV.2 (Analytic Expression)

Probability of a user falling within a particular unicast cell coverage

Given the above defined hybrid network with Gaussian distribution of the users with standard deviation σ , the probability $P_c(u \in C_i)$ that one user u of the network falls within the coverage are of one particular cell C_i of dimension c is approximated as

$$P_c(u \in C_i) \approx \frac{1 - Q_1\left(\frac{\delta_i}{\sigma}, \frac{\tilde{R}_c}{\sigma}\right)}{1 - Q_1\left(\frac{\Delta}{\sigma}, \frac{R_B}{\sigma}\right)} \quad \text{with } \tilde{R}_c = \sqrt{\frac{3\sqrt{3}}{2\pi}} c \quad (8.3)$$

where δ_i is the distance between the base station of the i th cell and the center of the Gaussian distribution, Δ is the distance between the center of the Gaussian distribution and the broadcast transmitter location.

► PDF of the attainable spectral efficiencies

The previously derived PDF of the distance between users and transmit stations can be translated into a PDF of the achievable rates of the users for each component of the hybrid network. To that end, one has to establish the link between the distance and the performance of the system. This is commonly obtained integrating some link budget relation into the model, and some tabulated physical layer performance results.

As far as the link budget is considered, each component of the hybrid network is generally associated with an adequate propagation attenuation model providing the path-loss $L(r)$ as a function of the distance of the receiver to the transmit station. In the case of broadcasting system from high-power transmitters, the Hata model is generally used [Hat80]. For cellular systems, the LTE specifications recommend the use of a dedicated model given in [2]. In both cases, the path-loss depends not only on the distance and carrier frequency, but also on the height of the transmit and receive antennas. From such models, it is easy to express the receive signal to noise ratio (SNR) $\Gamma(r)$ for each component of the hybrid network as,

$$\Gamma(r) = \Gamma_0 \left(\frac{R_{max}}{r} \right)^\alpha \quad (8.4)$$

with α the path-loss attenuation coefficient depending on the propagation model, R_{max} the maximum coverage distance of each component, i.e. $R_{max} = R_B$ for broadcast and $R_{max} = 2c$ for unicast, Γ_0 some minimal reference SNR. This latter can for instance correspond to the minimal required SNR at the boundary of the coverage area (broadcast or broadband) allowing for a transmission at a given QoS.

From the path-loss model, the next step is then to integrate the tabulated SNR results obtained from pure physical layer simulations over various channel models. For example, Table 8.1 gives the list of the spectral efficiencies related to various modulation and coding schemes of the DVB-T2 standard [v1.12a] at different levels of SNR assuming a binary error rate of 10^{-11} .

1. Semi-analytic analysis of dual mode Broadcast/Unicast Networks

index i	Γ_i (dB)	v_i (bit/s/Hz)
1	2.0	0.87
2	4.1	1.18
3	5.3	1.31
4	6.6	1.45
5	6.9	1.74
6	9.6	2.36
7	11.0	2.60
8	12.8	2.89
9	13.9	3.07
10	14.4	3.54
11	16.1	3.94
12	18.2	4.34
13	19.0	4.72
14	20.5	5.25
15	22.9	5.78
16	24.5	6.14
17	25.8	6.49

TABLE 8.1– Spectral efficiencies versus SNR for the DVB-T2 system. Target BER=10⁻¹¹.

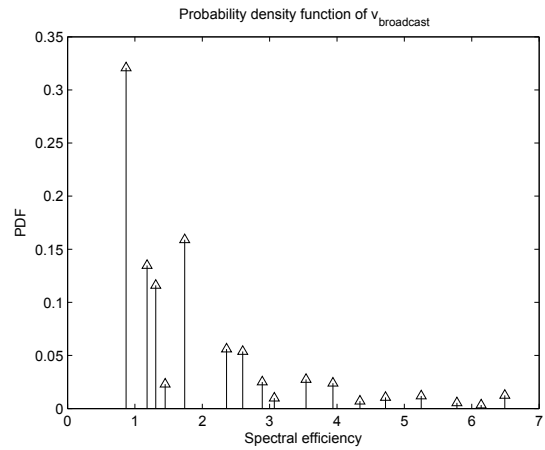


FIGURE 8.3– Probability density function of spectral efficiencies for the broadcast component

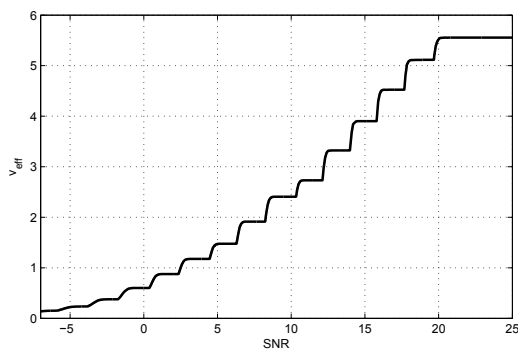


FIGURE 8.4– Effective spectral efficiency v_{eff} as a function of SNR for a LTE signal (AWGN channels)

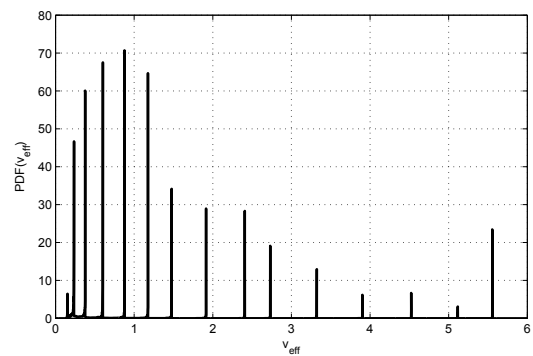


FIGURE 8.5– PDF of spectral efficiencies for the unicast component with HARQ mechanisms.

From such SNR tables, one can then compute the PDF $p_Y(v)$ of the spectral efficiencies which can be expected or which can be effectively granted to each user of the network. This is obtained through simple integration of the PDF of the distance over rings of coverage associated to the different levels of spectral efficiency of each standard assuming a predefined target bit or packet error rate. Such computation has been proposed and detailed in [C.36] and leads to the following expression.

Contribution IV.3 (Analytic Expression)

PDF of the achievable spectral efficiencies

Given the defined hybrid network, the probability density function $p_Y(v)$ of the spectral efficiency v which can be expected within the coverage area of each component of the hybrid network is

$$p_Y(v) = \sum_{i=0}^{N_i} \int_{r_{i-1}}^{r_i} p_R(r) \delta(v - v_i) dr \quad \text{with, } r_i = e^{\frac{1}{\alpha} \log\left(\frac{\Gamma_i R_{max}^\alpha}{I_0}\right)} \quad (8.5)$$

where $p_R(r)$ is the PDF of the distance defined in Contrib. IV.1, Γ_i is the minimum required SNR for spectral efficiency v_i as tabulated for a particular PHY and QoS.

This last result allows us to compute the probability to which a given user has the chance to benefit from a spectral efficiency v_i depending on the used sub-network. To illustrate this the PDF of the broadcast component using $\alpha = 2.5$, $F_p = 800\text{MHz}$, and $R_{max} = 100\text{km}$ has been computed and is depicted in Fig. 8.3. In the same way, the PDF of the unicast component can be exemplified on the basis of 3GPP-LTE specifications as

provided in [C.36]. In this latter case however, the system level model has to take into account the retransmission mechanisms used to improve the QoS of the system, namely the HARQ (Hybrid Automatic Repeat reQuest). The spectral efficiency values then translate into effective spectral efficiencies, integrating the statistical number of occurring repetitions. Hence, one can build a bijective function \mathcal{G} that links the effective spectral efficiency with the SNR as shown in Fig. 8.4. Such a function can be tabulated after PHY layer simulations and then be used to derive the PDF of the spectral efficiency. In that case, the PDF takes the form of a continuous function of ν instead of a discrete form as previously stated in Contrib. IV.3. The new PDF form is introduced in the contribution below and is exemplified in Fig. 8.5 in the LTE system case over Gaussian channels [C.36].

Contribution IV.4 (Analytic Expression)

PDF of the achievable spectral efficiencies with HARQ

Given the defined hybrid network, the probability density function $p_{\Upsilon}(\nu)$ of the spectral efficiency ν of the unicast component using HARQ is

$$p_{\Upsilon}(\nu) = p_{\text{R}}(r) \frac{2c}{\alpha\Gamma} \left(\frac{\mathcal{G}^{-1}(\nu)}{\Gamma} \right)^{\frac{1}{\alpha}-1} \mathcal{G}'(\nu) \quad (8.6)$$

where $p_{\text{R}}(r)$ is the PDF of the distance defined in Contrib. IV.1 for the unicast component and $\mathcal{G}(\nu)$ is the tabulated function of the effective spectral efficiency versus SNR involving HARQ mechanisms.

1.3 SEMI-ANALYTIC HYBRID NETWORK PERFORMANCE EVALUATION

From the derived PDFs, it is then possible to compute some statistical performance metrics of a network in which a broadcast and a unicast components are available. In such a hybrid network, indeed, a given service S can be transmitted through either the unicast component or the broadcast component. The choice of the component to use can be driven from various criteria according to objective criteria such as capacity, QoS, delay or energy considerations. In [C.36], we for instance defined two switching criteria based on spectral efficiency and energy efficiency gains denoted as $G_{\text{U} \rightarrow \text{B}}$ when selecting the broadcast component instead of the unicast one :

$$G_{\text{spectral}}^{\text{U} \rightarrow \text{B}} = \frac{\nu^{(\text{B})}}{\nu^{(\text{U})}} \quad \text{and,} \quad G_{\text{energy}}^{\text{U} \rightarrow \text{B}} = \frac{E^{(\text{U})}}{E^{(\text{B})}} \quad (8.7)$$

► Spectral efficiency switching criterion

A fundamental difference between the unicast and broadcast transmission modes is the way to adapt the spectral efficiency used to deliver a common service to multiple users. In the unicast mode, a so-called link adaptation is carried out to adapt the modulation and coding scheme regarding the quality of the channel (SNR). Hence, the resulting spectral efficiency at the scale of a cell corresponds to the average of the user spectral efficiencies. Contrary to that, in the broadcast case, the service is delivered using the same spectral resource for all the users of the coverage area. Hence, the choice of the modulation and coding scheme is based on the worst user channel conditions, that is of the users located at the boundary of the cell. On that basis, the gain in terms of spectral efficiency can be viewed as a random variable resulting from the fact that spectral resource is exploited with the latter two strategies. We showed that such a gain can from Eq. (8.7) be formally expressed as,

$$\lambda = G_{\text{spectral}}^{\text{U} \rightarrow \text{B}} = \min_k v_k^{(\text{B})} \times \sum_{k=1}^N \frac{1}{v_k^{(\text{U})}} \quad (8.8)$$

This expression already indicates that the potential gain obtained switching from a unicast to a broadcast transmission mode is depending on the number of users. If N is large, the right-hand side of the above expression corresponding to the cost in spectral efficiency of the unicast component dramatically increases, which comes

1. Semi-analytic analysis of dual mode Broadcast/Unicast Networks

in favor of the broadcast component hereby yielding a potentially high spectral gain. To go further, we provided the analytical expression of the PDF of the spectral gain as a function of the number of user [C.45]. This key result is stated in the following Contrib. IV.5. It can be analyzed that the obtained PDF depends both on the choice of the broadcast spectral efficiency $v_0^{(B)}$ and on the number N of users. If $v_0^{(B)} < 1$ and N is low, it can be shown that the switching gain is statistically negative. If $v_0^{(B)}$ is increased or N becomes sufficiently large, the gain can reach potentially high positive values. This has to be viewed as the user factorization gain naturally provided by the broadcast transmission mode. Further analyses namely given in [C.45] show that the spectral gain follows a modified Nakagami distribution which tends to be almost deterministic when N is large enough.

Contribution IV.5 (Analytic Expression)

PDF of the unicast-to-broadcast spectral gain

Given the defined hybrid network, the probability density function $p_{\Lambda}(\lambda)$ of the spectral gain λ obtained when switching from the unicast to the broadcast component to deliver a common service S is,

$$p_{\Lambda}(\lambda) = \frac{2m^m}{\Gamma(m)\omega^m} v_0^{(B)} \left(\lambda v_0^{(B)}\right)^{2m-1} e^{-\frac{m}{\omega} \left(\lambda v_0^{(B)}\right)^2} \quad (8.9)$$

where $v_0^{(B)}$ is the spectral efficiency selected for the broadcast component, and parameters ω and m defined as^a,

$$\omega = N^2(\mathbb{E}[v])^2 + N\mathbb{V}[v] \quad m = \frac{\omega^2}{4(\mathbb{E}[v])^2\mathbb{V}[v]N^3}$$

with N the number of users demanding service S in the network and v the random variable modeling the spectral efficiency of the unicast component which PDF is given by Contrib. IV.3 or Contrib. IV.4.

a. with $\mathbb{E}[\cdot]$ and $\mathbb{V}[\cdot]$ denoting the statistical expectation and variance, respectively.

► Energy efficiency switching criterion

The energy efficiency gain is similar to the spectral efficiency gain but integrates some complementary correction term in its expression regarding the transmit power level used for each component of the network. In the previously derived spectral gain, the transmit power of one component could indeed be arbitrarily augmented to positively influence that component, which lacks fairness. The energy efficiency gain takes the potential power imbalance between the two components into consideration as,

$$G_{energy}^{U \rightarrow B} = G_{spectral}^{(U \rightarrow B)} \times \frac{L^{(U)}(2c)}{L^{(B)}(R_B)} \frac{\Gamma_0^{(B)}}{\Gamma_0^{(U)}} \quad (8.10)$$

where $L(\cdot)$ are the maximum power attenuations experienced at the coverage boundaries for each component of the network (i.e. $2c$ or R_B) and computing from the adequate path-loss models as already discussed. Γ_0 are the minimum value of SNR that is required to guarantee a reliable reception for a signal which transmission is carried out at a the minimal spectral efficiency among the available ones for each component.

From this expression, it is understood that the maximal coverage distance of the broadcast component comes as a penalty compared to the cellular case since $L^{(B)}(R_B)$ is expected to be far higher than $L^{(U)}(2c)$. This penalty has to be compared to the user factorization gain discussed above. The simulation results presented in the following show how these two features jointly behave when N varies.

1.4 HYBRID ACCESS PERFORMANCE ANALYSIS

Many aspects can enter in consideration in the decision process between the activation of either the unicast or the broadcast transmission mode in a hybrid network in which both are available. Most of the already

conducted studies focus on the transmission of live mobile TV services [CHH08a, Bri08, UK06]. In that case, audience measurements provide a good criterion to decide which service has to be transmitted through the broadcast component. For other types of services, there is a lack of such a criterion. In the semi-analytical study summarized above, we have provided some statistical metrics allowing to easily evaluate the gain obtained when switching from the unicast to the broadcast component. Some of our results, published in [C.45] and [C.36], are reported below.

► Energy gain

Let us first investigate the gain obtained regarding the energy efficiency criterion as defined in (8.10). Our goal is to find which one of the components or sub-network can deliver a service to the users with the smallest overall power consumption, taking into account the spectral efficiency granted to the users. Fig. 8.6 gives the evolution of the global gain $G_{U \rightarrow B}$, which correspond to the broadcast gain over unicast, when the total number N of users changes within the proposed hybrid network. The given results are obtained using system and channel attenuation parameters specified in [v1.12a, 2]. Simulations results are obtained by direct numerical computation of the global gain $G_{U \rightarrow B}$ of (8.10) through uniform random locations of the N users. From these computations, curves corresponding to “average”, “minimum” and “maximum” cases are reported in the figure. The theoretical results are the average gains obtained with the proposed closed-form of Contrib. IV.5 which is verified to be very accurate as soon as $N > 10$. Then, it turns out that an average gain of 0dB is obtained when 5.0×10^3 users are active. This value represents the threshold that could drive the off-load of traffic from the unicast to the broadcast component of the hybrid network. This value can seem quite high, but recall that in the studied system, the area of the broadcast cell is 12.1×10^3 times greater than the area of a unicast cell. This means that the threshold eventually represent an average of 0.42 user per unicast cell, which correspond to less than 1 user every 2 cells. In other words, from energy considerations, the use of the large scale broadcast component is more favourable than the small scale unicast one as soon as one half of the unicast cells are requested for the same service delivery. This tends to prove that an hybrid unicast/broadcast coverage approach would allow global energy consumption reduction. In comparison, LTE-EMBMS-like systems are more flexible, allowing the switch from unicast to broadcast component cell by cell, but need that at least 2 users in the same cell use the same service for this switch to have an interest.

► Mixed broadcast/broadband strategy

In our study, further simulation have been led when changing the minimal spectral efficiency of the broadcast component. More precisely, instead of selecting the minimal spectral efficiency ν_1 and ensure a maximal coverage area, a higher ν_i is chosen to increase the throughput at the level of the broadcast component. If the transmit power of the broadcast station is not changed, the related coverage area is reduced. As such, we may switch from a pure unicast component to a mixed broadcast/unicast coverage : the users falling into the coverage area of the broadcast station may be served through the broadcast component and the other users will have no other possibility that the unicast component. In Fig. 8.7, we give how such a mixed strategy leads to some additional gain in terms of energy efficiency. Various “Mixed” modes according to switching spectral efficiency values ranging from ν_2 to ν_7 are tested, and the “Mixed Opt.” corresponds to the optimal mixed mode among all the possibilities.

► Unicast traffic off-load

The idea of data off-load can be applied to evaluate the reduction of the traffic load over the unicast component in some practical cases such as the periodic update of a given application. In that case, a large amount of terminals may be requested to download a common amount of data which could actually be pushed in advance in the memory of the terminals using a broadcast strategy. Based on some public information available in [Fra13], we took the example of the update of the Youtube application for Android terminals. In France for example, the average density of Android terminals is of about 26,4 per square km, hence leading to about $8,3^5$ terminals in the considered hybrid network of radius 100 km. Considering an average file weight of 6,6 Mo, the total traffic load to transmit such file to the whole terminals of the coverage area reaches 2,7 To in unicast mode, whereas it remains limited to 6,6 Mo in the broadcast mode if this mode is selected for the whole coverage area.

As previously used, we can also operate the hybrid network in a mixed broadcast/unicast strategy by reducing the broadcast coverage area while increasing the spectral efficiency. Fig. 8.8 gives the simulation results in such

1. Semi-analytic analysis of dual mode Broadcast/Unicast Networks

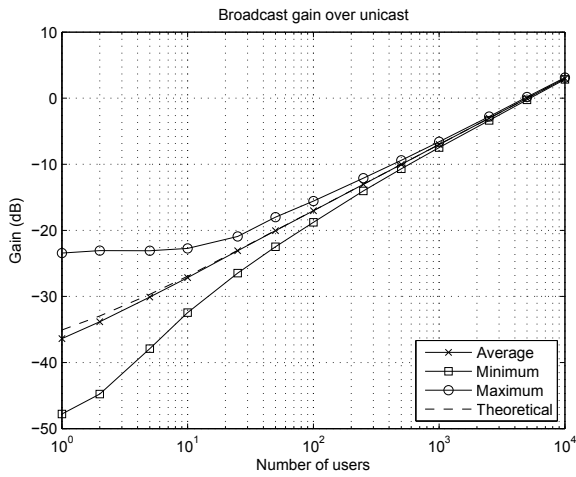


FIGURE 8.6– Analytical results and simulations of the energy efficiency gain versus the number of active users in a broadcast/unicast hybrid network with $R_B = 100$ km and $c = 1$ km.

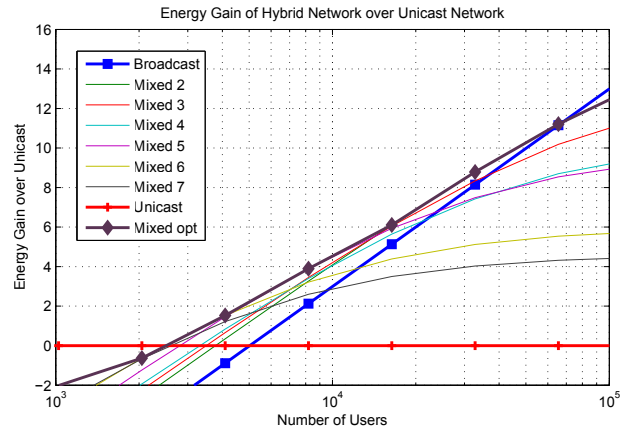


FIGURE 8.7– Energy efficiency gain versus the number of active users for the mixed broadcast/broadband strategy.

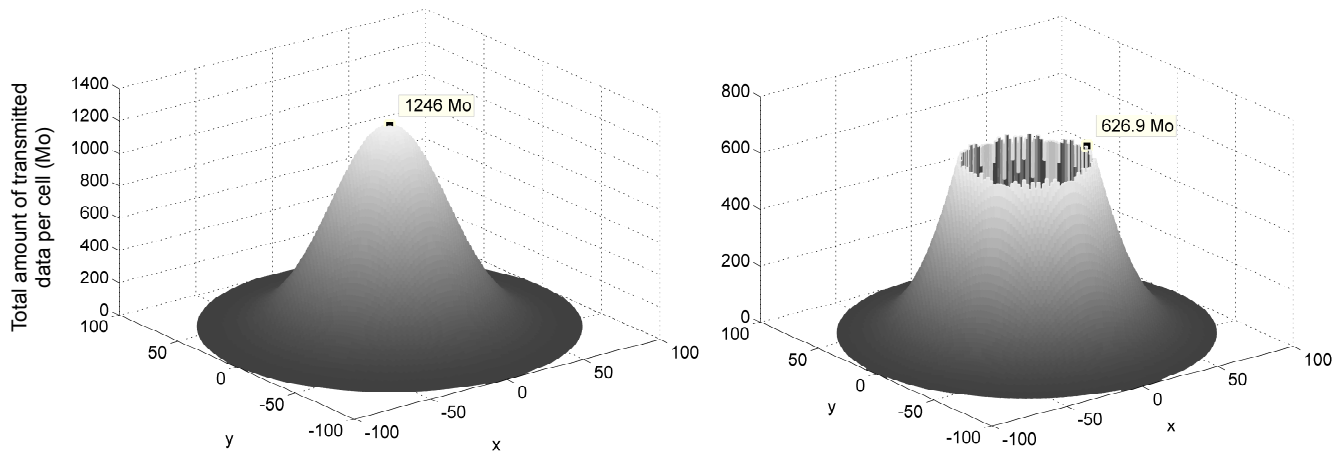


FIGURE 8.8– Distribution of the unicast traffic load per cell in a mixed broadcast/unicast transmission strategy. Left figure : unicast mode only. Right figure : broadcast mode activated $v = 4,34$ b/s/Hz.

a configuration for a Gaussian distribution of the users in the hybrid network and when the spectral efficiency of the broadcast component is set to 4,34 b/s/Hz. By this example, it is highlighted that a joint optimization of the broadcast and unicast components of a hybrid network can also be used to reduce the load of the unicast cells.

1.5 CONCLUSION

Network cooperation and convergence is a research topic that has taken an increased importance these last years since it opens new degrees of freedom in the optimization of communication systems. Most of the studies consider cooperation between cellular and local area networks as a major driver for increased system efficiency. The originality of our work has been to rather investigate cooperation aspects through the prism of the broadcast/unicast complementarity, hence addressing cooperation scenarios involving the conventional broadcast high-power high-tower infrastructure.

In this first PhD program conducted in the framework of the ANR MCube project, we have defined a new hybrid network topology and derived the related theoretical performance expressions based on a statistic model of the network metrics such as spectral and energy efficiency. On this basis, we have proposed switching criteria helping for the operation of the envisaged hybrid network. This led us to demonstrate the potential advantage

having a dual mode broadcast/unicast network.

During the work of the M-Cube project, we therefore promoted for a unified vision of the broadcast technologies, embedded in cellular networks to enable such cooperative scenarios. For instance, we contributed collectively with other partners to the organization of a dedicated Open Event at Orange Labs Paris gathering many industrials taking part in the DVB consortium and the 3GPP group. From an implementation perspective, we demonstrated in [R.8] how to specify a universal physical layer using a flexible signal to provide a common broadcasting system for the mobile broadband and TV broadcast networks. In the meantime, other initiatives such as the so-called dynamic broadcast [QNR11, NR12, QR13] or tower-overlay strategies [JR13, RIJ14] have emerged, with roughly the same idea of making cellular and broadcast network cooperate. In [RIJ14] in particular, the authors propose a cooperation scenario in which the LTE data traffic is offloaded to a DVB-T2 network, by using the DVB-T2 Future Extension Frame (FEF) concept together with the LTE carrier aggregation functionality, with the same philosophy as we introduced in [R.8]. All these ideas confirm that there is an advantage in such interworking between a broadcast and a unicast component, at least from a theoretical point of view.

Summary (PhD/Dissemination/Projects)

- 1 PhD (N. Cornillet)
- 1 International journal paper and 1 book chapter
- 3 communications in international conferences and workshops [C.36][C.45][C.51]
- 1 ANR Project (M-Cube)
- 1 presentation to an Open Event at Orange Labs

2 WIRELESS HYBRID BROADCAST/BROADBAND NETWORK OPTIMIZATION

2.1 MOTIVATION

Convergent network scenarios involving broadcast and broadband wireless networks have known a growing interest during the early 2010s. At the end of the PhD program summarized in the previous section, broadcast/unicast hybridization was even considered as a potential key technology in the perspective of the definition of the future 5th Generation mobile networks. The 5G vision of some industrials was consisting in a global standard unifying already existing network infrastructures and technologies, potentially also including broadcast networks. In addition, the definition in 2013 of the new MBMS operation on demand (MooD) mode in the 3GPP Release 12 [3GP15b] was a crucial step in the introduction of broadcast strategies in wireless broadband networks, since MooD allowed users to dynamically switch between unicast and broadcast transmission modes. This idea turned out to be very close to that we had investigated in our hybrid broadcast/broadband network studies and encouraged us to pursue our theoretical works on the optimization of hybrid operating modes and on the definition of efficient switching criteria.

In parallel to such an evolution, the upcoming 2015 Wireless Regulation Congress (WRC) putting again after the 2012 edition the UHF broadcasting band under high pressure for being partly attributed to mobile broadband operators [MGL⁺15, IR13, BR14], broadcast network operators were very interested in new strategies to demonstrate the advantage of operating such frequency bands using their high-power high-tower infrastructure. One promising approach for them was to enable cooperation strategies with wireless broadband networks.

In 2013, we then commonly defined with TDF and IRT-Bcom a new PhD program aiming at leading further investigations on broadcast/broadband hybrid network optimization. Some other works than ours, for instance [RECEH13c, RECEH13a], had shown that a broadcast/broadband network cooperation could be a promising and efficient solution, namely in the so-called broadcast coverage extension scenario. Broadcast coverage extension can be viewed as the dual scenario of the broadband off-load scenario previously introduced. As detailed later, a major common aspect of such scenarios relies on the coverage adaptation of the broadcast tower. In the PhD of P.A. FAM, started in 2013, we hence went on the hybrid network works initiated during the PhD of N. Cornillet

2. Wireless hybrid broadcast/broadband network optimization

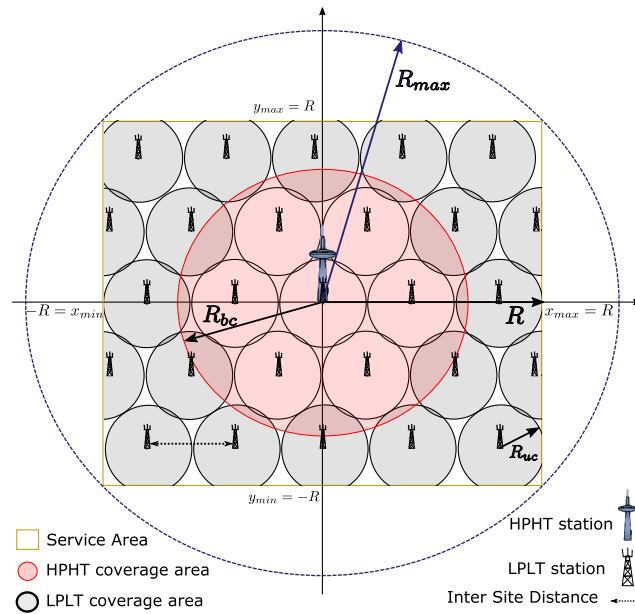


FIGURE 8.9– Hybrid network model with partial coverage of the broadcast station.

by integrating broadcast coverage adaptation. Our aim was to provide new theoretical results in term of hybrid network capacity and energy consumption and show in what extend a joint broadband/broadcast operation could lead to a better service coverage.

2.2 HYBRID NETWORK WITH ADAPTIVE BROADCAST COVERAGE

► Network model

As in the previous study, the hybrid network consists of two Orthogonal Frequency Division Multiplexing (OFDM) systems : a broadcasting system composed of a single High Power High Tower (HPHT) site located at the center of the service area and a mobile broadband system composed of N_c Low Power Low Tower (LPLT) sites. Based on the last discussions about the second digital dividend on the UHF broadcasting band around 2013, we will consider in this study that both the mobile broadband and broadcast systems operate in the UHF 700 MHz band which may be shared between the broadcast and the broadband networks. However, the two systems are supposed to be operated in two different frequency subbands, without any mutual interference. The broadcast system will benefit from a bandwidth $B^{(B)}$, while the each unicast cell will distribute between the users a number of N_{RB} resource blocks each having a bandwidth $B_{RB}^{(U)}$.

Contrary to the hybrid network model studied in the previous section, we consider in this work that the area of interest of radius R_{max} is jointly covered using the broadcast and broadband networks as represented Fig. 8.9. The broadcast station is assumed to have a coverage area of radius $R_B \leq R_{max}$. As such, the overall coverage is ensured for a common set of services to M users, some $M^{(B)}$ users being served by the central broadcast station, the other $M^{(U)}$ users located at outside the broadcast range being attached to the cellular base stations upon a unicast transmission mode. It is assumed that the service is always available and that the M considered users are demanding the service. A minimum capacity C_{req} is required for each user to properly receive the proposed service. This threshold capacity will hence govern the coverage area of the broadcast station, but also the spectral resource sharing for each unicast cell. In the latter case namely, a total

We are then interested in the study of the optimal planning parameters of the broadcast network i.e. the optimal broadcast coverage radius that maximizes a given utility function. We can for instance aim at maximizing the service capacity or the energy efficiency of the hybrid network given a targeted service rate. The useful metrics are introduced in the following paragraphs.

► Average Success Service Rate

Let us first define the average service capacity in the hybrid network. Such a definition was not used in the previous study. The service success rate η_s is defined as the number of users that have access to the proposed service over the total number M of users in the service area. Since the broadcast system is planned such that all users in the broadcast coverage area can access the service, therefore all users attached to the HPHT site have access to the service. However, for the unicast system, when the cells are overloaded, the access to the service is denied for some users. This is taken into account through the service success rate given at the level of the hybrid network by

$$\mathbb{E}[\eta_s] = \frac{1}{M} \left(\mathbb{E}[M^{(B)}] + \sum_{i=1}^{N_c} \mathbb{E}[\eta_i] \right) \tag{8.11}$$

in which η_i is the success rate for the i th cell. In practice, the number of users associated to each network component changes over time, hence the expectation. Considering a uniform distribution of the users in the network, a first contribution has been to derive a closed-form for the average service success rate as discussed later.

► Average Service Capacity

From the M users demanding the set of services in the hybrid network, the average service capacity is defined as the total average achievable rate gathering the contributive part of both components as,

$$\mathbb{E}[C_s^{(H)}] = \mathbb{E}[C^{(B)}] + \sum_{i=1}^{N_c} \mathbb{E}[C_i^{(U)}] \tag{8.12}$$

where $C^{(B)}$ is the total achieved capacity of the broadcast mode and $C_i^{(U)}$ is the capacity of the unicast mode in the i th cell of the wireless broadband network. The achieved rate of the broadcast mode will be directly influenced by the selected reference SNR $\Gamma_0^{(B)}$ yielding the coverage radius and the targeted spectral efficiency. As for the broadband network, the achieved rate will depend on the spectral resource sharing between users in each cell of the network, that is on the service success rate defined above.

► Energy Efficiency

Complementary to our previous study on hybrid network optimization, we have integrated here an accurate power consumption model extracted from the results of the EARTH project [RECEH13a]. According to [RECEH13a, DDG⁺12], base stations represent a dominant share of the total power consumption in unicast and broadcast networks. The proposed power model is based on a combination of the power consumption of base station components and sub-components such as analog Radio Frequency (RF), baseband (BB) processing, power amplifier and the power system (cooling). Furthermore, the power model uses a linear function that maps the consumed input power P of a base station to achieve a certain RF output power P_{max} at the antenna. Therefore, the power consumption P_{in} of a base station can be obtained from the following function,

$$P_{in} = \begin{cases} P_0 + \Delta_p P_{max} \rho & \text{if station in ON} \\ P_{sleep} & \text{otherwise} \end{cases} \tag{8.13}$$

where P_0 is a linear model parameter that represents the power consumption at the zero RF output power, P_{max} is the maximum RF output power at the antenna, P_{sleep} is the power consumption in sleep mode, Δ_p is the slope of the load-dependent power model and depends on the type of the base station, and ρ is the ratio of the number of carriers used to the total number of carriers, also called as the resource usage ratio. As an example, 8.2 shows power consumption model parameters for the different types of base stations used in this study, i.e. LPLT and

	P_{max} [W]	Δ_p	P_0 [W]	P_{sleep} [W]
LPLT ¹	40	4.75	260	150
HPHT ²	5000	3	260	150

TABLE 8.2– Power consumption parameters for the LPLT and HPHT transmitters.

2. Wireless hybrid broadcast/broadband network optimization

HPHT transmitters. Note that the resource usage ratio ρ should be set to 1, since all available subcarriers are used for data transmission in a broadcasting system. From such a model, the average power consumption of the hybrid network for the service delivery can be expressed as,

$$P_s^{(H)} = P_{in}^{(B)} + \sum_{i=1}^{N_c} P_{in,i}^{(U)} \quad (8.14)$$

2.3 SERVICE CAPACITY MAXIMIZATION

► Optimization Problem

We have first investigated the hybrid network optimization with adaptive broadcast range in the perspective of service capacity maximization. In other words, we have tried to show in what extend the cooperation between the unicast and broadcast components leverages the overall achievable rate of the network. Some intuitive reasoning can already be applied to understand the origin of the potential capacity gain when cooperation is processed. As stated in the previous section, the broadcasting system is usually planned to cover the entire service area using the worst case scenario, i.e. taking basis on the boundary SNR value. This planning strategy leads to a low service capacity with a high transmission power of the HPHT site. Furthermore, from (8.11) it can be seen that when the number of users in the unicast system increases, the service success rate decreases since the number of RBs available in a LPLT cell is limited. Based on these observations, we understand that finding an adequate coverage of the HPHT site should lead to a increase of the the service capacity of the hybrid network subject to a targeted service success rate η_{ref} . Therefore the service capacity maximization problem we have treated in our work can be stated as

$$\begin{aligned} \mathcal{P}1 : \quad & \max_{0 \leq r_B \leq 1} \mathbb{E}[C_s^H] \\ \text{subject to} \quad & \mathbb{E}[\eta_s] \geq \eta_{ref}, \end{aligned} \quad (8.15)$$

where $r_B = R_B/R_{max}$ is the normalized broadcast coverage radius with respect to the entire area of interest. The maximization of the service capacity in Problem $\mathcal{P}1$ can be viewed as the optimization of the offloading capacity of the hybrid network from its unicast to its broadcast component. Reversely, it can be understood as a maximization of the coverage area of the hybrid network, using the broadband component as a coverage extension means.

► Analytic formulation

To solve Problem $\mathcal{P}1$, we need to seek a more convenient analytical expression of the hybrid service capacity and service rate. As far as the broadcast component is considered, a straightforward expression of the service rate can be given assuming a uniform distribution of the users in the area of interest,

$$\mathbb{E}[C_s^{(B)}] = M r_B^2 B^{(B)} \log_2 \left(1 + \Gamma_0^{(B)} r_B^{-\alpha_B} \right) \quad (8.16)$$

where α_B is the path-loss exponent associated to the broadcast network. In the cellular system, the computation needs more effort since we need to express the average capacity $C_i^{(U)}$ of a cell in the network (see (8.12)). As detailed in [R.3], this can be achieved by first deriving the average achievable rate for one resource block RB and then getting the expression of the service success rate per cell. The main results we obtained are given in the following Contrib. IV.6 for a uniform distribution of the users. This result shows that the achievable rate corresponds to the minimal rate obtained at the boundary of the cells (the left term in (8.17)) augmented by an average rate given by the Beta function (the right term). This latter term from the uniform user distribution assumption. A different distribution would lead to a modified expression of such a term.

The expression given in Contrib. IV.6 is at the basis of any further statistical performance analysis at the level of the unicast cells. In particular, we have then derived the average service success rate per unicast cell, as given in the Contrib. IV.7. However, getting such a result theoretically depends on the resource allocation strategy carried out by the unicast station to serve multiple users in the cell, namely distributing the available

resource blocks among them. In a first attempt, a uniform allocation of the resource blocks among the users can be assumed. This approach can be seen as non realistic compared to practical allocation mechanisms, but we have shown through simulations that the impact of the average service rate is negligible [C.17], at least when the number of users is sufficiently high. Uniform RB allocation means that each user is assigned a fixed number of resource blocks based on the average capacity per resource block computed in Contrib. IV.6 and the total number of available resource block $N_{RB}^{(U)}$. Upon such assumption, the derivation of the average success rate per cell becomes tractable and yields the expression given in Contrib. IV.7 and detailed in [R.3].

Contribution IV.6 (Analytic Expression)

Average capacity of resource blocks with uniform user distribution

Given a uniform distribution of the users in the service area, and considering a minimum reference SNR $\Gamma_0^{(U)}$ at the boundary of the cells, the average capacity of a resource block in unicast mode is,

$$\mathbb{E}[C_{RB}^{(U)}] = B_{RB}^{(U)} \log_2(1 + \Gamma_0^{(U)}) + (\Gamma_0^{(U)})^{\alpha_U} \frac{B_{RB}^U}{\log 2} B\left(\frac{1}{1 + \Gamma_0^{(U)}}, \frac{2}{\alpha_U}, 1 - \frac{2}{\alpha_U}\right) \quad (8.17)$$

with α_U is the path-loss exponent in unicast mode, $B_{RB}^{(U)}$ the RB bandwidth and $B(.,.,.)$ the incomplete Beta function.

Contribution IV.7 (Analytic Expression)

Average service success rate per cell with uniform user distribution and resource allocation

Given a uniform distribution of M users in the service area and considering a unicast transmission mode based on a uniform resource allocation of the $N_{RB}^{(U)}$ resource blocks in each cell of radius R_U , the average service success rate per cell based upon a unicast transmission mode is,

$$\mathbb{E}[\eta_i^{(U)}] = \min\left(1, \frac{N_{RB} \mathbb{E}[C_{RB}^{(U)}]}{M r_U^2 C_{req}}\right) \quad (8.18)$$

where $r_U = R_U/R_{max}$ is the normalized cell coverage radius with respect to the entire area of interest, C_{req} is the required service capacity, N_{RB} is the total number of resource block per cell and $\mathbb{E}[C_{RB}^{(u)}]$ is given by Contrib. IV.6.

This expression of the average success rate yields a simple interpretation. If the number of users M is sufficiently low, the number N_{RB} of available resource blocks is higher than the number of required resource blocks to serve the users regarding the average rate given by Contrib. IV.6. Consequently, the ratio involved in the min function is greater than 1, hence leading to a 100% success rate. Otherwise, the ratio is less than 1 and directly gives the effective success rate.

From the latter two contributions, we have shown in [R.3] that Problem $\mathcal{P}1$ can be restated into the following analytic form,

$$\begin{aligned} \mathcal{P}1 : \quad & \max_{0 \leq r_B \leq 1} M \left[r_B^2 B^{(B)} \log_2 \left(1 + \Gamma_0^{(B)} r_B^{-\alpha_B} \right) + C_{req} (1 - r_B^2) \mathbb{E}[\eta_i^{(U)}] \right] \\ & \text{subject to} \quad r_B^2 + \mathbb{E}[\eta_i^{(U)}] (1 - r_B^2) \geq \eta_{ref}, \end{aligned} \quad (8.19)$$

► Problem solution

A major contribution of our work on broadband/broadcast hybrid network optimization has been to derive the closed-form solution to the above Problem $\mathcal{P}1$. A first important result was to prove the existence of an

2. Wireless hybrid broadcast/broadband network optimization

optimal operating point of the hybrid network in terms of achievable rate. Indeed, analyzing Problem $\mathcal{P}1$, we can interpret its utility function as an equilibrium function between two spectral efficiency terms,

$$f(x) = x^2 \log(1 + \delta_0 x^{-\alpha}) + (1 - x^2) \xi_0, \quad (8.20)$$

with,

$$\delta_0 = \Gamma_0^{(B)}, \quad \xi_0 = \frac{\log 2}{B^{(B)}} \quad \text{and,} \quad x = r_B^2 \quad (8.21)$$

The left term corresponds to the spectral efficiency term obtained from the broadcast component. The right term turns out to be homogeneous to a spectral efficiency and can be analyzed as the ratio between the average rate achieved by the users of the unicast component with the bandwidth available for the broadcast component. Hence, ξ_0 can be interpreted as the spectral efficiency a broadband network would offer if it would exploit the spectral resource of the broadcast network.

A first step has been to show that the utility function $f(x)$ is convex over the set of x values corresponding to practical situations and define a cooperation decision parameter helping us to find the optimal broadcast coverage radius R_B . This result has been discussed in [R.3], and is summarized in the following contribution.

Contribution IV.8 (Analytic Expression)

Convexity of the equilibrium function of Problem $\mathcal{P}1$

Given $\delta_0 \geq 0$, $\xi_0 \geq 0$ and $\alpha > 0$, the following function $f(x)$ $x \in [0, 1]$ is convex,

$$f(x) = x^2 \log(1 + \delta_0 x^{-\alpha}) + (1 - x^2) \xi_0, \quad (8.22)$$

such that $\exists x^* \in [0, 1]$, $f(x) \leq f(x^*) \forall x \in [0, 1]$ obeying to the following decision parameter s

$$s = \frac{\alpha}{2} - \log \frac{\alpha}{2} + \xi_0 \quad (8.23)$$

as,

$$x^* = \begin{cases} 1 & s < 1 \\ x^* \leftarrow \frac{df(x)}{dx} = 0 & s \geq 1 \\ 0 & s \rightarrow \infty \end{cases} \quad (8.24)$$

From this result, we conclude that there exists a unique optimal broadcast coverage radius $r_B^* = x^*$ which value goes from $r_b = 0$ (unicast mode only) to $r_b = 1$ (broadcast mode only) depending on the decision parameter s . This latter cooperation parameter s is mainly driven by ξ_0 which reports the average success rate in the cells of the broadband network. In other words, the optimal broadcast coverage radius directly depends on the load of the unicast cells. In the case when $s \geq 1$, the optimal radius needs still to be derived, which turns out not to be straightforward to obtain. In our study, we considered two solutions to give an analytic expression to the optimal solution : a first one based on a tabulated function, an a second one corresponding to an accurate approximation and relaxing the use of the tabulated function. These two solutions are gathered in the Contrib. IV.9. The way to extract such solutions is explained in [R.3].

The function $v(s)$ defined in Eq. (8.25) to express the optimal coverage radius is illustrated in Fig. 8.10. It is observed that $v(s)$ is monotonically decreasing $\lim_{s \rightarrow +\infty} v(s) = 0$. Thus when s becomes high enough (e.g. $s > 3$) the optimal solution can be approximated by omitting the tabulated function $v(s)$ in the optimal expression of r_B yielding the approximated result in (8.25). This observation is further highlighted in Fig. 8.11, which shows the optimal coverage radius as a function of the cooperation decision parameter s , with different values of $\Gamma_0^{(B)}$. We conclude that that the approximate solution is close to the exact solution even if for a low value of the cooperation decision parameter s and low SNR $\Gamma_0^{(B)}$, the approximation error increases. Indeed, we have shown in [R.3] that the approximation error can be further reduced by using an iterative approach.

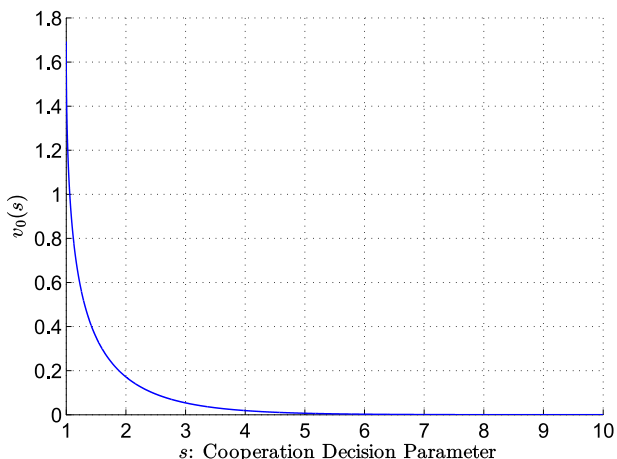


FIGURE 8.10– Illustration of the tabulated function $v(s)$ as a function of the cooperation decision parameter s .

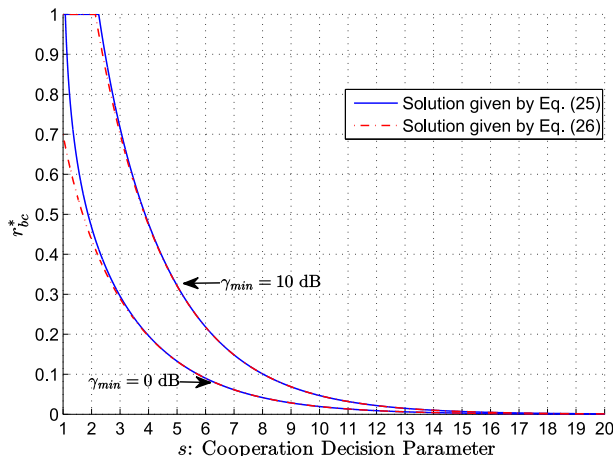


FIGURE 8.11– Optimal broadcast coverage radius as a function of the cooperation decision parameter s . Comparison of the exact and approximate solutions.

Contribution IV.9 (Analytic Expression)

Optimal broadcast coverage radius

Given the broadcast/broadband hybrid network previously defined, the normalized broadcast tower coverage radius r_B yielding maximal average service capacity is expressed as,

$$r_B^* = \left(\frac{\Gamma_0^{(B)}}{\frac{\alpha_B}{2} \frac{e^s}{1+v_0(s)} - 1} \right)^{\frac{1}{\alpha_B}} \approx \left(\frac{\Gamma_0^{(B)}}{\frac{\alpha_B}{2} e^s - 1} \right)^{\frac{1}{\alpha_B}} \tag{8.25}$$

with s introduced in Contrib. IV.8 and $v(s)$ a decreasing function defined over $[1, \infty]$ as,

$$\log(1 + v(s)) = e^{-s} (1 + v(s)). \tag{8.26}$$

From the last theoretical analysis, we have provided a means to set the coverage radius to maximize the global service capacity of the hybrid network. Nevertheless, the optimal r_B^* given by Contrib. IV.9 may not meet the service success rate constraint of Problem $\mathcal{P}1$. For example, if the total number of users M is very high, the optimal radius based on the overall hybrid network capacity optimization may lead to a success rate lower than the constraint. In such situations, it can be demonstrated that solution of the optimization is directly given by solving the constraint equation [R.3] as,

$$r_B^* = \sqrt{\frac{\eta_{ref} - \mathbb{E}[\eta_i^{(U)}]}{1 - \mathbb{E}[\eta_i^{(U)}]}} \tag{8.27}$$

which is valid only if $\mathbb{E}[\eta_i^{(U)}] \neq 1$. Finally, it can be shown that the solving the constraint Problem $\mathcal{P}1$ yields the solution summarized in the following contribution.

Contribution IV.10 (Analytic Expression)

Optimal solution to Problem P1

Given the broadcast/broadband hybrid network previously defined, the optimal setting for the broadcast station coverage radius for hybrid network capacity maximization under success rate constraint η_{target} is obtained through

$$r_B^* = \begin{cases} \text{from (8.25)} & \text{if } \mathbb{E}[\eta_i^{(U)}] < \frac{\eta_{ref} - r_B^2}{1 - r_B^2} \\ \text{from (8.27)} & \text{otherwise} \end{cases} \quad (8.28)$$

with $\mathbb{E}[\eta_i^{(U)}]$ computed from Contrib. IV.7.

► Simulation results

We give here some simulation results showing not only the accuracy of the proposed analytical solution of the hybrid network setting optimization, but also the performance gain obtained from the cooperation between the two components of the network. The Vienna LTE-A downlink system level simulator has been used to emulate the behavior of the hybrid model with a practical system and to provide the numerical results [TBK⁺15, MWI⁺09]. During the PhD of Pape FAM, a part of the work has been dedicated to add several features to the simulator to support the HPHT type of infrastructure. To follow the proposal published during the ANR MCube project in [R.3] and also suggested in [RIJ14], we used for the PHY layer a dedicated LTE broadcast system based on eMBMS++ specifications. This advanced feature of the Vienna simulator has been shown during a workshop in 2015 [C.17]. Using such a simulator closely reflects the behavior of a real systems since the SNR of each user is mapped to a channel quality indicator (CQI) relying on PHY layer performance results. Then to determine the throughput of the user, a modulation and coding scheme (MCS) is selected based on the reported CQI and the quality of service (QoS) requirements. We use this approach in our simulations using the SNR-to-CQI mapping function extracted from [MWI⁺09, 3GP15a].

For the presented simulations here, we consider the delivery of a high definition (HD) service to M users in a squared service area of $30 \times 30 \text{ km}^2$. The capacity requirement for the service is set to $C_{req} = 2 \text{ Mbps}$ and the reference SNR Γ_0 is set to 0 dB for both components. Further system parameter settings are available in [R.3] and [C.14]. Fig. 8.12 shows the evolution of the average service capacity as a function of the coverage radius of the HPHT cell without any specification of the targeted service success rate. The simulation results are presented along with the theoretical ones. As observed in this figure the analytical expressions of the optimal broadcast coverage radius are close to the optimal solution obtained from simulation, even considering the approximated closed-form. The difference observed about the capacity gain is due to the use of the theoretical Shannon capacity formula in the analytical model, whereas a practical SNR to capacity mapping function is used in the simulations. Nevertheless, the optimal broadcast coverage area is not that sensitive to such mismatch.

Complementary to the previous results, Fig. 8.13 shows the evolution of the average service success rate as a function of the broadcast coverage radius. The theoretical results are in agreement with the simulation ones. It is also observed that when the LPLT cells are not overloaded i.e. $M = 500$, the average service success rate is constant and equal to one. Thus all users in the service area can be served. On the other hand, when the LPLT cells become overloaded i.e. $M = 10000$, the average service success rate increases as the broadcast coverage radius increases. In this situation, the optimal broadcast coverage radius has to be computed from the constraint optimization problem solution given by Contrib. IV.10.

Further results given in Fig. 8.14 and 8.15 show how the cooperation between the broadcast and broadband networks can help in improving the service delivery performance depending on the user demand, either from a capacity or a success rate point of view. Such results, based on the previously derived theoretical expressions are important outputs of our work on broadcast/broadband cooperation.

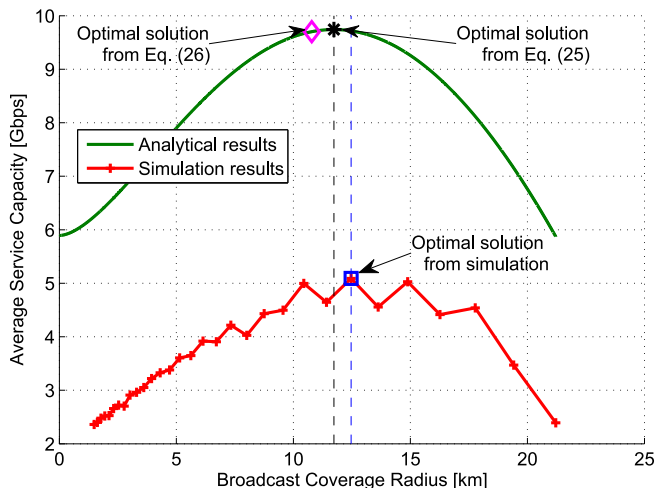


FIGURE 8.12– Average service capacity vs. broadcast coverage radius. Comparison between analytical and simulation results. M = 500 UEs

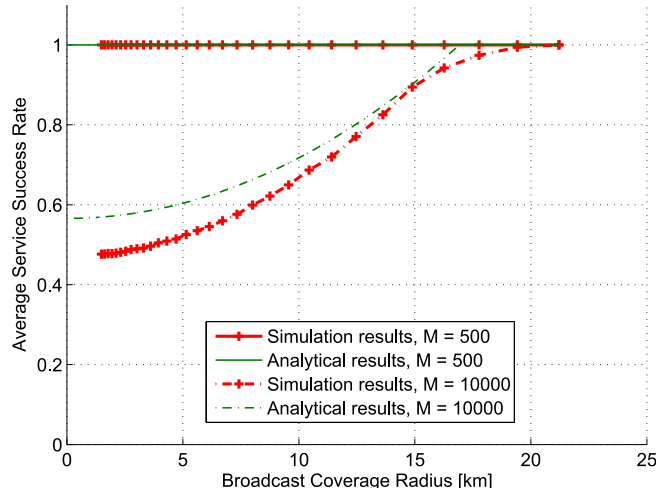


FIGURE 8.13– Average service success rate vs. broadcast coverage radius; analytical and simulation results; M = 500 and M = 10000 UEs.

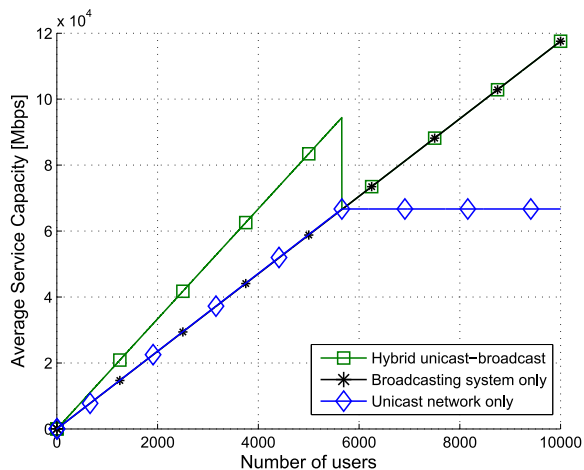


FIGURE 8.14– Average service capacity vs. the number of users in the service area; Comparison of the hybrid network, unicast network and broadcast network average service capacity.

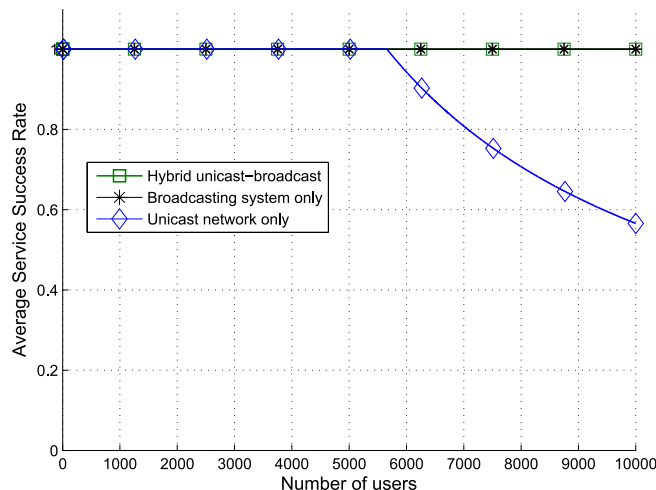


FIGURE 8.15– Average service success rate vs. the number of users in the service area; Comparison of the hybrid network, unicast network and broadcast network average service capacity.

2.4 ENERGY CONSUMPTION MINIMIZATION

► Problem formulation

In the previous section, we have investigated how to optimize the service capacity based on a joint operation of broadband and broadcast modes in a hybrid network. Using the accurate power consumption model complementary contributions in our work have been to optimize the energy efficiency metric of the hybrid network. Actually, considering the energy saving aspects, the LPLT sites within the coverage area of the broadcast network could be turned off to save more energy since there is no data to transmit. In the light of these observations, the aim is to find the optimal broadcast coverage radius that maximizes the energy efficiency (EE) metric of the hybrid network. The general related energy efficiency maximization problem states

$$\mathcal{P}2 : \quad \max_{0 \leq r_B \leq 1} \frac{\mathbb{E}[C_s^H]}{P_{in}^H} \tag{8.29}$$

$$\tag{8.30}$$

2. Wireless hybrid broadcast/broadband network optimization

with $\mathbb{E}[C_s^H]$ and P_{in}^H given from (8.12) and (8.14), respectively. Stated as it is, this problem turns out however to be mathematically untractable. To circumvent this, we formulated two subproblems, not equivalent to the main one, but following the energy efficiency approach. Indeed, the energy efficiency of the hybrid network is maximized either by increasing the capacity of the hybrid network for a fixed transmit power of the broadcast component or by reducing the power consumption of the broadcast component for a given capacity requirement. This leads to two different optimization problems which resolution become analytically feasible as detailed in the sequel.

► Power consumption minimization approach

In this subproblem, the energy efficiency is maximized by minimizing the power consumption of the broadcast component with respect to a target capacity at the edge of the broadcast coverage radius based on the service requirement. More precisely, in this approach the transmission power of the broadcast station is set according to the target capacity C_{req} , which leads to a minimum SNR $\Gamma_0^{(B)}$ as already discussed. After some manipulations, the energy efficiency of the hybrid network can be expressed as a function of the normalized broadcast coverage radius r_B . The optimization problem can thus be formally stated using the following objective function $f(x)$ with $x = r_b \in [0, 1]$ as,

$$f(x) = MC_{req} \left(\frac{\mathbb{E}[\eta_i^{(U)}]}{\Delta_p^{(B)} P_{max}^{(B)}} \right) \cdot \frac{1 + \theta_c x^2}{\sigma_{p1} - \sigma_{p2} x^2 + x_B^\alpha} \quad (8.31)$$

where $\mathbb{E}[\eta_i^{(U)}]$ is given by Contrib. IV.7, and

$$\theta_c = \frac{B^{(B)} \log_2(1 + \Gamma_0^{(B)})}{C_{req} \mathbb{E}[\eta_i^{(U)}]} - 1, \quad \sigma_{p1} = \frac{P_{in}^{(U)} + P_0^{(B)} r_U^2}{\Delta_p^{(B)} P_{max}^{(B)} r_U^2} \quad \text{and} \quad \sigma_{p2} = \frac{P_{in}^{(U)} + P_{sleep}^{(U)}}{\Delta_p^{(B)} P_{max}^{(B)} r_U^2} \quad (8.32)$$

Parameter θ_c is a parameter resulting from the difference between the average capacity of the broadcast component and the unicast component of the hybrid network, while parameters σ_{p1} and σ_{p2} are related to the power and system models introduced in (8.13).

In [C.1], we have shown that the function $f(x)$ is convex $\forall x \in [0, 1]$ and $\alpha \geq 2$. Therefore the optimal broadcast coverage radius is obtained by finding the root of the derivative function. We proved that only an approximated closed-form can be found to the optimal coverage radius, however providing a very accurate solution to the problem. The following contribution gives the proposed closed-form approximation.

Contribution IV.11 (Analytic Expression)

Approximated solution to power efficiency maximization through power minimization approach

Given the broadcast/broadband hybrid network previously defined, the optimal broadcast coverage radius for hybrid network energy efficiency maximization obtained through a power minimization approach is

$$r_B^* \approx \frac{s^{\frac{1}{\alpha_B - 2}}}{\sqrt{\theta_c \left(\frac{2}{\alpha_B} - 1 \right)}} \left(1 + \sum_{k=0}^2 \frac{k}{\alpha_B - 2} s^{\frac{2k}{\alpha_B - 2}} \right) \quad (8.33)$$

with s a cooperation decision parameter defined as,

$$s = \frac{2}{\alpha_B} (\theta_c \sigma_{p2} + \sigma_{p1}) \left[\theta_c \left(\frac{2}{\alpha_B} - 1 \right) \right]^{\frac{\alpha_B}{2} - 1} \quad (8.34)$$

► Capacity maximization approach

Instead of reducing the transmission power of the broadcast component, the energy efficiency is obtained by increasing the capacity of the broadcast component while the transmission power is kept constant. Given a uniform distribution of the location of the users in the service area, we have shown in [C.1] that the energy

efficiency of the hybrid network can be re-expressed as a function of the normalized broadcast coverage radius. Thus, the objective function to maximize in this case is written as

$$f(x) = M \left(\frac{B^{(B)}}{\Delta_P^{(B)} P_{max}^{(B)} \log 2} \right) \cdot \frac{x^2 \log \left(1 + \Gamma_0^{(B)} x^{-\alpha_B} \right) + (1 - x^2) v_c}{\sigma_{p1} - \sigma_{p2} x^2 + 1} \quad (8.35)$$

where $v_c = \frac{C_{req} \log 2}{B^{(B)}} \mathbb{E}[\eta_i^{(U)}]$. Finding the maximum operating point of such an objective function can not easily be obtained. A practical solution can however be provided by means of a tabulated function, following the same approach as that proposed to solve Problem $\mathcal{P}1$. The obtained solution which proof is detailed in [C.1] is given in the following contribution.

Contribution IV.12 (Analytic Expression)

Approximated solution to power efficiency maximization through capacity maximization approach

Given the broadcast/broadband hybrid network previously defined, the optimal broadcast coverage radius for hybrid network energy efficiency maximization obtained through a capacity maximization approach is

$$r_B^* \approx \left(\frac{\Gamma_0^{(B)}}{\frac{\alpha_B}{2S(v_p, v_c)} - 1} \right)^{\frac{1}{\alpha_B}} \quad (8.36)$$

with $v_c \in [0, +\infty]$ defined in (8.35), $v_p = \frac{\sigma_{p2}}{1 + \sigma_{p1}} \in [0, 1]$ and $S(v_p, v_c)$ a bivariate monotonously decreasing function defined as,

$$z - \log z + v_p \left(z \Gamma_0^{(B)} \right)^{\frac{2}{\alpha_B}} \left(\frac{\alpha_B}{2} - z \right)^{1 - \frac{2}{\alpha_B}} = \frac{\alpha_B}{2} - \log \frac{\alpha_B}{2} + v_c (1 - v_p) \quad (8.37)$$

with $z = S(v_p, v_c)$.

This last solution relies on a function for which no closed-form expression nor approximation has been found. However, it can be tabulated for predetermined parameters α_B and $\Gamma_0^{(B)}$.

► Simulation Results

Let us present some synthetic simulation results obtained by applying both proposed theoretical solutions. Fig. 8.16 gives the comparative results obtained in terms of energy efficiency carrying out the power minimization and the capacity maximization strategies. A first conclusion is that both approaches yield very close results. With a more detailed analysis, power minimization turns out to be slightly more favourable than capacity maximization unless the number M of users becomes very high. This means that the user factorization gain of the broadcast component is asymptotically more favourable to the capacity increase than to the power consumption decrease. Indeed, this can be also concluded through the analysis of the objective functions established in (8.31) and (8.35).

In Fig. 8.17 we focus on the sensitivity of the optimal broadcast coverage radius to the number of users M in the service area. It can be observed that the optimal broadcast coverage radius obtained using the capacity maximization approach is less sensitive to the variation of the number of users in the service area than the optimal broadcast coverage radius obtained with the power minimization approach. Therefore, from a network planning point of view, the capacity maximization approach may be more appropriate than the power minimization approach to optimize the energy efficiency of a hybrid unicast-broadcast network. From these results, a rule of thumb in terms of energy efficiency is to operate the hybrid network so as to ensure a broadcast coverage of about 40-50% of the whole service area.

2. Wireless hybrid broadcast/broadband network optimization

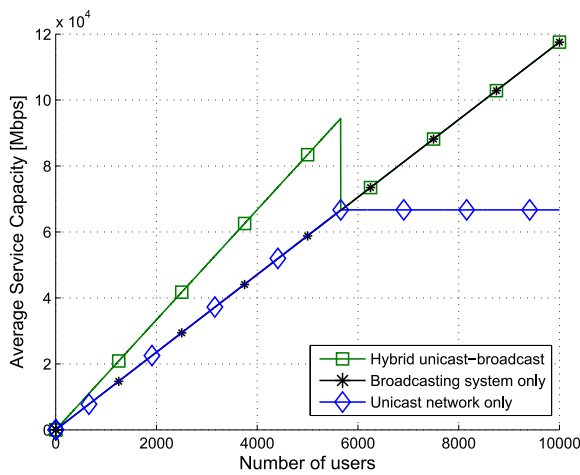


FIGURE 8.16– Maximum energy efficiency vs number of users M . Comparison between the capa-max and pwr-min approaches.

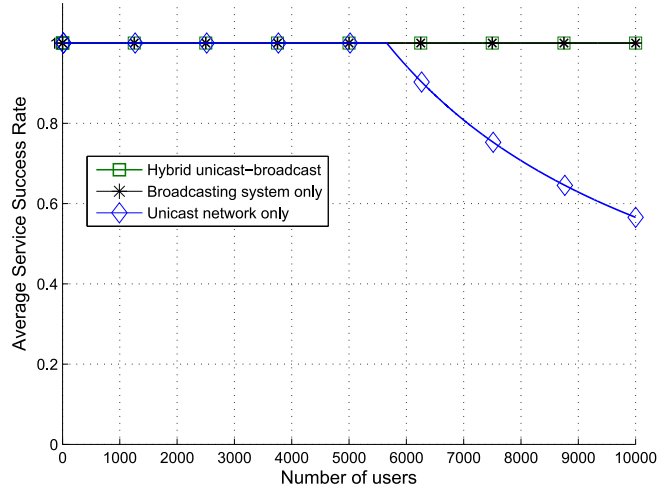


FIGURE 8.17– Optimal broadcast coverage radius vs number of users M . Comparison between the capa-max and pwr-min approaches.

2.5 CONCLUSION

The work achieved during the PhD of P.A. Fam gives further insight to the overall question of broadcast/broadband hybrid network optimization. This issue has been tackled with the definition of the MBMS operation on demand (MooD) in the 3GPP Release 12 [3GP15b]. MooD allows users to dynamically switch between unicast and broadcast transmission modes, nevertheless current deployments of LTE eMBMS are based on the Release 9 or 10 of LTE standard which does not implement this MooD enhancement.

In particular, authors in [CMGB15] have reviewed the state of the art and current trends in mobile multimedia delivery focusing on the potential opportunities and technical challenges of the convergence between mobile broadband and broadcast industries.

Further insights Yet, further theoretical investigations studies were needed to

Summary (PhD/Dissemination/Projects)

- 1 PhD (P.A. Fam)
- 1 International journal paper [R.3]
- 4 communications in international conferences and workshops [C.1][C.14][C.17]
- 1 IRT-Bcom Project (RS-COM)

The measure of greatness in a scientific idea is the extent to which it stimulates thought and opens up new lines of research.

– Paul A.M. Dirac –

1 GENERAL CONTEXT

2 PROPOSED RESEARCH TRACKS

2.1 UNIFIED MODEL OF HIGH POWER TRANSMITTERS EFFICIENCY

2.2 SPATIAL FILTERING FOR MMWAVE SYSTEMS

2.3 OPTIMIZED MULTI-MODE COMMUNICATION NETWORKS

- [1] ETSI TS 122 146. Digital cellular telecommunications system (phase 2+); universal mobile telecommunications system (umts); lte; multimedia broadcast/multicast service (mbms); stage 1. Technical report, ETSI, 2013. v11.1.0.
- [3GP15a] 3GPP. LTE; Evolved Universal Terrestrial Radio Access (E-UTRA); Physical layer procedures;. TS 136.213, 3rd Generation Partnership Project (3GPP), April 2015.
- [3GP15b] 3GPP. Multimedia Broadcast/Multicast Service (MBMS) improvements; MBMS operation on demand. TR 26.849, 3rd Generation Partnership Project (3GPP), June 2015.
- [2] ETSI TR 136 942. Lte; evolved universal terrestrial radio access (e-utra); radio frequency (rf) system scenarios. Technical report, ETSI, 2012. v11.0.0.
- [AHW07] O. Tirkkonen A. Hottinen and R. Wichman. *Multi-antenna Transceiver Techniques for 3G and Beyond*. WILEY, 2007.
- [Ala98] Siavash Alamouti. A simple transmit diversity technique for wireless communications. *Selected Areas in Communications, IEEE Journal on*, 16(8) :1451–1458, 1998.
- [ATS16] ATSC3.0. Atsc proposed standard : Physical layer protocol, a/322 :2016. Technical report, ATSC, sept. 2016.
- [BAT+11] M. Brandon, M. Ariaudo, S. Traverso, J. Bouvier, I. Fijalkow, and J.L. Gautier. Linearity improvement thanks to the association of Active Constellation Extension and digital predistortion for OFDM. In *New Circuits and Systems Conference (NEWCAS), 2011 IEEE 9th International*, pages 293–296, June 2011.
- [BC04] N.C. Beaulieu and J. Cheng. Precise error-rate analysis of bandwidth-efficient bpsk in nakagami fading and cochannel interference. *Communications, IEEE Transactions on*, 52(1) :149–158, Jan 2004.
- [BF82] S.A. Billings and S.Y. Fakhouri. Identification of systems containing linear dynamic and static nonlinear elements. *Automatica*, 18(1) :15 – 26, 1982.
- [BFH96] R. W. Bauml, R. F. H. Fischer, and J.B. Huber. Reducing the peak-to-average power ratio of multi-carrier modulation by selected mapping. *IEE Electronics Letters*, 32(22) :2056–2057, 1996.
- [BGP02] H. Bolcskei, D. Gesbert, and A. J. Paulraj. On the capacity of ofdm-based spatial multiplexing systems. *IEEE Transactions on Communications*, 50(2) :225–234, Feb 2002.
- [BHV09] E. Biglieri, Y. Hong, and E. Viterbo. On fast-decodable space-time block codes. *IEEE Transactions on Information Theory*, 55(2) :524–530, Feb 2009.
- [BLG02] P. Banelli, G. Leus, and G.B. Giannakis. Bayesian estimation of clipped Gaussian processes with application to OFDM. In *Signal Processing Conference, 2002 11th European*, pages 1–4, Sept 2002.
- [BLM+14a] N. Bhushan, J. Li, D. Malladi, R. Gilmore, D. Brenner, A. Damnjanovic, R. T. Sukhvasi, C. Patel, and S. Geirhofer. Network densification : the dominant theme for wireless evolution into 5g. *IEEE Communications Magazine*, 52(2) :82–89, February 2014.
- [BP08] Kitaek Bae and E. J. Powers. Distribution of envelope power using selected mapping in ofdm systems with nonlinearity. In *2008 IEEE International Conference on Acoustics, Speech and Signal Processing*, pages 3065–3068, March 2008.
- [BR14] R. Beutler and D. Ratkaj. Crystal ball, tea leaves or mathematics forecasting data traffic for mobile services. Rev. Q1, European Broadcasting Union (EBU), May 2014.
- [Bri08] A. Bria. *Mobile Multimedia Multicasting in Future Wireless Systems : A Hybrid Cellular-Broadcasting System Approach*. PhD thesis, KTH, Communication Systems, CoS, 2008.

- [BRV05] J. C. Belfiore, G. Rekaya, and E. Viterbo. The golden code : a 2 times ;2 full-rate space-time code with nonvanishing determinants. *IEEE Transactions on Information Theory*, 51(4) :1432–1436, April 2005.
- [BSHD13a] Emil Björnson, Luca Sanguinetti, Jakob Hoydis, and Mérouane Debbah. Designing multi-user mimo for energy efficiency : When is massive mimo the answer ? *arXiv preprint arXiv :1310.3843*, 2013.
- [CHH08a] D. Catrein, J. Huschke, and U. Horn. Analytic evaluation of a hybrid broadcast-unicast tv offering. In *Vehicular Technology Conference, 2008. VTC Spring 2008. IEEE*, pages 2864–2868, 2008.
- [Chr00] M. Chryssomallis. Smart antennas. *IEEE Antennas and Propagation Magazine*, 42(3) :129–136, June 2000.
- [CL14] In Kyeong Choi and Sok Kyu Lee. *Method and apparatus for allocating transmission power in multi input multi output system*. Google Patents, November 2014. US Patent 8,891,643.
- [CM04] Lai-U Choi and R. D. Murch. A transmit preprocessing technique for multiuser mimo systems using a decomposition approach. *IEEE Transactions on Wireless Communications*, 3(1) :20–24, Jan 2004.
- [CMGB15] J. Calabuig, J.F. Monserrat, and D. Gomez-Barquero. 5th generation mobile networks : A new opportunity for the convergence of mobile broadband and broadcast services. *Communications Magazine, IEEE*, 53(2) :198–205, Feb 2015.
- [CS03] Giuseppe Caire and Shlomo Shamai. On the achievable throughput of a multiantenna gaussian broadcast channel. *Information Theory, IEEE Transactions on*, 49(7) :1691–1706, 2003.
- [CY09] Li-Chung Chang and Chung-Ho Yang. A combined approach of MBAP/PR PAPR reduction and polynomial predistortion for performance enhancement. In *Information, Communications and Signal Processing, 2009. ICICS 2009. 7th International Conference on*, pages 1–5, Dec 2009.
- [D⁺04] Lei Ding et al. A robust digital baseband predistorter constructed using memory polynomials. *Communications, IEEE Transactions on*, 52(1) :159–165, Jan 2004.
- [DDG⁺12] C. Desset, B. Debaillie, V. Giannini, A. Fehske, G. Auer, H. Holtkamp, W. Wajda, D. Sabella, F. Richter, M. J. Gonzalez, H. Klessig, I. Gódor, M. Olsson, M. A. Imran, A. Ambrosy, and O. Blume. Flexible power modeling of lte base stations. In *2012 IEEE Wireless Communications and Networking Conference (WCNC)*, pages 2858–2862, April 2012.
- [Din04] Lei Ding. *Digital Predistortion of Power Amplifiers for Wireless Applications*. PhD thesis, School of Electrical and Computer Engineering, Georgia Institute of Technology, 2004.
- [DJ98] Esmael H Dinan and Bijan Jabbari. Spreading codes for direct sequence cdma and wideband cdma cellular networks. *Communications Magazine, IEEE*, 36(9) :48–54, 1998.
- [DT09] DVB-T2. Frame structure channel coding and modulation for a second generation digital terrestrial television broadcasting system (dvb-t2), en-302755 v1.1.1. Technical report, ETSI, sept. 2009.
- [DTF99] A. Derode, A. Tourin, and M. Fink. Ultrasonic pulse compression with one-bit time reversal through multiple scattering. *Journal of Applied Physics*, 85 :6343–6352, May 1999.
- [EAHAS⁺12] O. El Ayach, R.W. Heath, S. Abu-Surra, S. Rajagopal, and Zhouyue Pi. The capacity optimality of beam steering in large millimeter wave MIMO systems. In *2012 IEEE 13th International Workshop on Signal Processing Advances in Wireless Communications (SPAWC)*, pages 100–104, June 2012.
- [EVH⁺04b] Majid Emami, Mai Vu, Jan Hansen, Arogyaswami J Paulraj, and George Papanicolaou. Matched filtering with rate back-off for low complexity communications in very large delay spread channels. In *Signals, Systems and Computers, 2004. Conference Record of the Thirty-Eighth Asilomar Conference on*, volume 1, pages 218–222. IEEE, 2004.
- [Fin92] M. Fink. Time reversal of ultrasonic fields. i. basic principles. *IEEE Transactions on Ultrasonics, Ferroelectrics and Frequency Control*, 39(5) :555–566, Sept. 1992.
- [Fos96] Gerard J Foschini. Layered space-time architecture for wireless communication in a fading environment when using multi-element antennas. *Bell labs technical journal*, 1(2) :41–59, 1996.

Bibliographie

- [Fra13] Mobile Marketing Association France. Deuxième édition du baromètre trimestriel du marketing mobile, Juin 2013.
- [Fra16] Marcelo Jorge Franco. *Wideband digital predistortion linearization of radio frequency power amplifiers with memory*. PhD thesis, Drexel University, 2016.
- [FSY11] W. Fang, H. Sun, and L. Yang. Power allocation for maximizing sum capacity of multiuser mimo downlink with transmit precoding based on slnr. In *2011 IEEE 73rd Vehicular Technology Conference (VTC Spring)*, pages 1–5, May 2011.
- [GEPB06] M. J. Fernandez-Getino Garcia, O. Edfors, and J. M. Paez-Borralló. Peak power reduction for ofdm systems with orthogonal pilot sequences. *IEEE Transactions on Wireless Communications*, 5(1) :47–51, Jan 2006.
- [GH03] H. El Gamal and A. R. Hammons. On the design of algebraic space-time codes for mimo block-fading channels. *IEEE Transactions on Information Theory*, 49(1) :151–163, Jan 2003.
- [GMB05] P. Gilabert, G. Montoro, and E. Bertran. On the wiener and hammerstein models for power amplifier predistortion. In *2005 Asia-Pacific Microwave Conference Proceedings*, volume 2, pages 4 pp.–, Dec 2005.
- [Gol67] Robert Gold. Optimal binary sequences for spread multiplexing (corresp.). *Information Theory, IEEE Transactions on*, 13(4) :619–621, 1967.
- [GOU13] Oussoulaire Abel GOUBA. *Approche conjointe de la réduction du facteur de crête et de la linéarisation dans le contexte ofdm*. PhD thesis, Ecole Doctorale MATISSE, 2013.
- [GRJ+65] Izrail Solomonovich Gradshteyn, Iosif Moiseevich Ryzhik, Alan Jeffrey, Daniel Zwillinger, and Scripta Technica. *Table of integrals, series, and products*, volume 6. Academic press New York, 1965.
- [H+13] H. Hemesi et al. Analytical Modeling of MIMO-OFDM System in the Presence of Nonlinear Power Amplifier with Memory. *on IEEE Trans. Commun*, 61(1) :155–63, Jan. 2013.
- [Hat80] M. Hata. Empirical formula for propagation loss in land mobile radio services. *IEEE Transactions on Vehicular Technology*, 29(3) :317 – 325, 1980.
- [HB06] Jeremiah Hu and Norman C Beaulieu. Accurate closed-form approximations for the error rate and outage of equal gain combining diversity in nakagami fading channels. In *Communications, 2006. ICC'06. IEEE International Conference on*, volume 11, pages 5145–5152. IEEE, 2006.
- [HCPR12b] Hoon Huh, Giuseppe Caire, Haralabos C Papadopoulos, and Sean A Ramprasad. Achieving" massive mimo" spectral efficiency with a not-so-large number of antennas. *Wireless Communications, IEEE Transactions on*, 11(9) :3226–3239, 2012.
- [HCVG09] O. Hammi, S. Carichner, B. Vassilakis, and F. M. Ghannouchi. Effects of crest factor reduction on the predistortion performance for multi-carrier 3g rf power amplifiers. In *2009 IEEE MTT-S International Microwave Symposium Digest*, pages 1085–1088, June 2009.
- [Heu10] C. Heuck. An Analytical Approach for Performance Evaluation of Hybrid (Broadcast/Mobile) Networks. *IEEE Transactions on Broadcasting*, 56(1) :9–18, March 2010.
- [HH02] B. Hassibi and B. M. Hochwald. High-rate codes that are linear in space and time. *IEEE Transactions on Information Theory*, 48(7) :1804–1824, Jul 2002.
- [HH03] Babak Hassibi and Bertrand M Hochwald. How much training is needed in multiple-antenna wireless links? *Information Theory, IEEE Transactions on*, 49(4) :951–963, 2003.
- [HL05] Seung Hee Han and Jae Hong Lee. An overview of peak-to-average power ratio reduction techniques for multicarrier transmission. *IEEE Wireless Communications*, 12(2) :56–65, April 2005.
- [HLGHB01] Maryline Héliard, Rodolphe Le Gouable, Jean-Francois Héliard, and Jean-Yves Baudais. Multicarrier cdma techniques for future wideband wireless networks. *Annales des télécommunications*, 56(5-6) :260–274, 2001.
- [HTBD+13a] Jakob Hoydis, Stephan Ten Brink, Mérouane Debbah, et al. Massive mimo in the ul/dl of cellular networks : How many antennas do we need ? *IEEE Journal on selected Areas in Communications*, 31(2) :160–171, 2013.

- [HYW⁺12] Feng Han, Yu-Han Yang, Beibei Wang, Yongle Wu, and K.J.R. Liu. Time-reversal division multiple access over multi-path channels. *Communications, IEEE Transactions on*, 60(7) :1953–1965, July 2012.
- [IFS13] A. Ismail, J. Fiorina, and H. Sari. A new family of low-complexity stbcs for four transmit antennas. *IEEE Transactions on Wireless Communications*, 12(3) :1208–1219, March 2013.
- [INM89] N. Imai, T. Nojima, and T. Murase. Novel linearizer using balanced circulators and its application to multilevel digital radio systems. *IEEE Transactions on Microwave Theory and Techniques*, 37(8) :1237–1243, Aug 1989.
- [Ion03] D. M. Ionescu. On space-time code design. *IEEE Transactions on Wireless Communications*, 2(1) :20–28, Jan 2003.
- [IR13] ITU-R. Future spectrum requirements estimate for terrestrial IMT. Tech. Rep. ITU-R M.2290, International Telecommunications Union (ITU), December 2013.
- [Jaf01] H. Jafarkhani. A quasi-orthogonal space-time block code. *IEEE Transactions on Communications*, 49(1) :1–4, Jan 2001.
- [JAMV11] Jubin Jose, Alexei Ashikhmin, Thomas L Marzetta, and Sriram Vishwanath. Pilot contamination and precoding in multi-cell tdd systems. *Wireless Communications, IEEE Transactions on*, 10(8) :2640–2651, 2011.
- [JBS00] Michel C. Jeruchim, Philip Balaban, and K. Sam Shanmugan, editors. *Simulation of Communication Systems : Modeling, Methodology and Techniques*. Kluwer Academic Publishers, Norwell, MA, USA, 2nd edition, 2000.
- [JCS14] Jingon Joung, Yeow Khiang Chia, and Sumei Sun. Energy-efficient, large-scale distributed-antenna system (l-das) for multiple users. *Selected Topics in Signal Processing, IEEE Journal of*, 8(5) :954–965, Oct 2014.
- [JH05] H. Jafarkhani and N. Hassanpour. Super-quasi-orthogonal space-time trellis codes for four transmit antennas. *IEEE Transactions on Wireless Communications*, 4(1) :215–227, Jan 2005.
- [JKE08] S. Janaaththan, C. Kasparis, and B. G. Evans. A gradient based algorithm for papr reduction of ofdm using tone reservation technique. In *VTC Spring 2008 - IEEE Vehicular Technology Conference*, pages 2977–2980, May 2008.
- [JLL03] Jiho Jang, Kwang Bok Lee, and Yong-Hwan Lee. Transmit power and bit allocations for ofdm systems in a fading channel. In *Global Telecommunications Conference, 2003. GLOBECOM '03. IEEE*, volume 2, pages 858–862 Vol.2, Dec 2003.
- [JMZ⁺14] V. Jungnickel, K. Manolakis, W. Zirwas, B. Panzner, V. Braun, M. Lossow, M. Sternad, R. Apfelrojd, and T. Svensson. The role of small cells, coordinated multipoint, and massive mimo in 5g. *IEEE Communications Magazine*, 52(5) :44–51, May 2014.
- [JR13] F. Juretzek and U. Reimers. Point-to-multipoint-overlay (p2mp) for lte-advanced using dvb-t2 future extension frames. In *IEEE Broadcast Symposium (BTS)*, pages 1–10, 2013.
- [JWB94] A. E. Jones, T. A. Wilkinson, and S. K. Barton. Block coding scheme for reduction of peak to mean envelope power ratio of multicarrier transmission schemes. *Electronics Letters*, 30(25) :2098–2099, Dec 1994.
- [Kai02] S. Kaiser. Ofdm code-division multiplexing in fading channels. *Communications, IEEE Transactions on*, 50(8) :1266–1273, Aug 2002.
- [KBP⁺12] B. Koussa, S. Bachir, C. Perrine, C. Duvanaud, and R. Vauzelle. A comparison of several gradient based optimization algorithms for papr reduction in ofdm systems. In *CCCA12*, pages 1–6, Dec 2012.
- [KC06] J.S. Kenney and Jau-Horng Chen. Power Amplifier Linearization and Efficiency Improvement Techniques for Commercial and Military Applications. In *Microwaves, Radar Wireless Communications, 2006. MIKON 2006. International Conference on*, pages 3–8, May 2006.
- [KHNSL12] I. Kotzer, S. Har-Nevo, S. Sodin, and S. Litsyn. An Analytical Approach to the Calculation of EVM in Clipped Multi-Carrier Signals. *Communications, IEEE Transactions on*, 60(5) :1371–1380, May 2012.

Bibliographie

- [KJ03] B. S. Krongold and D. L. Jones. Par reduction in ofdm via active constellation extension. *IEEE Transactions on Broadcasting*, 49(3) :258–268, Sept 2003.
- [KK01] J. Kim and K. Konstantinou. Digital predistortion of wideband signals based on power amplifier model with memory. *Electronics Letters*, 37(23) :1417–1418, Nov 2001.
- [KPR12] F. Khan, Zhouyue Pi, and S. Rajagopal. Millimeter-wave mobile broadband with large scale spatial processing for 5g mobile communication. In *2012 50th Annual Allerton Conference on Communication, Control, and Computing (Allerton)*, pages 1517–1523, October 2012.
- [LAZ07] Jun Luo, J.H. Andrian, and Chi Zhou. Bit error rate analysis of jamming for ofdm systems. In *Wireless Telecommunications Symposium, 2007. WTS 2007*, pages 1–8, April 2007.
- [LC98] Xiaodong Li and L. J. Cimini. Effects of clipping and filtering on the performance of ofdm. *IEEE Communications Letters*, 2(5) :131–133, May 1998.
- [LC08] J. Liu and A. R. Calderbank. The icosian code and the e_8 lattice : A new $4, times, 4$ space-time code with nonvanishing determinant. *IEEE Transactions on Information Theory*, 54(8) :3782–3789, Aug 2008.
- [LdRT+04] G. Lerosey, J. de Rosny, A. Tourin, A. Derode, G. Montaldo, and M. Fink. Time reversal of electromagnetic waves. *Physical Review Letters*, 92 :193904, May 2004.
- [LdT+06] G. Lerosey, J. de Rosny, A. Tourin, A. Derode, and M. Fink. Time reversal of wideband micro-waves. *Applied Physics Letters*, 88(15), Apr. 2006.
- [LdTF07] G. Lerosey, J. de Rosny, A. Tourin, and M. Fink. Focusing Beyond the Diffraction Limit with Far-Field Time Reversal. *Science*, 315 :1120–, Feb. 2007.
- [LETM13] Erik G Larsson, Ove Edfors, Fredrik Tufvesson, and Thomas L Marzetta. Massive mimo for next generation wireless systems. *arXiv preprint arXiv :1304.6690*, 2013.
- [LH03] D.J. Love and R.W. Heath. Equal gain transmission in multiple-input multiple-output wireless systems. *Communications, IEEE Transactions on*, 51(7) :1102–1110, July 2003.
- [LLWZ14] Y. N. R. Li, J. Li, H. Wu, and W. Zhang. Energy efficient small cell operation under ultra dense cloud radio access networks. In *2014 IEEE Globecom Workshops (GC Wkshps)*, pages 1120–1125, Dec 2014.
- [Lo99] Titus KY Lo. Maximum ratio transmission. In *Communications, 1999. ICC'99. 1999 IEEE International Conference on*, volume 2, pages 1310–1314. IEEE, 1999.
- [LP08] Yves Louët and Jacques Palicot. A classification of methods for efficient power amplification of signals. *Annals of Telecommunications - annales des télécommunications*, 63(2008-08-07) :351–368, August 2008.
- [LV07] Y. Li and B. Vucetic. Design of differential space-time trellis codes. *IEEE Transactions on Wireless Communications*, 6(5) :1631–1637, May 2007.
- [Mar10a] Thomas L Marzetta. Noncooperative cellular wireless with unlimited numbers of base station antennas. *Wireless Communications, IEEE Transactions on*, 9(11) :3590–3600, 2010.
- [Med98] Jonas Medbo. Radio wave propagation characteristics at 5 ghz with modeling suggestions for hiperlan/2. *ETSI BRAN 3ERI074A*, 1998.
- [MGL+15] U. Meabe, X. Gil, C. Li, M. Velez, and P. Angueira. On the Coverage and Cost of HPHT Versus LPLT Networks for Rooftop, Portable, and Mobile Broadcast Services Delivery. *IEEE Transactions on Broadcasting*, 61(2) :133–141, June 2015.
- [MH97] S. H. Muller and J. B. Huber. Ofdm with reduced peak-to-average power ratio by optimum combination of partial transmit sequences. *Electronics Letters*, 33(5) :368–369, Feb 1997.
- [MMK+06] D. R. Morgan, Z. Ma, J. Kim, M. G. Zierdt, and J. Pastalan. A generalized memory polynomial model for digital predistortion of rf power amplifiers. *IEEE Transactions on Signal Processing*, 54(10) :3852–3860, Oct 2006.
- [MNP+10a] M. Mroué, A. Nafkha, J. Palicot, B. Gavalda, , and N. Dagonne. Performance and implementation evaluation of tr papr reduction methods for dvb-t2. *International Journal of Digital Multimedia Broadcasting*, 10 :1–10, August 2010.

- [MNP10b] M. Mroué, A. Nafkha, and J. Palicot. An innovative low complexity papr reduction tr-based technique for dvb-t2 system. In *International Congress on Ultra Modern Telecommunications and Control Systems*, pages 148–153, Oct 2010.
- [MPB11] P. Moss, T. Y. Poon, and J. Boyer. "a simple model of the uhfcross-polar terrestrial channel for dvb-ngh", white paper,. Technical report, BritishBroadcasting Corporation, 2011.
- [MWI+09] Christian Mehlführer, Martin Wrulich, Josep Colom Ikuno, Dagmar Bosanska, and Markus Rupp. Simulating the long term evolution physical layer. In *Proc. of the 17th European Signal Processing Conference (EUSIPCO 2009), Glasgow, Scotland*, volume 27, page 124, 2009.
- [NBEZ09] I.H. Naqvi, P. Besnier, and G. El Zein. Effects of time variant channel on a time reversal uwb system. In *IEEE Global Telecommunications Conference*, Dec. 2009.
- [NE08] V. K. Nguyen and J. S. Evans. Multiuser transmit beamforming via regularized channel inversion : A large system analysis. In *IEEE GLOBECOM 2008 - 2008 IEEE Global Telecommunications Conference*, pages 1–4, Nov 2008.
- [NG66] K. Narendra and P. Gallman. An iterative method for the identification of nonlinear systems using a hammerstein model. *IEEE Transactions on Automatic Control*, 11(3) :546–550, Jul 1966.
- [NKE07] Hung Tuan Nguyen, P. Kyritsi, and P.C.F. Eggers. Time reversal technique for multi-user wireless communication with single tap receiver. In *Mobile and Wireless Communications Summit, 2007. 16th IST*, pages 1 –5, july 2007.
- [NMDL13] Hien Quoc Ngo, Michail Matthaiou, Trung Q Duong, and Erik G Larsson. Uplink performance analysis of multicell mu-simo systems with zf receivers. *Vehicular Technology, IEEE Transactions on*, 62(9) :4471–4483, 2013.
- [NNB+13] T. Nakamura, S. Nagata, A Benjebbour, Y. Kishiyama, Tang Hai, Shen Xiaodong, Yang Ning, and Li Nan. Trends in small cell enhancements in LTE advanced. *IEEE Communications Magazine*, 51(2) :98–105, February 2013.
- [NR12] P. Neumann and U. Reimers. Live and time-shifted content delivery for dynamic broadcast : terminal aspects. *IEEE Transactions on Consumer Electronics*, 58(1) :53–59, February 2012.
- [NXP10] NXP. AN10945 174 MHz to 230 MHz DVB-T power amplifier with the BLF881. Technical report, NXP Semiconductors, 2010.
- [NZZK09] Hieu Nguyen, Zhao Zhao, Feng Zheng, and T. Kaiser. On the msi mitigation for mimo uwb time reversal systems. In *Ultra-Wideband, 2009. ICUWB 2009. IEEE International Conference on*, pages 295 –299, sept. 2009.
- [OHE+04] C. Oestges, J. Hansen, S. Emami, A. Kim, G. Papanicolaou, and A. Paulraj. Time reversal techniques for broadband wireless communication systems. *European Microwave Conference (Workshop)*, pages 49–66, Oct. 2004.
- [OI02b] H. Ochiai and H. Imai. Performance analysis of deliberately clipped ofdm signals. *IEEE Transactions on Communications*, 50(1) :89–101, Jan 2002.
- [OKPP05] C. Oestges, A.D. Kim, G. Papanicolaou, and A.J. Paulraj. Characterization of space-time focusing in time-reversed random fields. *Antennas and Propagation, IEEE Transactions on*, 53(1) :283 – 293, jan. 2005.
- [PFDB09] D. Panaitopol, J. Fiorina, and M.-G. Di Benedetto. Trade-off between the number of fingers in the prefilter and in the rake receiver in time reversal ir-uwb. In *IEEE International Conference on Ultra-Wideband*, pages 819 –823, Sept. 2009.
- [PKH+03] Jeongho Park, Changeon Kang, Daesik Hong, et al. Effect of partial band jamming on ofdm-based wlan in 802.11 g. In *Acoustics, Speech, and Signal Processing, 2003. Proceedings.(ICASSP'03). 2003 IEEE International Conference on*, volume 4, pages IV–560. IEEE, 2003.
- [Pop99] B.M. Popovic. Spreading sequences for multicarrier cdma systems. *Communications, IEEE Transactions on*, 47(6) :918–926, Jun 1999.
- [QNR11] J. Qi, P. Neumann, and U. Reimers. Dynamic broadcast. In *2011 14th ITG Conference on Electronic Media Technology*, pages 1–6, March 2011.

- [QR13] J. Qi and U. Reimers. A flexible signalling structure for content delivery in dynamic broadcast. In *2013 IEEE Third International Conference on Consumer Electronics \mathcal{I}^2 Berlin (ICCE-Berlin)*, pages 1–5, Sept 2013.
- [Rap91] C. Rapp. Effects of HPA-nonlinearity on a 4-DPSK/OFDM-signal for a digital sound broadcasting signal. In P. S. Weltevreden, editor, *ESA Special Publication*, volume 332 of *ESA Special Publication*, October 1991.
- [RECEH13a] A.A. Razzac, S.E. Elayoubi, T. Chahed, and B. El-Hassan. Comparison of LTE eMBMS and DVB-NGH mobile TV solutions from an energy consumption perspective. In *2013 IEEE 24th International Symposium on Personal, Indoor and Mobile Radio Communications (PIMRC Workshops)*, pages 16–20, September 2013.
- [RECEH13c] A.A. Razzac, S.E. Elayoubi, T. Chahed, and B. El Hassan. Planning of Mobile TV service in standalone and cooperative DVB-NGH and LTE networks. In *2013 11th International Symposium on Modeling Optimization in Mobile, Ad Hoc Wireless Networks (WiOpt)*, pages 609–614, 2013.
- [Rep14] ECC Report. Long term vision for the UHF broadcasting band. Technical report, Electronic Communications Comitee (ECC), 2014.
- [RHL⁺04] Heung-Gyoon Ryu, Tran Phuong Hoa, Kang Mi Lee, Sang-Woo Kim, and Jin-Soo Park. Improvement of power efficiency of HPA by the PAPR reduction and predistortion. *Consumer Electronics, IEEE Transactions on*, 50(1) :119–124, Feb 2004.
- [RIJ14] D. Rother, S. Ilsen, and F. Juretzek. A software defined radio based implementation of the tower overlay over lte-a+ system. In *2014 IEEE International Symposium on Broadband Multimedia Systems and Broadcasting*, pages 1–6, June 2014.
- [RL03] Heung-Gyoon Ryu and Yun-Hee Lee. A new combined method of the block coding and predistortion for the nonlinear distortion compensation. *Consumer Electronics, IEEE Transactions on*, 49(1) :27–31, Feb 2003.
- [RRE14] S. Rangan, T. S. Rappaport, and E. Erkip. Millimeter-wave cellular wireless networks : Potentials and challenges. *Proceedings of the IEEE*, 102(3) :366–385, March 2014.
- [SAHC14a] A. L. Swindlehurst, E. Ayanoglu, P. Heydari, and F. Capolino. Millimeter-wave massive mimo : the next wireless revolution ? *IEEE Communications Magazine*, 52(9) :56–62, September 2014.
- [Sal81] A. A. M. Saleh. Frequency-independent and frequency-dependent nonlinear models of twt amplifiers. *IEEE Transactions on Communications*, 29(11) :1715–1720, November 1981.
- [SC92] S. P. Stapleton and F. C. Costescu. An adaptive predistorter for a power amplifier based on adjacent channel emissions [mobile communications]. *IEEE Transactions on Vehicular Technology*, 41(1) :49–56, Feb 1992.
- [SEH⁺04] T. Strohmer, M. Emami, J. Hansen, G. Papanicolaou, and A.J. Paulraj. Application of time-reversal with mmse equalizer to uwb communications. In *IEEE Global Telecommunications Conference*, volume 5, pages 3123–3127, Dec. 2004.
- [SPCK04] R. Sperlich, Y. Park, G. Copeland, and J.S. Kenney. Power amplifier linearization with digital pre-distortion and crest factor reduction. In *Microwave Symposium Digest, 2004 IEEE MTT-S International*, volume 2, pages 669–672 Vol.2, June 2004.
- [SR09] K. P. Srinath and B. S. Rajan. Low ml-decoding complexity, large coding gain, full-rate, full-diversity stbcs for 2 times 2 and 4 times 2 mimo systems. *IEEE Journal of Selected Topics in Signal Processing*, 3(6) :916–927, Dec 2009.
- [SR13] K. P. Srinath and B. S. Rajan. Improved perfect space-time block codes. *IEEE Transactions on Information Theory*, 59(12) :7927–7935, Dec 2013.
- [SSH04] Quentin H Spencer, A Lee Swindlehurst, and Martin Haardt. Zero-forcing methods for down-link spatial multiplexing in multiuser mimo channels. *Signal Processing, IEEE Transactions on*, 52(2) :461–471, 2004.
- [SSS03] W. B. Sander, S. V. Schell, and B. L. Sander. Polar modulator for multi-mode cell phones. In *Custom Integrated Circuits Conference, 2003. Proceedings of the IEEE 2003*, pages 439–445, Sept 2003.

- [TBK⁺15] M. Taranetz, T. Blazek, T. Kropfreiter, M.K. Muller, S. Schwarz, and M. Rupp. Runtime Precoding : Enabling Multipoint Transmission in LTE-Advanced System-Level Simulations. *Access, IEEE*, 3 :725–736, June 2015.
- [TC98] J. Tellado and J. M. Cioffi. Efficient algorithms for reducing par in multicarrier systems. In *Proceedings. 1998 IEEE International Symposium on Information Theory (Cat. No.98CH36252)*, pages 191–, Aug 1998.
- [Tel99] Emre Telatar. Capacity of multi-antenna gaussian channels. *European transactions on telecommunications*, 10(6) :585–595, 1999.
- [TJC99] Vahid Tarokh, Hamid Jafarkhani, and A.R. Calderbank. Space-time block codes from orthogonal designs. *Information Theory, IEEE Transactions on*, 45(5) :1456–1467, Jul 1999.
- [TMoEE99] J. Tellado-Mourello and Stanford University. Dept. of Electrical Engineering. *Peak to Average Power Reduction for Multicarrier Modulation*. Stanford University, 1999.
- [TSC98] Vahid Tarokh, N. Seshadri, and A.R. Calderbank. Space-time codes for high data rate wireless communication : performance criterion and code construction. *Information Theory, IEEE Transactions on*, 44(2) :744–765, Mar 1998.
- [TvWA⁺16] M. Tercero, P. von Wrycza, A. Amah, J. Widmer, M. Fresia, V. Frascolla, J. Lorca, T. Svensson, M. H. Hamon, S. D. Roblot, A. Vijay, M. Peter, V. Sgardoni, M. Hunukumbure, J. Luo, and N. Vucic. 5g systems : The mmmagic project perspective on use cases and challenges between 6-100 ghz. In *2016 IEEE Wireless Communications and Networking Conference Workshops (WCNCW)*, pages 200–205, April 2016.
- [TZ06] Wojciech Tadej and Karol Życzkowski. A concise guide to complex hadamard matrices. *Open Systems & Information Dynamics*, 13(02) :133–177, 2006.
- [UK06] Peter Unger and Thomas Kürner. Radio network planning of dvh-h/umts hybrid mobile communication networks. *European Transactions on Telecommunications*, 17(2) :193–201, 2006.
- [UK09] Peter Unger and Thomas Kürner. Modeling and performance analyses of hybrid cellular and broadcasting networks. *International Journal of Digital Multimedia Broadcasting*, 2009, Article ID 329073, 9 pages, 2009.
- [V1.01] ETSI TR 101 290 V1.2.1. Digital video broadcasting (dvb); measurement guidelines for dvb systems. Technical report, ETSI, 2001.
- [v1.12a] ETSI TS 102 831 v1.2.1. Implementation guidelines for a second generation digital terrestrial television broadcasting system (dvb-t2). Technical report, Digital Video Broadcasting, 2012.
- [VRM01] J. H. K. Vuolevi, T. Rahkonen, and J. P. A. Manninen. Measurement technique for characterizing memory effects in RF power amplifiers. *IEEE Transactions on Microwave Theory and Techniques*, 49(8) :1383–1389, Aug 2001.
- [Was04] Hugo Durney Wasaff. *Adaptive Pre-Distortion for Nonlinear High Power Amplifiers in OFDM Systems*. PhD thesis, Universitat Politècnica de Catalunya, 2004.
- [WC09a] Y. Wang and J. Coon. Full rate orthogonal space-time block coding in ofdm transmission using time reversal. In *IEEE Wireless Communications and Networking Conference*, Apr. 2009.
- [WCDS12a] S. Wagner, R. Couillet, M. Debbah, and D. T. M. Slock. Large system analysis of linear precoding in correlated miso broadcast channels under limited feedback. *IEEE Transactions on Information Theory*, 58(7) :4509–4537, July 2012.
- [WCL14] Kongtao Wang, Zhiyong Chen, and Hui Liu. Push-based wireless converged networks for massive multimedia content delivery. *Wireless Communications, IEEE Transactions on*, 13(5) :2894–2905, May 2014.
- [WFGV98] P.W. Wolniansky, G.J. Foschini, G.D. Golden, and R. Valenzuela. V-blast : an architecture for realizing very high data rates over the rich-scattering wireless channel. In *Signals, Systems, and Electronics, 1998. ISSSE 98. 1998 URSI International Symposium on*, pages 295–300, Sep 1998.
- [WWGY10] J. Wang, X. Wang, Y. Guo, and X. You. A channel adaptive power allocation scheme based on slnr precoding for multiuser mimo systems. In *2010 IEEE 72nd Vehicular Technology Conference - Fall*, pages 1–4, Sept 2010.

Bibliographie

- [WWH⁺11] Beibei Wang, Yongle Wu, Feng Han, Yu-Han Yang, and KJ Ray Liu. Green wireless communications : a time-reversal paradigm. *Selected Areas in Communications, IEEE Journal on*, 29(8) :1698–1710, 2011.
- [WYZD13] Desheng Wang, Yifan Yang, Guangxi Zhu, and Xiaojiang Du. Distributed precoder design for inter-cell interference suppressing in multi-cell mu-mimo systems. In *2013 IEEE Wireless Communications and Networking Conference (WCNC)*, pages 1398–1403, April 2013.
- [XMH⁺17] Ming Xiao, Shahid Mumtaz, Yongming Huang, Linglong Dai, Yonghui Li, Michail Matthaiou, George K. Karagiannidis, Emil Björnson, Kai Yang, Chih Lin, and Amitava Ghosh. Millimeter wave communications for future mobile networks. *CoRR*, abs/1705.06072, 2017.
- [YM13b] Hong Yang and Thomas L Marzetta. Performance of conjugate and zero-forcing beamforming in large-scale antenna systems. *IEEE Journal on Selected Areas in Communications*, 31(2) :172–179, 2013.
- [ZDPC13] Wence Zhang, Bo Du, Cunhua Pan, and Ming Chen. Downlink sinr distribution in multiuser large scale antenna systems with conjugate beamforming. In *Global Communications Conference (GLOBECOM), 2013 IEEE*, pages 4163–4168. IEEE, 2013.
- [ZG02] Shengli Zhou and Georgios B Giannakis. Optimal transmitter eigen-beamforming and space-time block coding based on channel mean feedback. *Signal Processing, IEEE Transactions on*, 50(10) :2599–2613, 2002.
- [ZHG08] L. Zhao, J. Huber, and W. Gerstacker. Design and analysis of bit interleaved coded space-time modulation. *IEEE Transactions on Communications*, 56(6) :904–914, June 2008.
- [ZPLL06] S. Zabre, J. Palicot, Y. Louet, and C. Lereau. Socp approach for ofdm peak-to-average power ratio reduction in the signal adding context. In *2006 IEEE International Symposium on Signal Processing and Information Technology*, pages 834–839, Aug 2006.
- [ZZZ13] Long Zhao, Hui Zhao, and Kan Zheng. Energy efficient power allocation strategy for downlink MU-MIMO with massive antennas. *The Journal of China Universities of Posts and Telecommunications*, 20(3) :1–7, June 2013.

Partie

Annexes

Selected Article

S. Sindian, M. Crussière, J.F. H elard, A.E. Samhat et A. Khalil, "Admission Control and Resource Allocation Strategies for 802.15.5", EURASIP Journal on Wireless Communications and Networking, Springer, novembre 2014, DOI :10.1186/1687-1499-2014-197.

Abstract

In this paper, a novel two-tier mechanism for the access control and resource allocation of a two-hop high data rate IEEE 802.15.5 network is proposed. One of the main contributions in this proposal is the use of a dynamic superframe size in the IEEE 802.15.5. Additionally, the ideas of using a superframe utilization threshold and a channel time allocation period (CTAP) utilization threshold are incorporated, with the aim of allowing more devices to access the shared superframe. Using these thresholds, two new hop-1 resource allocation algorithms are described ; CTAP utilization threshold-based resource allocation algorithm (CTRA) and superframe utilization threshold-based resource allocation algorithm (STRA). These algorithms control the access of the hop-1 Mesh PicoNet Coordinators (MPNCs) and Mesh DEVICES (MDEVs) to the channel time resources in the superframe. Furthermore, an algorithm for the distribution of the hop-1 MPNCs' resources among the real-time (RT) and non-real-time (NRT) MDEVs at hop-2 is introduced. In this mechanism, a new flag metric is applied to provide higher priorities to MPNCs over MDEVs in the hop-1 algorithms and to the RT MDEVs over the NRT MDEVs in the hop-2 algorithm. Simulation results show the superiority of the proposed mechanism over others by providing a higher satisfaction factor and higher fairness among the competing devices at both hop-1 and hop-2 of the IEEE 802.15.5.

Keywords : IEEE 802.15.5, High data rate WPAN, Resource allocation, Fairness, Dynamic superframe

Admission control and resource allocation strategies for IEEE 802.15.5

Samar Sindian^{1,2*}, Matthieu Crussière¹, Jean-François Hélar¹, Abed Ellatif Samhat³ and Ayman Khalil^{1,2}

Abstract

In this paper, a novel two-tier mechanism for the access control and resource allocation of a two-hop high data rate IEEE 802.15.5 network is proposed. One of the main contributions in this proposal is the use of a dynamic superframe size in the IEEE 802.15.5. Additionally, the ideas of using a superframe utilization threshold and a channel time allocation period (CTAP) utilization threshold are incorporated, with the aim of allowing more devices to access the shared superframe. Using these thresholds, two new hop-1 resource allocation algorithms are described; CTAP utilization threshold-based resource allocation algorithm (CTRA) and superframe utilization threshold-based resource allocation algorithm (STRA). These algorithms control the access of the hop-1 Mesh PicoNet Coordinators (MPNCs) and Mesh Devices (MDEVs) to the channel time resources in the superframe. Furthermore, an algorithm for the distribution of the hop-1 MPNCs' resources among the real-time (RT) and non-real-time (NRT) MDEVs at hop-2 is introduced. In this mechanism, a new flag metric is applied to provide higher priorities to MPNCs over MDEVs in the hop-1 algorithms and to the RT MDEVs over the NRT MDEVs in the hop-2 algorithm. Simulation results show the superiority of the proposed mechanism over others by providing a higher satisfaction factor and higher fairness among the competing devices at both hop-1 and hop-2 of the IEEE 802.15.5.

Keywords: IEEE 802.15.5; High data rate WPAN; Resource allocation; Fairness; Dynamic superframe

1. Introduction

A new high data rate (HR) wireless personal area network (WPAN) standard has been developed by IEEE 802.15.3 task group (TG) [1]. The IEEE 802.15.3 standard is designed to provide low complexity, low cost, low power consumption, and high data rate wireless connectivity among portable consumer electronics and communication devices. HR WPAN is expected to play a crucial role in the formation of home area networks and is targeted to support high-end multimedia applications with high throughput requirements. However, HR WPAN has a limited operating range with a single-hop communication between devices. In order to extend this range and enable multi-hop communications, the mesh networking approach is utilized. A HR WPAN mesh network can be formed by interconnecting simultaneously operating piconets (SOPs). Hence, various problems may arise including inter-piconet interferences, beacon collisions,

throughput limitations, channel resource reservation collisions, etc. Different works [2-6] investigate the resource allocation mechanisms and propose solutions to overcome these limitations while trying to extend the coverage area of an IEEE 802.15.3-based WPAN. A detailed description of these works is presented in [7].

However, drawbacks in terms of system coverage and device connectivity are still evident despite the solutions presented in the works stated above. Consequently, and in order to extend the single-hop range of HR WPANs to multiple hops, the IEEE 802.15.5 standard was developed in 2009 to define the necessary specifications for HR WPANs operation in a mesh configuration [8]. The IEEE 802.15.5 [9] network is dynamically self-organized and self-configured, i.e., the nodes in the network automatically establish and maintain mesh connectivity among themselves. IEEE 802.15.5 provides the architectural framework enabling WPAN devices to promote interoperable, stable, and scalable wireless mesh topologies and, if needed, to provide the amendment text to the current WPAN standards that is required to implement this recommended practice [10].

* Correspondence: sindian_s@hotmail.com

¹INSA de Rennes, IETR, UMR 6164, F-35708 Rennes, France

²CCE Department, Faculty of Engineering, IUL, 30014 Khaldeh, Lebanon

Full list of author information is available at the end of the article



In the case of IEEE 802.15.5, multiple WPAN clusters compete for channel time in a shared superframe. Therefore, it is essential to determine the channel time requirements of each cluster with a certain number of devices and to determine how these clusters can compete to the shared channel time.

The work in [11] presents a distributed resource allocation scheme for meshed WPANs based on a utility function. In this paper, a novel centralized scheme for resource allocation in a two-hop IEEE 802.15.5 based on the centralized approach described in [12] is proposed. One of the main contributions in this proposal is the introduction of the notion of dynamic superframe size to the IEEE 802.15.5. This consequently leads to a much more efficient use of the superframe as it will be shown later by results. Additionally, the channel time requests (CTRqs) of both the hop-1 Mesh DEVICES (MDEVs) and Mesh PicoNet Coordinators (MPNCs) are taken into consideration. The latter are assigned higher priority and larger channel time allocations (CTAs) providing them with sufficient channel time resources for serving their clusters. The notion of utilization thresholds, which enables the allocation of variable CTA sizes for prompting fairness, is also introduced. Consequently, more devices are granted access to channel time resources but with smaller sizes. In this context, two types of utilization thresholds are proposed in order to be applied in two different hop-1 algorithms. Additionally, a mechanism for distributing the hop-1 MPNC resources among their hop-2 devices is proposed. Moreover, service differentiation is applied by providing higher priority and larger CTA allocations for RT over NRT traffic requests at hop-2. This proposal shows higher satisfaction and fairness by the introduction of a priority flag metric and by taking the devices' rejected requests into account.

The rest of this paper is organized as follows. Section II briefly describes the works related to resource allocation in IEEE 802.15.5. Section III introduces the IEEE 802.15.5 WPAN architecture. In Section IV, the standard resource allocation mechanism is described. In Section V, the new notions to be incorporated into the proposed mechanism are presented. This is followed by the presentation of the different IEEE 802.15.5 hop-1 and hop-2 resource allocation mechanisms in Section VI. In Section VII, the simulation results of the different mechanisms are presented. Finally, Section VIII concludes the paper.

2. Related work

Under the IEEE 802.15.5 umbrella, few research works [11,12] investigating the resource allocation mechanisms for the hop-1 of HR IEEE 802.15.5 have been conducted. But to the readers' knowledge, no work has already studied a resource allocation and admission control

mechanism at the IEEE 802.15.5 hop-2. Additionally, no work has introduced the notion of service differentiation among the real-time (RT) and non-real-time (NRT) devices in IEEE 802.15.5.

In [11], a distributed algorithm which calculates a fair share in the superframe for each requesting MPNC is proposed. It considers a cooperative approach in which the utility for each ref-MPNC is maximized in a way that the other requesting MPNCs benefit as well. However, the algorithm is based on the individual requests for each flow by the MPNC. The distributed allocation, although having some merits, has some drawbacks. In [9] and [11], as the number of devices increases in each cluster and also in the presence of a dense meshed WPAN with a high number of MPNCs, the probability of channel time request conflict increases. Additionally, due to the lack of an appropriate mechanism to determine a fair share for each MPNC, unfairness is likely in the reservations by the MPNCs in the mentioned distributed mechanisms.

The most relevant work for resource allocation in meshed WPANs is given in [12], where the resource allocation is done on a centralized basis for a two-hop neighborhood. In the centralized approach, one MPNC among each neighborhood of MPNCs which share a common beacon period (BP) in the superframe is selected as the reference MPNC (ref-MPNC) for the other MPNCs to synchronize their time slots with. In the centralized approach, the ref-MPNC keeps track of the time reservations in the superframe up to two hops and therefore assuring that there are no conflicts in channel time reservation. Another feature of the approach in [12] is that the channel time is reserved in bulk by the MPNCs rather than a request by request basis to reduce the amount of control overhead. The idea behind bulk reservation is to join a group of channel time requests in one large request, thus reducing the possibility of CTA conflicts in case of higher device density. The approach in [12] studies the satisfaction and fairness among the MPNCs at hop-1 of the IEEE 802.15.5. In spite of the advantages of this centralized approach over the distributed one, it does not take into consideration the channel time requirements of neither the hop-1 MDEVs in the ref-MPNC cluster nor the hop-2 MDEVs in the hop-1 MPNCs clusters. Moreover, it considers the fixed maximum superframe size (65,535 μ s) according to the IEEE 802.15.3 [1] which could be inefficiently utilized in case of low-loaded networks. Additionally, each MPNC estimates its channel requirements based on a history of previous flows. Therefore, inefficient superframe utilization can occur because of incorrect channel time estimation for a bulk reservation by each MPNC due to either overestimation or underestimation of the channel time requirement of a cluster.

3. Mesh WPAN based on the IEEE 802.15.5 standard

The recommendations for operation in a mesh configuration for WPANs are given in the IEEE 802.15.5 standard [9]. This standard has two parts in which one part defines necessary specifications for low data rate (LR) WPANs [13] and the other part for HR WPANs. The mesh-related functions and services reside over the IEEE 802.15.3 MAC sublayer as shown in Figure 1. Providing multi-hop services necessitates a slight amendment of the underlying MAC sublayer in the reference model.

The LR WPAN provides data rate of about 0.25 Mbps, which is not convenient to support high rate or real-time multimedia traffic. The work in [14] presents a new synchronization approach 'High-Performance Synchronization Algorithm for wireless mesh sensor networks (HIPESYN)', which is adapted to the LR IEEE 802.15.5 standard for synchronous communications. However, because of the low data rate provided by the LR WPAN, our work focuses on the HR WPAN which provides a high data transmission of 55 Mbps that is suitable for supporting RT applications.

3.1 IEEE 802.15.5 architecture

The IEEE 802.15.5 Recommended Practice is a member of the WPAN standard family. It is developed based on IEEE 802.15.3-2003/2005 MAC/PHY layer specifications [10]. The architectural framework of the HR WPAN mesh is to allow multiple MPNCs and MDEVs to participate in communications across multiple piconets. The communication between MDEVs and MPNCs of different piconets is called inter-PAN communication while communication between devices in the same piconet is called intra-PAN communication (Figure 2). Additionally, since all the MPNCs could be connected to each other using the mesh topology, there is no single point of failure in the mesh network. Moreover, IEEE 802.15.5 enables the MAC to handle multiple connections at a given time using different channels.

3.2 IEEE 802.15.5 superframe

A MPNC manages the synchronization and controls the data traffic of the system. In a meshed WPAN, communications between MPNCs and within their piconets take place in a shared superframe. The superframe can

be used for transmission of beacons from MPNCs and data communication. It is composed of three main parts (Figure 3):

- The beacon period: the beacon (Figure 4) is transmitted periodically by a MPNC to provide information about neighbor reservations and provide timing information that aids in synchronization. This helps in avoiding beacon reservation conflicts.
- The channel access period (CAP) is carrier sense multiple access with collision avoidance (CSMA/CA) based and it can be used for sending association requests and other commands. The CAP is shared among the MPNCs.
- The channel time allocation period (CTAP) is time division multiple access (TDMA) based. It is divided into equal length medium access slots (MASs) used to address medium reservations between MPNCs. A MAS is composed of CTAs that are used by devices to exchange data connections. The smallest channel time unit is referred to as time unit (TU). A TU is a unit of time of the CTA with a resolution of 1 μ s to make the allocation of time easier for the MPNC.

4. IEEE 802.15.5 standard resource allocation mechanism

Before allocating the channel time resources, a device calculates the necessary number of TUs per superframe. The device then indicates the minimum and the desired number of TUs it requires through a CTRq command (Figure 5) to the MPNC. The MPNC after getting the CTRq from the device checks the available capacity of the superframe, and if suitable, it sends a channel time response command (CTRp) (Figure 6). Using the CTRp, a MPNC indicates to the requesting device the available number of TUs and also notifies the neighbor MPNCs of the new reservation.

The IEEE 802.15.5 standard in [9] identifies that the MPNCs which are in a single-hop transmission range of each other need to synchronize their boundaries to a common ref-MPNC to avoid time slot overlaps due to synchronization issues. The procedure given in [9] for time reservation by a MPNC for intra-PAN flows is

Mesh Sublayer	IEEE 802.15.5 – WPAN Mesh									
MAC/PHY layers	Low Rate WPAN							High Rate WPAN		
	15.4b	15.4a	15.4c	15.4d	15.4e	15.4f	15.4g	15.3	15.3b	15.3c

Figure 1 IEEE 802.15.5 layers.

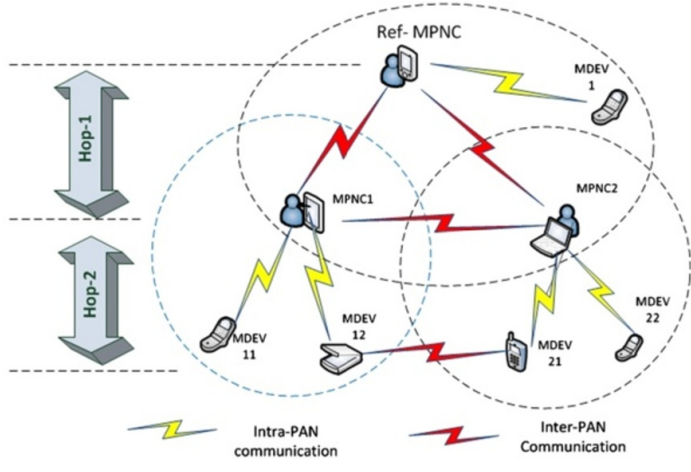


Figure 2 Two-hop IEEE 802.15.5 mesh configuration.

different from inter-PAN flows. But in both cases, if the MPNC reserves channel time in the superframe, it indicates the time reserved via a CTA status information element (IE) and then via a CTA IE in its beacon frame (Figure 4). The other MPNCs, upon checking these IEs, check if the reserved time conflicts with any of the time slots already reserved by them. In case there is a conflict, the other MPNCs can raise an objection IE in their beacon and the MPNC which reserved the time can shift the reserved time slots to another location on the superframe and then wait for an objection again. If there is no objection raised, the MPNC finalizes the reserved time. Since this mechanism is distributed, thus as the number of devices increases in each piconet of a dense meshed WPAN with a higher number of MPNCs, the probability of channel time request conflict increases. Furthermore, the distributed superframe sharing can cause fairness issues because there is no mechanism to determine the requirement of each MPNC and monitor a fair allocation to each MPNC. These are the main drawbacks of the resource allocation mechanism of the IEEE 802.15.5 standard.

5. IEEE 802.15.5 proposed admission control schemes

If a MPNC allocates the channel time to a device based on the available time in the superframe only, then most of the devices might not get a fair share of the superframe. While allocating the channel time, the MPNC should ensure an approach such that the maximum number of devices in the piconet gets a fair share of the superframe time based on their requirements.

With the novel proposed admission control approach, a centralized two-tier mechanism for coordinating the resource allocation algorithms of both the hop-1 (between the ref-MPNC and its member hop-1 MDEVs/MPNCs) and hop-2 (between the hop-1 MPNCs and their member hop-2 RT/NRT MDEVs) of the IEEE 802.15.5 is carried out. With this scheme, the ref-MPNC is used for allocating the channel time to each requesting device at hop-1. Some of the introduced notions are used by both hop-1 and hop-2 access mechanisms, namely, bulk channel time requests and flag metric notions. Other notions are introduced only to the hop-1 resource allocation mechanism, namely dynamic superframe

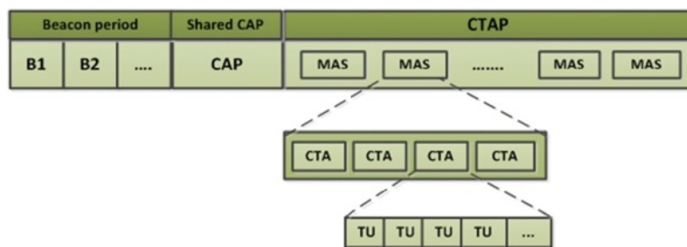


Figure 3 Superframe sharing in IEEE 802.15.5.

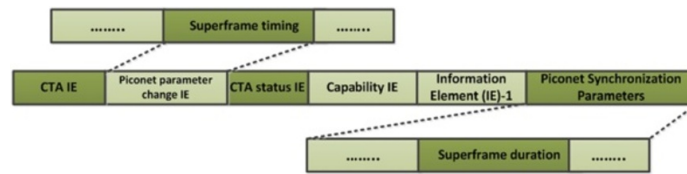


Figure 4 Beacon frame.

and utilization threshold notions. Under the utilization thresholds, two different thresholds are proposed to be used in the resource allocation mechanisms at hop-1, the superframe utilization threshold and the CTAP threshold.

5.1 Dynamic superframe size

With this proposal, the notion of dynamic superframe size starting with a minimum value as identified in [1] is introduced. The increase in the superframe size is restricted by the maximum size of the superframe. There exist two different policies that could be used to manage CTAs according to devices' needs. The first is to start off with a maximum superframe length and try to manage the growing number of CTRq commands by proper allocation of CTAs. The second method is to have an initial small superframe length and adjust its length any time it is necessary. The superframe duration can be extracted from the 'superframe duration field' in the 'piconet synchronization parameters' (see Figure 4) that are broadcasted in the beacon.

The size of the superframe is managed by the ref-MPNC which, based on the novel proposal, recomputes the new superframe size after each CTA request decision. In case of an accepted CTRq, the new allocated channel time size is added to the superframe size and this new size is broadcasted to the devices in the 'superframe timing' field in the piconet parameter change IE (Figure 4) in the beacon. In such cases, the waiting time to start a new superframe is avoided if the maximum superframe size is not reached. Thus, the QoS requirements for real-time traffic in IEEE 802.15.5 can be much satisfied by minimizing the delay between two consecutive CTAs of the same device. Additionally, the superframe capacity is efficiently utilized especially when the network is not overloaded. Consequently, only a portion of the superframe size is used (instead of using its maximum size), thus avoiding the wastage of the superframe capacity.

5.2 Bulk channel time requests model

The notion of bulk CTRq (BCTRq) sent by the MPNCs to the ref-MPNC at hop-1 is also considered. In the proposed mechanism, the BCTRqs sent by a MPNC to the ref-MPNC are based on the aggregate of the received CTRqs from its members' MDEVs at hop-2. As highlighted in Figure 5, the MPNCs send BCTRq for requesting CTAs from the ref-MPNC by identifying the 'minimum number of TUs' and the 'desired number of TUs' fields. After receiving the requests, the ref-MPNC can decide to accept or deny the request according to the proposed algorithms, and it notifies the requesting device by sending a CTRp (see Figure 6). The ref-MPNC decision to allocate channel time is based on prioritizing the MPNCs over the MDEVs by granting the MPNCs more TUs.

5.3 Flag metric notion

In addition to the use of utilization thresholds, fairness and different priorities are also induced in the proposed mechanism by the use of a priority flag metric (*Flag*). The ref-MPNC keeps a global record of flag metrics for its members' MDEVs and MPNCs at hop-1. Each hop-1 MPNC also keeps a record of *Flag* for its member RT and NRT MDEVs at hop-2. Each device is identified at the ref-MPNC by a device identifier (*Dev_id*) as defined in [9]. Each raised *Flag* (i.e., its value is greater than zero) refers to a rejected CTRq or BCTRq. The flag metrics list is kept along all the superframe durations. If a device's request is rejected, its flag metric is incremented by one. Otherwise, this metric is decremented, provided that its value is greater than zero (to avoid having a negative flag metric). The flag metrics list is utilized by the ref-MPNC at the CAP of the next superframe to generate a priority list P that includes the flag metrics sorted in a descending order. Then, the ref-MPNC uses P to sort the *Dev_id* list accordingly, i.e., *Dev_id* of the device having first metric in P is set at the head of the new *Dev_id* list. At the CAP of the next superframe, the

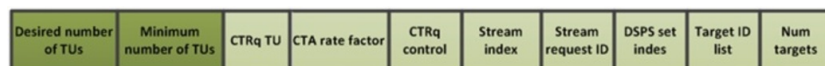


Figure 5 Channel time request block field format.



Figure 6 Channel time response command format.

devices' requests are served according to this new *Dev_id* list. Moreover, the initial flag metrics assigned to the hop-1 MPNCs and hop-2 RT MDEVs are higher than that of hop-1 MDEVs and hop-2 NRT MDEVs, respectively.

5.4 Utilization thresholds

In order to attract more devices, the network must be able to offer a comparatively satisfactory service to the devices to reduce the loss of devices. However, because of a limited superframe capacity, some devices' requests are rejected in order to satisfy other devices' requirements. Obviously, it is not fair to guarantee the requesting devices' QoS by rejecting more devices. Consequently, a compromise between the devices satisfaction and the requests' rejection rate is applied by the use of utilization thresholds at the hop-1 resource allocation mechanism. These thresholds are the CTAP utilization threshold and the superframe utilization threshold.

5.4.1 CTAP utilization threshold

In the proposed mechanism, the CTAP threshold ($CTAP_{TL}$) is introduced to split the CTAP into two sub-CTAPs, MPNC-CTAP, and MDEV-CTAP. The sizes of these two sub-CTAPs are referred to as $CTAP_{MPNC_size}$ and $CTAP_{MDEV_size}$, respectively. These sizes are adjusted according to Φ as:

$$CTAP_{MPNC_size} = \Phi \times size_{max}, \text{ where } (0 < \Phi < 1) \tag{1}$$

and

$$CTAP_{MDEV_size} = (1-\Phi) \times size_{max} \tag{2}$$

where $size_{max}$ is the maximum size of the superframe. For providing higher priority for the MPNCs over the MDEVs, a larger CTAP portion is reserved for the

MPNCs, i.e., $CTAP_{MPNC_size} > CTAP_{MDEV_size}$, by adjusting the value of Φ to be greater than $(1 - \Phi)$.

Then, a MPNC threshold ($MPNC_{TL}$) is introduced in the CTAP_MPNC and is used by the ref-MPNC to adjust the size of the channel time resources to be granted for the requesting MPNCs. Similarly, a MDEV threshold ($MDEV_{TL}$) is introduced in the CTAP_MDEV which, in its turn, is used by the ref-MPNC to adjust the size of the channel time resources to be granted for the requesting MDEVs (Figure 7). These thresholds are defined as follows:

$$MPNC_{TL} = \beta_1 \times CTAP_{MPNC_size}, \text{ where } (0 < \beta_1 < 1) \tag{3}$$

$$MDEV_{TL} = \beta_2 \times CTAP_{MDEV_size}, \text{ where } (0 < \beta_2 < 1) \tag{4}$$

where the values of these thresholds are adjusted according to β_1 and β_2 , respectively. As long as the total allocated channel size in the CTAP_MPNC and CTAP_MDEV is below the $MPNC_{TL}$ and the $MDEV_{TL}$, respectively; the channel times are granted in a way such that the requesting devices are highly satisfied, i.e., the granted channel times are approximately equal to the requested channel times. Otherwise, the ref-MPNC applies a control procedure that minimizes the size of the granted resources in order to allow more devices to get channel access. This is in condition that the granted resources remain greater than or equal to the minimum requested channel times.

5.4.2 Superframe utilization threshold

The proposed mechanism applies a common superframe utilization threshold (T_L) for the hop-1 devices (MPNCs and MDEVs) in another hop-1 resource allocation

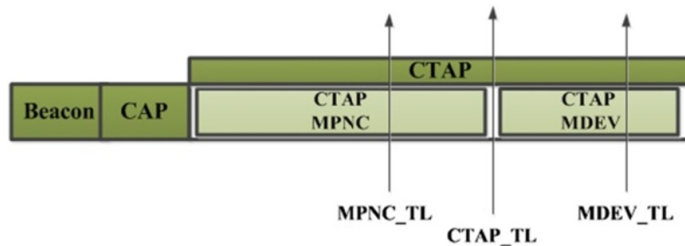


Figure 7 CTAP utilization thresholds.

algorithm. Then, the prioritization of the MPNCs over MDEVs is applied within this algorithm. The use of T_L is such that whenever the total CTAP allocated channel time size is below T_L , the requesting devices are highly satisfied. Then when the total allocated superframe size exceeds this threshold, the ref-MPNC reduces the granted resource size to allow more devices to get channel access. Nevertheless, it is guaranteed that the granted channels are still greater than or equal to the minimum requested resources by a device. The threshold T_L is defined as:

$$T_L = \text{size}_{\max} - 2 \times \alpha \times \text{TU} \times N \quad (5)$$

where TU is the duration of a time unit in microseconds, N is the total number of devices and α is a factor through which different values of T_L can be obtained as illustrated in Figure 8. All the other parameters for calculating T_L are considered to be constant in a certain scenario. The reason of the choice of $(2 \times \text{TU} \times N)$ is to ensure that two TUs, as minimum, are available for each of the associated devices to be capable of communicating with the ref-MPNC (one TU for uplink stream and another for downlink stream).

6. IEEE 802.15.5 proposed resource allocation mechanisms

The block diagram shown in Figure 9 represents the proposed two-hop IEEE 802.15.5 mechanism which can be decomposed into five stages. It is a two-tier mechanism of hop-1 resource allocation algorithms for the MDEVs and MPNCs and a hop-2 resource allocation algorithm for the RT and NRT MDEVs. For the hop-1, two different algorithms are proposed at stage (3) and the hop-2 algorithm takes place at stage (5). It is important to mention that the implementation of the hop-2 algorithm is related to the validity of the condition that the hop-1 device is a MPNC with granted channel time resources as shown in Figure 9. In the sequel, each block is described in details. These algorithms can be defined as follows:

Hop-1 algorithms: control the admission and resource allocation between the ref-MPNC and its member MDEVs/MPNCs belonging to the parent piconet. Individual CTRqs are sent from MDEVs to ref-MPNC

and BCTRqs are sent from MPNCs to ref-MPNC. For the hop-1 mechanism, two algorithms are proposed: the first one is the CTAP utilization threshold-based resource allocation algorithm (CTRA) and the second one is the superframe utilization threshold-based resource allocation algorithm (STRA).

Hop-2 algorithm: controls the admission and resource allocation between the hop-1 MPNCs and their member RT/NRT MDEVs. The concerned MPNC applies the hop-2 algorithm which is a service differentiation-based resource allocation algorithm (SDRA) to distribute the CTAs among the RT and NRT MDEVs.

6.1 Hop-1 resource allocation algorithms

According to the novel proposal, we have two hop-1 resource allocation algorithms, CTRA and STRA. Each of these algorithms can be divided into several stages. These stages are common between both of these algorithms except for the 'hop-1 channel time calculations' stage which is particular for each of these two algorithms. These stages, identified in Figure 9, are described as follows and are detailed accordingly in the form of block diagrams from Figures 10, 11, 12, 13, 14, 15, and 16:

Stage (1) - Initialization and hop-1 Priority list creation: The flow chart corresponding to this stage is described in Figure 10. At the initial stage, the minimum and maximum superframe sizes (size_{\min} and size_{\max}) are set. The ref-MPNC initializes the devices ID list (Dev_id1) of its hop-1 MPNCs and MDEVs. In each superframe S , the *Flag* metric list is generated with initial values for each device. Higher flag metrics are assigned to the MPNCs to give them higher priority than MDEVs. Prior to its channel time requests decision, a ref-MPNC creates a priority list ($P1$) from the *Flag* metric list sorted in a descending order. The Dev_id1 list is then sorted according to $P1$. The abbreviations' descriptions of all the flowcharts are presented in Table 1.

Stage (2) - Receiving channel time requests: The flowchart of this stage is shown in Figure 11. Whenever the ref-MPNC receives a CTRq/BCTRq, it serves it according to the sorted Dev_id1 list. Since the MPNCs are assigned higher flag metrics at the initialization

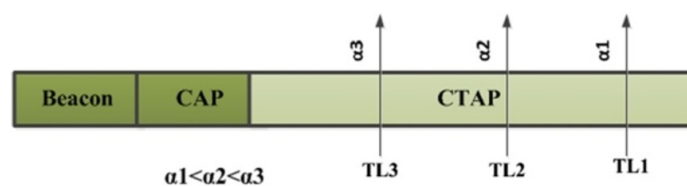
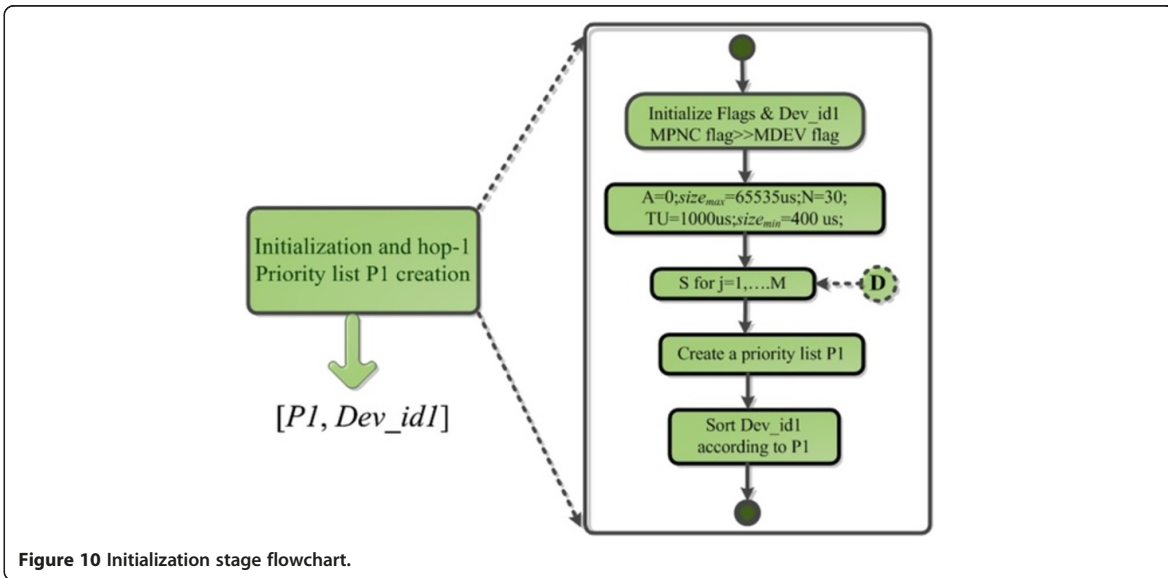
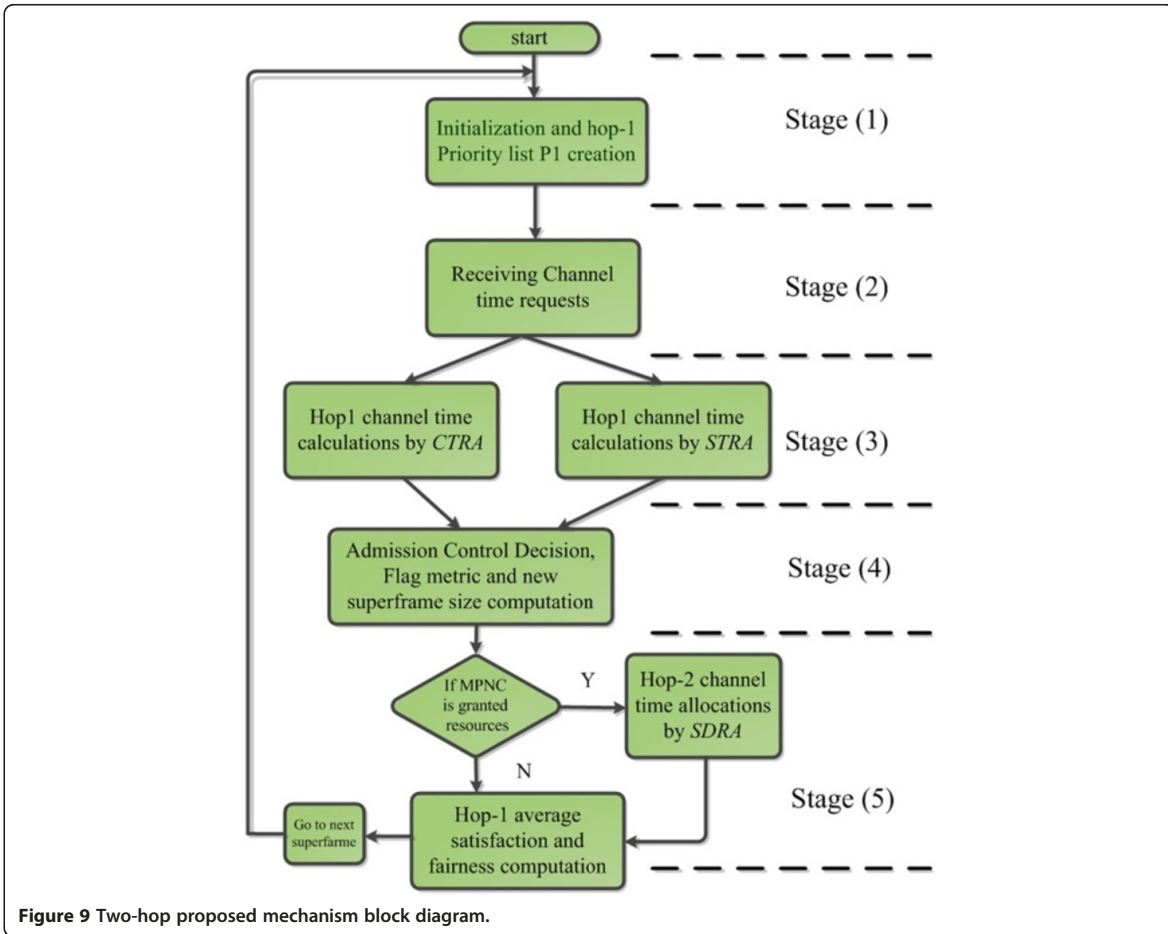


Figure 8 Superframe utilization threshold for different α .



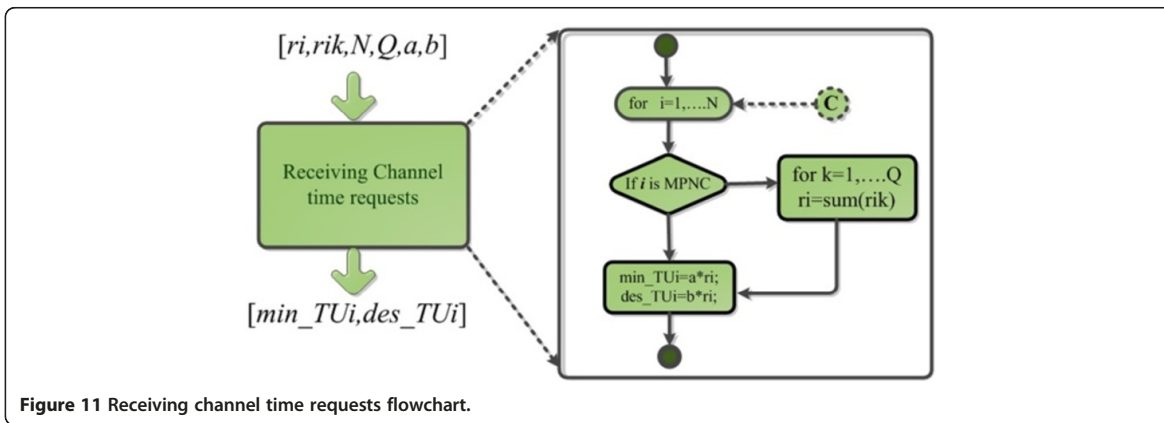


Figure 11 Receiving channel time requests flowchart.

stage, then they occupy the first positions of the Dev_id1 list. The values of the minimum number of TUs (min_TU_i) and the desired number of TUs (des_TU_i) of each device i are equal to a fraction of its requested channel time resources (r_i), i.e., $(a.r_i)$ and $(b.r_i)$, respectively, where a and b values are less than 1. Stage (3) - Hop-1 channel time calculations: In this stage, the behavior of the two hop-1 algorithms is differentiated as follows:

6.1.1 CTAP utilization threshold-based resource allocation algorithm

Firstly, the ref-MPNC checks if the request received is sent by a MPNC or a MDEV (see Figure 12). Consequently, it checks the $MPNC_TL$ or $MDEV_TL$, and it then grants the channel times accordingly. Additionally, the ref-MPNC has to grant channel times for the MPNCs from the $CTAP_MPNC$ portion in the shared superframe according to the $MPNC_TL$. As long as the total allocated $CTAP_MPNC$ channel time (A_{mpnc}) does not exceed $MPNC_TL$, the ref-MPNC grants up to the des_TU_i for a BCTRq. Otherwise, it indicates to the

attached devices in the capability IE in the beacon (Figure 4) about the new capacity constraints and it reduces the size of the granted channel times to the average of the min_TU_i and des_TU_i for the requesting MPNC.

Similarly for the MDEV CTRqs, when the total allocated $CTAP_MDEV$ channel time (A_{mdev}) is below $MDEV_TL$, the MDEVs are granted up to the average of the min_TU_i and des_TU_i . When the total MDEVs' allocated resources exceed $MDEV_TL$, the ref-MPNC indicates to the attached devices in the capability IE about the new capacity constraints. From now on, the ref-MPNC accepts requests with new constraints by granting up to the min_TU_i for the requesting MDEVs. In the proposed algorithms, the calculated channel times are referred to as rqi , then if these resources are granted successfully we refer to them as g_i .

6.1.2 Superframe utilization threshold-based resource allocation algorithm

The algorithm flowchart of the proposed mechanism is shown in Figure 13. The ref-MPNC grants up to the des_TU_i for a BCTRq, while it grants up to the average

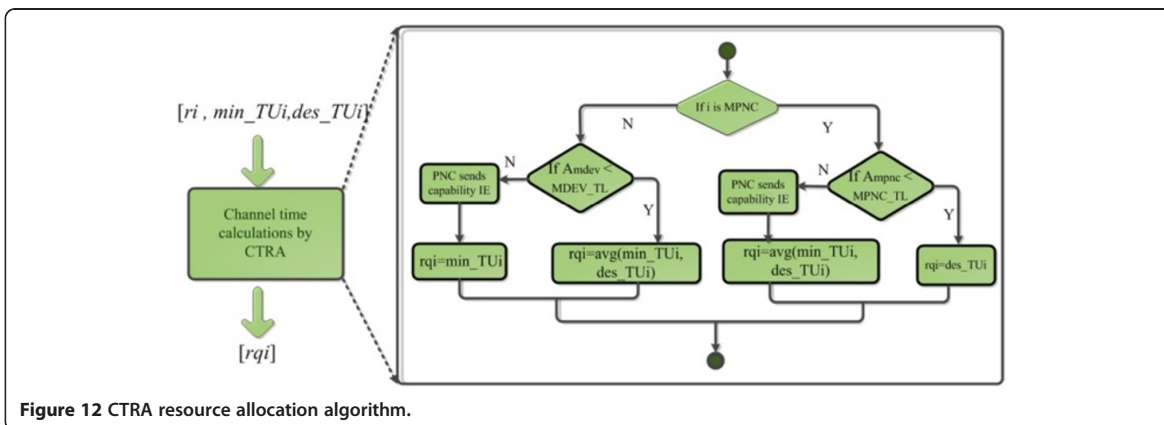


Figure 12 CTAP resource allocation algorithm.

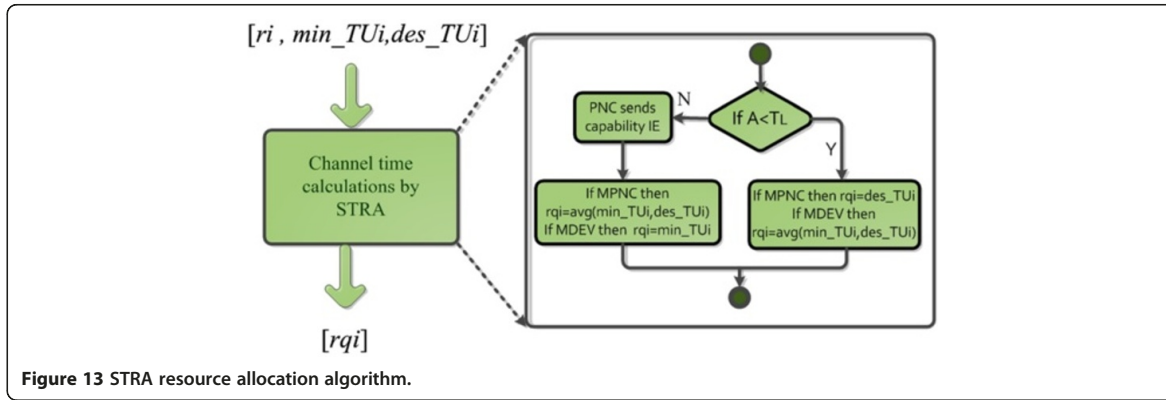


Figure 13 STRA resource allocation algorithm.

of the min_TU_i and des_TU_i for a CTRq. This is applied as long as the total allocated channel time (A) is below a certain superframe utilization threshold T_L . When the allocated resources exceed T_L , the ref-MPNC indicates to the attached devices in the capability IE (in the beacon) about the new capacity constraints the ref-MPNC is capable of handling. Later on, the ref-MPNC accepts requests with new constraints, it grants up to the average of the min_TU_i and des_TU_i for MPNCs and up to the min_TU_i for the MDEVs.

Stage (4) - Admission control decision: the flowchart of this stage is shown in Figure 14. For both hop-1 algorithms, the conditions applied on the size of channel time to be granted (rqi) are applied as long as the summation of (A) and (rqi) does not exceed the superframe maximum capacity ($size_{max}$); otherwise, the requests are rejected. In the case where a BCTRq/CTRq is rejected, the *Flag* metric of the concerned MPNC/MDEV is incremented and a negative CTRp is sent by the ref-MPNC. Otherwise, a positive CTRp is received by the device with the granted channel time resources (g_i) and its *Flag* metric is decremented by one. In both CTRA

and STRA, a satisfaction factor of each device ($satfi$) is calculated as defined in Equation 7. The new granted resources amount (g_i) is added to the total allocated resources (A) during a superframe. The new superframe size (S_z) is then calculated by the addition of (A) to $size_{min}$ as follows:

$$S_z = size_{min} + A \tag{6}$$

The satisfaction factor of a device i is defined to be equal to the ratio of granted TUs (g_i) divided by the desired TUs (des_TU_i) requested by a device i as:

$$satfi = \frac{g_i}{des_TU_i} \tag{7}$$

Stage (5) - Average satisfaction and fairness computation: Before moving to the next superframe ($j + 1$), the hop-2 resource allocation algorithm is applied to the hop-2 members only if the hop-1 member is a MPNC and it has been granted channel time resources, i.e., $g_i > 0$ (Figure 15). Then the algorithm returns back to the point number (C) identified in Figure 11 to repeat stages (2) and

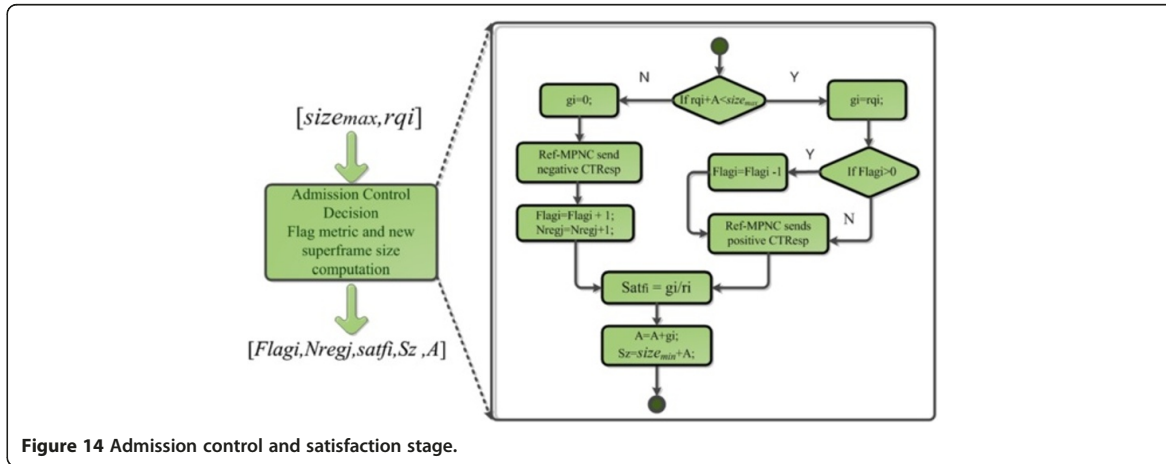


Figure 14 Admission control and satisfaction stage.

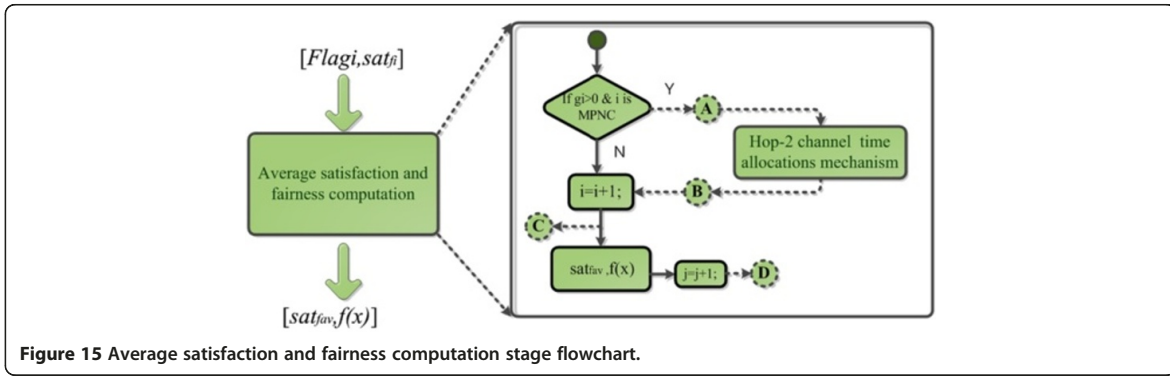


Figure 15 Average satisfaction and fairness computation stage flowchart.

(3) for all the other hop-1 devices until i reaches N . Next, it calculates the average satisfaction factor of all the devices after calculating the device satisfaction factor at stage (3). The average satisfaction factor is defined as:

$$sat_{f_{av}} = \frac{\sum_i sat_{f_i}}{n} \quad (8)$$

where n represents the number of devices (MPNCs or MDEVs). Using only $sat_{f_{av}}$ value is not enough to determine the fairness of the proposed resource allocation mechanism. It is highly desirable to find a method and, preferably, an index to measure and compare the degree of fairness of a particular allocation policy [15]. Many general purpose fairness indexes (Gini, Jain's Fairness,

min-max) have been frequently used to measure fairness of different resource allocation schemes [16,17]. We apply the Jain's Fairness index on the satisfaction factor which is in function of granted resources and requested resources as defined in Equation 7. The Jain's Fairness index is defined as follows:

$$f(x) = \frac{(\sum_i sat_{f_i})^2}{N \sum_i sat_{f_i}^2} \quad \forall i = 1, 2, ..N \quad (9)$$

where $f(x = sat_f)$ is the Jain's Fairness index and N is the total number of devices. The fairness index value is a positive number with max value 1 indicating a 100% fair system.

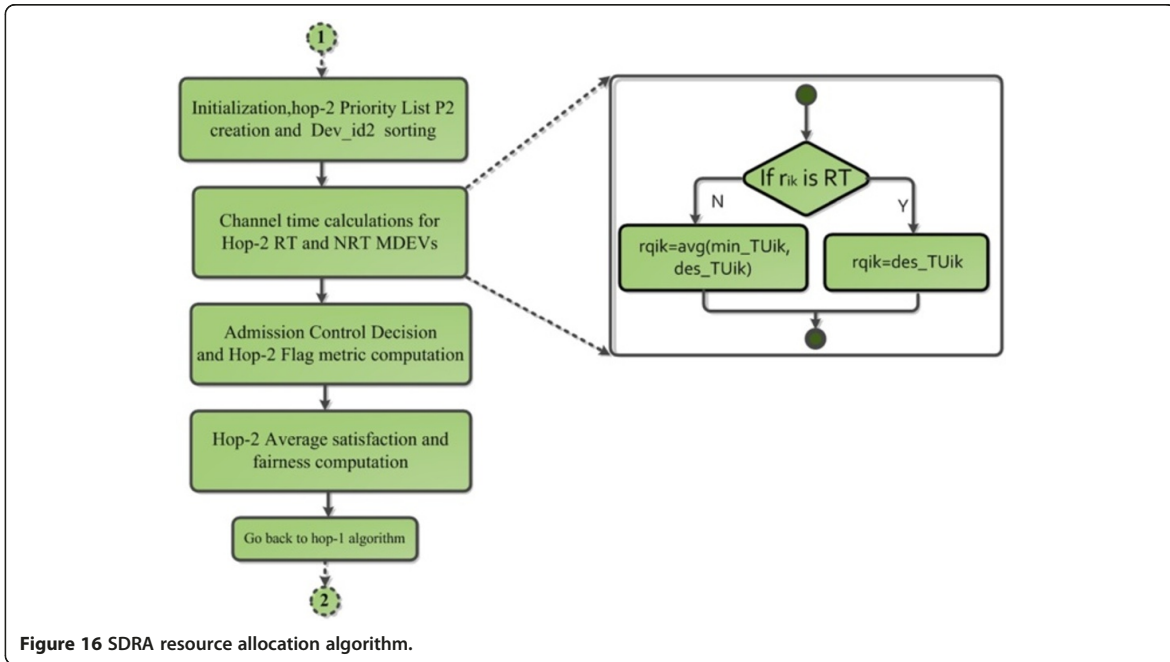


Figure 16 SDRA resource allocation algorithm.

Table 1 Flowcharts abbreviations

Abbreviation	Description
Dev_id1, Dev_id2	Array of device ID for the devices at hops 1 and 2, respectively
P1, P2	Priority lists at hops 1 and 2, respectively
A	Total allocated channel time of the superframe
A _{mpnc} , A _{mdev}	Total allocated channel time by hop-1 MPNCs and MDEVs, respectively
S	Number of superframes
S _z , size _{max} , size _{min}	Current, maximum and minimum sizes of superframe (μs)
r _i , r _{ik}	Requested channel time by a device at hops 1 and 2, respectively
rq _i , rq _{ik}	Size of channel time size to be granted to a device if available at hops 1 and 2, respectively
g _i	Granted channel time to device according to different algorithms
N, Q	Number of devices at hops 1 and 2, respectively
MPNC_T _L , MDEV_T _L	MPNC and MDEV CTAP utilization threshold, respectively
N _{regj}	Number of rejected requests in a superframe j
TU	Duration of a time unit (μs)
min_TU _i , des_TU _i	Minimum and desired number of TUs requested by a device i
a, b	Ratio of min_TU and des_TU, respectively, with respect to request
sat _i , sat _{av}	Calculated satisfaction factor for a device i and average satisfaction for n devices
f(x)	Jain's Fairness index

After that, the algorithm proceeds to the next superframe by returning back to point (D) identified in Figure 10.

6.2 Hop-2 service differentiation-based resource allocation algorithm

The most relevant work for resource allocation for hop-1 WPANs mesh is given in [12] as previously mentioned. In addition to the already identified drawbacks, the work in [12] does not present a mechanism for distributing the MPNCs' resources among their piconets' member MDEVs. In this scheme, a hop-2 centralized service differentiation-based resource allocation algorithm (SDRA) in IEEE 802.15.5 is proposed using the approaches that are applied by the hop-1 algorithms. Whatever the applied hop-1 algorithm (CTRA or STRA) is, the hop-2 algorithm (SDRA) does not change. This algorithm is proposed for fairly sharing the hop-1 MPNC resources among its hop-2 RT and NRT MDEVs. Additionally, this algorithm prioritizes RT over NRT MDEVs and grants them larger CTA allocations. SDRA, which is started at the point number (A) in Figure 15, can be divided into the same stages

described for the hop-1 algorithms as illustrated in Figure 16 but with the following differences:

- 1) In SDRA, all the stages described for the hop-1 algorithms are performed by the hop-1 MPNC instead of the ref-MPNC.
- 2) At the initialization stage, initial higher priority is given to the RT MDEVs over the NRT MDEVs by assigning the former higher *Flag* metrics than the latter.
- 3) Different rules are applied at the 'channel time calculations' stage where a MPNC *i* has to distribute the channel time among its MDEVs according to their requested resources with service differentiation. The MPNC checks if the CTRq of a device *k* is for RT or NRT MDEV. Accordingly, it then sets the size of resources to be granted for an RT CTRq (*rq_{ik}*) to *des_TU_{ik}*, and to the average of *min_TU_{ik}* and *des_TU_{ik}* for an NRT CTRq.
- 4) At the admission control stage, the sum of the total allocated resources is compared with the time granted to a MPNC *i* (*g_{impnc}*) instead of the maximum superframe size.
- 5) After computing the average satisfaction factor and fairness for the hop-2 RT and NRT MDEVs at the 'average satisfaction and fairness computation' stage, the algorithm returns back to the applied hop-1 algorithm at point (B) identified in Figure 15. It is necessary to highlight the point that the QoS requirements (for example delay) for the RT CTRqs are included in the demanded *des_TU*, thus in the calculated RT satisfaction factor.

In the proposed scenarios, when applying the CTRA as the hop-1 algorithm with SDRA at hop-2, the two-hop mechanism is referred to as CTAP utilization threshold-service differentiation-based mechanism (CTSD). Similarly, when applying the STRA as the hop-1 algorithm with SDRA at hop-2, the two-hop mechanism is referred to as superframe utilization threshold-service differentiation-based mechanism (STSD).

7. Simulations and results

The proposed algorithms aim to identify the number of TUs to be allocated to each device as described above. To study the performance of these algorithms and without loss of generality, a two-hop meshed scenario with a ref-MPNC having 20 MDEVs and 10 MPNCs as hop-1 members is considered. Then each MPNC embeds 2 RT and 3 NRT MDEVs as its piconet members as illustrated in Figure 17. Therefore, we have a total of 30 devices at hop-1 and 50 devices at hop-2 distributed among 10 hop-2 piconets. This can be considered as a large number of

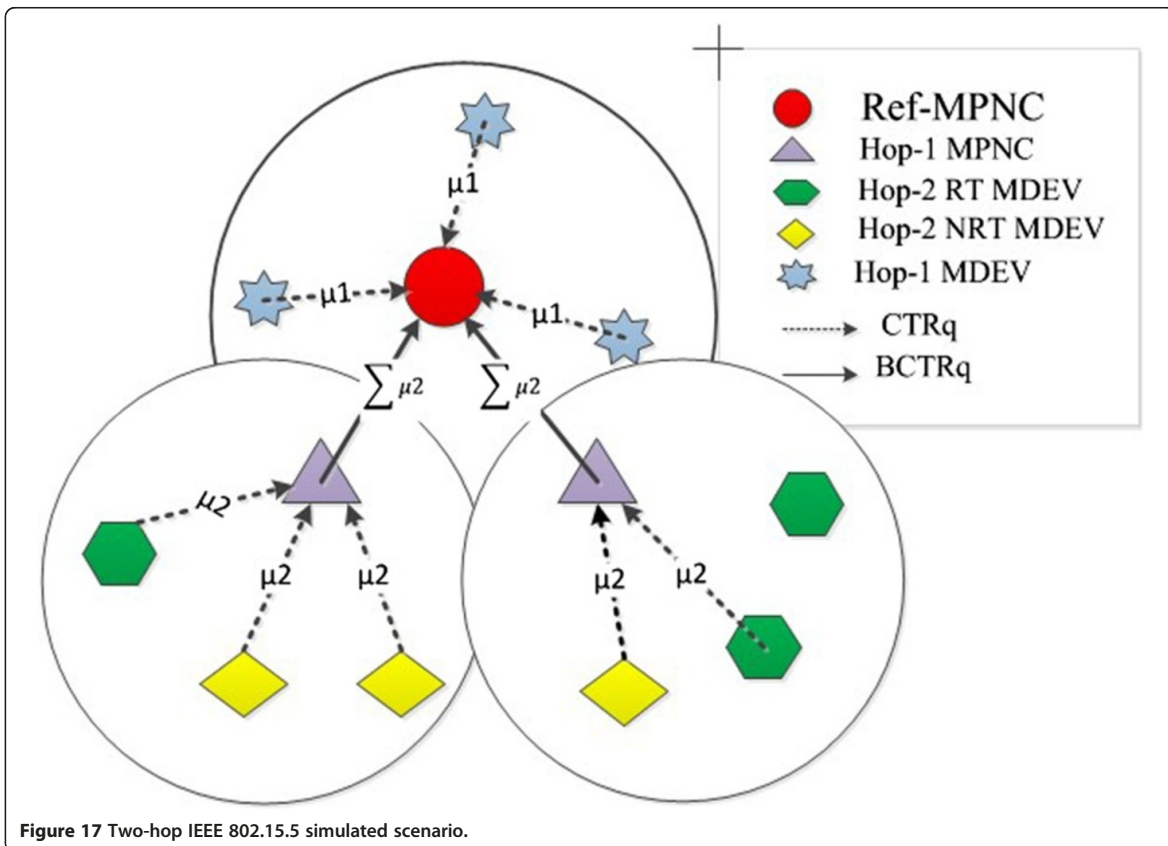


Figure 17 Two-hop IEEE 802.15.5 simulated scenario.

devices in a two-hop WPAN whose piconets do not exceed a 10-m coverage range.

The requests sent by the hop-2 MDEVs to their MPNCs are considered to follow an exponential distribution with mean equals to (μ_2) microseconds. The (μ_2) refers to the mean of the individual requests sent by the hop-2 MDEVs to their hop-1 MPNCs. Then, the aggregate of these requests ($\Sigma\mu_2$) is sent by the hop-1 MPNCs to the ref-MPNC (Figure 17). Additionally, the hop-1 MDEVs send individual requests to the ref-MPNC, which follow an exponential distribution with mean equals to (μ_1) μs . One request per each device is sent during a CAP. Several MATLAB simulations were run by using the parameters' values that are summarized in Table 2, while taking different values of the means (μ_1) and (μ_2) as specified in the sequel. The satisfaction factor, the average requests' rejection rate, the average superframe utilization and the fairness index variations are studied.

Figure 18 shows a comparison of the superframe utilization for different loads (μ_1) when using the dynamic superframe size proposal or fixing the superframe size to its maximum value. It is shown that in case of

the proposed mechanism, the superframe is efficiently utilized (100%) since its size increases regarding the network load. However, in case of the fixed superframe size, where the maximum size is always used, the superframe is inefficiently utilized in cases of low- and medium-loaded networks. This consequently imposes more delay between two CTAs for a certain device in two subsequent superframes especially for real-time application devices.

Table 2 Simulation parameters

Parameter	Value
TU duration	1,000 μs
min_TU	0.4r
des_TU	0.9r
Number of MPNCs at hop 1	10
Number of MDEVs at hop 1	20
Number of RT MDEVs at hop 2 per 1 MPNC	2
Number of NRT MDEVs at hop 2 per 1 MPNC	3
Φ, β_1, β_2	0.6, 0.7, 0.7
Number of superframes S	10^5

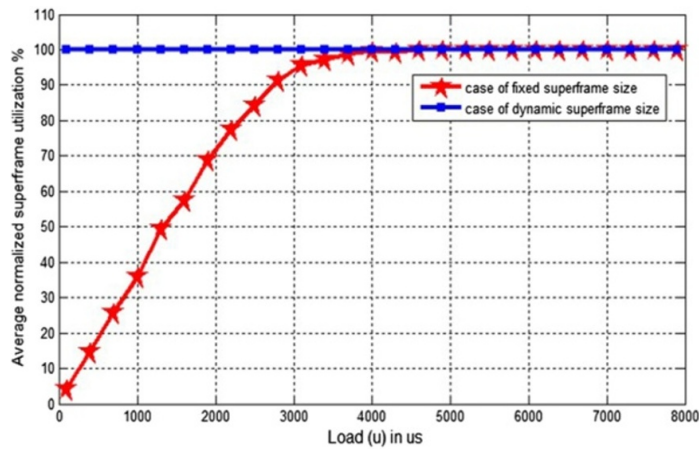


Figure 18 Comparison of average superframe utilization between dynamic and fixed superframe size approaches for different μ_1 .

Figure 19 and Figure 20 show the average satisfaction factor of MPNCs/MDEVs and RT/NRT MDEVs, respectively, when applying each of the hop-1 algorithms (CTRA and STRA) in combination with SDRA at hop-2, thus leading to the already defined CTSD and STSD approaches. Therefore, the results presented in the sequel show the performance of the whole two-hop simulated scenario for each of the hop-1 and hop-2. The simulation time is equal to 10^5 superframe durations, and constant values of μ_1 and μ_2 for both hops are considered. It is shown that the MPNCs satisfaction (Figure 19) and

the RT MDEVs satisfaction (Figure 20) are very high, and reach 0.9 when applying STSD. This refers to the maximum satisfaction since the des_TU is set to $(0.9r)$. Consequently, if the des_TU has been set to r , the satisfaction would have reached 1.

When applying STSD, the CTAP is shared among the MPNCs and the MDEVs with one common threshold T_L . Additionally, the MPNCs are assigned higher priorities than the MDEVs, thus the MPNCs dominate the shared CTAP channel times and reserve their required resources at hop-1. Then, the remaining CTAP channel

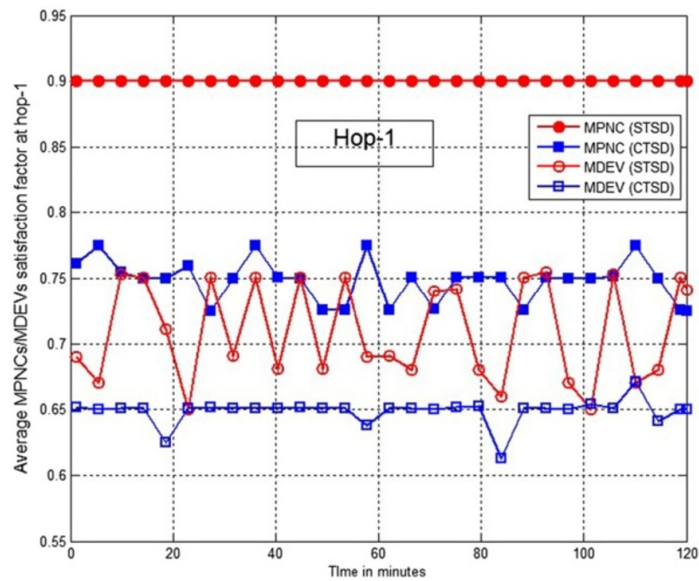


Figure 19 Average MPNCs/MDEVs satisfaction factor at hop-1 for fixed μ_1 and μ_2 .

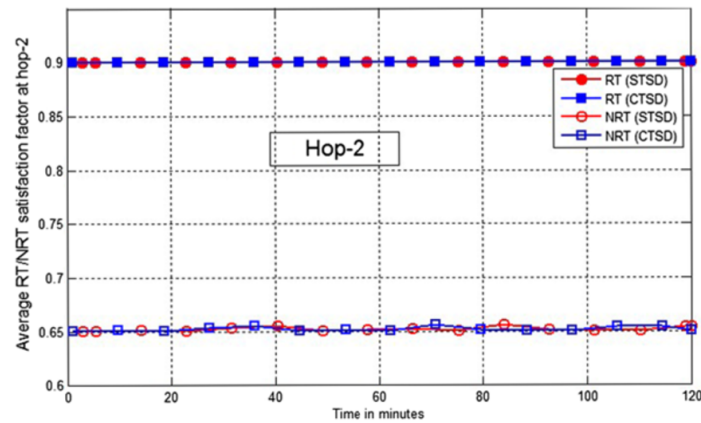


Figure 20 Average RT/NRT MDEVs satisfaction factor at hop-2 for fixed μ_1 and μ_2 .

times are distributed among the MDEVs according to their *Flag* metrics. This explains the much higher MPNCs satisfaction factor compared to the MDEVs satisfaction as illustrated in Figure 19. On the other hand, each of the MPNCs and MDEVs is reserved a CTAP portion when applying CTSD, thus the MPNCs do not grip the MDEVs' channel times. This explains the smaller difference between MPNCs and MDEVs satisfaction in comparison with that using STSD. However, the MPNCs CTAP portion and the MPNCs priorities are higher than those of MDEVs, thus the MPNCs satisfaction is greater than that of MDEVs.

Nevertheless, the same satisfaction factor is achieved by the RT and NRT MDEVs at hop-2 using either STSD or CTSD (see Figure 20) for fixed load. This is because the hop-2 algorithm grants the resources to the hop-2 devices in the same manner regardless of the applied hop-1 algorithm. Moreover, the hop-2 algorithm is applied only in case the hop-1 MPNC is granted its requested resources which are the sum of its hop-2 MDEVs requests; therefore, these MDEVs are granted all their requested resources. Additionally, since RT MDEVs are assigned higher priorities, their satisfaction factor is much greater than that of the NRT MDEVs. Finally, compared to the results obtained by applying CTSD, STSD provides much better results for MPNCs and MDEVs at hop-1 but the RT and NRT satisfaction at hop-2 remains the same regardless of the applied hop-1 algorithm.

In the following simulations, the impact of varying the load of both hops on the satisfaction factor, the rejection rate and the Jain's Fairness index, is studied. We take different hop-1 load values (μ_1) ranging from low-, medium-, to high-loaded networks, and three values of load μ_2 (200, 1,000, and 2,000 μs) that refer to low-, medium-, and high-loaded hop-2 networks, respectively.

Figure 21 and Figure 22 show the variations of the average satisfaction factor of MPNCs and MDEVs when the load at hop-1 increases. Various curves are given for both STSD and CTSD algorithms and for different loads at hop-2. It can be shown that for both algorithms, the MPNCs satisfaction is always higher than that of MDEVs. It is also shown that applying the STSD provides higher satisfaction for both MPNCs and MDEVs for different loaded hop-1 and hop-2 networks. Figure 21 also shows that the MPNCs satisfaction is maintained at 0.9 when applying STSD, whereas it decreases with the increase of the load at both hops when applying CTSD. This is because the CTAP channel times are shared among the MPNCs and MDEVs when applying STSD. Since higher priority is given to the MPNCs, then they usually get all their requested channel times. While for the MDEVs, their satisfaction decreases as the load on both hops decreases as shown in Figure 22. However, in the case of applying CTSD, the CTAP is divided into two parts, one is reserved for the MPNCs and the other for the MDEVs. So even though the MPNCs are provided with higher priority than the MDEVs, they cannot use the resources reserved for the MDEVs. Thus, as the load increases, the same behavior is shown for both MPNCs and MDEVs where the possibility of rejecting or granting smaller channel times than the requested by MPNCs or MDEVs increases. This explains the decrease in the MPNCs and MDEVs satisfaction and the increase in the rejection rate as the load increases as shown in Figure 23. However, the MPNCs satisfaction is still much higher than that of the MDEVs because the MPNCs reserved CTAP portion is larger than that of MDEVs.

Comparing the RT and NRT results at hop-2, it can be shown in Figure 24 and Figure 25 that the RT satisfaction is higher than that of the NRT. In addition, it is

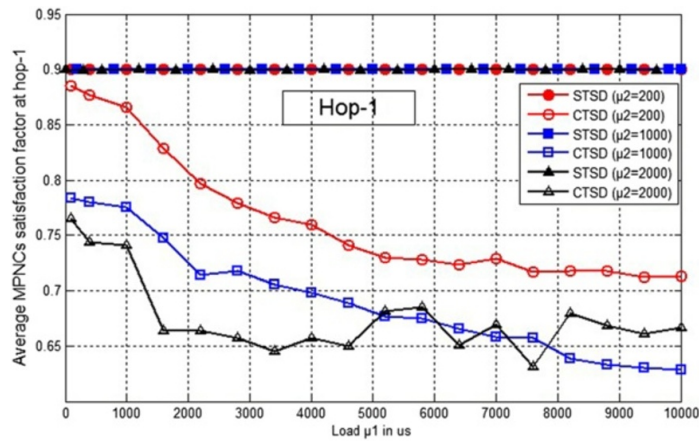


Figure 21 MPNC satisfaction at hop-1 for different μ_1 and $\mu_2 = 200, 1,000, 2,000 \mu s$.

noticed that the RT satisfaction remains the same regardless of the applied hop-1 algorithm and for different loads at both hops. This is because the RT requests are provided with higher priority than the NRT requests, so they get their requested channel times (this is why satisfaction is 0.9) and larger CTA sizes. It is also shown in Figure 25 that applying STSD at hop-1 gives better satisfaction for the NRT than applying the CTSD because the NRT satisfaction depends on the size of available hop-1 MPNC channel resources. Since STSD provides larger CTA allocations for the MPNCs than the CTSD, then the capacity of the hop-1 MPNCs is larger when applying the STSD, which finally translates into better results at hop-2.

In Figure 26, it is shown that the average rejected request rate is negligible at hop-2 when applying any of

the hop-1 algorithms for different loaded networks. This is because the hop-2 algorithm is implemented only if the hop-1 MPNC is granted its requested channel times. This guarantees that the hop-2 devices are approximately granted their desired channel time size. However, a minor request rejection rate is noticed at high-loaded hop-2 networks ($\mu_2 = 2,000 \mu s$) when applying CTSD since the latter achieves the lowest MPNC satisfaction factor (i.e., the granted resource size) for $\mu_2 = 2,000 \mu s$ as already shown in Figure 21.

For the Jain's Fairness index shown in Figure 27 and Figure 28, it is obvious that both algorithms provide an approximate of 100% fairness for hop-2 devices for different hop-1 loaded networks and for both algorithms (Figure 28). This is because of the same reason explained in the previous paragraph which states that the hop-2

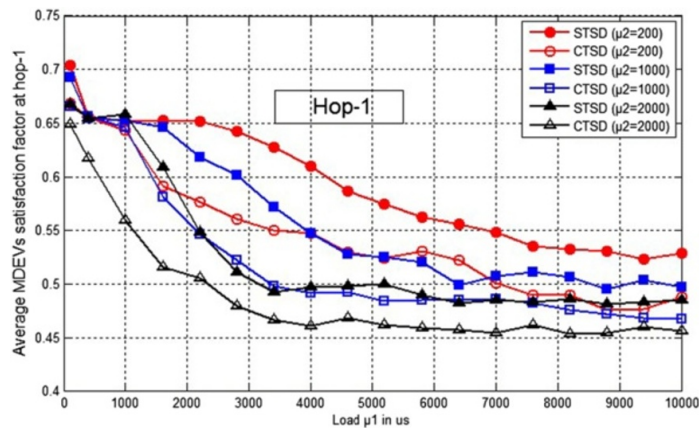


Figure 22 MDEV satisfaction at hop-1 for different μ_1 and $\mu_2 = 200, 1,000, 2,000 \mu s$.

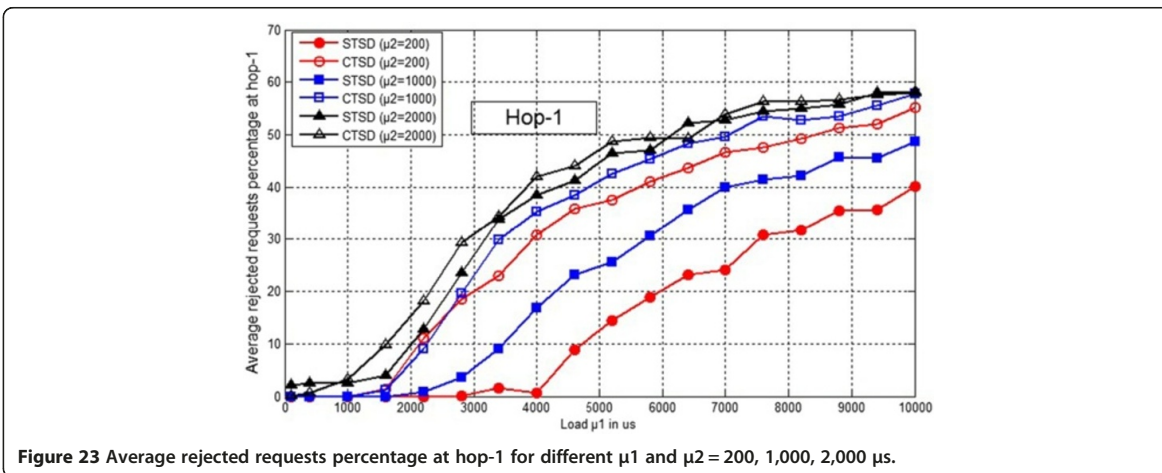


Figure 23 Average rejected requests percentage at hop-1 for different μ_1 and $\mu_2 = 200, 1,000, 2,000 \mu\text{s}$.

devices are granted their desired channel time size. However, the fairness at hop-1 is very high at low-loaded hop-1 and hop-2 networks and starts to decrease as load at both hops increases (Figure 27). It is also noticed that better fairness is obtained when applying the STSD compared to applying CTSD. This is because higher MPNCs and MDEVs satisfaction rate and lower rejection rate are obtained when applying the STSD which implement the T_L notion. Thus, using T_L makes the system more adaptive inducing a compromise between the satisfaction and the rejection rate of the devices (as explained previously).

Concerning the hop-2 simulation results shown above, it is worthy to mention that studying only the performance of SDRA independently of the hop-1 algorithms cannot be implemented in this work. This is because the implementation of SDRA is dependent on the validity of the condition that the hop-1 MPNC is granted resources by the running hop-1 algorithm as mentioned previously.

After showing in Figure 18 that the superframe dynamicity enhances the superframe utilization and the delay, we try to show the usefulness of the use of the *Flag* metric and the utilization thresholds in this part. Therefore, a comparison of the MPNCs/MDEVs satisfaction and fairness indexes between the proposed mechanism that jointly applies the utilization thresholds and priority list and without applying this mechanism is conducted. Since it is concluded from the previous analyses that STSD (i.e., STRA at hop-1) outperforms CTSD (i.e., CTRA at hop-1), only STRA is applied in the sequel. Therefore, comparing the resultant satisfaction factor and the average Jain's Fairness of the proposed mechanism with and without STRA is directly reflecting and showing the usefulness of applying the *Flag* metric and the superframe utilization threshold which are the basis of STRA.

Figure 29 shows a comparison of the MPNCs and the MDEVs average satisfaction factor for different loads μ_1

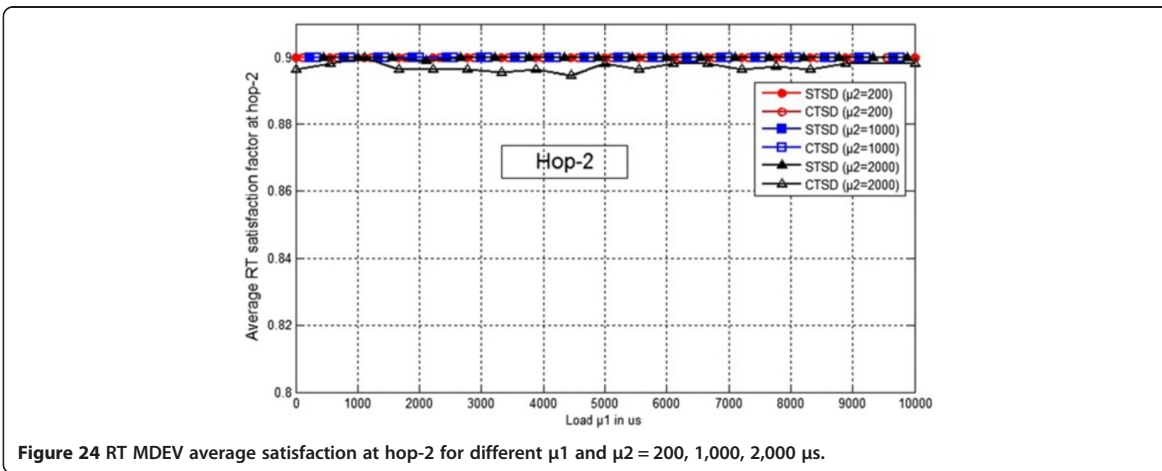


Figure 24 RT MDEV average satisfaction at hop-2 for different μ_1 and $\mu_2 = 200, 1,000, 2,000 \mu\text{s}$.

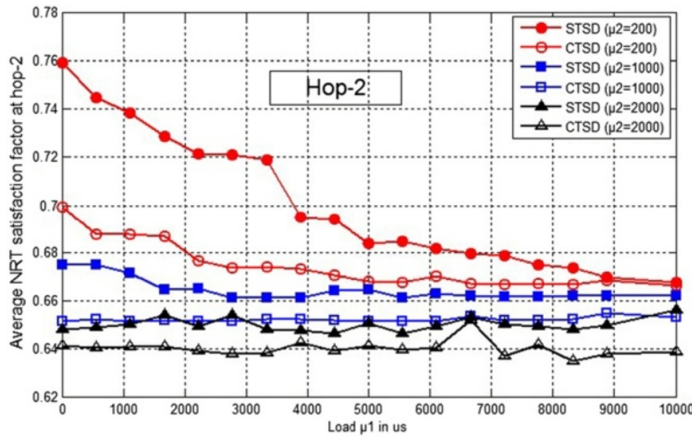


Figure 25 NRT MDEV average satisfaction at hop-2 for different μ_1 and $\mu_2 = 200, 1,000, 2,000 \mu s$.

with or without applying STRA. It is shown that much higher satisfaction is obtained thanks to the STRA for both MDEVs and MPNCs. Moreover, the variations obtained in the case of the STRA reveal the use of the threshold T_L , since the STRA adjusts the size of channel time values according to T_L . In contrast to that, the satisfaction factor remains constant when the STRA is not carried out. To better reflect the importance of the proposed mechanism, Figure 30 shows a comparison of the system average Jain's Fairness index for different loads applying or not STRA. It is shown that the overall fairness is much higher when applying STRA and it reaches an approximate of 100% in the case of low-loaded networks. This is due to the various advantages achieved when applying STRA as it has been previously explained.

In the literature, only few works ([11] and [12]) study the resource allocation for the HR mesh WPAN as previously mentioned. While [11] presents a distributed solution for the mesh WPAN, [12] presents a centralized solution which is the most relevant work for the resource allocation in the HR mesh WPAN. Since the work in [12] studies only the hop-1 MPNCs satisfaction, then the hop-1 algorithm (STRA) is solely applied to perform this comparison. Thus, the performance of the proposed mechanism is compared with that of [12] on the level of the MPNCs satisfaction and fairness index.

For this comparison, the same simulation environment of [12] is considered. Thus, we consider scenarios of 8, 10, and 12 MPNCs with a 274,663 superframe duration as studied in [12]. Since the authors in [12] do not study

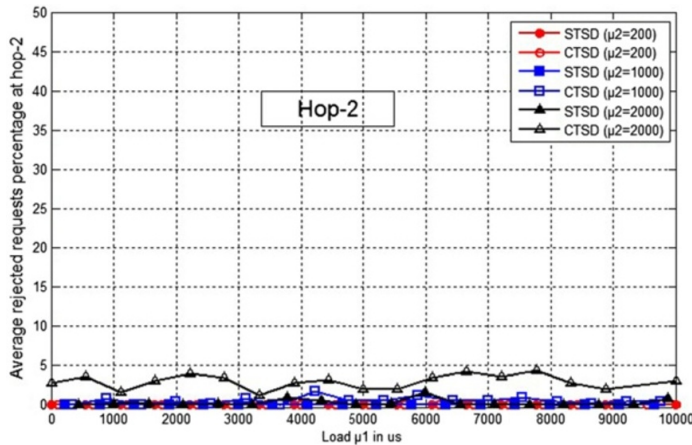


Figure 26 Average rejection rate at hop-2 for different μ_1 and $\mu_2 = 200, 1,000, 2,000 \mu s$.

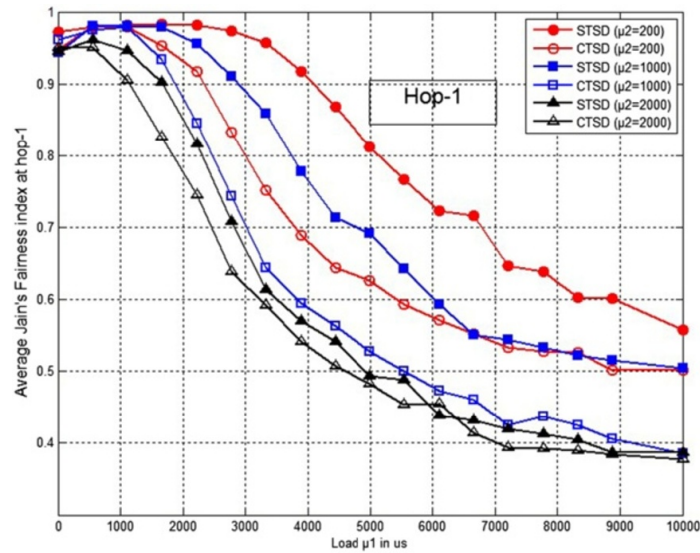


Figure 27 Jain's Fairness index at hop-1 for different μ_1 and $\mu_2 = 200, 1,000, 2,000 \mu s$.

the satisfaction of the hop-1 MDEVs, only the hop-1 MPNCs satisfaction obtained by running STRA is studied in Figure 31. It is shown that the satisfaction factor achieved in [12] is less than that achieved by STRA for different numbers of MPNCs. Additionally, Figure 32

shows a comparison of the average Jain's Fairness index for the number of MPNCs (8, 9, 10, and 11) studied in [12]. It is also shown that the overall fairness is much higher when applying STRA compared to that obtained in [12].

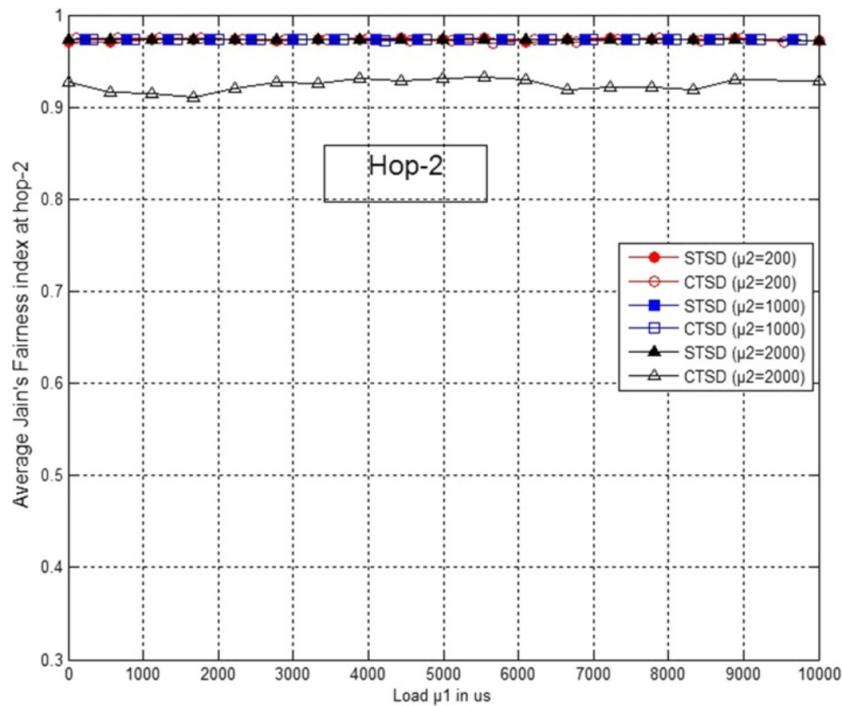


Figure 28 Jain's Fairness index at hop-2 for different μ_1 and $\mu_2 = 200, 1,000, 2,000 \mu s$.

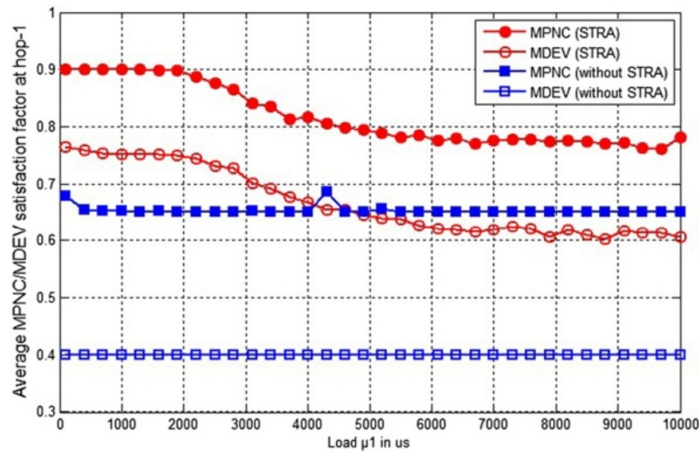


Figure 29 Comparison of average MPNC/MDEV satisfaction with and without applying T_L and P (STRA).

For summarizing the obtained results, we identify herein the reasons for obtaining better results using the proposed mechanism in comparison with [12]. These reasons can be described as follows:

Firstly, in addition to the bulk reservation mode, we add the dynamic superframe size, whereas [12] considers the fixed superframe size which could be inefficiently utilized in case of low-loaded networks. Additionally, each MPNC estimates its channel requirements based on a history of previous flows in [12]. Therefore, inefficient superframe utilization can occur because of incorrect channel time estimation for a bulk reservation by each MPNC due to either overestimation or underestimation of the channel time requirement of a cluster.

Secondly, the proposed algorithm considers the channel time requirements of both hop-1 (MPNCs and MDEVs)

and hop-2 devices (MDEVs), whereas [12] does not consider the channel time requirements of neither the hop-2 MDEVs in the ref-MPNC cluster nor the hop-2 MDEVs in the hop-1 MPNCs' clusters.

Thirdly, the use of the *Flag* metric and the priority list assigns higher priority for the devices with a higher number of unserved requests to ascertain that their requests are served in the subsequent superframes. This ensures higher satisfaction and consequently higher fairness among the competing devices compared to [12].

Fourthly, the introduction of the utilization thresholds induces a tradeoff between the satisfaction factor and the rejection rate which directly affects the fairness. This plays an important role in obtaining better fairness using our proposed mechanism compared to [12].

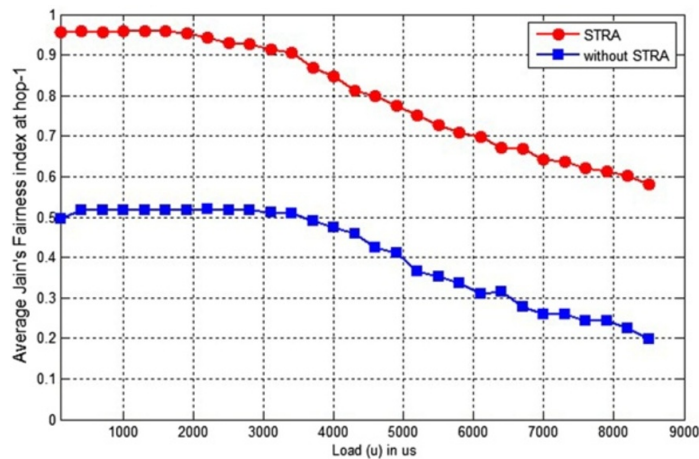


Figure 30 Comparison of Jain's Fairness index with and without applying T_L and P (STRA).

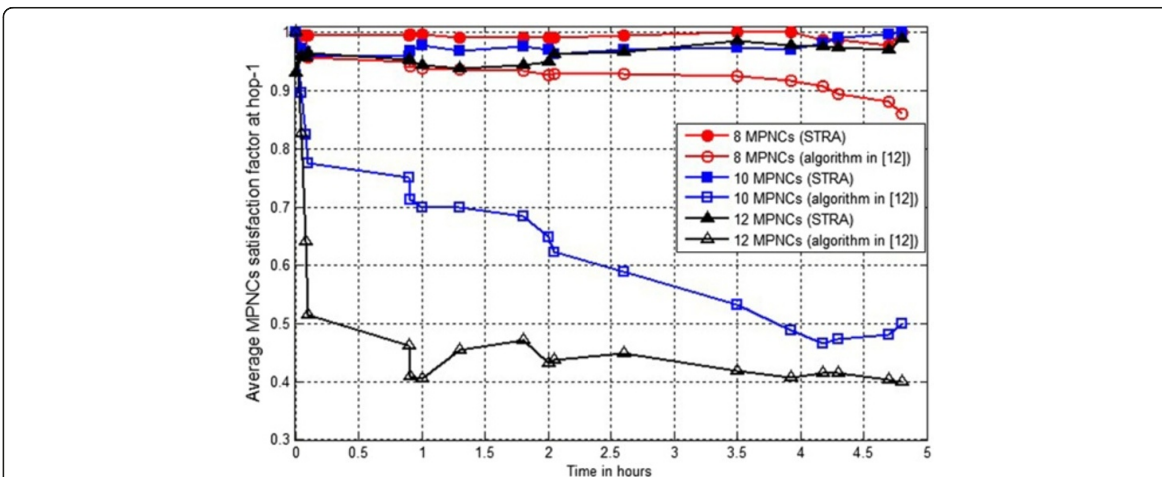


Figure 31 Comparison of average MPNC satisfaction for fixed μ_1 between STRA and algorithm in [12].

Finally, the better results achieved by STRA reflect the advantages of the various new notions that are introduced in this mechanism, namely, the utilization threshold T_L , the *Flag* metric, and the priority list. These advantages have already been thoroughly revealed and discussed throughout the various simulation result analyses and the algorithm descriptions.

8. Conclusions

In this paper, a two-hop IEEE 802.15.5 resource allocation mechanism, adopting the dynamic superframe size, was proposed. In this mechanism, two algorithms for resource allocation of two-hop IEEE 802.15.5 were defined. A CTAP utilization threshold, a superframe utilization threshold, a *Flag* metric, and a priority list were introduced.

The conducted simulations illustrated that the superframe is 100% efficiently utilized when using the proposed mechanism. Additionally, it was demonstrated that this mechanism achieves higher satisfaction and fairness by the use of the utilization thresholds and *Flag* metric. It was also illustrated that this mechanism prioritizes the MPNCs over the MDEVs at hop-1 and the RT over NRT MDEVs at hop-2 for a two-hop IEEE 802.15.5. Moreover, comparing the results obtained by the proposed mechanism with other works showed that the proposed mechanism provides better performance on the level of satisfaction factor and fairness.

Finally, the proposed mechanism is fully compliant with the IEEE 802.15.5 standard and is completely relying on the information elements and frames defined in this standard. Thus, this mechanism could be integrated

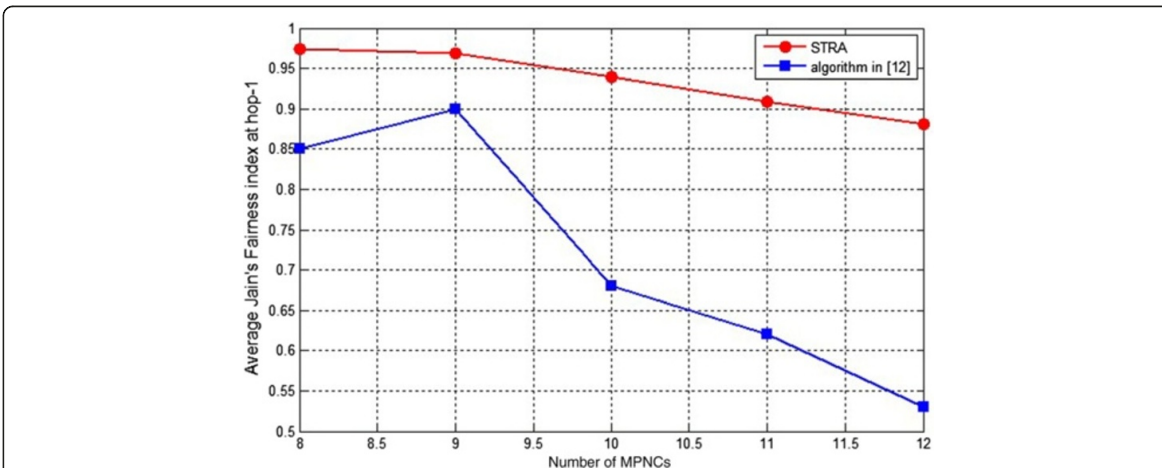


Figure 32 Comparison of Jain's Fairness index for fixed μ_1 between STRA and algorithm in [12].

in practice to improve the HR mesh WPAN performance and efficiency as illustrated by the conducted simulation results.

Competing interests

The authors declare that they have no competing interests.

Author details

¹INSA de Rennes, IETR, UMR 6164, F-35708 Rennes, France. ²CCE Department, Faculty of Engineering, IUL, 30014 Khaldeh, Lebanon. ³Faculty of Engineering, Lebanese University, Rafic Hariri Campus, Hadath, Lebanon.

Received: 4 April 2014 Accepted: 5 November 2014

Published: 23 November 2014

References

1. IEEE Standard 802.15.3-2003, "Part 15.3: wireless medium access control (MAC) and physical layer (PHY) specifications for high rate wireless personal area networks (WPANs)", 2003, pp. 1–315
2. SB Jung, S-B Yim, TJ Lee, S-D June, HS Lee, TG Kwon, JW Cho, Multipiconet formation to increase channel utilization in IEEE 802.15.3 high-rate WPAN". Springer-Verlag Lect. Notes Comput. Sci. **3392**, 1041–1049 (2006)
3. F Da Costa, "Dynamic Beacon Alignment in Simultaneously Operating Piconets (SOP) Using the Heart Beat Approach," IEEE Standard P802.15-04/135r0, 2004
4. Z Fan, "Multi-hop mesh networking for UWB-based 802.15.3 coverage extension", in *Proceedings of the 20th international Conference on Advanced Information Networking and Applications*, vol. 1, 2006, pp. 920–925
5. S Jung, H Kim, S Yim, T Lee, "Channel Time Allocation and Routing Algorithm for Multi-hop Communications in IEEE 802.15.3 High-Rate WPAN Mesh Networks", in *Proceedings of the 7th international Conference on Computational Science*, 2007, pp. 457–465
6. P Xue, P Gong, D Kim, Enhanced IEEE 802.15.3 MAC protocol for efficient support of multiple simultaneously operating piconets. IEEE Trans. Veh. Technol. **57**(4), 2548–2559 (2008)
7. S Sindian, A Khalil, A Samhat, M Crussière, J-F H elard, Resource allocation in high data rate mesh WPAN: a survey paper. Wirel. Pers. Commun. **74**(2), 909–932 (2014)
8. S Khan, H Al-Raweshidy, K Sivarajah, Meshed high data rate personal area networks". IEEE Commun. Surv. Tut. **10**(1), 58–69 (2008)
9. IEEE Standard 802.15.5-2009, "Part 15.5: Mesh topology capability in Wireless Personal Area Networks (WPANs)", 2009, pp. 1–166
10. M Lee, R Zhang, C Zhu, TR Park, C-S Shin, Y-A Jeon, S-H Lee, S-S Choi, Y Liu, S-W Park, Meshing wireless personal area networks: introducing IEEE 802.15.5". IEEE Commun. Mag. **48**(1), 54–61 (2010)
11. MS Park, B Lee, SH Rhee, Distributed multiple access control for the wireless mesh personal area networks. Trans. Inform. Syst. **E91**(2), 258–263 (2008)
12. S Mahmud, S Khan, HS Al-Raweshidy, A resource allocation strategy for meshed high data rate WPANs. IEEE Commun. Lett. **14**(6), 524–526 (2010)
13. IEEE Standard 802.15.4-2006, "Part 15.4: Wireless LAN Medium Access Control (MAC) and Physical Layer (PHY) Specifications for Low-Rate Wireless Personal Area Networks (LR-WPANs)", 2006
14. DR Herr aiz, A-J Garc a-S anchez, F Garc a-S anchez, J Garc a-Haro, On the synchronization of IEEE 802.15.5 wireless mesh sensor networks: shortcomings and improvements". EURASIP J. Wirel. Commun. Netw. **2012**(198), 5958–5995 (2012)
15. M Dianati, X Shen, S Naik, "A New Fairness Index for Radio Resource Allocation in Wireless Networks". 5th IEEE Wireless Communications and Networking Conference vol 2, 2005, pp. 712–717
16. A Kumar, J Kleinberg, "Fairness measures for resource allocation", in *IEEE Symposium on Foundation of Computer Science*, 2000, pp. 568–578
17. R Jain, D Chiu, W Hawe, A quantitative measure of fairness and discrimination for resource allocation in shared computer system. DEC Tech. Rep. **301**, (1984)

doi:10.1186/1687-1499-2014-197

Cite this article as: Sindian et al.: Admission control and resource allocation strategies for IEEE 802.15.5. *EURASIP Journal on Wireless Communications and Networking* 2014 **2014**:197.

Submit your manuscript to a SpringerOpen® journal and benefit from:

- Convenient online submission
- Rigorous peer review
- Immediate publication on acceptance
- Open access: articles freely available online
- High visibility within the field
- Retaining the copyright to your article

Submit your next manuscript at ► springeropen.com

Selected Article

[M. Crussière, C. Douillard, C. Gallard, M. Le Bot, A. Bouttier, A. Untersee, "A unified broadcast layer for horizon 2020 delivery of multimedia services", IEEE Transaction on Broadcasting, Vol. 60, Issue 2, pp 193–207, June 2014, DOI :10.1109/TBC.2014.2315764](#)

Abstract

It is expected that, in the coming years, the video data traffic carried by mobile networks will increase drastically. Among the different ways of facing this "mobile data tsunami", the cooperation of several complementary access technologies offers promising prospects. In the context of such a cooperative approach, this paper proposes the definition of a unified broadcast layer, close to the 3GPP LTE technology, and therefore liable to be easily integrated in mobile devices and infrastructure equipment. The general technical requirements for the design of such a common physical layer are detailed and a practical example based on the 3GPP LTE/E-MBMS and DVB-T2 standards is described. The verification of the proposed approach is performed through simulation results and validation tests carried out on a hardware platform.

Keywords : Access network cooperation, broadband networks, broadcast networks, common physical layer, hardware demonstrator, satellite channels, terrestrial channels, 3GPP LTE/E-MBMS.

A Unified Broadcast Layer for Horizon 2020 Delivery of Multimedia Services

Mathieu Crussière, *Member, IEEE*, Catherine Douillard, *Senior Member, IEEE*, Christian Gallard, Marie Le Bot, Benjamin Ros, Arnaud Bouttier, and Alain Unterseer

Abstract—It is expected that, in the coming years, the video data traffic carried by mobile networks will increase drastically. Among the different ways of facing this “mobile data tsunami,” the cooperation of several complementary access technologies offers promising prospects. In the context of such a cooperative approach, this paper proposes the definition of a unified broadcast layer, close to the 3GPP LTE technology, and therefore liable to be easily integrated in mobile devices and infrastructure equipment. The general technical requirements for the design of such a common physical layer are detailed and a practical example based on the 3GPP LTE/E-MBMS and DVB-T2 standards is described. The verification of the proposed approach is performed through simulation results and validation tests carried out on a hardware platform.

Index Terms—Access network cooperation, broadband networks, broadcast networks, common physical layer, DVB-T2, hardware demonstrator, satellite channels, terrestrial channels, 3GPP LTE/E-MBMS.

I. INTRODUCTION

GLOBAL mobile data traffic will increase 13-fold between 2012 and 2017”. “Two thirds of the world’s mobile data traffic will be video by 2017”. These words extracted from [1] and often referred to as the so-called “mobile data tsunami” describe how strong the phenomenon of data traffic growth is expected to be in the coming years. With such figures in mind, one can question how mobile operators will be able to face this challenge.

The evolution in network topologies, from current macrocells to future small cells (picocells, femtocells), will provide more capacity locally. The counterparts of such a network densification are twofold. On the one hand, interference will increase and will have to be managed in a not too complex way; technical solutions are currently being studied in the 3GPP standardization groups. On the other hand, backhauling

issues will also have to be solved: how to connect so many small cells to the core network, in a cost-efficient way, while guaranteeing the desired quality of experience for the end user?

In order to provide higher throughput services, a mobile operator can also acquire more spectrum, as data rates are closely related to the amount of available spectrum. To this end, the digital dividend in the 800 MHz band has already been allocated to mobile operators and the 700 MHz band allocation will be discussed during the World Radio-communication Conference in 2015. Consequently, one can imagine that the spectrum size allocated to mobile operators could be roughly doubled by 2020. Nevertheless, such investments in spectrum have a non-negligible cost for mobile operators. A longer term perspective, in terms of spectral resources, could be the use of millimeter waves where huge bandwidths could be available for small cells, due to the short coverage capability at such high frequencies. For instance, the 60 GHz band has been identified as a promising band: a huge amount of unlicensed spectrum is available and acceptable attenuation levels are observed for these frequencies.

Another alternative is to rely on the cooperation of different access technologies. One current example of such cooperation involves offloading part of the mobile traffic over WiFi access networks: in indoor environments such as homes, offices, or airports, the mobile traffic can be diverted to private or public WiFi access points when available. In order to improve the cooperation, enhancements are about to be carried out in 3GPP LTE (Long Term Evolution), release 12, and WiFi standard (known as High Efficiency WiFi [2]).

A well-known technology which can be also very helpful in delivering video services is broadcasting. Indeed, broadcasting should not be restricted to live TV delivery. It can also beneficially provide other kinds of multimedia services in the coverage area of the network and can then be considered as an efficient “point-to-area” service distribution technology. In particular, taking advantage of the huge amount of memory available in devices, broadcasting is well suited for predictive datacasting services. Different types of contents, such as e-magazines, “top-10” music video-clips, software and application updates, etc., can be pushed to device cache prior to their consumption by the end user, who can then access the contents, even without any connection, with a perfect quality of service. Besides, such a service based on broadcast access technology and known as NOTTV [3] is already available in Japan since April 2012.

Manuscript received July 15, 2013; revised March 18, 2014; accepted April 1, 2014. Date of publication April 29, 2014; date of current version June 4, 2014. This work was supported by the French National Research Agency, Project Mobile MultiMedia (M³, ANR-2010-VERS-0010).

M. Crussière is with the INSA-IETR Laboratory, Rennes, France.
C. Douillard is with the Telecom Bretagne/Lab-STICC Laboratory, Brest, France.

C. Gallard and M. Le Bot are with Orange Labs, Rennes, France.
A. Bouttier is with Mitsubishi Electric R&D Centre Europe, Rennes, France.

A. Unterseer is with TeamCast, Rennes, France.
B. Ros is with CNES, Toulouse, France.
Color versions of one or more of the figures in this paper are available online at <http://ieeexplore.ieee.org>.

Digital Object Identifier 10.1109/TBC.2014.2315764

0018-9316 © 2014 IEEE. Personal use is permitted, but republication/redistribution requires IEEE permission.
See http://www.ieee.org/publications_standards/publications/rights/index.html for more information.

In the framework of the DVB-NGH (Digital Video Broadcasting—Next Generation Handheld) standardization process, it was proposed in February 2010 to re-use 3GPP E-MBMS (Evolved Multimedia Broadcast Multicast Services), *i.e.*, the 4G broadcast mode, as a basis for NGH specifications. The purpose of this proposal was to avoid market fragmentation between standards, while making it easier the integration of broadcast chipsets in mobile devices (e.g., smartphones and tablets).

However, 3GPP E-MBMS as currently specified in Release 9 [4] is not able to meet all the usual broadcasters' requirements. For instance, terrestrial broadcast networks can usually cover areas within a radius of several tens of kilometres. In contrast, E-MBMS signals transmitted in a shared-carrier mode with LTE unicast data can only reach users at a maximum distance of 5 km from the base station, if no specific processing is performed on the receiver side. Moreover, as latency is not an issue for broadcasting services, deep time interleaving can be applied in such systems, which leads to improved performance in terms of quality of service, particularly in mobile conditions. For the development of the LTE standard, one of the initial requirements was conversely the reduction of latency compared to 3G; so no specific time interleaver has been designed for the LTE broadcast mode.

In November 2010, the DVB Forum decided to knock at 3GPP's door in order to propose a common definition for a unified broadcast standard. After an initial phase of mutual presentations of DVB and 3GPP broadcast state-of-the-art standards, a small group of 3GPP companies decided to propose, in May 2011, the creation of a study item dealing with converged mobile broadcast support for LTE. Unfortunately, due to the lack of support from mobile key players (due to unclear business model, uncertain potential profit for operators, etc.), the study item creation proposal was rejected in the end.

The various past attempts to propose pure broadcast solutions to the mobile ecosystem turned out to be vain. DVB-H, the first generation of DVB broadcast standard to handhelds standardized in 2004 [5], which was promoted by Nokia, has met a rather mixed success. DVB-H chipsets have been integrated into Nokia handsets, some services over DVB-H networks have been launched, e.g., in Finland, Austria, and Italy, but most of these services have now been switched off. On the other side of the Atlantic, Qualcomm promoted a proprietary solution known as MediaFLO [6] and got this technology standardized by the European Telecommunications Standards Institute (ETSI) in 2009 [7]. FLO TV services have been launched in the U.S. starting from 2007. Some devices able to receive such services were introduced by LG and Samsung in 2006. Nevertheless, in 2010 Qualcomm decided not to support the MediaFLO technology any longer and sold the spectrum they owned in the 700MHz band to AT&T. A second trial on the DVB side with DVB-SH (Satellite Services to Handhelds) [8], mainly promoted by Alcatel Lucent, did not meet the expected commercial success either.

A few lessons can then be learnt from these experiences:

- 1) A mobile broadcast standard would more likely become a market success if supported by a worldwide ecosystem, e.g., by 3GPP actors. Without having mobile vendors in the loop from day one, convincing them to embed a

non-3GPP broadcast chipset in their devices afterwards seems to be difficult.

- 2) Deploying and managing a broadcast network in addition to a mobile network also seems hard to achieve. This is mainly due to cost issues since significant investments have to be made to deploy this second network.
- 3) Beyond historical broadcast services (live TV and radio), additional multimedia services must be considered in order to assess the actual interest in deploying a broadcast solution.

The original approach described in this paper consists in defining a universal broadcast layer, close to the LTE technology, and therefore liable to be easily integrated in mobile devices and infrastructure equipment, which is an essential enabling factor for a worldwide adoption.

This paper is organized as follows. Section II analyses general requirements for a common physical layer (CPHY) and compares the main features of the DVB-T2/NGH standard with the broadcast mode of 3GPP LTE. A set of CPHY specifications based on LTE/E-MBMS is then proposed in Section III. Section IV describes a hardware demonstration implementing the proposed CPHY and presents the different validation tests carried out so far through simulations and laboratory tests. Section V concludes the paper.

II. FOUNDATIONS FOR A COMMON PHYSICAL LAYER

In this section, we introduce the concept of CPHY specifications for a convergent broadband/broadcast network. The technical challenges to obtain such a unified system are first detailed from a general point of view according to the specific requirements of point-to-area transmissions. Then, a comparison between the broadcast systems coming from DVB and 3GPP standardization bodies is carried out to better understand the key features that should govern the technical choices of a future common broadcast physical layer.

A. Common Physical Layer Challenges

The CPHY specifications have to be devised to act as an enabler for the deployment of broadcasting transmission modes over various network infrastructures, whether it be conventional terrestrial broadcast, broadband networks or satellite ones. Such a unified system should allow a common baseband chip embedded in a handheld receiver to demodulate and decode any service delivered through a broadcast transmission mode whatever the bearer network responsibility of the transmission. In other words, baseband operations for broadcast reception should become network agnostic. In this perspective, many basic features have to be guaranteed to make the CPHY well suited for point-to-area transmissions whatever the network environment, *i.e.*, whatever the point (the transmission station) and whatever the area (the radio links).

At first, the CPHY waveform should be sufficiently scalable to be fully compatible with the radio deployment plans of the targeted networks in terms of frequency bands, coverage areas and frequency planning strategies. For instance,

the CPHY has to be able to address at once typical frequency bandwidths for mobile communications and Digital TV (DTV). Moreover, as the cell range of cellular networks is far different from the coverage areas targeted by terrestrial or even satellite DTV networks, the CPHY waveform has to be shaped in order to ensure the coverage of cells whose size ranges from a few hundred meters to several tens of kilometers. This is of particular importance when considering Single Frequency Network (SFN) planning for which the coverage distance is mainly driven by the waveform immunity against inter-cellular interference.

Secondly, CPHY should take advantage of the full downlink feature of broadcast transmissions by defining long frame durations. In a pure broadcast mode, transmission frames can indeed be designed without any delay or latency considerations due to the uplink channel constraints. As far as modulation and coding schemes are concerned, using long frames allows the constellations and coding rates to be optimized for large codeword lengths, making the system perform closer to the Shannon limit. Over time-varying channels typical of mobile reception scenarios, interleaving schemes should also be applied over a large time spread to take advantage of time diversity. The increase of the interleaving depth and codeword length should actually essentially be limited by the maximum memory size that can be embedded in nomadic terminals.

Finally, the CPHY specifications should be based on a framing structure adapted to point-to-area transmissions. Such transmissions ensure a universal coverage, *i.e.*, they are not user specific and they deliver a common content to all the terminals within the coverage area whatever their individual situations. This implies that a given user should be able to access the broadcast contents at every time without engaging complex high-level process such as session control protocols. Besides, the user terminal should be able to easily and rapidly extract the multimedia service of interest among the whole delivered content. This involves designing frames with their own embedded signaling messages, giving all the necessary information about the frame structure and service content. Additionally, the frame structure should allow fast synchronization and sounding procedures.

B. Comparison of the DVB-T2/NGH and 3GPP LTE Standards

This Section analyses the state-of-the-art terrestrial DVB and 3GPP cellular broadcasting technologies. In Europe, the DVB standardization body proposes specifications for signal transmission over terrestrial, satellite, and cable broadcast networks. More specifically, the DVB-T2 [9] and DVB-NGH [10] systems define a family of frames able to operate broadcasting in various network topologies. On the other hand, the 3GPP working groups in charge of LTE have introduced the E-MBMS broadcast mode for cellular network operation [4]. These two systems can thus be viewed as reference systems for this study and the targeted CPHY has been designed taking their specifications as bases.

The first stage of comparison deals with the framing approach. Figs. 1 and 2 give the overall frame structure

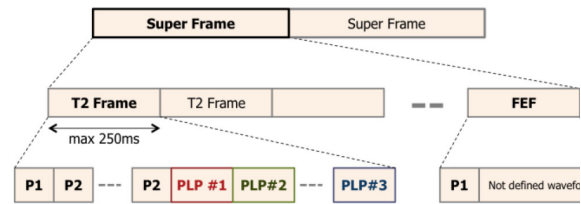


Fig. 1. Schematic view of the DVB-T2 frame structure highlighting P1 P2 preambles, multiple physical layer pipes (PLP) multiplexing, and future extension frame (FEF) insertion.

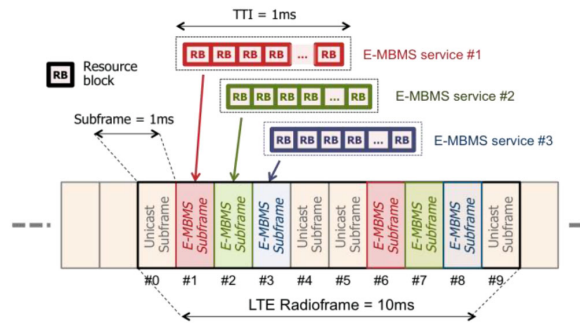


Fig. 2. Schematic view of the LTE radioframe structure (in FDD mode) highlighting the resource block allocation units and showing the unicast E-MBMS services multiplexing approach.

in both systems. DVB-T2 is based on a super-frame time segmentation possibly containing different families of frames whose duration can reach 250 ms. It can be noticed that DVB-T2 framing provides the concept of Future Extension Frames (FEF) for the transmission of non-DVB-T2 frames. In LTE, Fig. 2 gives the framing structure defined for downlink in the Frequency Division Duplex (FDD) mode. In this mode, LTE radio interface supports radioframes of 10 ms subdivided into ten sub-frames of 1ms each. This sub-frame duration is a reference value for the LTE system and is referred to as Transmission Time Interval (TTI). As shown in the figure, a subset of downlink sub-frames can be configured to deliver E-MBMS broadcast services/signals and E-MBMS services are multiplexed with classical unicast services within the radioframe. Both systems allow several services to be multiplexed within a frame.

This feature is provided by Physical Layer Pipes (PLP). In DVB-T2, each PLP being associated to a given set of physical layer parameters (modulation order, coding rate, interleaving depth) corresponding to a particular quality of service. In LTE, service multiplexing is inherent to the broadband nature of the systems. Each LTE service is first allocated to a set of elementary containers called Resource Blocks (RB) which are mapped onto the subframes. Last but not least, the two systems are based on very different signaling approaches.

On the DVB side, multiplexes of linearly programmed TV services are self-documented (the Electronic Program Guide gives information on multiplexed services and programmed contents), requiring the receivers to discover the services. On that basis, DVB-T2 frames are provided with dedicated preambles, namely P1 and P2 (see Fig. 1), to all

TABLE I
COMPARISON OF DVB-T2 LITE AND 3GPP E-MBMS PHYSICAL LAYERS

	3GPP E-MBMS	DVB-T2 Lite
Frequencies		
Main Frequency bands in Europe [MHz]	[791-862] [2,500-2,690]	[174-446] [470-790]
Main Channel Bandwidths [MHz]	5 ; 10 ; 15 ; 20	5 ; 6 ; 7 ; 8
OFDM parameters		
	Bandwidth 5 MHz	Bandwidth 8 MHz
FFT size	From 128 to 2k	From 2k to 16k
Δf [kHz]	15	From 4.464 to 0.558
Symbol duration [μ s]	67	From 224 to 1792
Guard Interval [μ s]	16.67	From 14 to 448
Cell radius [km]	5	From 4 to 133
Channel coding		
Code family	Binary turbo-code	LDPC code
Codeword size [bits]	Variable $K = \{40 \dots 6144\}$	Fixed $N = 16200$
Code rate	From 0.1172 to 0.9258	From 1/3 to 11/15
Interleav. Depth [ms]	1 ms max (TTI length)	250 ms max
Channel Sounding		
Scattered pilots	Fixed pattern (see [4])	8 Pilot patterns

the terminal to be fast synchronized and to easily extract the desired service from the frame payload. On the LTE side, broadband services are intermittently using the transmission resources and then are sustained by session opening/closing procedures implemented through a control channel using the bidirectional wireless connection. Hence, synchronization and signaling information is shared between unicast and broadcast services and is distributed across the whole radioframe.

To go further in the system comparison, Table I gives a summary of the main physical layer characteristics of these two broadcast standards. On the DVB side, DVB-T2 Lite parameters are taken as a reference. They constitute a subset of the DVB-T2 specifications that is well suited for mobile reception. As far as 3GPP is concerned, the LTE E-MBMS downlink parameters have been reported in the table, based on the FDD mode of the LTE standard.

These physical layers have a number of commonalities. Firstly, they use an OFDM modulating waveform, due to the fact that they have both been designed to cope with time and frequency selective channels. Various modulation and coding schemes are available in each standard as well, in order to provide flexible system performance. Such flexibility is exploited at the user level on the LTE side whereas it is viewed on the DVB side as the ability for the operator to select sets of parameters according to the targeted network deployment. Besides, DVB and LTE systems carry out a similar approach for channel sounding, using dedicated pilot symbols spread over the OFDM spectrum according to specific patterns. As a last common feature, both systems define SFN modes. For DVB systems, this is actually a basic feature used for the conventional deployment of a terrestrial network.

Apart from these similarities, both systems differ on various key aspects as highlighted in Table I. First of all, both systems operate in different frequency bands. Terrestrial DVB

systems were assigned the VHF and UHF bands whereas LTE systems address bandwidths in the frequency regions around 2.6 GHz. Note however, that the S band between 2 and 4 GHz is envisaged for the future DVB-NGH satellite link. In addition, some countries have recently taken the opportunity of the digital dividend to reallocate the upper band of the UHF spectrum to LTE systems, namely between 790 and 862 MHz. Concerning bandwidths, typical values for DTV broadcast are 6, 7 and 8 MHz for the terrestrial link and 5 MHz for the satellite link. LTE systems are mainly based on bandwidths defined as multiples of 5 MHz. So, it turns out that the two systems are not natively compatible in terms of spectrum usage, which is a first degree of harmonization to deal with (see Section III).

As a second major difference, the analysis of the OFDM parameters shows that they have not been chosen following the same strategy. Concerning the LTE standard, the OFDM waveform is governed by a fixed inter-carrier spacing of 15 kHz, the desired OFDM spectrum width being actually obtained through the activation of an adequate number of subcarriers at the FFT stage. Such a large inter-carrier spacing value allows strong Doppler effects to be handled. LTE has in fact been designed to support high mobility scenarios in frequency bands that can be located at 2.6 GHz. In addition, larger values of the inter-carrier spacing are more convenient to limit uplink synchronization constraints. As a consequence of this choice, the time domain OFDM symbol length remains constant, namely 67 μ s, whatever the effective signal bandwidth. Hence, considering a maximum ratio of 1/4, the guard interval duration is restricted to 16.67 μ s. On the other hand, the DVB-T2 Lite OFDM parameters result from a trade-off between Doppler effect mitigation and guard interval increase. Actually, DVB-T2 Lite offers several FFT sizes for each of the possible bandwidths. This leads to variable inter-carrier spacing values and thus to a variable degree of resistance against Doppler effect. Basically, this gives rise to various symbol and guard interval durations. From Table I, we can note for instance that the inter-carrier spacing for an 8 MHz bandwidth ranges from 0.558 kHz to 4.464 kHz, yielding guard interval values between 14 μ s and 448 μ s. The idea behind the guard interval adjustment is to adapt the OFDM signal to various coverage ranges if the system is operated in SFN mode. In such a network configuration, the guard interval is chosen according to the distance between two neighboring transmit towers so that it is able to absorb the echoes of the signals coming from each transmission link. In other words, the guard interval duration can be directly translated into maximum coverage distance according to the propagation speed, as reported in Table I. As an example, a maximum cell radius of 133 km is given for the DVB-T2 Lite system considering an 8 MHz bandwidth, which is far larger than the 5 km obtained for the LTE standard. However, LTE specifies an SFN mode allowing the inter-carrier spacing to be reduced to half of its nominal value, *i.e.*, 7.5 kHz, and leads to cells with an increased 10 km radius. This value still remains 13 times smaller than the maximum radius in terrestrial DVB-T2 Lite. From this comparison, we can conclude that LTE systems are mainly designed for Doppler effect mitigation, whereas DVB-T2 Lite systems are tailored to fit large coverage areas. The search

adequate OFDM parameters for a common broadcast PHY under coverage and mobility constraints is investigated in Section III.

The last significant contrast between DVB and LTE specifications can be analyzed from a Forward Error Correction (FEC) coding and interleaving point of view. At a first level, the two systems exploit different families of error correcting codes: DVB is based on LDPC codes while LTE makes use of turbo codes. However, when properly designed, both code families display comparable performance for similar implementation complexity. Consequently, the FEC code family does not represent a key criterion in our analysis. We rather focus on the FEC block size and time interleaving duration values. On the DVB side, the coded block size is fixed and is equal to 16,200 bits; the information block size thus depends on the coding rate. Then, bit interleaving is carried out at the FEC block level and time interleaving is applied to the constellation symbols within the so-called interleaving frames, which can contain a variable number of FEC blocks. As a result, the overall interleaving depth can reach the maximum frame duration, *i.e.*, 250 ms (see Table I and Fig. 1). It can even be extended to larger values with the inter-frame interleaving option which allows each interleaving frame to be mapped across several T2 frames. In this case, the improvement of the interleaving depth comes at the price of a bit-rate reduction and latency increase and has thus to be decided accordingly.

For the satellite case, which is the most sensitive to time selectivity, an interleaver with a time spread of several seconds could be envisaged [14]. From these considerations, it appears that DVB systems have been designed to benefit from high time/frequency diversity in a full downlink transmission mode. On the 3GPP side, the followed strategy is different. Table I indicates that various information block sizes (before coding) ranging from 40 to 6,144 bits are available. Compared to the DVB specifications, the LTE system thus offers more flexibility with respect to the block size, which can be explained by the need to adapt each link to users' requirements in cellular networks. Consequently, interleaving essentially relies on the interleavers used by the turbo code and on the so-called rate-matching functionalities, thus limiting the interleaving depth to a single code block. Each code block is then allocated to the resource blocks defined as the atomic allocation unit in LTE systems. In E-MBMS with SFN operation, these resource blocks are mapped without any additional interleaving process onto the subframes introduced in Fig. 2. Eventually, the maximum time spread in LTE E-MBMS is limited to the 1ms TTI value, which is far lower than what is carried out on the DVB side. The reason for such a difference comes from the fact that the LTE systems have to manage bidirectional communications governed by delay constraints. Nevertheless, LTE FEC functionalities include retransmission procedures that provide the base station with the possibility to transmit additional redundancy in case of erroneous packet reception at the terminal side, hereby implicitly exploiting channel time diversity. In a pure downlink broadcast transmission, such an approach can obviously not be carried out. Hence, in the perspective of a convergent

E-MBMS/DVB system, interleaving is a fundamental issue to be addressed.

III. CPHY SPECIFICATIONS PROPOSAL

Mobile broadcasting can be viewed as standing at the confluence of the DVB and 3GPP worlds. Aiming at defining a unified physical layer for mobile broadcasting scenarios is highly desirable to take advantage of both system designs. Our approach involves starting from the LTE/E-MBMS specifications and making them evolve to integrate broadcast requirements in the perspective of a deployment of the CPL over traditional broadcasting infrastructures, terrestrial and satellite.

Regarding the comparison analysis made in Section II, the E-MBMS specifications are modified according to the following steps:

- 1) Define a frame structure compatible with the DVB-T2 framing approach;
- 2) Modify the OFDM parameters in order to address typical broadcasters' bandwidths;
- 3) Increase the OFDM guard interval duration for SFN operation at the scale of typical broadcasters' cells;
- 4) Increase time diversity exploitation with time interleaving;
- 5) Design appropriate pilot patterns according to the previous modifications.

A. Framing

As detailed in Section II-B, E-MBMS services are multiplexed with unicast services within the LTE radioframes. Time-related synchronization and signaling procedures rely on information available in the unicast part of the frame. Since CPL signals should be delivered through downlink-only transmissions, it should be rather viewed as a dedicated carrier from the 3GPP world. The CPHY system has to embed its own synchronization and signaling information. Even if this paper is not intended to give complete solutions about signaling and synchronization mechanisms, some basic concepts are discussed hereafter. A simple solution is for instance to follow the preamble concept offered by the DVB-T2 specifications previously described and depicted in Fig. 1. A dedicated symbol can be defined to enable quick synchronization and to carry some preliminary signaling. To go further, the CPL can be considered as a particular FEC and can be multiplexed in time with already existing DVB-T2 frames, the dedicated preamble P1 guaranteeing its proper identification. This is sketched in Fig. 3. To keep the CPHY system as close as possible to the E-MBMS specifications, the new frame can benefit from the resource allocation strategy defined in 3GPP. In practice, we propose to build CPHY frames from radioframes of 10 ms made of subframes of fixed duration and relying on the elementary RB containers used by the 3GPP LTE systems. This approach gives a solution to the deployment of CPHY frames either in a TDM fashion with DVB-signals or directly embedded in a LTE radioframe. The practical implementation of a time multiplex with native sampling frequencies of each system (DVB and 3GPP) is discussed in Section IV-B.

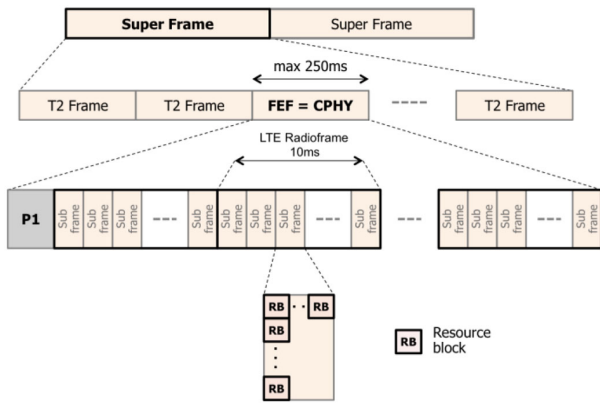


Fig. 3. CPHY framing structure proposal as a particular DVB-T2 FEF. The resource allocation principles of 3GPP LTE, based on resource block units and sub-frame segmentation, are maintained.

B. Bandwidth Harmonization

As previously mentioned in Section II-B, three native bandwidths of the DVB-T2 standard, *i.e.*, 6 MHz, 7 MHz and 8 MHz, are not addressed by current E-MBMS specifications. As a universal system, CPHY should be compatible with these bandwidth values. Reminding that 3GPP LTE is somehow bandwidth agnostic, it is actually fairly simple to adapt E-MBMS signals to these three new bandwidth cases. This is achieved through the activation of the adequate number of subcarriers for a fixed inter-carrier spacing and a given FFT size. Following 3GPP terminology, this translates into the allocation of a variable number of RBs per OFDM symbol, one RB corresponding to 180 kHz. As an example, one can easily achieve the 6, 7 or 8 MHz bandwidths starting from the existing 10 MHz E-MBMS case by progressively reducing the number of modulated subcarriers. Following this idea, one can calculate the number of subcarriers, or alternatively the number of RBs, being allocated according to the system bandwidth. Table II reports the parameters obtained under the 15 kHz and 7.5 kHz legacy E-MBMS subcarrier spacing and considering 1024- and 2048-point FFTs respectively. Note that a similar approach can be followed starting from a 5 MHz bandwidth with a 512-point FFT and then increasing the number of RBs. The choice between these two possibilities can actually be related to implementation strategies.

It is worth noting that the above proposal keeps approximately the same bandwidth occupancy as in the legacy E-MBMS standard, in such a way that the ratio of effective bandwidth over the total bandwidth is around 90%. Hence, this proposal retains the spectrum usage policy in use on the 3GPP side and could be considered as a "3GPP compatible" allocation mode. On the DVB side, an extended bandwidth planning is traditionally adopted to increase the system capacity. With this goal in mind, a second bandwidth allocation mode called "DVB compatible" can be considered with improved bandwidth occupancy, yet respecting DVB spectrum usage. The figures for these two modes are reported in Table III, highlighting an improvement of around 5% of the spectral occupancy when the extended mode is activated.

TABLE II
CPHY PARAMETERS FOR UHF BANDWIDTHS COMPATIBILITY, START FROM THE LTE-NATIVE 10 MHz BANDWIDTH

Radio Bandwidth	Inter-carrier spacing	FFT size	Number of RBs	Activated subcarriers	Effective Bandwidth
10 MHz	15 kHz	1024	50	600	9 MHz
	7.5 kHz	2048		1200	
8 MHz	15 kHz	1024	40	480	7.2 MHz
	7.5 kHz	2048		960	
7 MHz	15 kHz	1024	35	420	6.3 MHz
	7.5 kHz	2048		840	
6 MHz	15 kHz	1024	30	360	5.4 MHz
	7.5 kHz	2048		720	

TABLE III
CPHY PARAMETERS FOR UHF BANDWIDTHS, CONSIDERING NORM. MODE FOR LTE COMPATIBILITY AND EXTENDED MODE FOR DVB COMPATIBILITY. INTERCARRIER SPACING IS 7.5 KHZ, FFT SIZE IS 20

Mode	Radio Bandwidth	Number of RBs	Effective Bandwidth	Bandwidth occupancy
LTE compatible	8 MHz	40	7.2 MHz	90 %
	7 MHz	35	6.3 MHz	90 %
	6 MHz	30	5.4 MHz	90 %
DVB compatible	8 MHz	42	7.56 MHz	94.5 %
	7 MHz	37	6.66 MHz	95.14 %
	6 MHz	32	5.76 MHz	96 %

C. Coverage Area Extension

From the analysis of Section II, we pointed out that 3GPP LTE system suffers from a very short coverage area for SFN terrestrial operation compared to DVB-T2/NGH systems. The increase of the coverage is thus a crucial issue to be addressed for the design of the CPHY based on E-MBMS standard in the perspective of a deployment in SFN network. Since, in that context, the coverage size is directly proportional to the guard interval duration, set to 1/4 of the OFDM symbol size in the current E-MBMS standard, a possible solution involves increasing the OFDM symbol size. This is obtained by reducing the subcarrier spacing, however leading to lower immunity to Doppler effect. This issue has then to be analyzed as a trade-off between Doppler resistance and echo resistance. Interestingly, with a CPHY deployment in VHF/UHF bands, the Doppler spread values are expected to be much lower than those encountered in classical LTE bands, thus offering more flexibility for system optimization. Taking the practical assumption widely used in wireless communications stating that the admissible Doppler value may not exceed 10% of the subcarrier spacing, it is possible to compute the Doppler resistance for various guard interval values.

Table IV summarizes the maximum Doppler frequency shifts and echo resistances obtained in the UHF band, evaluated at 600 MHz, when dividing the current E-MBMS inter-carrier spacing values, namely 15 kHz (normal mode) and 7.5 kHz (SFN mode), by factors of 2, 3 and 6, respectively. From these results, we first note that the maximum Doppler shifts supported by the original LTE systems when operated at a center frequency of 600 MHz are 1500 Hz and 750 Hz. These values correspond to velocities of 2700 km/h and 1350 km/h respectively, which are way too far beyond a realistic situation. After inter-carrier spacing reduction, it comes that

TABLE IV
CPHY PARAMETERS FOR COVERAGE AREA ENHANCEMENT IN THE UHF
BAND (BANDWIDTH: 8 MHz, CENTRAL FREQUENCY: 600 MHz)

System	Inter-carrier spacing	Possible FFT size	Guard interval duration	Coverage radius	Max. Doppler shift	#OFDM symbols per subframe
LTE	15 kHz	1024	16.67 μ s	5 km	1500 Hz	12
LTE SFN	7.5 kHz	2048	33.33 μ s	10 km	750 Hz	6
CPHY	3.75 kHz	2048	66.67 μ s	20 km	375 Hz	3
	2.5 kHz	3072	100 μ s	30 km	250 Hz	2
	1.25 kHz	6144	200 μ s	60 km	125 Hz	1

maximum coverage can be increased up to 60 km, leading in counterpart to a sacrifice of the Doppler resistance down to 125 Hz in the worst case. In the UHF band however, this actually corresponds to a maximal supported velocity of 225 km/h, which is fairly acceptable. Note that reducing the inter-carrier spacing has also an impact on resource allocation since the OFDM symbol duration increases. Such an effect is reported in the last column of Table IV indicating the number of OFDM symbols to map to subframes. Eventually, the smallest value of inter-carrier spacing, namely 1.25 kHz, is still compatible with the subframe segmentation and leads to the allocation of a single OFDM symbol per subframe.

D. Interleaving Depth Increase

As explained in Section II, the time interleaving depth offered by the 3GPP specifications is significantly smaller than those specified in the DVB-T2/T2-Lite standards, due to latency constraints. Two main strategies detailed hereafter are proposed to circumvent this limitation of the physical layer:

- 1) Intra- and inter-frame interleaving schemes based on enlarged TTI and time slicing concept,
- 2) Retransmission-based interleaving schemes reusing the Hybrid Automatic Repeat reQuest (HARQ) concept.

Note that both approaches can only be carried out if additional soft buffer resources are made available at the terminal.

1) *Inter-Frame and Intra-Frame Interleaving*: A simple way to increase the frequency/time diversity of the 3GPP E-MBMS system is to incorporate an interleaving scheme at the Multicast Channel (MCH) level while increasing the TTI value. In current 3GPP systems, an MCH is mapped onto a single TTI of 1 ms based on the resource allocation approach depicted in Fig. 2. Keeping the same mechanism, the TTI value could actually be increased to 2 ms for instance, while adding an intra-frame interleaving applied on the coded blocks mapped onto the RBs. Following this example, data allocation within the frame is simply carried out as described in Fig. 4. This principle can also be extended up to a 5 ms TTI in a 10 ms radioframe, or to even larger values if the LTE nominal radioframe duration is extended. Complementary to this, time slicing mechanisms can easily be carried out at the resource allocation level. This concept, originally proposed in the context of DVB-H [5], allows separating in time several fragments of the interleaved and coded data. These fragments, called slices of length T_{slic}^u , are spread over the radioframes according to a delay T_{slic}^Δ between each slice. Thereby, channel time

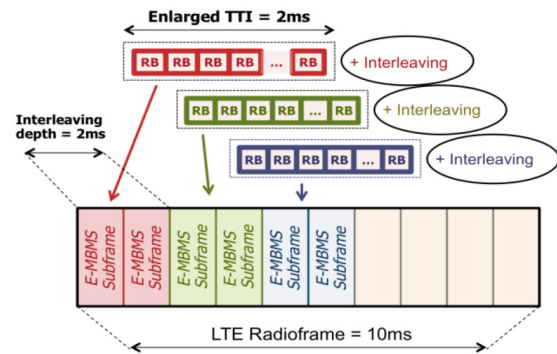


Fig. 4. Intra-frame interleaving and TTI enlargement of 2 ms.

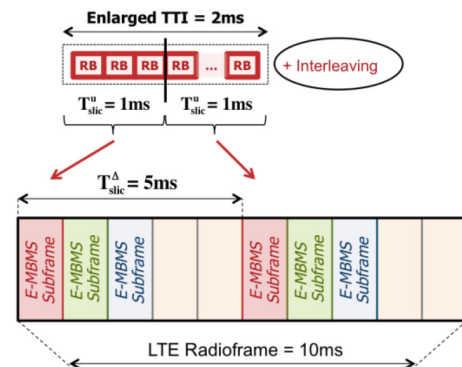


Fig. 5. Intra-frame interleaving combined with time slicing concept. TTI enlarged to 2 ms, slice duration is 1 ms, and delay between slices is 5 ms

diversity can be better exploited and the power consumption of the receiver can be lowered. This approach is depicted in Fig. 5 considering an enlarged TTI of 2 ms, slices of length 1 ms and a delay of 5 ms. Note that time slicing can be used to inter-frame interleaving as soon as the delay exceeds the radioframe duration. In that case, the data of a single MCH would be mapped onto several frames.

2) *Retransmission-Based Scheme*: Another way of taking advantage of time diversity is to exploit HARQ concepts already defined in the LTE unicast transmission mode. However, since no acknowledgment feedback signals are available in a broadcast mode, HARQ mechanisms have to be based on automatic retransmissions at the MCH level. A better approach can consist in simply sending the same coded bits for each retransmission. In that case, a Chase Combining process can be used at the receiver side. Such a scenario is illustrated in Fig. 6 in order to reach a code rate of 1/3, three retransmissions with code rate 1 can be used in three 1 ms subframes located in different frames. The delay between retransmissions corresponds to the interleaving depth equal to 21 ms in the example. Note that this method avoids the enlargement of TTI duration as well as the definition of an additional time interleaver.

A more elaborate technique could be based on an incremental redundancy mechanism: a given CPHY is broadcast during an initial subframe, and additional redundant bits corresponding to the same information bits can

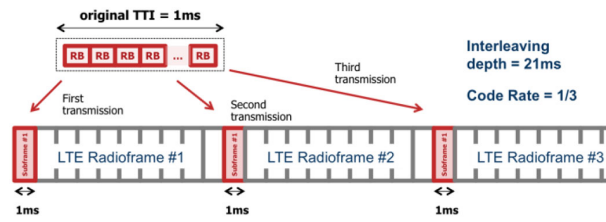


Fig. 6. Time interleaving based on automatic retransmissions.

automatically retransmitted in subsequent subframes, after some predefined delays. Then, through the observation of the initial transmission content and of the additional redundancy, each receiver improves the decoding of the information.

Such an automatic retransmission approach results in a reduced code rate but yields increased diversity exploitation if the channel has sufficiently changed between two transmissions. It could only be implemented for push services, not for live TV or radio services, and in situation of limited data traffic, during the night for instance. A typical example of application would be data carousels, repeatedly delivering data in a continuous cycle during a sufficient period, allowing most of the receivers in the coverage area to retrieve the transmitted data.

E. Sounding Pattern Design

At this stage of the study, all the physical layer parameters of the proposed CPHY waveform have been identified and selected. Since the inter-carrier spacing values and the guard interval durations have been substantially modified, the Pilot Patterns (PP) specified by the LTE E-MBMS standard are no more suitable. Indeed, scattered PPs can be viewed as a time-frequency sampling grid which granularity has to meet certain constraints to properly measure the time and frequency variations of the channel response. These constraints can be computed according to the Nyquist criterion (see [11], Section 10.3.2.3.2 for more details):

$$T_{Nyquist} = \max \left\{ \frac{N_{FFT}}{F_s} \cdot \frac{X}{Y}, \frac{4}{3} \cdot GI \right\}, \quad (1)$$

$$D_{Nyquist} = \frac{F_s}{2N_{FFT} \cdot (1 + GI) \cdot X}, \quad (2)$$

where X denotes the spacing between 2 pilots in time domain and Y denotes the spacing between 2 pilots in frequency domain. A convenient PP should hence be designed such that $T_{Nyquist}$ and $D_{Nyquist}$ remain greater than the guard interval duration and the maximum Doppler shift, respectively.

From these relations, it is then possible to propose PPs suitable for the different parameters of the CPHY, namely considering the inter-carrier spacing and guard interval values introduced in Table IV. In order to remain as close as possible to the LTE specifications, such PPs could be obtained following the same pattern shape as the one used in the LTE standard. However, since the PPs have to be unchanged from one TTI to another, such a strategy would lead to a dramatic increase of the overhead when the intercarrier spacing

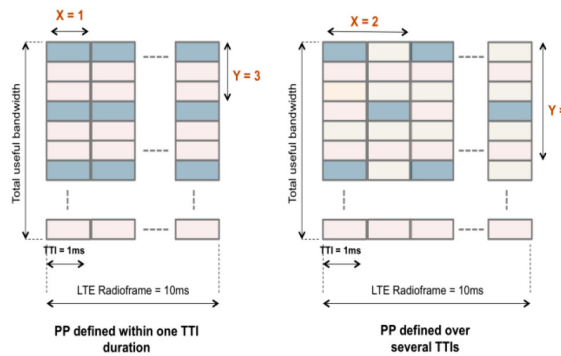


Fig. 7. Comparison of PPs defined in the 1.25 kHz inter-carrier spacing configuration. On the left, the PP is restricted to the TTI time spread whereas it is defined over 2 TTIs on the right.

is reduced (see [12] for more details). Relaxing this constraint, *i.e.*, allowing defining a PP over several TTIs, leads to more efficient PPs. As an example, Fig. 7 compares two suitable PPs with respect to the Nyquist criterion for 1.25 kHz inter-carrier spacing configuration. The first PP (on the left) strictly fulfils the LTE requirements by constraining the pattern to be entirely defined within a single TTI duration. The second PP (on the right) is built over two consecutive TTIs, thus leading to an overhead reduction by a factor of two. Note that the second approach would be compatible and particularly adequate in the case of an enlarged TTI, as proposed in Section III-D for time interleaving improvement.

F. Impact on Terminals

The resulting impact of CPHY implementation in receivers in terms of complexity and power consumption highly depends on the way the proposed generic CPHY is deployed and used. In the case it is deployed by a mobile or broadcast network operator on a dedicated carrier, a specific chipset is necessary to decode it. Conversely, in the case the CPHY is used in a mixed mode by a broadcast network operator (e.g., embedded CPHY frames in Future Extension Frames of DVB-T2) or a mobile network operator (e.g., a time multiplex of LTE-Advanced/5G frames and CPHY frames in a shared-carrier mode), the addition of the new broadcast capabilities requires a multi-mode receiver whose complexity can be higher than the basic receiver. However, in the case of a time multiplexed LTE-Advanced and CPHY in a shared-carrier mode, the corresponding receiver should not differ very much from existing LTE-Advanced receivers with E-MBMS capabilities, due to the numerous commonalities between the proposed CPHY and E-MBMS.

IV. VERIFICATION AND IMPLEMENTATION OF THE CPHY CONCEPT

Beyond the analysis and the specifications proposed in previous sections, the validity of the CPHY concept is verified by means of simulations and implementation of a time demonstrator.

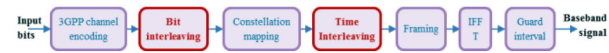


Fig. 8. Introduction of new interleaving blocks (in red) into the LTE transmission chain (terrestrial link).

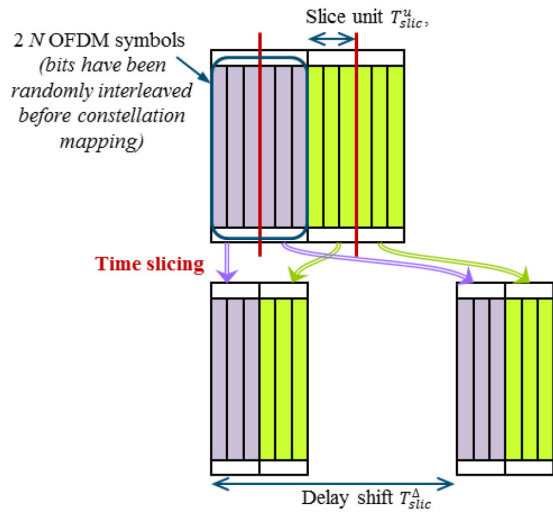


Fig. 9. Proposed time slicing principle (terrestrial link).

Simulations were mainly carried out to assess the gains obtained when increasing the time interleaving depth according to Section III-D, for both terrestrial and satellite channels. Besides, the demonstrator was built in two phases and was assigned two main objectives:

- 1) Implementing a stand-alone CPHY transmission in order to assess the CPHY concept in transmissions over real Radio Frequency (RF) channels;
- 2) Implementing CPHY and DVB-T2 combined together, in order to illustrate the feasibility of converged operation of the proposed CPHY and of a DVB-T2 signal in a single RF channel.

A. Validation of the CPHY Concept

1) *Validation of CPHY Time Interleaving Enhancements:* Due to strong low-latency requirements, the LTE physical layer does not include any time interleaver. Nevertheless, as explained in Section III-D such an interleaver can profitably be inserted into the CPHY in order to take advantage of the time diversity offered by the fading environment.

Therefore, for terrestrial transmission channels, a time interleaver coupled with a bit interleaver was introduced at the output of the coding and rate matching modules of the LTE transmission chain, as illustrated in Fig. 8. The simulated time interleaver structure is based on random interleaving combined with time slicing as proposed in Section III-D and illustrated in Fig. 9. In this way, the set of bits interleaved together are split into two slices of duration T_{slic}^u and separated in time by the time slicing shift T_{slic}^Δ . The bit interleaver depth is then equal to $2T_{slic}^u$ while time diversity spans on $T_{slic}^\Delta + T_{slic}^u$.

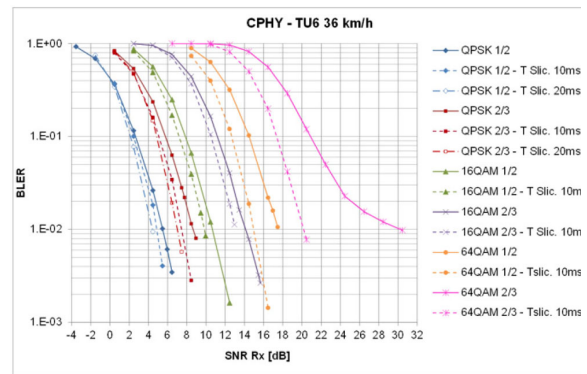


Fig. 10. Simulation results for the CPHY scenario of Table IV with and without time interleaving.

The impact of the time slicing algorithm on performance was assessed through simulations for the CPHY with a carrier frequency of 800 MHz and with the intercarrier spacing to 1.25 kHz as proposed in Table IV. QPSK, 16QAM, and 64QAM constellations were considered with coding rates of 1/2 and 2/3. Two different time slicing configurations corresponding to different values of slice duration T_{slic}^u and time slicing shift T_{slic}^Δ were tested:

- 1) $T_{slic}^u = 1$ ms and $T_{slic}^\Delta = 10$ ms,
- 2) $T_{slic}^u = 2$ ms and $T_{slic}^\Delta = 20$ ms.

The channel model is the normalized typical urban mobile channel with 6 paths (TU-6) described in the DVB-T2 implementation guidelines [11]. The mobile velocity is equal to km/h, corresponding to a Doppler shift of 26.67 Hz.

Fig. 10 shows the Block Error Rate (BLER) curves versus Signal to Noise Ratio (SNR) at the receiver side for the different simulated modulation and coding parameters, with and without time slicing. In the area of interest for broadcasting that is for target BLERs lower than 10^{-2} , this very simple time slicing algorithm brings a significant gain, ranging from 1 dB to 2 dB, for most examples under study. In the particular case of 64QAM constellation with coding rate 2/3, an error floor is observed when no time interleaving is implemented. This is due to the imperfect estimation of the Doppler shift performed by the channel equalizer, this effect being stronger for high order constellations. In this particular case, the simple introduction of the time interleaver significantly lowers the error floor so that a huge gain (around 10 dB) can be observed in the 10^{-2} BLER region.

Performance enhancements due to time interleaving can also be demonstrated in satellite channels. Actually, satellite vehicular channels can suffer from fast fading events coupled with deep or average shadowing events whose correlation values can reach several meters [13]. Note that the CPHY waveform parameters in the satellite case can remain very close to those of the 3GPP LTE system, because of strong similarities in terms of frequency bands (5 MHz bandwidth around 2 GHz) and owing to the fact that the coverage range is more governed by the guard interval duration. Simulations have been performed with the LTE native intercarrier spacing

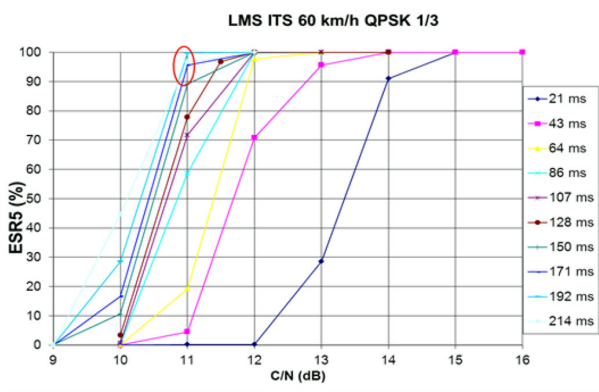


Fig. 11. Satellite case simulations results, LMS ITS channel.

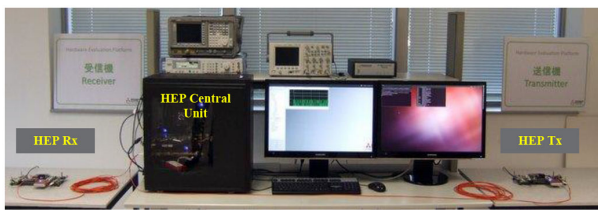


Fig. 12. Overview of the CPHY real-time implementation platform.

i.e., 15 kHz, and a guard interval of 1/14, corresponding to a guard interval duration of 4.69 μ s. The carrier frequency is set to 2.2 GHz. To address a very large scale of time interleaving values, simulations were obtained using a simple row-column matrix permutation.

Differently from the terrestrial channels, the BLER measurement is not currently used as a quality criterion for video reception over satellite mobile channels. In DVB-SH implementation guidelines [14], the Errored-Second-Ratio at 5 % (ESR5) criterion is preferred to assess the transmission quality in mobile channels. In Land Mobile Satellite (LMS) channels, an ESR5 90 % fulfillment ratio is sought to ensure good video quality on a mobile device.

A first set of simulations were carried out in LMS with Intermediate Tree Shadowing (ITS) channel, with 40° elevation for the satellite [13], and 60 km/h mobile speed. The corresponding results are given in Fig. 11. One can observe that interleaving depths greater than or equal to 150 ms make the ESR5 90 % fulfillment ratio to be achieved at a minimum C/N around 11 dB. This C/N value is quite achievable with a well-designed satellite payload and a vehicular category 1 terminal [14]. Significant interleaving gains exceeding 3 dB can be observed because of the severity of the considered LMS channel.

2) *CPHY Demonstrator*: In order to validate the relevance of the CPHY specifications under realistic conditions, the CPHY system has been implemented in hardware using an FPGA platform. Fig. 12 depicts the overall architecture of the so-called Hardware Evaluation Platform (HEP) that is made of three entities, a main computing unit, the HEP Central Unit, and two secondary units, HEP Tx and HEP Rx.

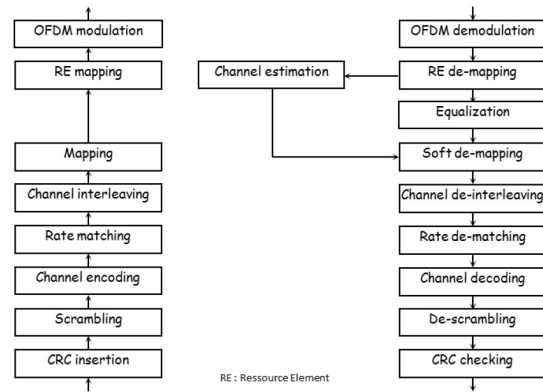


Fig. 13. Functional diagram of the CPHY platform.

Both the transmitter and the receiver are implemented with the same equipment, namely the HEP Central Unit, which made of a FPGA PCIe board embedded within a PC with a real-time operating system for control and monitoring. In order to allow for transmissions over distant locations, the main processing board is connected to the secondary units HEP Tx and HEP Rx via full-duplex optical links running 5 Gbps. The HEP Tx unit implements the Digital-to-Analog Conversion (DAC) on an Intermediate Frequency (IF) while the HEP Rx unit implements the Analog-to-Digital Conversion (ADC) from IF down to baseband. The HEP Tx and Rx units can interconnect in analog with RF front-ends or with channel emulators, terrestrial or satellite. The CPHY platform is based on an existing design implementing a simplified version of the 3GPP LTE (Release 8) physical layer in downlink [1]. The reference platform was dedicated to the evaluation and validation of physical layer technologies. There is thus no support of the signaling channels. Table V provides the parameters of the reference 3GPP LTE system implemented in the platform.

Fig. 13 depicts the functional diagram of the CPHY transmitter and receiver in baseband. This version of the system does not support any time and frequency synchronization mechanism so far. The subset of CPHY specifications supported by the HEP platform is summarized in Table VI.

The main purpose of this first-generation demonstrator is to prove that the current 3GPP E-MBMS broadcasting component can easily be modified to enable broadcasting over land cells, as argued in Section III-C. In the so-called Multicast Broadcast Single Frequency Network (MBSFN) mode E-MBMS, all the cells are tightly synchronized in time and transmit over the same frequency. MBSFN transmission enables highly efficient MBMS, allowing for over-the-air combining of multi-cell transmissions in the User Equipment (UE). An extended cyclic prefix is used to compensate for the difference in propagation delays, thus making the MBSFN transmission appear to the UE as a transmission from a single cell. The advantage of this SFN mode is precisely to allow for data transmission from a small number of very large cells.

TABLE V
GENERAL PARAMETERS OF THE CPHY PLATFORM

BASIC SYSTEM PARAMETERS	
Carrier frequency	Low-IF = 70 MHz
Symbol duration	66.66 μ s
Short cyclic prefix duration (symbols 1-6 / 7)	4.69 / 5.21 μ s
Total symbol duration	71.35 μ s
Subcarrier spacing	15 kHz
Slot duration	0.5 ms
Number of symbols per slot	7
Frame duration	10 ms
Number of subframes in a frame	10
Number of subcarriers in a Resource Block	12
SYSTEM PARAMETERS FOR 20 MHz CHANNELS	
Channelization bandwidth	20 MHz
Sampling frequency	30.72 MHz
Number of samples per slot	15,360
FFT size	2,048
Number of null subcarriers	848
Number of modulated subcarriers	1,200
Number of available RBs	100

TABLE VI
CPHY FEATURES IMPLEMENTED IN HARDWARE

Parameters	Supported values
Bandwidth	6, 7, 8 and 10 MHz
Inter-carrier spacing	1.25, 2.5, 3.75, 7.5 and 15 kHz
FFT size	0.5k, 1k, 2k, 4k, 8k, 12k and 24k
Pilot patterns	X=2, 6 Y=1, 2, 4 and 6 (see section III.E)

The radius of the cells is actually limited by the duration of the guard interval of the OFDM symbols whose task is to avoid the inter-symbol interference due to long echoes coming from distant transmitters (see Fig. 14).

In order to demonstrate the gain provided by the CPHY system in terms of coverage area, the five different physical modes detailed in Table IV have been implemented for a 10 MHz bandwidth. An essential guideline that directed the design of these physical modes was keeping maximum commonality with the 3GPP LTE system, especially the sampling frequency and the 1 ms duration of the 3GPP LTE TTI. With the normal 3GPP LTE subcarrier spacing mode and the SFN reduced subcarrier spacing modes, the system is able to transmit 12, 6, 3, 2 or 1 OFDM symbols per TTI as illustrated in Fig. 15. The most favorable case provides a guard interval of 200 μ s, compatible with a coverage radius of 60 km (see Table IV). Note that the reduction of the subcarrier spacing also reduces the robustness to Doppler and that the selection of the mode to be deployed in practice depends on the operating frequency.

3) *Validation Tests Carried Out With the CPHY Demonstrator*: The five framing modes of the CPHY specifications have been implemented on the HEP platform with the ability to dynamically switch from one mode to

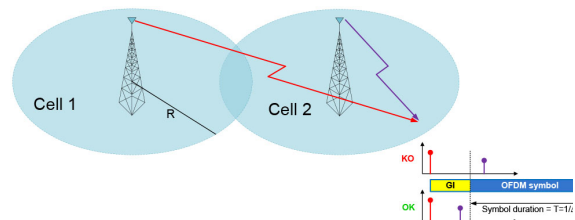


Fig. 14. Illustration of the impact of the distance between SFN transmitters on OFDM.

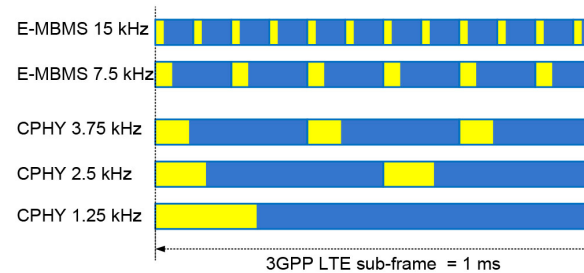


Fig. 15. Illustration of the guard interval duration with respect to the CF modes.

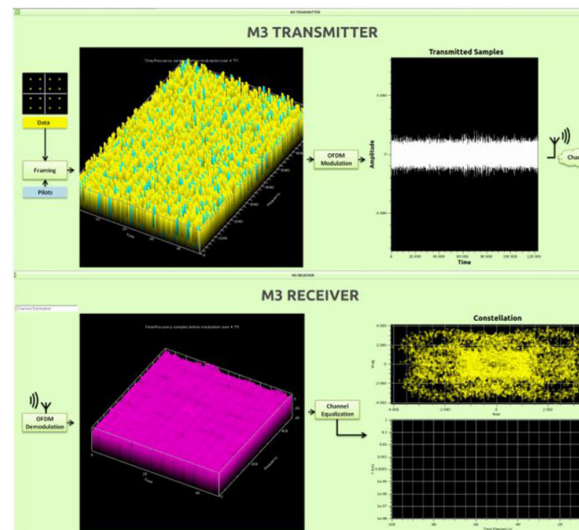


Fig. 16. Impact of a two-path channel with 160 μ s delay on E-MBMS $\Delta f = 15$ kHz.

another. Fig. 16 and Fig. 17 provide an overview of HEP monitoring interface where the platform transmits E-MBMS signal through a hardware channel emulator. In that particular case, the interface shows:

- 1) **at the transmitter side**, the 3D representation of time and frequency samples in the framing module and the transmitted signal in the time domain;
- 2) **at the receiver side**, the 3D representation of the channel estimation samples and the constellation points at the output of the equalizer.

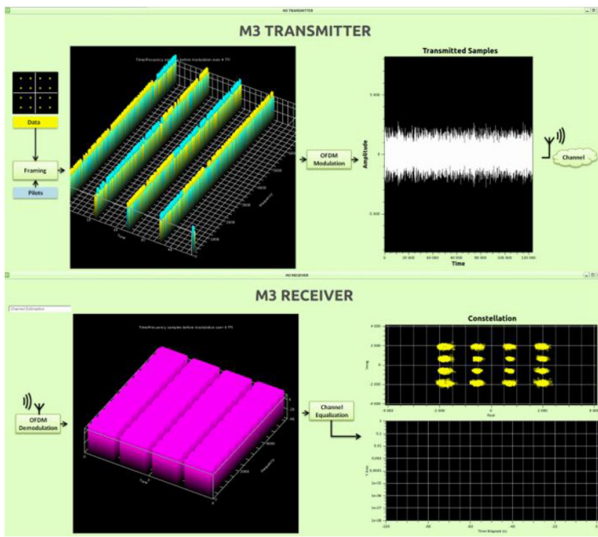


Fig. 17. Impact of a two-path channel with 160µs delay on CPHY with $\Delta f = 1.25$ kHz.

To demonstrate the robustness of the CPHY system towards long echoes, a simple channel featuring two paths 160 µs apart has been implemented. Fig. 16 illustrates the impact of this channel on the E-MBMS signal when the subcarrier spacing of 15 kHz sets the guard interval duration to 16.7 ms. The signal is obviously degraded due to inter-symbol interference. Once the platform configured to transmit the CPHY signal with the lowest subcarrier spacing value $\Delta f = 1.25$ kHz, the guard interval of 200 µs is large enough to handle the channel delay and inter-symbol interference is no longer observed at the receiver side, as shown in Fig. 17.

B. Embedding a CPHY Waveform Into DVB-T2 FEF Frames

The second phase of the demonstrator implementation combines two end-to-end real time transmission chains:

- 1) The CPHY chain, including transmitter, channel emulator, and receiver, as described in the previous subsection;
- 2) A DVB-T2 transmission chain also including transmitter, channel emulator, and receiver.

As illustrated in Fig. 18, the digital output of the CPHY modulator feeds the DVB-T2 modulator, which inserts the CPHY frames into reserved slots of the T2 signal, by means of the FEF mechanism offered by the DVB-T2 standard. The resulting signal is a sequence of DVB-T2 and CPHY frames in a classical time division multiplexing scheme. At the receiver side, the DVB-T2 demodulator first provides channel estimation and overall synchronization, then extracts the CPHY frames and forwards them to the CPHY demodulator. On the one hand, the DVB-T2 frames are demodulated by the DVB-T2 demodulator which delivers the data to a standard audio/video (AV) decoder and a wide screen. On the other hand, the CPHY frames are demodulated by the CPHY demodulator which delivers the received data to the upper layers for display. Both demodulators provide indications about the quality of the received signals.

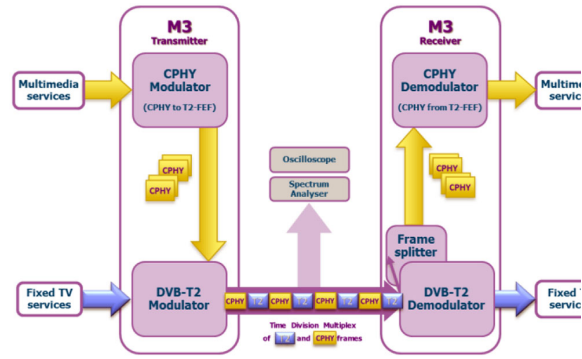


Fig. 18. Functional description of the demonstrator combining CPHY and DVB-T2 waveforms.

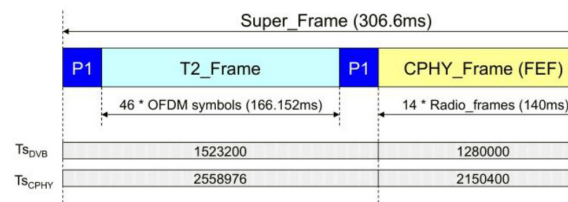


Fig. 19. T2 and CPHY frame combination.

The structure of the DVB-T2 super-frame structure adopted for the combination of regular T2 frames and CPHY frames is given in Fig. 19 and the parameters of the T2 and CPHY frames are detailed in Table VII. The super-frame duration has been chosen to contain an integer multiple of both the DVB-T2 and CPHY elementary periods, Ts_{DVB} and Ts_{CPHY} . The configuration of the T2 frame is derived from the regular “U mode”, i.e., it targets fixed receivers at home, with wide high definition (HD) screens. Moreover, the super-frame structure was defined to have approximately the same duration for both the T2 and CPHY frames.

1) Validation Tests for a Combined DVB-T2/CPHY Transmission: Three types of validation tests have been defined and carried out so far in order to show that CPHY frames can actually be transmitted within a T2 signal without disturbing the regular T2 reception:

- 1) **Transmitter test:** Verify with a spectrum analyzer and an oscilloscope the correct insertion of the CPHY-FEF into the T2 frame. When the CPHY signal is not present, the RF signal contains a null FEF corresponding to the CPHY-FEF duration. When the CPHY signal is present, the transmitter generates a continuous RF signal, shown in Fig. 20 (the power for the CPHY and DVB-T2 signals have intentionally been set to different values in order to distinguish the FEFs).
- 2) **End-to-end go/no-go test (video test):** Check the video on the T2 receiver and on the CPHY receiver with a camera. This scenario actually constitutes the convergence demonstration.

TABLE VII
SUPER-FRAME PARAMETERS OF THE DVB-T2/CPHY PLATFORM

Frame format	1 T2 frame + 1 FEF
Bandwidth	8 MHz
T2 FRAME PARAMETERS	
DVB-T2 mode	Mode A (1PLP) – SISO
T_{SDVB}	7/64 μ s (109 ns)
# OFDM symbols in T2 frame	46
FFT size	32K extended (27,841)
Δf (kHz)	0.279
Guard interval duration	1/128 (28 μ s)
Pilot pattern	PP7
PAPR reduction	No
LI constellation	64QAM
LDPC codeword length	64K
Code rate	2/3
Constellation	Rotated 256QAM
Time interleaver	intra-frame
High efficiency mode	Yes
T2 bitrate (Mbit/s)	21.69
CPHY FRAME PARAMETERS	
T_{SCBS}	1/30.72 μ s (32.5 ns)
# Radio frames in CPHY FEF (10ms)	14
FFT size	12k
Δf (kHz)	2.5
Guard interval	1/4 (33.33 μ s)
# RBs	40
# Occupied subcarriers	2880
Effective BW (MHz)	7.2
TTI duration	1 ms
# OFDM symbols per TTI	2
# OFDM symbols in CPHY frame	280
Pilot pattern	(a)
Constellation	16QAM
Code rate	1/2
CPHY bitrate (Mbit/s)	~3.5

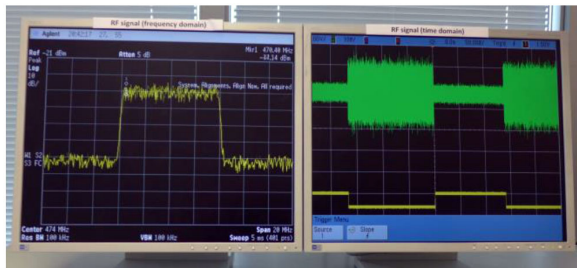


Fig. 20. Observation of a combined T2 and CPHY signal.

- 3) **Test in Additive White Gaussian Noise (AWGN) channel:** Perform a rough assessment of system performance, in presence of noise, for the transmission of the DVB-T2 and CPHY signals. The validation criterion is a video without error. The minimum carrier-to-noise ratio requested for good reception is then compared to the values obtained by simulation.

The complete assembled “CPHY in T2” demonstrator used to carry on these tests is shown in Fig. 21 and Fig. 22.

2) *Future Work:* The first-generation demonstrators presented in this paper have been used to demonstrate both the CPHY concept and a possible broadband/broadcast convergent scenario with the insertion of CPHY traffic within DVB-T2 FEFs. However, only a limited set of the CPHY system parameters have been implemented and tested so far. The next tasks will involve implementing the missing modes in the CPHY demonstrator in order to achieve performance assessment.

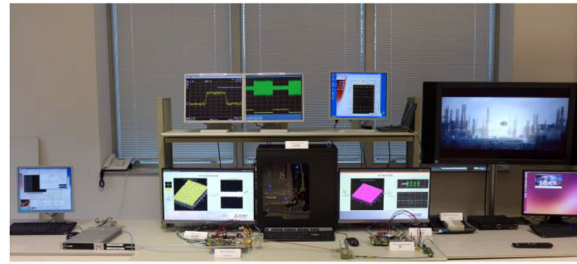


Fig. 21. “CPHY in T2” overall platform: (from left to right) the DVB and CPHY video sources, the DVB-T2 and CPHY transmitters, the DVB frame splitter and CPHY receiver, the CPHY receiver control displays, DVB-T2 receiver control display, the HD widescreen for DVB-T2 video, the screen for the low-resolution CPHY video.

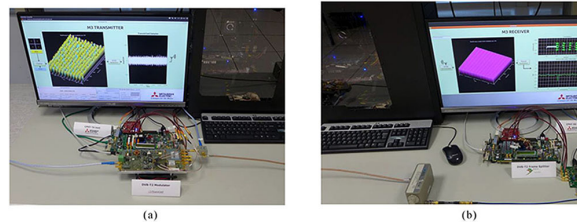


Fig. 22. (a) “CPHY in T2” transmitter: The DVB-T2 modulator (front) the CPHY Tx interface board (rear), the CPHY transmitter control display (b) “CPHY in T2” receiver: The DVB-T2 frame splitter (front), the CPHY Rx interface board (rear), the CPHY receiver control display.

V. CONCLUSION

This paper argues in favor of a broadband-broadcast convergence through the concept of common physical layer, providing a good basis for coverage cooperation between broadcast and mobile networks, while relying on non-dedicated mobile receivers.

General technical requirements for the design of such specifications have been given and a practical example of common physical layer based on the 3GPP LTE/E-MBMS and DVB-T2 standards has been described. Then, the successive steps of the proof of concept demonstration of proposed unified broadcast layer have been presented: simulation results have proved the advantages of introducing time interleaving into 3GPP E-MBMS; the implementation of a hardware platform and subsequent validation tests have demonstrated the common physical layer feasibility as well as its embedding into a DVB-T2 future extension frame (FEF).

Additional laboratory tests with terrestrial/satellite hardware channel emulators and field trials have still to be carried out in order to complete the overall proof of concept demonstration. Nevertheless, the work already done has proved the technical feasibility and the relevance of such a common physical layer approach. Such a convergent approach appears to be a relevant work item in FoBTv’s work on the next generation terrestrial broadcast systems.

The remaining issues mainly concern upper layers, signaling and, beyond physical layer, the idea of cooperation/convergence at the network architecture level has to be considered. In particular, some kind of synchronization

would be required between both networks and network infrastructures should be modified in order to create interconnections and insert gateways.

ACKNOWLEDGMENT

The authors would like to warmly thank all the Mobile MultiMedia (M³) project partners for the numerous and fruitful discussions that contributed to the maturation of the concepts outlined in this paper.

REFERENCES

- [1] CISCO White Paper. (2013, Feb.). "Cisco visual networking index: Global mobile data traffic forecast update, 2013–2018." [Online]. Available: http://www.cisco.com/c/en/us/solutions/collateral/service-provider/visual-networking-index-vni/white_paper_c11-520862.html
- [2] [Online]. Available: http://www.ieee802.org/11/Reports/hew_update.htm
- [3] [Online]. Available: http://www.nttdocomo.co.jp/english/binary/pdf/corporate/technology/rd/technical_journal/bn/vol14_3/vol14_3_051en.pdf
- [4] [Online]. Available: <http://www.3gpp.org/Release-9>
- [5] *Digital Video Broadcasting (DVB), Transmission System for Handheld Terminals (DVB-H)*, ETSI Standard EN 302 304, V1.1.1, Nov. 2004.
- [6] [Online]. Available: <http://en.wikipedia.org/wiki/MediaFLO>
- [7] *Forward Link Only Air Interface; Specification for Terrestrial Mobile; Multimedia Multicast*, ETSI Standard TS 102 589, V1.1.1, Feb. 2009.
- [8] *Digital Video Broadcasting (DVB), Framing Structure, Channel Coding and Modulation for Satellite Services to Handheld Devices (SH) Below 3 GHz*, ETSI Standard EN 302 583, V1.1.1, Mar. 2008.
- [9] *Digital Video Broadcasting (DVB); Frame Structure Channel Coding and Modulation for a Second Generation Digital Terrestrial Television Broadcasting System (DVB-T2)*, ETSI Standard EN 302 755, V1.3.1, Oct. 2011.
- [10] *Digital Video Broadcasting (DVB); Next Generation Broadcasting System to Handheld, Physical Layer Specification (DVB-NGH)*, DVB Bluebook Standard A160, Nov. 2012.
- [11] *Digital Video Broadcasting (DVB); Implementation Guidelines for a Second Generation Digital Terrestrial Television Broadcasting System (DVB-T2)*, ETSI Standard TS 102 831, V1.2.1, Feb. 2012.
- [12] C. Gallard *et al.*, "Universal DVB-3GPP broadcast layer: An enabler for new business in mobile broadcasting landscape," in *Next Generation Mobile Broadcasting*, D. Gómez-Barquero Ed. Hoboken, NJ, USA: CRC Press, 2013.
- [13] F. Pérez-Fontán, M. Vázquez-Castro, C.E. Cabado, J. Pita García, and E. Kubista, "Statistical modelling of the LMS channel," *IEEE Trans. Veh. Tech.*, vol. 50, no.6, pp. 1549–1567, Nov. 2001.
- [14] *Digital Video Broadcasting (DVB); DVB-SH Implementation Guidelines*, ETSI Standard TS 102 584, V1.2.1, Jan. 2011.
- [15] *3rd Generation Partnership Project (3GPP) Long Term Evolution (LTE); Evolved Universal Terrestrial Radio Access (E-UTRA); Physical Channels and Modulation (3GPP TS 36.211 Release 8)*, ETSI standard TS 136 211 V8.9.0, Jan. 2010.



Matthieu Crussière received the M.Sc. and Ph.D. degrees in electrical engineering from the National Institute of Applied Sciences (INSA), Rennes, France, in 2002 and 2005, respectively. Since 2005, he has been an Associate Professor with the Department of Telecommunications and Electrical Engineering at INSA, and currently leads his research activities with the Electronics and Telecommunications Institute of Rennes, Rennes, France. His current research interests include digital communications and signal processing techniques.

His works focus on the optimization of high-bit rate communications, resource allocation mechanisms, adaptive system design based on multicarrier, and multi-antenna schemes. He is the author or co-author of over 80 technical papers in international conferences and journals. He has been involved in several European and French national research projects in the field of powerline, broadcasting, ultra wideband, and mobile radio communications.



Catherine Douillard received the engineer degree in telecommunications from the Ecole Nationale Supérieure des Télécommunications Bretagne, Plouzané, France, in 1988, the Ph.D. degree in electrical engineering from the University of Western Brittany, Brest, France, in 1992, the accreditation to supervise research from University of Southern Brittany, Lorient, France, in 2004. She is currently a Professor with the Electronics Department of Telecom Bretagne, Plouzané, France, where she is in charge of the Algorithm-Silicon Interaction Research team. Her current research interests include turbo codes and iterative decoding, iterative detection, the efficient combination of high spectral efficiency modulation and turbo coding together with diversity techniques and turbo processing for multicarrier, multi-antenna, multiple access transmission systems. In 2009, she received the SEE/II Glavieux Award for her contribution to standards and related industrial impacts.



Christian Gallard received the engineering degree from the Ecole Supérieure d'Électronique de l'Océan (ESEO), Angers, France, in 1996. From 1996 to 2000, he worked with Matra Communications in the area of digital communications applications for Professional Mobile Radio. From 2000 to 2002, he worked on digital communications in a UMTS context with Philips Consumer Communications (France) for layer simulations. From 2002 to 2004, he worked as a sub-contractor with France Telecom, working on speech processing, UMTS FDD, and MIMO issues. He joined France Telecom in 2004. From 2005 to 2006, he worked on WiMAX issues (WiMAX Forum, link layer simulations). From 2006 to 2007, he was involved in elaboration of 3GPP LTE standard (RAN1 meetings, system level simulations, link layer simulations). Since the end of 2007, he has been involved in the definition of broadcasting systems (standardization of DVB-T2, DVB-NGH, B21C, ENGINES Celtic projects). From 2010 to 2013, he led the French collaborative M3 (Mobile Multi-Media) project. He is currently a Research Project Coordinator inside Orange (studies on enablers in digital communications, propagation channel modelling, antennas design for future networks including 5G).



Marie Le Bot received the engineering degree from the Ecole Centrale de Nantes, Nantes, France, in 1997, and the Ph.D. degree in electronics and communications from the Conservatoire National des Arts et Métiers, Paris, France, in 2001. Since then, she has been working as a Research Engineer with Orange Labs, Rennes, France, in digital signal processing, dimensioning and resource management in wireless networks (GSM, UMTS, HSPA, LTE), and power-line communications. Her current research interests include mobile broadcasting systems and the reduction of energy consumption in home networks.



Benjamin Ros graduated from the University of Rennes 1, Rennes, France, in electrical and telecommunications engineering in 2005. He has first worked on signal processing algorithms for GNSS receivers. Since 2007, he has been working as an Air Interface Engineer with the Telecommunications Department at French Space Agency on topics such as waveforms optimization over satellite mobile channel, channel sounding, and satellite system optimization.



Arnaud Bouttier was born in Le Mans, France, in 1969. In 1992, he received the Master of Sciences in signal processing from the University of Rennes 1, Rennes, France. He graduated from the Engineering School Ecole Nationale Supérieure des Télécommunications de Bretagne, Plouzané, France, in 1994. He received the Ph.D. degree from the University of Rennes 1 in 2000. During his Ph.D., his research was focused on blind equalization by means of adaptive trellis filtering. He joined MERCE, formerly ITE-TCL, in 2000, with the task

to acquire on knowledge digital implementation of telecommunication systems. He is currently a Project Leader with the development of hardware evaluation platforms in the Wireless Communication Systems team with an emphasis on satellite and terrestrial broadcasting. He was involved in several collaborative projects dealing with broadband and broadcasting technologies (IST 4MORE, ANR APOGEE, CELTIC WINNER+, CELTIC ENGINES, and ANR M3).



Alain Untersee received the engineering degree in electronics from the National Electronics Engineering School, Grenoble, France. After spending several years in large French groups, in 1988, he co-founded the Innovation in Telecommunications, Image, and Sound (ITIS) Company, where he held the position as a Sales Director. He developed the worldwide sales of professional equipment for Terrestrial Digital TV and Digital Radio networks. He joined TeamCast in 2007, where he is taking care of the involvement of TeamCast in collabora-

tive research projects at the French and international levels (preparation of proposals, management of projects).

Selected Article

M. Liu, M. Crussière, J.F. Héland, "A novel data-aided channel estimation with reduced complexity for TDS-OFDM systems", IEEE Transaction on Broadcasting, Vol. 58, Issue 2, pp 247–260, June 2012, DOI :10.1109/TBC.2012.2184152

Abstract

In contrast to the classical cyclic prefix (CP)-OFDM, the time domain synchronous (TDS)-OFDM employs a known pseudo noise (PN) sequence as guard interval (GI). Conventional channel estimation methods for TDS-OFDM are based on the exploitation of the PN sequence and consequently suffer from intersymbol interference (ISI). This paper proposes a novel data-aided channel estimation method which combines the channel estimates obtained from the PN sequence and, most importantly, additional channel estimates extracted from OFDM data symbols. Data-aided channel estimation is carried out using the rebuilt OFDM data symbols as virtual training sequences. In contrast to the classical turbo channel estimation, interleaving and decoding functions are not included in the feedback loop when rebuilding OFDM data symbols thereby reducing the complexity. Several improved techniques are proposed to refine the data-aided channel estimates, namely one-dimensional (1-D)/two-dimensional (2-D) moving average and Wiener filtering. Finally, the MMSE criteria are used to obtain the best combination results and an iterative process is proposed to progressively refine the estimation. Both MSE and BER simulations using specifications of the DTMB system are carried out to prove the effectiveness of the proposed algorithm even in very harsh channel conditions such as in the single frequency network (SFN) case.

Keywords : TV broadcasting, Channel estimation, iterative method, OFDM, TDS-OFDM

Selected Article

A. Khalil, M. Crussière, J.F. Hélard, "Time-frequency spectrum sharing scheme for next generation OFDM systems", *EURASIP Journal on Wireless Communications and Networking*, December 2010, DOI :10.1155/2010/598707

Abstract

Spectrum sharing and multiple-access techniques are challenging matters for future wireless communication systems. Orthogonal frequency division multiplexing (OFDM) has been considered as the most important physical layer candidate for the next generation wireless systems. Alternatively, multiband OFDM (MB-OFDM) approach has shown some novelty and efficiency for high-rate (HR) WPAN applications and so has been selected for future HR ultrawideband (UWB) systems. Based on an optimization problem formulation, we jointly consider resource allocation and scheduling to define a novel dynamic time-frequency spectrum sharing mechanism based on the MB-OFDM approach. Viewed as a cross-layer solution, the proposed MB-OFDM multiple-access (MB-OFDM-MA) scheme can achieve an efficient multiuser spectrum sharing under QoS constraints. While the optimization formulation results in a high-complexity time-frequency sharing solution, we propose a low-complexity suboptimal solution able to jointly provide fairness provision with the QoS support. Compared with traditional orthogonal frequency division multiple access (OFDMA), the simple time-frequency MB-OFDM-MA approach ensures a high level of fairness among the users while satisfying high-priority users having strict QoS requirements.

Keywords : MB-OFDM, WPAN, Resource allocation, Spectrum sharing, Optimization

Research Article

Time-Frequency Spectrum Sharing Scheme for Next Generation OFDM Systems**Ayman Khalil, Matthieu Crussière, and Jean-françois H elard***European University of Brittany (UEB) and Institute of Electronics and Telecommunications of Rennes (IETR), INSA, 20 Avenue des Buttes de Co smes, 35708 Rennes, France*

Correspondence should be addressed to Ayman Khalil, ayman.khalil@insa-rennes.fr

Received 23 July 2010; Revised 17 November 2010; Accepted 13 December 2010

Academic Editor: Kwan L. Yeung

Copyright   2010 Ayman Khalil et al. This is an open access article distributed under the Creative Commons Attribution License, which permits unrestricted use, distribution, and reproduction in any medium, provided the original work is properly cited.

Spectrum sharing and multiple-access techniques are challenging matters for future wireless communication systems. Orthogonal frequency division multiplexing (OFDM) has been considered as the most important physical layer candidate for the next generation wireless systems. Alternatively, multiband OFDM (MB-OFDM) approach has shown some novelty and efficiency for high-rate (HR) WPAN applications and so has been selected for future HR ultrawideband (UWB) systems. Based on an optimization problem formulation, we jointly consider resource allocation and scheduling to define a novel dynamic time-frequency spectrum sharing mechanism based on the MB-OFDM approach. Viewed as a cross-layer solution, the proposed MB-OFDM multiple-access (MB-OFDM-MA) scheme can achieve an efficient multiuser spectrum sharing under QoS constraints. While the optimization formulation results in a high-complexity time-frequency sharing solution, we propose a low-complexity suboptimal solution able to jointly provide fairness provision with the QoS support. Compared with traditional orthogonal frequency division multiple access (OFDMA), the simple time-frequency MB-OFDM-MA approach ensures a high level of fairness among the users while satisfying high-priority users having strict QoS requirements.

1. Introduction

Orthogonal frequency division multiplexing (OFDM) is a powerful scheme that is slated to be employed in the next generation wireless systems such as Long-Term Evolution (LTE), Worldwide Interoperability for Microwave Access (WiMAX), and high-speed WLAN standards such as 802.11n. It is expected to provide good performance at the physical layer and to enable efficient multiple-access mechanisms by employing orthogonal frequency multiple access (OFDMA) technique [1]. Thereby, in a multiuser context, the performance of OFDMA has to be linked to efficient and low-complexity spectrum sharing schemes that can respect the wireless channel conditions and satisfy the different users demands.

In the literature, the spectrum sharing issue is addressed either as a resource allocation problem using optimization strategies or as a time scheduling problem. Several studies investigate adaptive resource allocation for OFDMA systems using constrained optimization techniques [2–4]. Either

considering margin adaptive or rate adaptive optimization techniques, all the resulting algorithms are nonlinear and have high computational complexity. Suboptimal algorithms are thus proposed in these studies to reduce the complexity. On the other hand, the studies that deal with scheduling in the time domain do not consider physical layer issues [5]. Few research works consider jointly the scheduling and the resource allocation matters. In [6], scheduling algorithms are developed for IEEE802.16d OFDMA-based broadband wireless access systems. In these algorithms, radio resource is dynamically shared by the users in both time and frequency domains. Fairness is ensured in this study but performance of the proposed algorithms is not examined for real-time applications. The authors in [7] define a joint resource allocation and scheduling scheme for IEEE 802.16 systems but without investigating optimization issues.

Alternatively to OFDM, multiband OFDM (MB-OFDM) is a new transmission technique proposed for high-rate (HR) ultrawideband (UWB) systems and supported by the WiMedia alliance [8, 9]. It consists in combining OFDM with

TABLE 1: WiMedia data rates and associated parameter λ .

Data rate (Mbps)	Modulation	Coding rate (r)	Frequency domain spreading	Time spreading factor (TSF)	Code bits per OFDM symbol	λ
53.3	QPSK	1/3	Yes	2	100	1.49
80	QPSK	1/2	Yes	2	100	1.57
110	QPSK	11/32	No	2	200	1.52
160	QPSK	1/2	No	2	200	1.57
200	QPSK	5/8	No	2	200	1.82
320	DCM	1/2	No	1	200	1.85
400	DCM	5/8	No	1	200	1.82
480	DCM	3/4	No	1	200	1.80

multiband technique that divides the available bandwidth into subbands or blocks of subcarriers. Spectrum sharing and resource allocation are topics of interest in MB-OFDM-based systems. To this date, however, related research works are still limited.

Some research studies on MB-OFDM UWB systems have been strictly devoted to physical layer issues or have addressed the question of resource allocation yet without taking into consideration the MAC layer constraints. In [10], for instance, in order to improve the BER performance, an adaptive carrier selection and power allocation is proposed. An optimal algorithm with Lagrange multiplier method is derived. Based on the channel state information (CSI), the carriers and the power are dynamically allocated with the constraint of fixed data rate and fixed total power. In [11], the authors propose two power allocation schemes to maximize the total capacity for single-band OFDM UWB transmissions with space-time codes, under the assumption of perfect and partial CSI at the transmitter. The results show that the water-filling scheme provides the smallest outage probability while the scheme with limited CSI feedback has lower feedback overhead and slight performance loss. In [12], a power allocation scheme is proposed for clustered MB-OFDM. In this study, a cluster which is a group of subcarriers is dynamically assigned a unique power in order to maximize the total system throughput. The results show that the proposed solution, with its low complexity, has a performance close to the one of a standard water-filling scheme.

A cross-layer subband and power allocation scheme is proposed in [13] for the multiband UWB systems. The subband and power assignment problem is formulated as an optimization problem whose goal is to minimize the total power under the condition that all users achieve their requested data rates. A low-complexity fast suboptimal algorithm is also proposed to reduce the complexity of the formulated problem. Although this latter study exploits information laying in the physical and MAC layers, some aspects are not ensured in the proposed resource allocation scheme. The QoS support, for instance, is not fully exploited since no service differentiation scheme is defined.

Based on optimization problem formulation and with respect to a study on the multiuser resource allocation for MB-OFDM UWB systems [14], the goal of this paper is to

define a novel time-frequency MB-OFDM multiple-access (MB-OFDM-MA) scheme using a cross-layer approach and a joint consideration of resource allocation and scheduling. This scheme should be able to overcome the complexity limitation of the resource allocation in OFDMA systems while guaranteeing a high system performance and a good level of QoS and fairness provision. The paper is organized as follows. In Section 2, we present the MB-OFDM system model. An analytical study based on optimization problem formulation is given in Section 3. A joint resource allocation and scheduling optimization is derived leading to a time-frequency spectrum sharing optimization model. In order to reduce the complexity of the defined joint optimization, we present in Section 4 a novel low-complexity time-frequency spectrum sharing solution based on suboptimal subband allocation and scheduling solutions. The new proposed multiuser spectrum sharing scheme proves its ability to provide jointly fairness among users and QoS support for high-priority users. Finally, Section 5 presents simulation results showing the efficiency of the new multiuser scheme by evaluating the performance of the different users in terms of multiple QoS satisfaction metrics. Besides, some comparisons between the novel MB-OFDM-MA solution and the OFDMA scheme are drawn.

2. MB-OFDM System Model

In this section, we present the MB-OFDM solution as proposed by the WiMedia solution [8]. Thereby, the WiMedia MB-OFDM scheme consists in combining OFDM with a multiband technique that divides the available band into 14 subbands of 528 MHz each. An OFDM modulation with 128 subcarriers is applied on each subband separately. Different data rates from 53.3 to 480 Mbps are obtained with the combined use of forward error correction (FEC), frequency-domain spreading (FDS), and time-domain spreading (TDS), as presented in Table 1. The constellation applied to the different subcarriers is either a quadrature phase-shift keying (QPSK) for low data rates or a dual carrier modulation (DCM) for high data rates. Note that in Table 1, a new parameter λ is introduced. This parameter will be defined in the next section and used for the exploitation of the CSI. Moreover, it is possible in the

WiMedia solution to exploit the two or three subbands of one band group through the use of a so-called time frequency code (TFC). TFC defines frequency hopping patterns applied to consecutive OFDM symbols. Without considering the resource allocation matter, TFC allows each user to benefit from frequency diversity over a bandwidth equivalent to the two or three subbands of one channel. However, the TFC strategy lacks in the ability to allocate bands optimally since the available bands are not assigned to each user according to its channel condition. We have thus to look for an alternative of the TFC in order to allocate the resources in an adaptive way that responds to the heterogeneous QoS requirements.

3. Analytical Study

3.1. Channel Information. In order to be aware of the physical conditions in the perspective of the resource allocation scheme, there is a need to exploit some channel parameters reflecting the channel quality of each user aiming at accessing the network. Assuming that the instantaneous signal to interference and noise ratio (SINR) for each subcarrier is known by each user through the CSI acquisition, it is possible to estimate the system level performance in terms of BER by using the effective SINR approach [15]. Note that the CSI is simply obtained through channel estimation process at each user station. Proposed in the 3GPP standardization, the effective SINR approach has been used as an effective link to system mapping method. The basic idea is to find a compression function that maps each sequence of varying SINRs to a single value that is correlated with the BER. This can be stated as

$$\text{SINR}_{\text{eff}} = -\lambda \left[\frac{1}{N} \sum_{i=1}^N \exp\left(-\frac{\text{SINR}_i}{\lambda}\right) \right], \quad (1)$$

where N is the number of subcarriers in a subband, SINR_i is the ratio of signal to interference and noise for the i th subcarrier, and λ is a scaling factor that depends on the selected modulation and coding scheme (MCS).

In order to apply the effective SINR mapping method to MB-OFDM systems, we evaluate the value of λ for the eight data rate modes of the WiMedia system as presented in Table 1.

In practice, based on the CSI knowledge, each user is capable to compute the effective SINR value in each subband by using (1). For instance, in the case of one channel divided into $B = 3$ subbands, and with $K = 3$ users, the physical layer information is reduced to the knowledge of only $B \times K = 9$ effective SINR scalar values.

3.2. Optimization Problem Formulation. In order to meet the QoS requirements of multimedia and real-time services, we formulate an optimization problem based on a service differentiation principle. A two-class-based model is defined as follows: class 1 is referred to as hard-QoS class for real-time or multimedia applications that require strict QoS requirements (i.e., multimedia applications), and class 2 is referred to as soft-QoS class for nonreal-time or data applications having less QoS constraints (i.e., data applications).

We consider a system that consists of K UWB users aiming at accessing the network. The users are classified into two groups; the first K_h users are hard-QoS users and the remaining $K - K_h$ users are soft-QoS users. We first derive the expression of the rate used for the problem formulation. The rate of a user k in a subband b is expressed as

$$r_{k,b} = \log_2(1 + P_{k,b}E_{k,b}), \quad (2)$$

where $P_{k,b}$ is the allocated power of user k in subband b and $E_{k,b}$ the effective SINR of user k in subband b . The optimization problem can thus be formulated as

$$\max_{S_k, P_{k,b}} \sum_{k=K_h+1}^K \sum_{b \in S_k} r_{k,b}$$

$$\text{subject to } \sum_{b \in S_k} r_{k,b} \geq R_k, \quad k = 1, \dots, K_h \quad (3)$$

$$\sum_{k=1}^K \sum_{b=1}^B P_{k,b} \leq P_T,$$

where B is the total number of subbands, R_k is the hard-QoS user k required data rate, and S_k is the set of subbands assigned to user k . In our case, S_1, S_2, \dots, S_K are disjoint and each user is assigned one subband during one time interval. This problem is a mixed integer linear programming problem since S_k are integer variables. Consequently, the problem is classified as NP-hard. A method that makes the problem solvable is to relax the constraint that each subband is assigned to one user only. The idea is to allow the users to time-share each subband by defining a new parameter $\omega_{k,b}$, which represents the time-sharing factor for user k in subband b . The optimization problem can then be stated as

$$\max_{P_{k,b}, \omega_{k,b}} \sum_{k=K_h+1}^K \sum_{b=1}^B \omega_{k,b} \log_2 \left(1 + \frac{P_{k,b}E_{k,b}}{\omega_{k,b}} \right)$$

$$\text{subject to } \sum_{b=1}^B \omega_{k,b} \log_2 \left(1 + \frac{P_{k,b}E_{k,b}}{\omega_{k,b}} \right) \geq R_k, \quad k = 1, \dots, K_h,$$

$$\sum_{k=1}^K \omega_{k,b} = 1, \quad \forall b \quad 0 \leq \omega_{k,b} \leq 1 \quad \forall k, b,$$

$$\sum_{k=1}^K \sum_{b=1}^B P_{k,b} \leq P_T. \quad (4)$$

Consequently, using the properties of a convex optimization problem, we derive the Lagrangian of the problem

$$\begin{aligned} L = & \sum_{k=K_h+1}^K \sum_{b=1}^B \omega_{k,b} \log_2 \left(1 + \frac{P_{k,b}E_{k,b}}{\omega_{k,b}} \right) \\ & + \sum_{k=1}^{K_h} \alpha_k \left(\sum_{b=1}^B \omega_{k,b} \log_2 \left(1 + \frac{P_{k,b}E_{k,b}}{\omega_{k,b}} \right) - R_k \right) \\ & + \sum_{b=1}^B \beta_b \left(1 - \sum_{k=1}^K \omega_{k,b} \right) + \gamma \left(P_T - \sum_{k=1}^K \sum_{b=1}^B P_{k,b} \right), \end{aligned} \quad (5)$$

where α_k , β_b , and γ are the Lagrange multipliers for the different constraints of the optimization problem. Besides, to find the optimal solution of the problem, we need the Karush-Kuhn-Tucker or KKT conditions. Let $\omega_{k,b}^*$ and $P_{k,b}^*$ denote the optimal solution, the KKT conditions of the formulated problem are given by

$$(1) \begin{cases} \frac{\partial L}{\partial P_{k,b}} = 0, & P_{k,b}^* > 0, \\ < 0, & P_{k,b}^* = 0 \end{cases}$$

$$(2) \begin{cases} < 0, & \omega_{k,b}^* = 0 \\ \frac{\partial L}{\partial \omega_{k,b}^*} = 0, & \omega_{k,b}^* \in]0, 1[, \\ > 0, & \omega_{k,b}^* = 1 \end{cases} \quad (6)$$

$$(3) \alpha_k \left(\sum_{b=1}^B \omega_{k,b} \log_2 \left(1 + \frac{P_{k,b} E_{k,b}}{\omega_{k,b}} \right) - R_k \right) = 0.$$

Applying the first KKT condition, we obtain

$$P_{k,b}^* = \omega_{k,b} \left(\frac{\alpha_k}{\gamma \ln 2} - \frac{1}{E_{k,b}} \right), \quad \text{for } k = 1, \dots, K_h, \quad (7)$$

$$P_{k,b}^* = \omega_{k,b} \left(\frac{1}{\gamma \ln 2} - \frac{1}{E_{k,b}} \right), \quad \text{for } k = K_h + 1, \dots, K.$$

Then, the second KKT condition derives

$$\alpha_k \left[\log_2 \left(1 + \frac{E_{k,b} P_{k,b}}{\omega_{k,b}} \right) - \frac{1}{\ln 2} \left(\frac{E_{k,b} P_{k,b}}{\omega_{k,b} + E_{k,b} P_{k,b}} \right) \right] - \beta_b = 0, \quad \text{for } k = 1, \dots, K_h,$$

$$\log_2 \left(1 + \frac{E_{k,b} P_{k,b}}{\omega_{k,b}} \right) - \frac{1}{\ln 2} \left(\frac{E_{k,b} P_{k,b}}{\omega_{k,b} + E_{k,b} P_{k,b}} \right) - \beta_b = 0, \quad \text{for } k = K_h + 1, \dots, K. \quad (8)$$

Substituting (7) into (8), we get

$$\alpha_k \left[\log_2 \left(\frac{\alpha_k E_{k,b}}{\gamma \ln 2} \right) - \frac{1}{\ln 2} \left(1 - \frac{\gamma \ln 2}{\alpha_k E_{k,b}} \right) \right] - \beta_b = 0, \quad \text{for } k = 1, \dots, K_h, \quad (9)$$

$$\log_2 \left(\frac{E_{k,b}}{\gamma \ln 2} \right) - \frac{1}{\ln 2} \left(1 - \frac{\gamma \ln 2}{E_{k,b}} \right) - \beta_b = 0, \quad \text{for } k = K_h + 1, \dots, K.$$

After having used the time-sharing factor to find the optimal solution, we now go backward and enforce that one subband is assigned to one user only during one time interval. Therefore, we consider that $\omega_{k,b}$ cannot take values other than 0 or 1. Consequently,

$$\omega_{k,b}^* = \begin{cases} 1, & H_{k,b} > \beta_b \\ 0, & H_{k,b} < \beta_b, \end{cases} \quad (10)$$

where $H_{k,b}$ is defined as

$$H_{k,b} = \alpha_k \left[\log_2 \left(\frac{\alpha_k E_{k,b}}{\gamma \ln 2} \right) - \frac{1}{\ln 2} \left(1 - \frac{\gamma \ln 2}{E_{k,b}} \right) \right], \quad \text{for } k = 1, \dots, K_h, \quad (11)$$

$$H_{k,b} \log_2 \left(\frac{E_{k,b}}{\gamma \ln 2} \right) - \frac{1}{\ln 2} \left(1 - \frac{\gamma \ln 2}{E_{k,b}} \right), \quad \text{for } k = K_h + 1, \dots, K.$$

We conclude that, for a selected subband b , the user k having the highest $H_{k,b}$ is assigned the subband. In other words, for a subband b , if $H_{k,b}$ are different for all k , then

$$\omega_{k',b}^* = 1, \quad \omega_{k,b}^* = 0 \quad \forall k \neq k', \quad (12)$$

where

$$k' = \arg \max_k H_{k,b}. \quad (13)$$

Afterwards, we derive the last KKT condition that characterizes the hard-QoS users rate constraint

$$R'_{k,b} = \sum_{b=1}^B \omega_{k,b} \log_2 \left(1 + \frac{P_{k,b} E_{k,b}}{\omega_{k,b}} \right) \geq R_k. \quad (14)$$

Substituting (7) into (14), we get

$$R'_{k,b} = \sum_{b=1}^B \omega_{k,b} \log_2 \left(\frac{\alpha_k E_{k,b}}{\gamma \ln 2} \right) \geq R_k. \quad (15)$$

As a result, to obtain the optimal solution, we have to compute the optimal power allocation function $P_{k,b}$ and the optimal subband allocation function $H_{k,b}$. To do so, we need to find the set of α_k such that the hard-QoS users rate constraint given in (15) is satisfied.

3.3. Optimal Spectrum Allocation Algorithm. To solve the formulated optimization problem, we first study the characteristics of the subband and power allocation functions given in (7) and (11), respectively. These two functions have the following properties. (i) First, they are monotonically increasing with respect to $E_{k,b}$. This means that, for a selected subband, the user having better channel conditions has more chance to be assigned this subband with a good power level. (ii) Second, the two allocation functions are monotonically increasing with respect to α_k . This can be viewed as a result of the service differentiation principle. In other terms, the functions depend on the user priority, and, thus, the stricter the user requirements, the higher the value of α_k and consequently the higher the value of these functions. (iii) Third, we conclude from the hard-QoS users constraint given in (15) that α_k is monotonically increasing with respect to R_k . As a result, the power and the subband allocation functions depend on the rate constraints of the users, in particular the hard-QoS users which have strict data rate requirements.

Based on the above observations, we propose an iterative algorithm for the search of the optimal subband allocation.

- (1) **Initialization**
 $\alpha = 1$;
 $\alpha_k = \alpha + \delta$, for $k = 1, \dots, k_h$
- (2) **Subband allocation**
 (a) **for** subband $b = 1, \dots, B$
 compute $H_{k,b}$ using (11) for all k
 obtain $\omega_{k,b}$ and k' using (12) and (13)
 (b) **for** $k = 1, \dots, k_h$
 compute R'_k using (15)
 (c) **for** $k = 1, \dots, k_h$
 find \tilde{k} with $R'_k < R_{\tilde{k}}$ and $R'_k - R_{\tilde{k}} \leq R'_k - R_k$
 (d) **while** $R'_k < R_{\tilde{k}}$
 $\alpha_{\tilde{k}} = \alpha_{\tilde{k}} + \delta$
 repeat (a), (b) and (c)
- (3) **Power allocation**
 (a) compute $P_{k,b}$ using (7) for all k
 (b) compute $P'_T = \sum_{k=1}^K \sum_{b=1}^B P_{k,b}$
 (c) **if** $P'_T < P_T$
 $\alpha_{\tilde{k}} = \alpha_{\tilde{k}} + \delta/2$
 else
 $\alpha_{\tilde{k}} = \alpha_{\tilde{k}} - \delta/2$
 repeat (2) and (3) until $P'_T = P_T$

ALGORITHM 1: Iterative algorithm for optimal power and subband allocation.

The process consists in incrementing α_k iteratively by a small value δ until reaching the hard-QoS users data rate request while respecting the power constraint.

As shown in Algorithm 1. We first start by initializing α_k by a value slightly greater than one. Then, we process the subband allocation based on the defined α_k value by computing $H_{k,b}$ using (11) and finding $\omega_{k,b}$ and k' using (12) and (13). We test afterwards the rate constraint of the hard-QoS users by using (15). While there are hard-QoS users not satisfying their rate constraints, we increment their corresponding α_k values by δ .

Next, based on the obtained α_k values we process the power allocation by using (7). We then check the total power constraint. If we find that the total power exceeds the imposed total power, we decrement the α_k values by half the value of δ ; otherwise, we increment it by half of the same value.

Interestingly, due to the banding approach, MB-OFDM-MA reduces the complexity of the subcarrier assignment required in OFDMA which is considered as a combinatorial optimization problem with high computational complexity. On the other hand, an additional complexity arises in the derived optimal subband allocation. This complexity resides in the iterative process required by the optimal subband allocation function to find the set of α_k .

3.4. Time-Frequency Spectrum Sharing Optimization. From a physical perspective, metrics such as spectrum efficiency and minimum BER are the most important constraints to be considered. On the other hand, from a user perspective, QoS as well as fairness among the users are of great importance. Thereby, in order to increase the freedom

level of the frequency resource allocation, we propose a joint resource allocation and scheduling model leading to a multiuser time-frequency spectrum sharing scheme. Based on the optimal allocation function derived in (11), we define hereafter a multiuser time-frequency optimization scheme that should allow different users to coexist in one subband while respecting the QoS requirements.

In the WiMedia solution, the channel time is divided into superframes; a superframe is the basic timing structure for frame exchange and is composed of two major parts: the beacon period (BP) and the data transfer period (DTP). The duration of the superframe is specified as $65536 \mu s$, and the superframe consists of 256 medium access slots (MASs), which are all of equal length, $256 \mu s$.

Thereby, three users can coexist in the same channel that consists of three subbands in the case of one MB-OFDM channel. The idea is thus to share the MASs of a superframe among multiple users whereas three users can transmit simultaneously in each MAS.

While B and K are the number of subbands and the total number of users, respectively, the idea is to classify the K users into two groups: a high-priority (HP) group of B users and a low-priority (LP) group of $K - B$ users. To do so, we arrange the K users in a decreasing order according to their $H_{k,b}$ values given by (11).

A first subband allocation is achieved; the HP users are assigned subbands according to their priority order; the highest priority user is assigned its most powerful subband, that is the subband having the greatest $E_{k,b}$ value.

After the first allocation, the remaining $K - B$ LP users are reclassified according to a new allocation function defined as the average of their $H_{k,b}$ values over the B subbands

$$\bar{H}_{k,b} = \frac{\sum_{b=1}^B H_{k,b}}{B}, \quad k = B + 1, \dots, K. \quad (16)$$

This modified metric is justified by the fact that these $K - B$ users do not have any assigned subband yet and that all the available subbands are already assigned to the HP users. Actually, we have to allow the LP group to share the assigned subbands with the HP group in an efficient time sharing way that respects all the QoS constraints. As this time sharing principle should respect the QoS support, the new allocation problem consists in finding, for each user in the LP group, the corresponding subband that maximizes its rate while minimizing the loss of rate of the HP user already occupying the subband. The problem can be formulated as

$$\begin{aligned} \max_b r_{k',b}, \quad k' = B + 1, \dots, K \\ \text{subject to } r_{k,b} \geq R_{k \min}, \quad k = 1, \dots, B, \end{aligned} \quad (17)$$

where $R_{k \min}$ is the minimum tolerable data rate value of the HP user k . To solve this optimization problem, we introduce a subband sharing factor τ_b defined as

$$\tau_b = \frac{H_{k,b}}{\bar{H}_{k',b}}, \quad (18)$$

where $H_{k,b}$ and $\bar{H}_{k',b}$ are the allocation functions for the HP user k and the LP user k' , respectively. This sharing factor

actually represents the spectrum usage advantage of the HP users on the LP users. Consequently, the sharing coefficients of HP user k and LP user k' in subband b are, respectively, defined as

$$\tau_{k,b} = \frac{\tau_b}{1 + \tau_b}, \quad \tau_{k',b} = \frac{1}{1 + \tau_b}, \quad (19)$$

and it is important to note that $\tau_{k,b} + \tau_{k',b} = 1$, which indicates that the subband is occupied at 100% of the time. As a result, the new data rates of users k and k' sharing the same subband b are now defined by

$$r_{k,b}^* = \tau_{k,b} r_{k,b}, \quad r_{k',b}^* = \tau_{k',b} r_{k',b}. \quad (20)$$

The solution of the sharing optimization problem given in (20) is then obtained by using a priority-based approach. Indeed, the time sharing is processed according to the classification of the LP users. Thus, the highest priority user in this LP group first starts a heuristic search for the corresponding subband that responds to (17) by using (20). The process is iterated for all the remaining LP users.

To better illustrate the proposed optimization spectrum sharing scheme, we present hereafter a case of six users aiming at sharing the three subbands of the WiMedia solution. We consider the following user classification:

$$\underbrace{U_1 > U_2 > U_3}_{\text{high-priority}} > \underbrace{U_4 > U_5 > U_6}_{\text{low-priority}}, \quad (21)$$

which results from the allocation functions computation given by $H_{k,b}$ and $\bar{H}_{k',b}$. Initially, suppose that the HP users are first assigned the subbands according to their $H_{k,b}$ values. Then, suppose that, after the computation of (18) and (20) and solving (17), we obtain the following matrix containing the $\tau_{k,b}$ values for all the users in the subbands they aim at sharing:

$$\begin{pmatrix} \tau_{U_1,1} & 0 & 0 \\ 0 & 0 & \tau_{U_2,3} \\ 0 & \tau_{U_3,2} & 0 \\ 0 & \tau_{U_4,2} & 0 \\ 0 & 0 & \tau_{U_5,3} \\ \tau_{U_6,1} & 0 & 0 \end{pmatrix}. \quad (22)$$

The latter matrix gives a possible optimized sharing scheme for the six users, where U_4 shares subband 2 with U_3 , U_5 shares subband 3 with U_2 , and U_6 shares subband 1 with U_1 .

4. Proposed Low-Complexity Time-Frequency Spectrum Sharing Solution with Fairness Provision

Optimizing the use of the spectrum by adjusting the main transmission parameters is the main purpose. However, the spectrum sharing solution presented in the previous section has a high computation cost. The complexity of the defined spectrum sharing scheme lies on two main aspects. First, the

iterative process defined for the subband allocation and the computation of the optimal allocation function $H_{k,b}$ require a high computation complexity. Second, the heuristic search proposed to schedule the users also involves an additional computation cost into the heuristic search proposed to schedule the users also involves an additional computation cost. We present in this section a low-complexity and practical cross-layer spectrum sharing scheme.

Since the complexity of the optimal spectrum sharing solution resides in the complexity of both resource allocation optimization and scheduling optimization, we will reduce the whole complexity by defining suboptimal subband allocation and suboptimal time scheduling solutions.

4.1. Suboptimal Subband Allocation Function. By analyzing the optimal allocation function given by (11), it comes that this function is monotonically increasing with respect to $E_{k,b}$ and α_k . In addition, α_k is monotonically increasing with respect to R_k as given by (15). Thus, the allocation function depends on the user rate requirement. In order to reduce the complexity due to the computation of α_k , we define a new parameter having the same mathematical characteristics as α_k , but requiring a lower complexity computation. This new parameter is the user data rate weight r_k defined as

$$r_k = 1 + \frac{R_k - R_{\min}}{R_{\max} - R_{\min}}, \quad (23)$$

where R_k , R_{\min} , and R_{\max} are, respectively, the requested data rate of user k , the lowest and highest data rates taken from WiMedia rate modes (Table 1). Provided by the MAC layer, this weight definition scheme ensures an adaptive rate classification of the different users according to their requirements and to the system model. Consequently, we define a low-complexity cross-layer allocation function $H'_{k,b}$, having the same mathematical behaviors as the optimal function $H_{k,b}$, and based on the product of the user rate weight by the user effective SINR in a subband. It is given by

$$H'_{k,b} = r_k E_{k,b}. \quad (24)$$

4.2. Suboptimal Time-Scheduling Solution. To reduce the complexity of the optimal sharing solution, we propose a novel time scheduling mechanism called the nearest priority sharing (NPS) based on a priority principle that shares the time among the users in a simple way according to their priority order. As described before, the different users are arranged according to their allocation function and then classified into two groups: HP and LP. While the HP users are first assigned the B subbands, the LP users aim at sharing these assigned subbands with them during one superframe. The idea of the NPS mechanism is depicted in Figure 1; the users of the LP group share, in a priority order, the same subband assigned to their nearest-priority user of the HP group, provided that this latter user has the minimum number of users already sharing the same spectrum with.

This suboptimal scheduling solution has the same characteristics as the optimal solution resulting from the

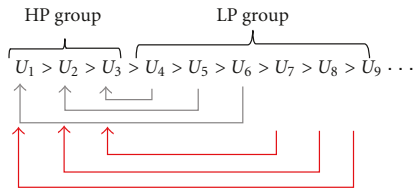


FIGURE 1: The principle of the NPS mechanism.

optimization problem given by (17). Indeed, the optimal sharing is done in a priority-based principle. Similarly, the NPS mechanism respects the same priority-based approach, yet forces the LP users to share the subbands with the HP users by using the inverted priority order, that is the highest priority user of the LP group coexists with the lowest priority user of the HP group, and the lowest priority user of the LP group coexists with the highest priority user of the HP group.

4.3. Low-Complexity Time-Frequency Spectrum Sharing with Fairness Provision. As stated before, a priority-based approach is used to arrange the users in a decreasing order according to a weight value. The weight \mathcal{Q} of each user k is defined as its highest cross-layer suboptimal allocation function value over the subbands. It is given by

$$\mathcal{Q}_k = \max_b H'_{k,b}. \quad (25)$$

Then, since the suboptimal time-scheduling principle provides a high level of simplicity and flexibility, we define a fair time-frequency scheduling mechanism called Weighted Cyclic Rounding (WCR) based on the NPS principle. The idea behind this mechanism is to share the time proportionally to the users weights \mathcal{Q}_k while permuting cyclically, after each user round, the priority order of the users for the subband assignments. Thereby, while each frame time (superframe) is shared dynamically among the users, a user round O_k , which consists of a certain number of MASSs, is defined as follows:

$$\frac{\mathcal{Q}_1}{O_1} = \frac{\mathcal{Q}_2}{O_2} = \dots = \frac{1}{T_F}, \quad (26)$$

where $\mathcal{Q}_1, \mathcal{Q}_2, \dots, \mathcal{Q}_k$ are the normalized users weights and T_F is the total superframe duration. The WCR is achieved using a priority-based circular shift approach as illustrated in Figure 2(a). For example, the highest priority user U_1 is assigned first its best subband for a round cycle equal to O_4 ; then a first permutation is applied so that the second priority user U_2 is placed at the top of the priority order and assigned its best subband for a round cycle equal to O_2 and so on.

4.3.1. Multiuser Round Sharing. In order to share one round cycle among multiple users in a multiuser scenario, we define a round sharing scheme. The idea is to time-share the MASSs of one round cycle among multiple users whereas, in frequency, B users can transmit simultaneously during one MASS duration.

Similarly to the optimal scheme, the HP users are assigned subbands according to their priority order; the highest priority user is assigned its most powerful subband, that is the subband that has the greatest $E_{k,b}$ value. Secondly, the users of the LP group have to share the already assigned subbands with the HP group users during one round cycle.

In The Frequency Domain. The sharing is done according to the NPS principle. For instance, the highest priority user of the LP group shares the same subband with the lowest priority user of the HP group and so on.

In The Time Domain. A time-sharing factor of user k in subband b is defined as follows:

$$\tau_{k,b} = \frac{\mathcal{Q}_{s_b^k}}{\sum_{s_b^k} (\mathcal{Q}_{s_b^k})}, \quad (27)$$

where s_b^k is the disjoint set of users sharing the subband b obtained by applying the NPS mechanism. This sharing factor represents the spectrum usage advantage of the HP users on the LP users. As a result, multiple users can share, using a priority-based principle, one subband during one round cycle of a superframe as illustrated in Figure 2(b).

Depicted in Figure 3, the low-complexity time-frequency spectrum sharing can be considered as an answer to the multiuser access problem in the WiMedia solution where the use of TFC is limiting the number of users aiming at sharing one superframe in one WiMedia channel to three users only.

5. Performance Evaluation

5.1. Channel Model. The channel used in this study is the one adopted by the IEEE 802.15.3a committee for the evaluation of UWB proposals [16]. This model is a modified version of Saleh-Valenzuela model for indoor channels [17], fitting the properties of UWB channels. A log-normal distribution is used for the multipath gain magnitude. In addition, independent fading is assumed for each cluster and each ray within the cluster. The impulse response of the multipath model is given by

$$h_i(t) = G_i \sum_{z=0}^{Z_i} \sum_{p=0}^{P_i} \alpha_i(z, p) \delta(t - T_i(z) - \tau_i(z, p)), \quad (28)$$

where G_i is the log-normal shadowing of the i th channel realization, $T_i(z)$ the delay of cluster z , and $\alpha_i(z, p)$ and $\tau_i(z, p)$ represent the gain and the delay of multipath p within cluster z , respectively.

Independent fading is assumed for each cluster and each ray within the cluster. The cluster and path arrival times can be modeled as Poisson random variables. The path amplitude follows a log-normal distribution, whereas the path phase is a uniform random variable over $[0, 2\pi]$. Four different channel models (CM1 to CM4) are defined for the UWB system modelling, each with arrival rates and decay factors chosen to match different usage scenarios and to fit line-of-sight (LOS) and non-line-of-sight (NLOS) cases.

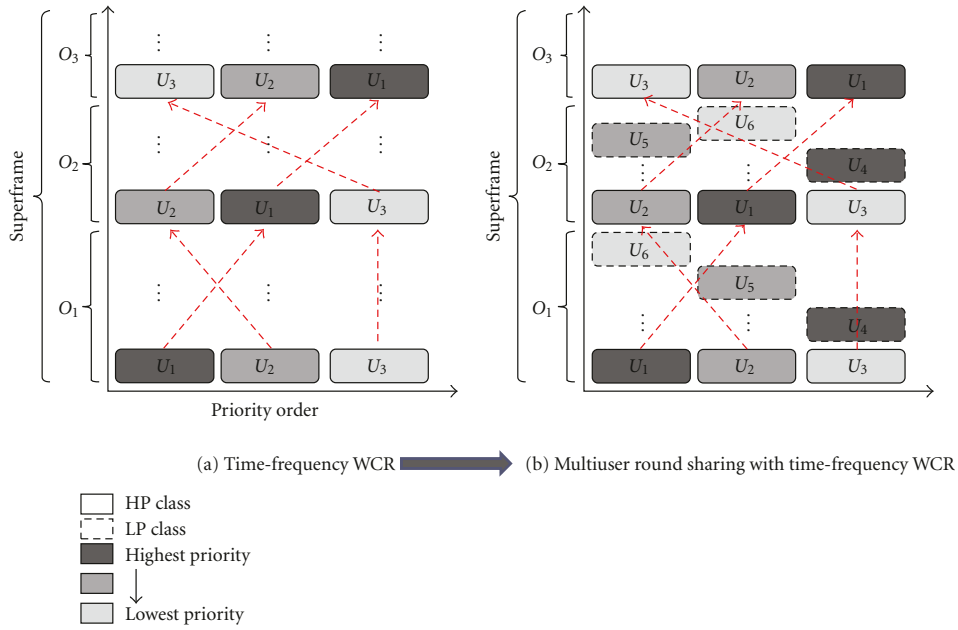


FIGURE 2: Weighted cyclic rounding mechanism and the associated round sharing principle.

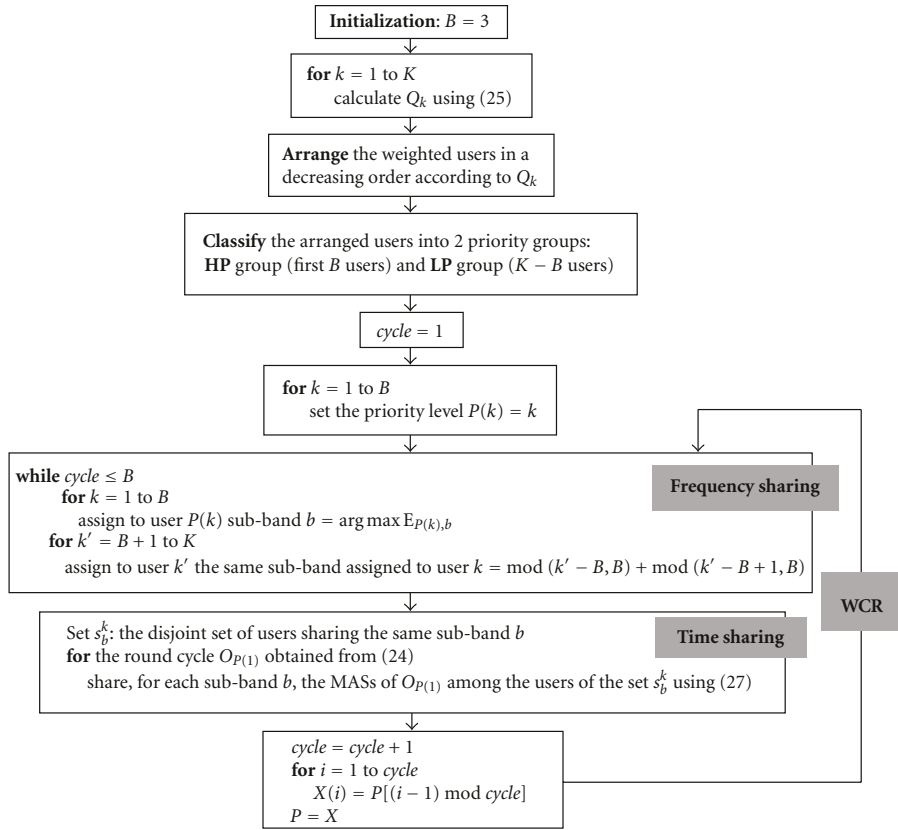


FIGURE 3: Proposed time-frequency spectrum sharing algorithm.

For the simulation scenarios, we use the proposed WiMedia data rates requests defined in Table 1, and we consider the first WiMedia channel (3.1–4.7 GHz) for CM1 channel model.

5.2. Simulation Results. In this section, we present the simulation results for the proposed spectrum sharing scheme, and we compare the performance of the optimal solution with the proposed low-complexity suboptimal solution. The system performance will be evaluated in terms of time-frequency QoS satisfaction. Two metrics are thus considered for the QoS evaluation: one frequency metric related to the channel and rate satisfaction represented by the channel Satisfaction Index (SI), and another time metric representing the time delay of the scheduled users to assess the efficiency of the time-scheduling scheme. Moreover, we compare the performance of the proposed MB-OFDM-MA solution to the OFDMA scheme as well as to the single-user WiMedia solution.

5.2.1. Channel Satisfaction Index Comparison. For performance comparison purpose, we introduce a cross-layer performance metric called the Satisfaction Index (SI) defined as

$$SI_k = \frac{E_{k,b}}{\max_b E_{k,b}}. \quad (29)$$

This new evaluation metric is defined to reflect the cross-layer aspect of the proposed scheduling scheme. It evaluates the channel satisfaction level of a user k assigned a subband b by using the effective SINR value which is correlated to its BER and its effective data rate via parameter λ as given in Table 1. It will be equal to one if the user is fully satisfied since it is assigned its best subband. The SI is consequently a QoS parameter and can be used to evaluate the fairness among the users.

In Figure 4, we compare the user SI level obtained in the optimal and the suboptimal allocation functions given by (11) and (24), respectively, for different possible rates of the WiMedia solution. We consider a scenario consisting of three users aiming at sharing the three subbands of one WiMedia channel: one hard-QoS user requesting the highest data rate, that is 480 Mbps, and two soft-QoS users requesting data rates between 53.3 and 200 Mbps. While the SI of the hard-QoS user is equal to one in the optimal and suboptimal solutions since it is assigned its best subband in both cases, soft-QoS users SI varies according to their data rates. This is due to the fact that the users channel gain is represented by the effective SINR which depends on the data rate by means of parameter λ (see Table 1). Thus, we evaluate the performance of the highest and lowest priority users for the first five data rates. As shown in the figure, the suboptimal subband allocation solution with its low-complexity computation performs close to the iterative optimal solution; an average of 10% of outperformance is outlined for the sake of the optimal solution.

5.2.2. Time Delay Comparison. In Figure 5, we evaluate the QoS support in the proposed time-frequency sharing scheme

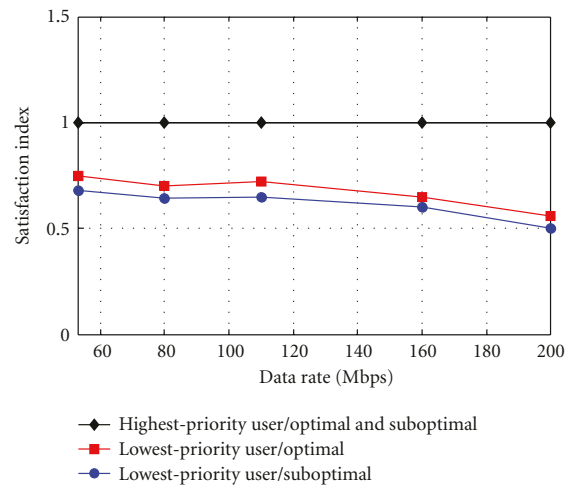


FIGURE 4: Satisfaction Index of the highest and lowest priority users in the optimal and suboptimal solutions.

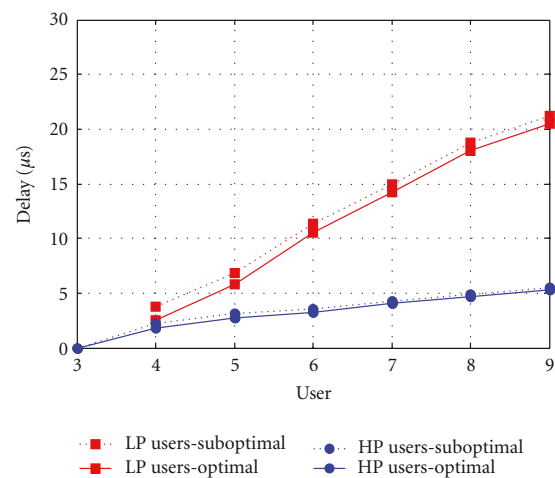


FIGURE 5: The delay of high-priority (HP) and low-priority (LP) users in a multiuser sharing scenario.

in terms of average delay per MAS duration. We consider thus the case of nine users aiming at sharing one superframe by using the proposed optimal and suboptimal spectrum sharing solutions. The nine users are requesting 480, 400, 320, 200, 160, 110, 80, 53.3, and 53.3 Mbps, respectively. The users are arranged according to their priority order and classified into HP and LP users. As shown in the figure, when the first three HP users share the spectrum, there is no delay since there is no time sharing. However, when the LP users time-share the spectrum with the HP users, the performance degrades and the delay increases. Nevertheless, we observe that the delay of the HP users is considerably less than the delay of the LP users in both optimal and suboptimal solutions. The QoS of the HP group is thus well guaranteed since the average of the sum of the delays of the HP users

is relatively low when nine users are sharing the same superframe. On the other hand, the delay in the LP group is more considerable. This can be tolerable when the services of this group are data or BE services, which have tolerance for delay. However, note that if the LP group consists of some hard-QoS users, the performance of these hard-QoS users will degrade and the QoS will not be ensured. Consequently, the ideal case is to have only three hard-QoS users forming the HP group and the other users are soft-QoS users.

Besides, it is noticed that the optimal and suboptimal solutions perform very close in the time-frequency sharing scheme especially in the case of HP users. This proves that the performance difference between optimal and suboptimal allocation functions is reduced in the time domain when combining the frequency allocation with the time scheduling.

5.2.3. Performance Comparison of the Proposed MB-OFDM-MA Solution with the OFDMA Scheme and the Single-User WiMedia MB-OFDM Solution. In order to assess the efficiency of the proposed MB-OFDM-MA spectrum sharing scheme, we compare its performance to two other schemes: the first one is the traditional OFDMA, which allocates subcarriers to users according to their channel power and the second one is the differentiated OFDMA (D-OFDMA), which takes into account the QoS support. The latter solution results from the application of our proposed QoS-aware resource allocation solution on OFDMA, that is using the cross-layer allocation function defined in (24). Moreover, we consider two versions of the proposed scheme: (i) the optimal solution without fairness provision and (ii) the suboptimal with fairness provision, that is using the WCR mechanism. In Figure 6, we evaluate the performance of three users transmitting simultaneously during one MAS duration in terms of average SI. The requested data rates of the users are 480, 200, and 53.3 Mbps, respectively. As shown in the figure, although the first two users are very well satisfied in the case of D-OFDMA and the optimal MB-OFDM-MA, the third user satisfaction level is relatively low. On the other hand, the OFDMA and the low-complexity WCR-MB-OFDM-MA perform almost the same and ensure a very good level of fairness among the three users. This is due to the subband permutation achieved in the WCR mechanism which allows the low-priority users to benefit from best channel qualities for a time proportional to their weights.

In Figure 7, we compare the performance of our suboptimal multiuser allocation solution to the single-user WiMedia solution. The plotted curves represent the E_b/N_0 required to reach a BER level of 10^{-4} for each of the WiMedia data rates. The same “nine-users” scenario considered in Figure 5 is used here. As shown in the figure, the highest priority user has a considerable gain compared to the lowest priority user. For example, at a data rate equal to 200 Mbps, the highest priority user outperforms the lowest priority user with a 2.3 dB gain. On the other hand, the lowest priority user performance is slightly degraded compared to the WiMedia solution. This proves that the fixed TFC as defined in the WiMedia solution does not give advantage to high-priority users that are privileged in the proposed

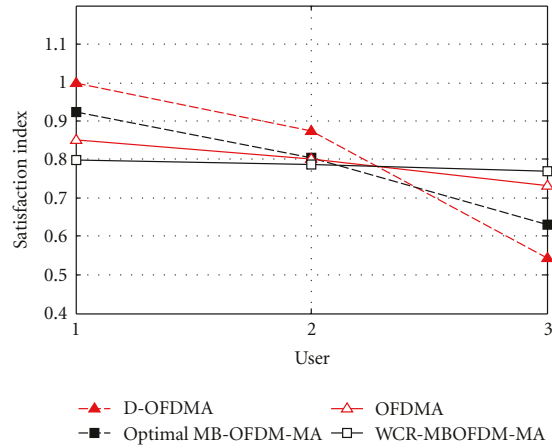


FIGURE 6: Comparison of the proposed MB-OFDM-MA solution with other multiuser schemes.

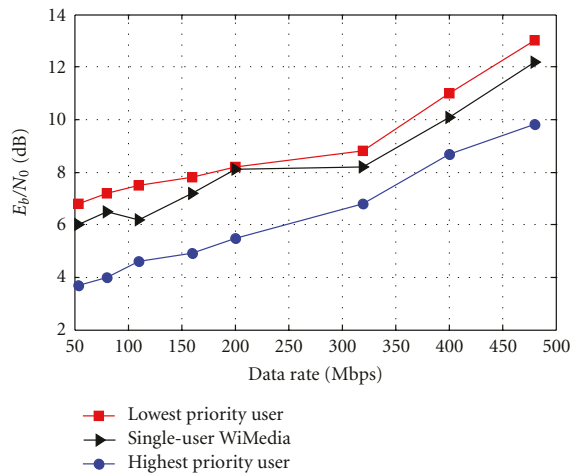


FIGURE 7: Performance of the highest and lowest priority users for the different WiMedia data rate modes.

multiuser spectrum sharing solution since the allocation is achieved proportionally to the users priorities.

6. Conclusion

In this paper, we have proposed a novel spectrum sharing scheme based on a cross-layer MB-OFDM-MA approach. This new scheme has considered both the frequency resource allocation and the time scheduling issues by deriving a joint optimization model resulting in an MB-OFDM time-frequency spectrum sharing scheme. However, to reduce the complexity of the optimal spectrum sharing solution, a low-complexity suboptimal spectrum sharing model has been proposed based on suboptimal resource allocation and scheduling solutions. The low-complexity time-frequency spectrum sharing solution takes into account the fairness provision jointly with the QoS support. It uses a mechanism

that interchanges the priority among the users by offering them the opportunity to choose their best-quality channels during a fraction of the superframe proportionally to their priority weights. Combined with the priority-based time-frequency sharing approach, the fair scheduling mechanism ensures a good level of fairness among the users while respecting the concept of prioritization among them. Compared with the single-user WiMedia solution and the high-complexity OFDMA scheme, the low-complexity MB-OFDM-MA can be a solution for the multiuser medium access problem in WiMedia UWB systems as well as in next generation OFDM systems.

Acknowledgment

The research leading to these results has received funding from the European Community's Seventh Framework Programme no. FP7/2007-2013 under Grant Agreement no. 213311 also referred as OMEGA.

References

- [1] J. Moon, J. Y. Ko, and Y. H. Lee, "A framework design for the next-generation radio access system," *IEEE Journal on Selected Areas in Communications*, vol. 24, no. 3, pp. 554–564, 2006.
- [2] J. Jang and K. B. Lee, "Transmit power adaptation for multiuser OFDM systems," *IEEE Journal on Selected Areas in Communications*, vol. 21, no. 2, pp. 171–178, 2003.
- [3] C. Y. Wong, R. S. Cheng, K. B. Letaief, and R. D. Murch, "Multiuser OFDM with adaptive subcarrier, bit, and power allocation," *IEEE Journal on Selected Areas in Communications*, vol. 17, no. 10, pp. 1747–1758, 1999.
- [4] I. Kim, I. S. Park, and Y. H. Lee, "Use of linear programming for dynamic subcarrier and bit allocation in multiuser OFDM," *IEEE Transactions on Vehicular Technology*, vol. 55, no. 4, pp. 1195–1207, 2006.
- [5] Y. Shang and S. Cheng, "An enhanced packet scheduling algorithm for QoS support in IEEE 802.16 wireless network," in *Proceedings of the International Conference on Communications, Networking and Mobile Computing (ICCNMC '05)*, vol. 3619 of *Lecture Notes in Computer Science*, pp. 652–661, Zhangjiajie, China, August 2005.
- [6] V. Singh and V. Sharma, "Efficient and fair scheduling of uplink and downlink in IEEE 802.16 OFDMA networks," in *Proceedings of the IEEE Wireless Communications and Networking Conference (WCNC '06)*, vol. 2, pp. 984–990, April 2006.
- [7] L. Badia, A. Baiocchi, A. Todini et al., "On the impact of physical layer awareness on scheduling and resource allocation in broadband multicellular IEEE 802.16 systems," *IEEE Wireless Communications*, vol. 14, no. 1, pp. 36–43, 2007.
- [8] WiMedia Alliance, Inc., "Multi-band OFDM physical layer specification," Release 1.1, July 2005.
- [9] A. Batra, J. Balakrishnan, G. R. Aiello, J. R. Foerster, and A. Dabak, "Design of a multiband OFDM system for realistic UWB channel environments," *IEEE Transactions on Microwave Theory and Techniques*, vol. 52, no. 9, pp. 2123–2138, 2004.
- [10] Z. Chen, D. Wang, and G. Ding, "An OFDM-UWB scheme with adaptive carrier selection and power allocation," in *Proceedings of the International Conference on Wireless Communications, Networking and Mobile Computing (WiCOM '06)*, pp. 1–4, Wuhan, China, September 2006.
- [11] J. Wang, G. Zhu, and J. Jin, "Optimal power allocation for space-time coded OFDM UWB systems," in *Proceedings of the International Conference on Wireless Communications, Networking and Mobile Computing (WCNM '05)*, vol. 1, pp. 169–172, September 2005.
- [12] Z. Xu and L. Liu, "Power allocation for multi-band OFDM UWB communication networks," in *Proceedings of the 60th IEEE Vehicular Technology Conference (VTC '04)*, pp. 368–372, Los Angeles, Calif, USA, September 2004.
- [13] W. P. Siriwongpairat, Z. Han, and K. J. R. Liu, "Power controlled channel allocation for multiuser multiband UWB systems," *IEEE Transactions on Wireless Communications*, vol. 6, no. 2, pp. 583–592, 2007.
- [14] A. Khalil, M. Crussière, and J. F. Hélar, "Differentiated multiuser resource allocation scheme for multi-band UWB systems," in *Proceedings of the 10th IEEE Workshop on Signal Processing Advances in Wireless Communications (SPAWC '09)*, pp. 707–711, Perugia, Italy, June 2009.
- [15] 3GPP TSG-RAN-1, "R1-030999: considerations on the system performance evaluation of HSDP using OFDM modulations," RAN WG1 #34.
- [16] J. Foester, "Channel modeling sub-committee report (final)," IEEE P802.15.-02/490r1-SG3a, 2003.
- [17] A. A. M. Saleh and R. A. Valenzuela, "A statistical model for indoor multipath propagation," *IEEE Journal on Selected Areas in Communications*, vol. 5, no. 2, pp. 128–137, 1987.

Selected Article

O.P. Pasquero, M. Crussière, Y. Nasser, J.F. Hélar. "Efficient space code block code mimo channel estimation for future mobile video broadcasting", In Proceedings of the IEEE Wireless Communications and Networking Conference (WCNC), pp 1– 6, April 2009, DOI :10.1109/WCNC.2009.4917703

Abstract

In this paper, we propose a novel and simple MIMO channel estimation technique based on 2D spread pilots. Taking advantage of the simplicity and flexibility of 2D spread pilot channel estimation, we easily combine the Alamouti code with the Walsh-Hadamard codes to obtain a space code block code (SCBC) MIMO scheme. We demonstrate that our proposed system is much more efficient in high mobility scenario than the classical STBC scheme. The performance evaluated over a realistic channel model shows the efficiency of this technique which turns out to be a promising MIMO channel estimation technique for the future mobile video broadcasting systems.

Keywords : Linear Precoded OFDM, space code block code, MIMO, TV broadcasting, channel estimation

PROCES VERBAL DE SOUTENANCE DU 24/11/2017 A 10h30

ANNEE UNIVERSITAIRE 2017/2018

Etudiant : M. MATTHIEU CRUSSIÈRE né le : 22/10/1979

Diplôme : HABILITATION DIRIGER DES RECHERCHES ELECTRONIQUE

Lieu de soutenance : Amphi Bonin - INSA de Rennes - 20 Avenue des Buttes de Coesmes

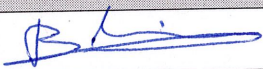
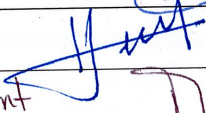
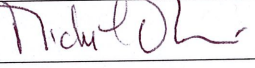
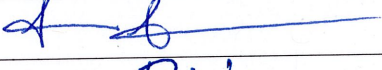
La soutenance est publique.

Résultat : *Admis*

Mention :

Avis de reproduction : *Avis favorable*

Membres du Jury

Nom	Qualité	Etablissement	Rôle	Signature
Mme GENEVIEVE BAUDOIN	PROFESSEUR DES UNIVERSITES	ESIEE PARIS		
Mme MARIE-LAURE BOUCHERET	PROFESSEUR DES UNIVERSITES			
Mme CATHERINE DOUILLARD	PROFESSEUR DES UNIVERSITES			
M. JEAN-MARIE GORCE	PROFESSEUR DES UNIVERSITES	INST NAT SC APPLIQ VILLEURBANN		
M. JEAN-FRANCOIS HELARD	PROFESSEUR DES UNIVERSITES	INSA DE RENNES		
M. MICHEL TERRE	PROFESSEUR DES UNIVERSITES	CNAM	Président	
M. ANDREA TONELLO	PROFESSEUR DES UNIVERSITES	Univ. Klagenfurt		
M. BERNARD UGUEN	PROFESSEUR DES UNIVERSITES	UNIVERSITE DE RENNES 1		
M. LUC VANDENDORPE	PROFESSEUR DES UNIVERSITES	UNIVERSITE CATHOLIQUE DE LOUVAIN		

HABILITATION A DIRIGER LES RECHERCHES
mention ELECTRONIQUE
par Matthieu CRUSSIÈRE le 24 novembre 2017

RAPPORT DE SOUTENANCE

(signature obligatoire de tous les membres du jury)

Président de jury : M. Teuve'

Rapporteur du jury : M. Teuve'

Monsieur Matthieu Crussière a effectué un excellent exposé de sa carrière. Il a parfaitement démontré son implication dans le domaine de l'enseignement et il a synthétisé toutes ses activités de recherche en les regroupant, de manière très intelligente, dans trois grands domaines. Son exposé extrêmement pédagogique et synthétique, mais aussi particulièrement précis sur des sujets scientifiques complexes, a permis au jury d'apprécier son très grand recul sur des questions liées à plusieurs types de systèmes de télécommunications.

Le jury a été particulièrement sensible à la polyvalence de Monsieur Mathieu Crussière, qui a toujours su maintenir un parfait équilibre entre des résultats théoriques fondamentaux et des considérations très pragmatiques et opérationnelles, sur le fonctionnement réel des systèmes de diffusion et d'accès large bande. Lors de son exposé, Monsieur Matthieu Crussière a parfaitement illustré les nombreuses et importantes solutions analytiques qu'il a établies au cours de sa carrière.

Le jury a été impressionné par la forte implication de Monsieur Matthieu Crussière dans la vie scientifique de son laboratoire de recherche (IETR) et par le grand nombre de doctorants qu'il a pu encadrer, en veillant toujours à publier avec eux dans de très bonnes revues et congrès.

Il est apparu clairement au jury que Monsieur Matthieu Crussière possédait une très grande autonomie scientifique et avait l'expérience nécessaire, non seulement pour encadrer des doctorants, mais aussi pour initier et piloter des nouvelles thématiques de recherches.

A l'issue de ce remarquable exposé le jury a considéré que Monsieur Matthieu Crussière était un enseignant chercheur brillant et lui a décerné, à l'unanimité, l'habilitation à diriger des recherches de l'Université de Rennes 1.

J.M. Teuve'

B. Baudouin

M. Bouchet

B. UGUEN

J-F HELARD

Nicholas

L. VANNIER

A. Fanel

C. Bouill...

Campus de Beaulieu
263, avenue du Général Leclerc
CS 74205
35042 Rennes Cedex
www.univ-rennes1.fr

☎ : 02 23 23 63 23
☎ : 02 23 23 55 11